19th International Conference
ENGINEERING MECHANICS 2013
Svratka, Czech Republic, May 13 – 16, 2013

REPAIRING AND REINFORCING LOAD BEARING ELEMENTS OF TIMBER STRUCTURES, DAMAGED BY BIO-DEGRADATION

P. Agel*, A. Lokaj**

Abstract: *Many historical timber constructions are damaged by biodegradation especially by ligniperdous insect. Sometimes the degradation is so high, that some construction members need to be replaced or reinforced. In common buildings we can use many known methods to repair damage. But in historical buildings we must mind visual aspect and Bureau of care of historical monuments. According to their demands we are not able to replace whole members also repaired timber element must look like original members. This article describes the method which can be used in such cases.*

Keywords: ***reinforcing, timber, bio-degradation, structure, element***

1. Introduction

At the reconstructions and repairs of historical roof structures it is often necessary to deals with load bearing members damaged by biodegradation. Best way to repair such structure will be to replace whole damaged member. This is often against position of Bureau of care of historical monument which we must mind when dealing with historical buildings. Main goal of the bureau is to maintain visual (historical) look of the construction.

One of many solutions of this situation is to remove damaged truss reinforce it and return back to its original place. In part 2 of the article there is detailed description of repair technology which maintains member look and its former strength.

For reliable design of load bearing member repairs it is to be to set construction principles which are based on calculation procedures and methods proved by laboratory test on appropriate samples.

Fig. 1: Timber members damaged by ligniperdous insect with embed reinforcing core

* Ing. Petr Agel: Faculty of Civil engineering, Technical Univesity of Ostrava. Ludvika Podeste 1875/17, 708 33 Ostrava – Poruba, e-mail: petr.agel@vsb.cz
** doc. Ing. Antonín Lokaj, Ph.D.: Faculty of Civil engineering, Technical Univesity of Ostrava. Ludvika Podeste 1875/17, 708 33 Ostrava – Poruba, e-mail: antonin.lokaj@vsb.cz

Acknowledgement

Article was funded from the SGS project at the FAST VŠB-TU Ostrava.

References

ČSN EN 408(2004): *Timber structures – Timber and gluelaminated timber. Set of physical and mechanical properties*

Euro code 5.(2006):*Design of timber structures – Part 1-1:General - Common rules and rules for buildings*

Janas, P., Krejsa, M., Krejsa, V.(2009) *Structural reliability assessment using a direct determined probabilistic calculation.* In Proceedings of the 12th International Conference on Civil Structural and Environmental Engineering Computing. Funchal, Madeira

Lokaj, A., Vavrušová K., Rykalová E.(2011) *Application of laboratory tests results of dowel joints in cement-splinter boards VELOX into the fully probabilistic methods (SBRA method).* Applied Mechanics and Materials, 2011, 187. 1. pp. 95-99.

Lokaj, A., Marek, P.(2009) Simulation-*based Reliability Assessment of Timber Structures.* In Proceedings of the 12th International Conference on Civil Structural and Environmental Engineering Computing. Funchal, Madeira

Lokaj, A., Vavrušová K., Agel, P.(2011) The *embedment strength of dowel joints in cement-splinter boards Velox,* Transactions of the VŠB-Technical University of Ostrava Civil Engineering Series, 11. 2. pp. 43-48.

Reinprecht, L.(2008) *Timber protection*. Technical University of Zvolen

19th International Conference
ENGINEERING MECHANICS 2013
Svratka, Czech Republic, May 13 – 16, 2013

ELASTIC CRITICAL BUCKLING STRESS OF THE WEB GIRDER SUBJECTED TO TRANSVERSE FORCE

I. Baláž*, Y. Koleková**

Abstract: *Beam subjected to a single concentrated load or transverse uniformly distributed partial load (relative loading length $0 \leqslant c/a \leqslant 1$). Buckling coefficients $k_{\sigma,b}$ for a long rectangular plate $(4 \leqslant \alpha \leqslant 40)$ stiffened at longitudinal edges by flanges with different relative normal flange rigidity $(0 \leqslant \delta \leqslant 3)$ and subjected to a symmetric transverse load only at one longitudinal edge. Comparison of the buckling coefficients k_σ computed by various authors for plate without flanges. Conclusions made from a parametrical study, part of which is presented in the paper. Program PLII was used in the parametrical study.*

Keywords: ***Buckling coefficient, critical stress, patch loading, parametrical study, comparisons.***

1. Introduction

Already in the older editions of the modern codes DIN 18800 (1989), ENV 1993-1-5 (1997) the rules for the resistance of a web to the patch loading (*Fig.1*) use the same format as the other buckling rules. In the design procedure it is necessary to calculate:

- the yield resistance in the form of the stress f_y DIN 18800 (1989), or the force F_y ENV 1993-1-5,
- the elastic buckling stress σ_{cr} DIN 18800 (1989), or the buckling force F_{cr} ENV 1993-1-5 (1997),
- the relative slenderness $\lambda = \sqrt{f_y / f_{cr}}$ DIN 18800 (1989), or $\lambda = \sqrt{F_y / F_{cr}}$ ENV 1993-1-5 (1997),
- the reduction factor $\kappa = f(\lambda)$ DIN 18800 (1989), or $\chi = f(\lambda)$ ENV 1993-1-5 (1997),
- the resistance of web to patch loading $\sigma_R = \kappa f_y$ DIN 18800 (1989), or $F_R = \chi F_y$ ENV 1993-1-5.

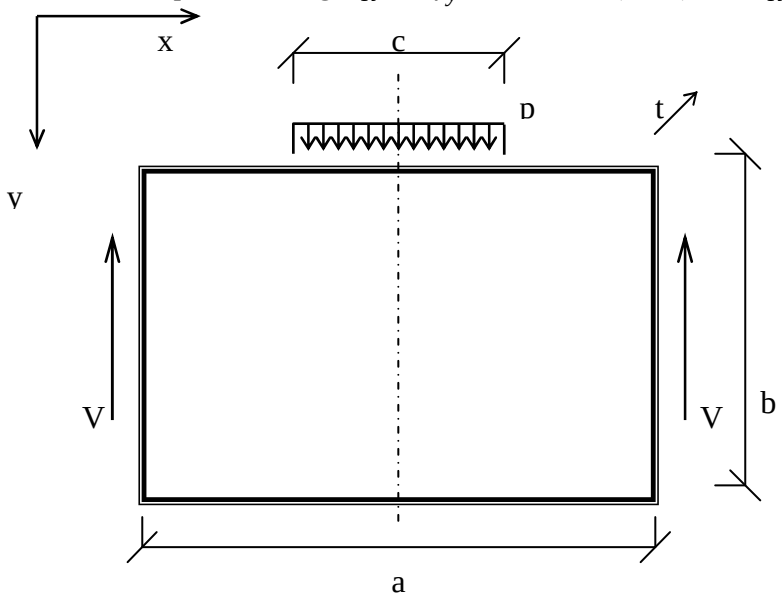

Fig. 1: Notation

* Prof. Ing. Ivan Baláž, PhD.: Department of Metal and Timber Structures, Faculty of Civil Engineering, Slovak University of Technology, Radlinského 11; 813 68, Bratislava; SK, e-mail: ivan.baláž@stuba.sk

** Assoc. Prof. Ing. Yvona Koleková, PhD.: Department of Structural Mechanics, Faculty of Civil Engineering, Slovak University of Technology, Radlinského 11; 813 68, Bratislava; SK, e-mail: yvona.kolekova@stuba.sk

Despite of the formal similarity in the design procedures, there are important differences in the details between the both codes DIN 18800 (1989) and ENV 1993-1-5 (1997).
One of the most important step in a design procedure is calculating of the elastic buckling stress σ_{cr} .

2. Elastic buckling stress

The elastic buckling force is written as

$$F_{cr} = \sigma_{cr} ct \tag{1}$$

where

c is the length over which the applied transverse force is distributed,
t the thickness of the plate,
$\sigma_{cr} = k_\sigma \sigma_E$ the critical stress and the Euler critical stress are as follows

$$\sigma_E = \frac{\pi^2 E}{12\left(1-\nu^2\right)\left(\frac{b}{t}\right)^2}, \quad \sigma_{\mathrm{E,steel}} = \frac{189\,800}{\left(\frac{b}{t}\right)^2}\ \left[\mathrm{N/mm^2}\right], \quad \sigma_{\mathrm{aluminium}} = \frac{\sigma_{\mathrm{E,steel}}}{3} = \frac{63\,267}{\left(\frac{b}{t}\right)^2}\ \left[\mathrm{N/mm^2}\right] \tag{2}$$

b is the breadth of the plate or depth of the web,
b/t the slenderness of the plate or the web,
k_σ the buckling coefficient,
E Young's modulus of elasticity (210 GPa for steel, 70 GPa for aluminium alloys),
v Poisson's ratio in elastic stage (0,3 for steel and aluminium alloys).

The buckling coefficient k_σ depends generally on the

- type of the action (also on the relative loading length $\beta = c/a$ in the case of transverse action),
- boundary conditions (also on the flange rigidities, e.g. on the relative normal rigidity of the flange $\delta = A_f/(bt)$, where A_f is the area of the flange cross-section),
- longitudinal and/or transverse stiffeners locations and their rigidities,
- shape of the plate (e.g. on the aspect ratio of the plate $\alpha = a/b$, in the case of rectangular plate, where a is the length of the investigated plate – the spacing of the transverse stiffeners),

The numerical values of the buckling coefficient k_σ may vary a lot and therefore sometimes for the purpose of diagrams the more convenient forms of the buckling coefficients $k_{\sigma,a}$ and $k_{\sigma,b}$ are used. For instance Petersen (1993), von Berg (1989) and Ravinger (1979) use instead of the above defined buckling coefficient k_σ the buckling coefficient $k_{\sigma,a}$:

$$F_{cr} = \sigma_{cr} ct = k_\sigma \sigma_E ct = (k_\sigma \frac{c}{a})\sigma_E at = k_{\sigma,a}\sigma_E at \tag{3}$$

Kutzelnigg (1982) and Protte (1994) use instead of the coefficient k_σ the buckling coefficient $k_{\sigma,b}$:

$$F_{cr} = \sigma_{cr} ct = k_\sigma \sigma_E ct = (k_\sigma \frac{c}{b})\sigma_E bt = k_{\sigma,b}\sigma_E bt \tag{4}$$

The following formulae are valid

$$k_{\sigma,a} = k_\sigma \frac{c}{a} = k_{\sigma,b}\frac{b}{a} = \frac{k_{\sigma,b}}{\alpha} = k_\sigma \beta \tag{5}$$

$$k_{\sigma,b} = k_\sigma \frac{c}{b} = k_{\sigma,a}\frac{a}{b} = k_{\sigma,a}\alpha = k_\sigma \alpha\beta \tag{6}$$

Acknowledgements

Project No. 1/0748/13 was slightly supported by the Slovak Grant Agency VEGA.

References

There is a list of references in the full text paper.

19th International Conference
ENGINEERING MECHANICS 2013
Svratka, Czech Republic, May 13 – 16, 2013

PROTECTIVE SCREEN AND ITS INFLUENCE ON THE RELIABILITY OF THE CONTROL VALVE OPERATION

L. Bednář*, L. Tajč, M. Miczan*****

Abstract: *The standard version of the control and stop valve of steam turbines is mentioned. The pressure loss caused by the screen at the valve entrance is assessed. The results of different experiments and the 3D numeric simulation are presented. The influence of the screen on the loss, the suitability of the direction openings and the input spin of the flow in the valves is described. The pressure loss in the combined valve and the influence of the screen on even distribution under the valve cone is mentioned.*

Keywords: ***Turbine, valve, screen, experiments, flow.***

1. Introduction

The screens in the control and stop valves shall prevent penetration of the extraneous particles to the blade section of the steam turbines. They have become an integral part of all valves as a protective element. However, the screens have the influence on the pressure distribution as well as on the pressure loss. The screens are placed in the entrance chamber of the valve, the size of their holes has stabilized at 8 up to 12 mm. The angled holes in the bottom part of the screen make the part of the flow rotate in a certain extent, which has a positive influence on the flow stabilization in the output diffuser.

2. The pressure loss in the valves

The characteristic arrangement of non-lightweight control valves is shown in the Fig. 1.

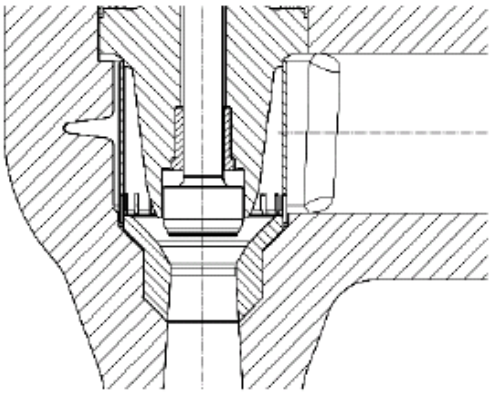

Fig. 1: The detail section of the control valve with the protective screen

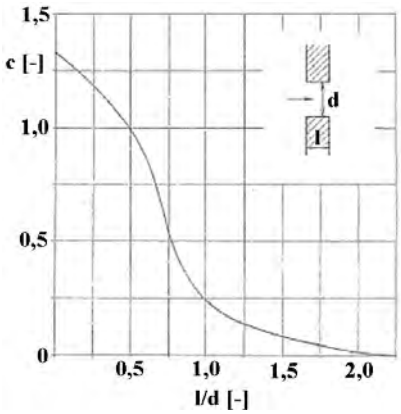

Fig. 2: Coefficient c depending on the ratio of the plate thickness to the diameter of the circular section

The pressure loss in the valve is determined by the difference between the total pressures before and behind the valve. The pressure loss in the screen is a part of this loss. This may be determined using the loss coefficient ζ. The following shall be applied:

* Ing. Lukáš Bednář: Doosan Škoda Power, s.r.o., Tylova 1/57, 301 28 Plzeň; CZ, e-mail: lukas.bednar@doosan.com
** Ing. Ladislav Tajč, CSc.: Doosan Škoda Power, s.r.o., Tylova 1/57, 301 28 Plzeň; CZ, e-mail: ladislav.tajc@doosan.com
*** Ing. Martin Miczán: Doosan Škoda Power, s.r.o., Tylova 1/57, 301 28 Plzeň; CZ, e-mail: martin.miczan@doosan.com

$$\Delta p = \zeta \cdot \rho \frac{w_0^2}{2}$$

w_0 is the speed before the screen. The following relation indicates the loss coefficient

$$\zeta = \frac{\zeta_v + c(1-f_n) + (1-f_n)^2 + \lambda \ell / d}{f_n^2} \qquad (1)$$

whereas $f_n = F_1 / F_2$ – area ratio of the holes to the total area

ℓ / d - proportional depth of the hole of the screen

λ - frictional loss coefficient

c – additional experimental coefficient

ζ_v – coefficient of the curvature on the flow.

For the screens made of the thicker plate the following is indicated: ζ = 0.5 and c is changed depending on ℓ / d, see the Fig. 2.

3. The aerodynamic characteristic of the valves

The 3D numeric study enabling to assess the mutual influence of the rib and the directional holes in the screen has been carried out. In the Fig. 3 there is a flow field in the middle section of the supply pipe and the screen in the area of the circular holes. The rib on the opposite side to the steam inlet helps to create the symmetrical arrangement of the flow. A radical entrance to the screen is well visible. Another situation occurs in the part with the directional holes. The relevant flow field is shown in the Fig. 4.

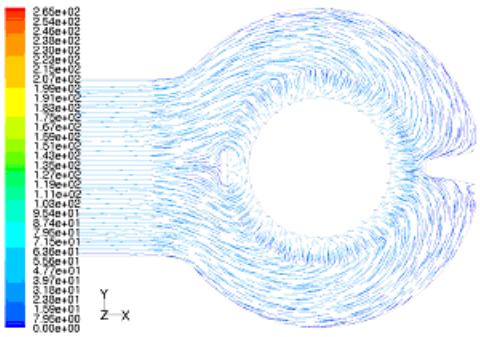

Fig. 3: The flow field in the section of the screen in the area of the circular holes (ε = 0.98)

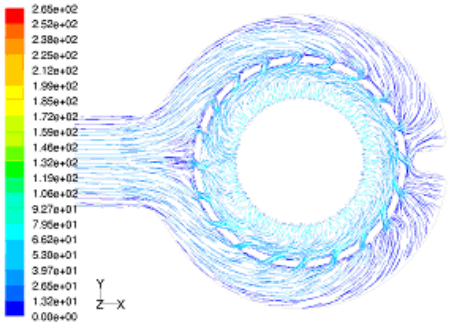

Fig. 4: The flow field in the part of the directional holes (ε = 0.98)

4. Conclusions

The steam discharge from the bypass valve in its middle part helps, due to the ejection effect, to separate the main flow from the wall of the diffuser. It is the source of the impulses, pressure pulsations and pipe vibrations. The location of the outflow in the peripheral part of the big cone helps to stabilize the flow along the wall of the diffuser. It performs the same function as a damper or the flow rotation.

The valves without the screen show the lowest pressure loss. They provide a greater unevenness of the pressure and velocity fields or step changes in the pressure.

The screen helps to balance the pressure and velocity fields in the valve. It is the source of the pressure loss, which may be 0.2 ÷ 0.5 % of the input pressure.

The screen with the directional holes for the rotation of the flow has better aerodynamic properties than the screen having only the drilled holes.

19th International Conference
ENGINEERING MECHANICS 2013
Svratka, Czech Republic, May 13 – 16, 2013

Numerical modeling of several cases of the stratified flow

L. Beneš [1]

1. Mathematical model and numerical scheme

The article deals with the numerical simulation of the stratified incompressible flows over the body and over the isolated hill. Different obstacle models and boundary conditions are tested.

The mathematical model is based on the system of Navier-Stokes equations for viscous incompressible flow with variable density. These equations are simplified by the Boussinesq approximation.

The AUSM MUSCL scheme in the finite volume formulation has been used for spatial semidiscretization. For the time integration BDF method of the second order has used. Arising set of nonlinear equations is then solved by the artificial compressibility method in the dual time τ by the explicit 3-stage second-order Runge-Kutta method. For validation of obtained results the other two different schemes have been used in the selected cases. The first of this schemes is the WENO scheme combined with the projection method, the second scheme is the compact finite–difference scheme. All schemes were validated in our previous studies. The schemes have been successfully used for simulation of the flow field around moving bodies in 2D and 3D stratified fluid for wide range of Richardson numbers see (1), (2), (3).

2. Computational setup and numerical results

The gravity waves are generated by the moving of the thin horizontal strip $0.025 \times 0.002\ m$ in the towing tank. The flow field is initially at rest with the exponential profile of stratification $\varrho_0 = \varrho_{00} \exp \frac{x_2}{\Lambda}$, $\varrho_{00} = 1008.9\ kg/m^3$, $\Lambda = 47.735\ m$, the kinematic viscosity is $\nu = 10^{-6} m^2/s$. Three different models of the body was tested. The first one is the classical body fitted mesh. The second one is based on the penalization technique and the obstacle is modeled as the permeable body with high resistance parameter. The last approach is based on the immersed boundary method.

The second computational case is given by the low smooth sine-shaped hill. The domain has dimensions $90 \times 30\, m$. The hill height is $h = 1m$.

The background density field is given by $\varrho_0(x_2) = \varrho_w + \gamma x_2$ with $\varrho_w = 1.2\, kg \cdot m^{-3}$ and $\gamma = -0.01\, kg \cdot m^{-4}$, the viscosity $\nu = 0.001$. Three different boundary conditions on the outlet are tested and compared each to other.

[1] Doc. Ing. Luděk Beneš PhD Dept. Of Technical Mathematics, Faculty of Mechanical Engineering, Czech Technical University in Prague, Karlovo nám 13, 121 35, Prague 2, tel. +420 224357543, e-mail benes@marian.fsik.cvut.cz

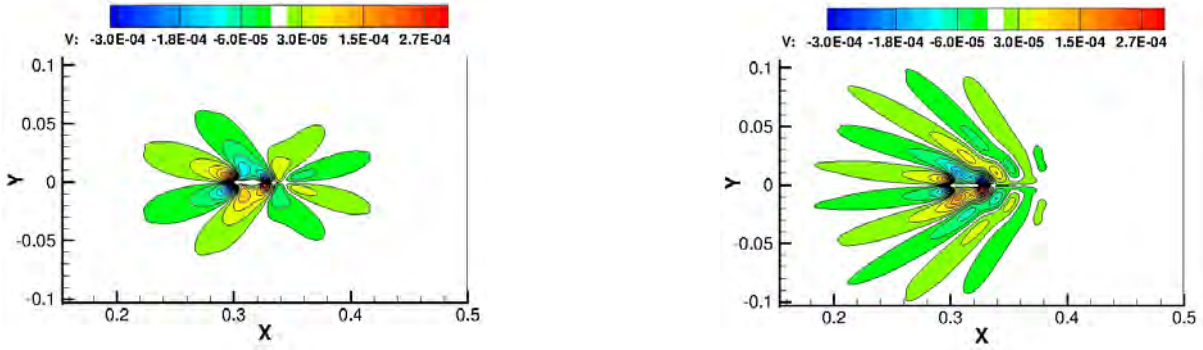

Figure 1: Developing of the internal waves. Isolines of u_2– velocity component, two different times.

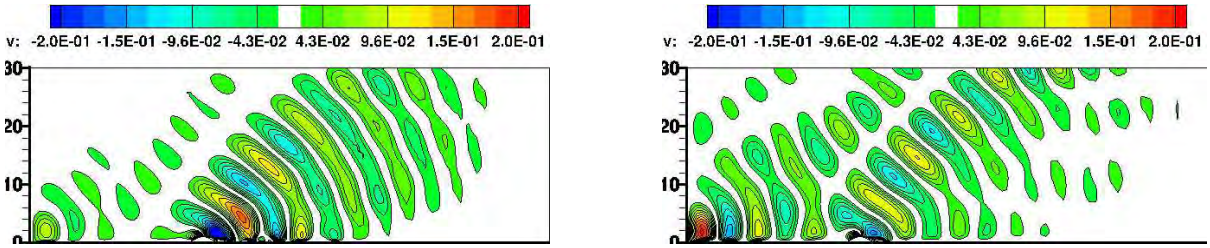

Figure 2: Gravity waves pattern for different boundary conditions. BC 1 – left, BC 3 –right

Presented results show suitability of all models for modeling of this type of problems. Both wave structure far away the obstacle and boundary layer are well resolved. The flow pattern is practically identical for all obstacle models. The number, position and wave length are practically the same. While the u_1–velocity component is similar in all models (including the boundary layer), greatest differences are in the prediction of the u_2–velocity component. The more significant differences are mainly close to the corners and in the case of permeable model in the wake close to the obstacle. The boundary layer on the sides of the obstacle is resolved well. In the case of boundary conditions, the flow was significantly influenced by the boundary condition for pressure on the outlet.

Acknowledgments: This work was supported by TACR Project TA01020428 and grant CTU SGS13/174/OHK2/3T/12.

3. References

[1] Beneš L., Fürst J., Fraunié Ph.: Numerical simulation of the towing tank problem using high order schemes. BAIL 2008 - Boundary and Interior Layers. Lecture Notes in Computational Science and Engineering 69, Springer 2009 ISSN 1439-7358.

[2] Beneš L., Fürst J., Fraunié Ph.: Numerical simulation of the stratified flow using high order schemes. *E*ngineering Mechanics, 16(1):39–48, 2009. ISSN 1210-2717.

[3] Beneš L., Fürst J., Fraunié Ph.: Comparison of two numerical methods for the stratified flow. *J*. Computers & Fluids,in press, doi:10.1016/j.compfluid.2011.02.003.

19th International Conference
ENGINEERING MECHANICS 2013
Svratka, Czech Republic, May 13 – 16, 2013

HYDRAULIC AND STRUCTURAL ANALYSIS OF FLAP GATES

M. Brouček*, M. Králík and P. Nowak*****

Abstract: *Undesirable vibrations of either structural or technological parts of gated weirs are often observed during the service life of these hydraulic structures. Such vibrations cause inconvenience to the environment due to the induced excessive noise as well as shift the design point of view to fatigue capacity of the appropriate parts. Nowadays, flap gate present the most frequently designed type of gate for weirs in river engineering. Despite their many advantages, such as uniform load of the foundation structure, good regulation of water level, favourable hydraulic properties, when lowered, and most importantly good price to gated head ratio, they suffer from vibration issues. The paper presents results and comparison of in-situ measurements, laboratory experiments and numerical modelling.*

Keywords: ***flap gates, vibrations, in-situ measurements***

The necessity of detailed study of potential vibrations of flap gates and their foundation structure results from operational and service life reasons as well as from hygienic standards setting safety limits for noise and vibrations. Although no dam or spillway failures have been reported in Czech Republic in recent years, several gates, some of them are brand new, are experiencing undesirable vibrations. Due to the complexity of the phenomenon, is it extremely difficult to completely eliminate the possibility of vibration affecting the construction during the design stage (ICOLD, 1996) and therefore evaluation of the possible impact based on the measured data must take place. Theoretical part of the paper focuses on the discharge over the edge of the gate.

The experimental part presents methods and procedures used for measurement and evaluation of selected variables on both laboratory model and in-situ. Forces in operating rods under steady conditions and accelerations and deformations of the gate are also presented. An example of the visible effects of the vibrations, which were captured using video camera and digital camera, is presented in the final part of the paper.

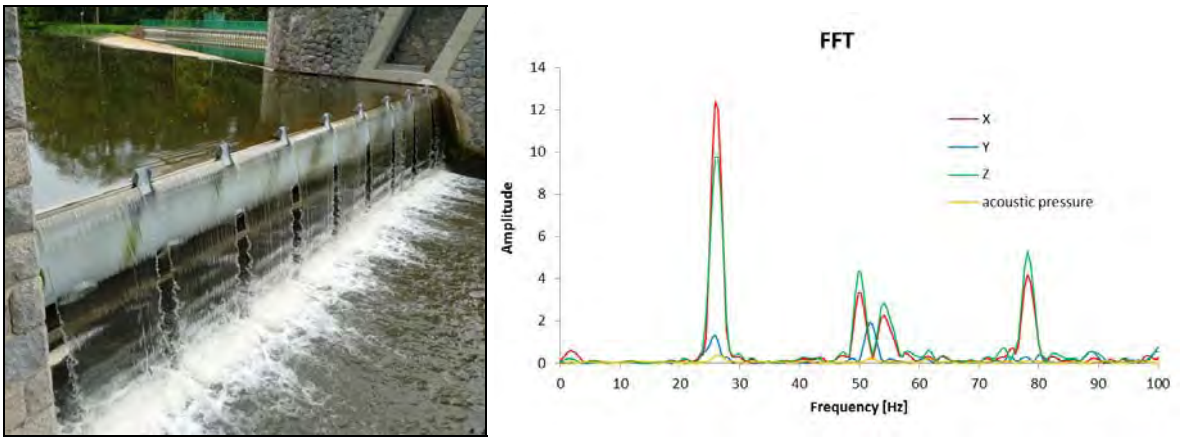

Fig. 1: Oscillation of the overflowing nappe and FFT analysis of acceleration and acoustic pressure

* Ing. Miroslav Brouček: Czech Technical University in Prague, Faculty of Civil Engineering, Thákurova 7; 166 29, Prague; CZ, e-mail: miroslav.broucek@fsv.cvut.cz

** Ing. Martin Králík, Ph.D.: Czech Technical University in Prague, Faculty of Civil Engineering, Thákurova 7; 166 29, Prague; CZ, e-mail:kralik@fsv.cvut.cz

*** Dr. Ing. Petr Nowak: Czech Technical University in Prague, Faculty of Civil Engineering, Thákurova 7; 166 29, Prague; CZ, e-mail: petr.nowak@fsv.cvut.cz

Measured data were used for calibration of numerical models created in ANSYS Workbench environment, while using ANSYS CFX code for modelling of flow and ANSYS Mechanical code for structural analysis.

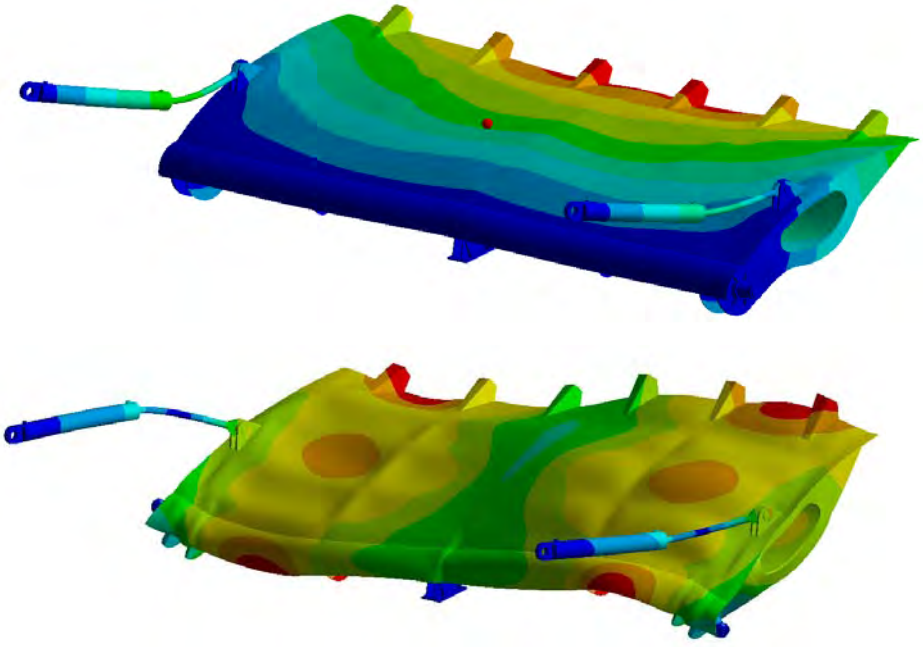

Fig. 2: First two eigenshapes for flap gate with operating rods on both sides – D and S shape

It is shown that applying all three approaches, i.e. in-situ measurements, laboratory experiments and numerical modeling, results in robust analysis which allows for solid assessment and practical recommendations for mitigation or elimination of the undesirable vibrations.

Reliability analysis and impact on service life assessment cannot be done without numerical model, as neither in-situ measurement nor laboratory model can provide sufficient information about the stress state in the whole gate body, joints and operating rods.

Laboratory model on the other hand allows for design recommendations related to the shape of the edge or position of the baffle blocks which would eliminate the vibrations without affecting the hydraulic characteristics of the spillway in undesirable way. The laboratory model can also serve other purposes such as confirmation of the effect of aeration or forces in lifting rods in different positions of the gate.

In-situ measurements serve for the calibration purpose in case of numerical models and verification in case of laboratory model. It provides for correct selection of the eigenshape and assessment of the impact of vibration to the adjacent areas in terms of excessive noise and vibration pollution.

Apart from design recommendations to adjustments on the real construction it is also usually possible to avoid the impact of vibrations by restricting the time of action in the handling manuals to the flap gate. Although such approach does eliminate the cause of vibrations it presents the least demanding and in Czech Republic the most often used way to minimize the negative impact of undesirable vibrations.

Acknowledgement

The financial support of the project No. VG20102014056 provided by the Ministry of the Interior of the Czech Republic is gratefully acknowledged.

References

International Commision of Large Dams – ICOLD (1996). Vibrations of hydraulic equipment for dams. *ICOLD Bulletin 102*

19th International Conference
ENGINEERING MECHANICS 2013
Svratka, Czech Republic, May 13 – 16, 2013

AEROELASTIC SENSITIVITY ANALYSIS OF AIRLINER WING

J. Čečrdle[*]; O. Vích [**]

Abstract: *This paper describes the airliner wing flutter sensitivity analysis. The sensitivity coefficients define the influence of the structural parameters changes to the structure eigenvalue and flutter stability characteristics. Evaluated structural parameters represent the possible changes of the structure due to the installation of the smart high-lift devices at the leading and trailing edge region. In general, we can suppose the increasing of the mass and mass moment of inertia around the elastic axis and decreasing of the stiffness. Described effects are ordinarily considered destabilizing regarding the flutter. The main aim of the presented work is to evaluate the impact of components to the stability and to define the most critical regions or parameters.*

Keywords: ***aeroelasticity, flutter, eigenvalue, sensitivity***

The submitted paper describes the airliner wing flutter sensitivity analysis. The sensitivity coefficients define the influence of the structural parameters changes to the flutter stability. Evaluated structural parameters represent the possible changes of the structure due to the installation of the smart high-lift devices at the leading and trailing edge region. In general, we can suppose the increasing of the mass and mass moment of inertia around the elastic axis and decreasing of the stiffness. Described effects are ordinarily considered destabilizing regarding the flutter. The main aim of the presented work is to evaluate the impact of components to the stability and to define the most critical regions or parameters.

Fig.1: Structural model

Firstly, the structural model of the wing / engine component (fig.1) was adjusted in order to match the target modal frequencies. Also the Guyan reduction (static condensation) in order to filter out local modes was performed. The aerodynamic model (fig.2) is based on the Doublett - Lattice panels, the nacelle is modeled by means of cross-surface scheme. The interpolation between both models was realized by means of the infinite surface splines. In order to identify the flutter behavior the standard flutter analysis was performed. The PK method was applied for the stability solution, 14 modes including the wing bending and torsional

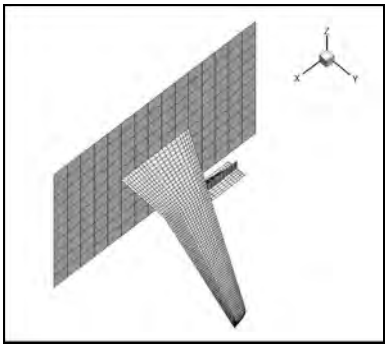

Fig.2: Aerodynamic model

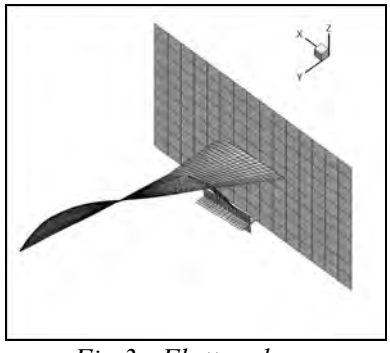

Fig.3: Flutter shape

* Ing. Jiří Čečrdle, Ph.D.: Výzkumný a zkušební letecký ústav a.s., Beranových 130; 199 05 Praha - Letňany; tel.: +420.225 115 123, fax: +420 283 920 018; e-mail: cecrdle@vzlu.cz
** Ing. Ondřej Vích: Výzkumný a zkušební letecký ústav a.s., Beranových 130; 199 05 Praha - Letňany; tel.: +420 225 115 123, fax: +420 283 920 018; e-mail: ondrej.vich@vzlu.cz

vibrations as well as the engine vibration modes were included. The structural damping was included via common value of the damping ratio of 1%. The density was considered $\rho = 1.225\ kg.m^{-3}$ (ISA value for $H = 0$ which is ordinarily considered as the most critical for the bending - torsional type of flutter). The analysis had a character of non-matched analysis for the fixed altitude. The reference Mach number ($M = 0$) for the whole range of velocities was used and the aerodynamic terms were given from this reference Mach number. Thus analysis velocities did not match the Mach number and the results have a character of artificial states. Such approach is frequently used in the flutter analysis, because it allows to evaluate the rate of reserve in the flutter stability with respect to the specific velocity (e.g. certification velocity). There was found the bending - torsional flutter state (fig.3) with the velocity of $V_{FL} = 400.04\ m.s^{-1}$; the flutter frequency was $f_{FL} = 13.87\ Hz$. The primary flutter mode was *1st wing torsion*, the main contributing modes were *1st and 3rd wing bending*.

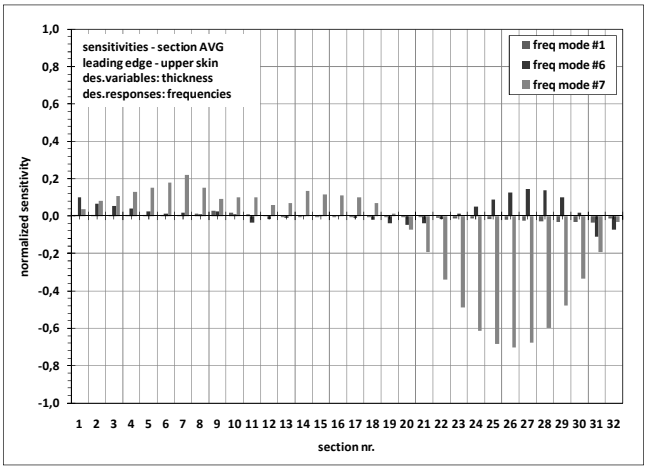

Fig.4: Eigenvalue response normalized sensitivities

The sensitivity coefficients were calculated with respect to the eigenvalue type of responses (natural frequencies of flutter contributing modes) and flutter type of response (decay rate for the flutter primary mode at a velocity of 420 $m.s^{-1}$ and average of decay rate within the evaluated velocity region). Eigenvalue response sensitivities are calculated by:

$$\frac{\partial \lambda_n}{\partial x_i} = \frac{\{\phi_n\}^T \left(\frac{\partial [K]}{\partial x_i} - \lambda_n \frac{\partial [M]}{\partial x_i} \right) \{\phi_n\}}{\{\phi_n\}^T [M] \{\phi_n\}} \qquad (1)$$

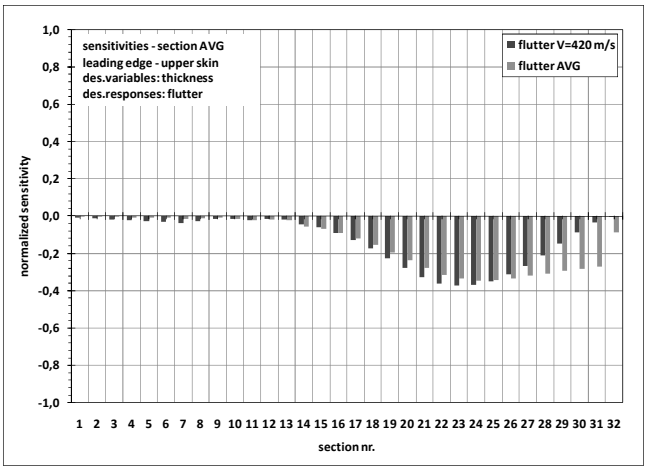

Fig.5: Flutter response normalized sensitivities

whereas flutter response sensitivities are given as rates of change of transient decay coefficient γ with respect to changes of the design variables. Flutter equation

$$\left[M_{hh} p^2 + \left(B_{hh} - \frac{1}{4} \rho \bar{c} V \frac{Q_{hh}^{\mathrm{Im}}}{k} \right) p + \left(K_{hh} - \frac{1}{2} \rho V^2 Q_{hh}^{\mathrm{Re}} \right) \right] \{u_h\} = 0 \qquad (2)$$

where $p = \omega(\gamma \pm j)$ is differentiated with respect to the design variables for the quantity $(\partial\gamma / \partial x_i)$.

There were used both stiffness and inertia characteristics of out-of wing box region as design variables. The fig. 4 and 5 shows the results. The fig.4 shows the normalized sensitivities of the leading edge upper skin thickness to the eigenvalue responses whereas fig.5 shows the sensitivities to the flutter responses. The inertia design variables have much higher sensitivities. As apparent from the fig.5, flutter sensitivities are negative at the leading edge region (increasing of the design variable have a stabilizing effect). The maximal destabilizing effect has the increasing of the mass at the trailing edge region around the spanwise section 23.

Climent, H. - Johnson, E.H. (1993) *Aeroelastic Optimization Using MSC/NASTRAN*, International Forum on Aeroelasticity and Structural Dynamics (IFASD), May 1993, Strasbourg, France

19th International Conference
ENGINEERING MECHANICS 2013
Svratka, Czech Republic, May 13 – 16, 2013

IMPACT OF SEISMIC EVENT ON RUPTURE PROBABILITY OF CIRCUMFERENTIALLY CRACKED LARGE-DIAMETER PIPING

K. Demjančuková[*], L. Pečínka[**]

Abstract: *Historically, the safety of nuclear power plants (NPPs) is based on the ability to eliminate the large loss-of-coolant accident (large LOCA) which is represented by the double ended guillotine break of the primary circuit piping. As a matter of experience with operation of many nuclear units, US NRC prepared the so- called redefinition of large LOCA which is based on the theory of transition break size (TBS). For the PWR (Pressurized Water Reactor) the TBS is characterized by the piping with diameter of 360 mm. The regulatory body has to prove that the postulated circumferential crack satisfies the requirements of ASME Code, Section XI. In the paper a numerical example will be presented.*

Keywords: ***Large LOCA, redefinition, transition break size, circumferential break.***

1. Introduction

When solving the problem of safety of nuclear power plants' (NPP's), a lot of various extreme effects and influences have to be involved. Even if these events are exceptional and highly improbable, they can induce unexpected impacts and vibrations and consecutively environmental, health and biological hazard and naturally a heavy economic loss.

The occurrence of these extreme effects on NPP's equipment and structures is expected with the probability less than 10^{-1}/year and more than 10^{-6} to 10^{-7}/year, i.e. the combination of unexpected events that do not eliminate each other, and decrease of NPP's system function, if the probability of appearance of such a combination is more than 10^{-6} to 10^{-7}/year. Selected combinations or separate extreme events determine the extreme cases essentials for NPP's projects.

Historically, the safety of NPPs is based on the ability to eliminate the large loss-of-coolant accident (large LOCA) which is represented by the double ended guillotine break of the primary circuit piping. The loss of coolant accident is one of the most limiting design-basis accidents that cause the loss of ability of the coolant to remove heat from the fuel. Even small losses of fluid (or loss of coolant flow) may have important consequences (US NRC, 2008).

2. Determining Seismic Risk Contributions

The goal of the analysis is to determine whether the risk associated with the direct, seismically induced failure of the primary reactor cooling piping (PLP) is significantly less than the failure risk caused by the expected loading histories considered in NUREG-1829. For any of the following three criteria satisfied at each analyzed location, the seismic risk of direct failure of PLP is considered negligible:

1. The critical flaw depths are greater than 30% of the through-wall thickness.
2. The critical flaw depths are greater than the ASME Code, Section IX, flaw acceptance criteria.
3. The ISI programs are sufficient for detecting flaws before reaching critical flaw depths calculated according to US NRC (2009), Section 2.2.2.4.2.

[*] Ing. Kateřina Demjančuková: Faculty of Mechanical Engineering, Unviersity of West Bohemia, Univerzitni 22; 306 14 Plzen; CZ, e-mail: demjanck@kke.zcu.cz

[**] Ing. Ladislav Pečínka, CSc.: UJV Rez, a. s., Hlavni 130; 250 68, Husinec – Řež, CZ, e-mail: pel@ujv.cz

3. Example Calculation

This example will be used to demonstrate the principle of numerical procedure. The individual steps are enumerated in the following text.

3.1. Determine seismic hazard curve coefficients

At the very beginning of the calculation we need to find the seismic hazard of the locality, which will be labeled as Step 1.

1. The seismic hazard curve is determined by the Weibull equation fit for peak ground acceleration (PGA) versus the probability of occurrence

$$P(x) = Scale.\alpha.\beta^{-\alpha}\, x^{\alpha-1}\, e^{-(\frac{x}{\beta})\alpha}, \qquad (1)$$

where parameters α and β are determined as a matter of geophysical research. The values depend on the given country and site.

3.2. Next steps

After having determined the seismic hazard the following steps have to be proceed:

2. Obtain SSE (safe shut-down earthquake) design PGA value.
3. Solve for PGA value at $1x10^{-6}$ probability of occurrence, and obtain ratio of PGA at $1x10^{-6}$ to PGA at SSE.
4. Determine the highest SSE stress location.
5. Determine the materials of interest at the critical localization.
6. Determine the pipe cross-sectional dimensions at critical location.
7. Determine normal operating conditions/stresses.
8. Determine strength values for materials of interest.
9. Determine the SSE stresses.
10. Determine the linearly scaled seismic stresses for the $1x10^{-6}$ seismic even.t
11. Apply seismic scaling factor for plant site to correct the linearly scaled stresses from Step 10 and add the normal operating conditions.
12. Apply nonlinear correction factor to the elastic N + $1x10^{-6}$ seismic stresses from Step 11 to obtain the nonlinear stress S_{NL}.
13. Determine the elastic-plastic correction factor (Z-factor) for the critical flaw size evaluation.
14. Determine EPFM-corrected stress S_{EC} for use in limit-load equations.
15. Determine the minimum critical surface flaw depth from limit-load equations.
16. Calculate the a/t value corresponding to ASME Service Level D loading.
17. Compare BE a/t value to the ASME Code a/t value from Step 16.

4. Conclusions

The so-called redefinition of large LOCA prepared by US NRC is based on the theory of transition break size (TBS). For the reactors of PWR type the TBS is characterized by the piping with diameter of 360 mm. In the paper a numerical example is presented to prove that the postulated circumferential crack satisfies the requirements of ASME Code, Section XI.

References

US NRC (2009) Plant-Specific Applicability of 10 CFR 50.46 Technical Basis. Washington, DC.

US NRC (2008) *Seismic Considerations For the Transition Break Size*. NUREG – 1903. Washington, DC.

US NRC (2008) *Estimating Loss-of-Coolant Accident (LOCA) Frequencies Through the Elicitation Process.* NUREG-1829. Washington, DC.

19th International Conference
ENGINEERING MECHANICS 2013
Svratka, Czech Republic, May 13 – 16, 2013

PROBLEMS OF FEM SIMULATION OF MAGNETORHEOLOGICAL CLUTCH'S MAGNETIC CIRCUIT

J. Dlugoš, J. Roupec, Z. Strecker, I. Mazůrek *

Abstract: *The article deals with Magnetostatic analysis of a magnetorheological (MR) clutch. The analysis is needed for acquiring information about magnetic saturation of iron parts in operation mode. This paper describes a comparison of FEM model and experimentally measured data in the clutch´s working gap filled with the air. The most important parameters such as use of linear and nonlinear material (iron parts, MR fluid), element type and size, effect of measuring groove for Hall sensor on magnetic field distribution, which significantly improved the FEM model of the simulation were determined, and they are also mentioned bellow. Simulation based on the verified FEM model of magnetic circuit with MR fluid was completed. Results showed places, where it is possible to reduce the material without any changes to the magnetic flux density in the working gap. With this knowledge, we reduced the weight by 13,2%.*

Keywords: ***magnetorheological clutch, MR clutch, FEM simulation, magnetic circuit***

1. Introduction

MR clutches are characterized by very good controllability of transmitted torque and very short reaction times. The biggest advantage over the conventional clutches lies in their X-by-wire handling without any need for a mechanism. There are two types of MR clutches - *disc shaped* and *bell shaped* clutch (Lampe *et al.*, 1998; Saito & Ikeda, 2007; Kielan *et al.*, 2011; Barber & Carlson, 2010). Main MR clutch's components are made of steel which shows significant nonlinearity in magnetic behavior represented by *B-H curve*. At some level any increase in the magnetic field strength will have little or no effect. This point, where the flux density reaches its limit, is called *magnetic saturation*. Our goal during reducing weight is to stay in the section of the B-H curve, where the input electrical current is used in the most effective way. This limitation, caused by the magnetic saturation, applies on MR fluids (MRF) as well. We have been investigating MR clutch with two rotor disks. Complete documentation of this MR clutch is made as a master's thesis (Nováček, 2011).

2. Methods and Procedures

First of all, the flux density in the measure groove had to be measured. Hall sensor *STD18-0404*; *F. W. Bell 5180 Gauss/Tesla meter* and DC power supply *Manson SDP2603* were used. Clutch was powered by constant current 1,5A and data were measured. Hall sensor's thickness 1mm is greater than the thickness of the working gap 0,5mm. Therefore, the 0,8mm measure groove has to be created. Hall sensor has air permeability. Therefore, sensor significantly affects magnetic field in the measure groove in MR clutch filled with the MRF (relative permeability 4-6). That's why initial FEA were run on models with the air working gap. Only after successful solution of these analyses, comparison of computed and measured data can be made. Complex information about magnetic field of MR clutch filled with MRF can be obtained only by FEA. With relatively accurate FEM model, we can simulate operation mode by solving FEA with working gap filled by *MRF Lord 140 CG*. Results of the analysis carry information about magnetic saturation in metallic components of MR clutch. Much higher magnetic flux density is expected. Only if some parts lie within the effective section of B-H curve, these components can by lightened. Next, design of MR clutch weight relief is verified by FEA. Only after simulation, reducing weight is actually done on existing MR clutch. At last, we measure the flux density in the air filled lightened clutch using Hall sensor and compare obtained data with FEA results.

* Faculty of mechanical Engineering, Brno University of Technology, Technická 2, 616 69, Brno, Czech Republic

3. Results

Groove's impact on the air filled working gap is shown in Fig. 1. Difference between FEA and measured data is 2%. The FEM model with MRF has much higher magnetic flux density than model with an air working gap (Fig. 2). The flux density limits weight reducing possibilities. The parts of our concern are the heaviest parts such as housing, stator and rotor disks. *Housing* reaches its magnetic saturation with MRF at the face areas, but the outer radius area has the magnetic flux density low enough to allow us to reduce 2mm of the diameter (Fig. 2a). FEA results and comparison with experimentally measured data (air filled MR clutch) are shown in Fig. 3. The magnetic flux density flows perpendicular to *the rotor and stator disks* and therefore reducing thickness of these parts has no effect. To prove this prediction, two rotor disks' thickness was reduced by 2mm. Results of FEA confirm premises.

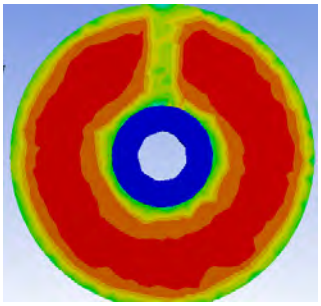

Fig. 1 Impact of measure groove on magnetic flux density

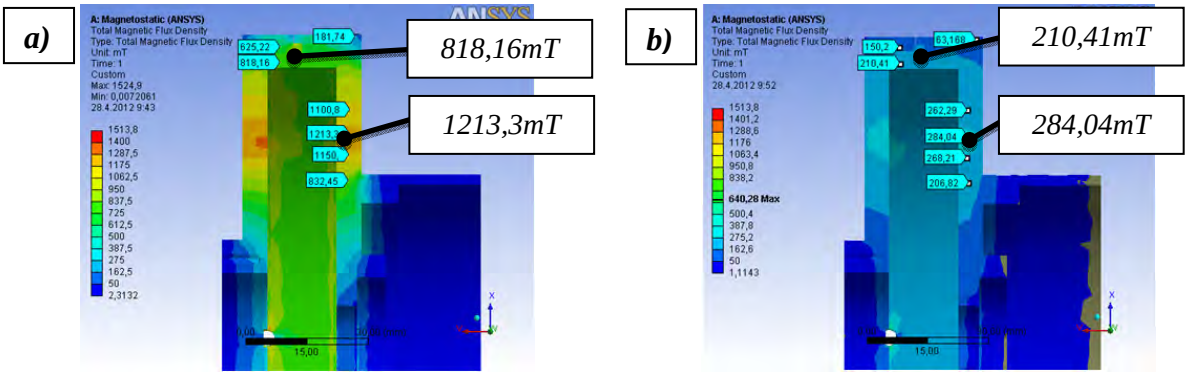

Fig. 2 Magnetic flux density in clutch filled by: a) MR fluid, b) an air

4. Conclusions

This work is focused on creating FEM model of constructed MR clutch (Nováček, 2011). Before FEA of MR clutch, only experimentally data measured in the groove with air were available. We had no information about course of magnetic flux density and saturation level inside iron components of clutch with MR fluid. FEA of MR clutch in operation mode (with MRF) led to reducing weight by 13.2% with minimal influence on the magnetic flux density in other parts. Thanks to this work, more MR clutch modifications can be based on knowledge of the computed magnetic circuit.

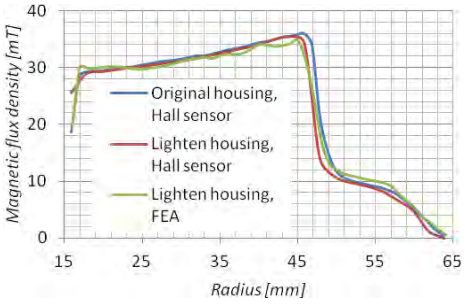

Fig. 3 Magnetic flux density in lighten housing clutch

Acknowledgement

This work was developed with the support of grants GAČR 13-31834P and CZ.1.07/2.3.00/30.0039.

References

Barber, D. E. & Carlson, J. D. (2010) Performance Characteristics of Prototype MR Engine Mounts Containing Glycol MR Fluids. *Journal of Intelligent Material Systems and Structures*; vol. 21, 15; pp.1509-1516.

Kielan, P., Kowol, P. & Pilch, Z. (2011) Conception of the electronic controlled magnetorheological clutch. R87. PRZEGLĄD ELEKTROTECHNICZNY (Electrical Review), pp. 93-95.

Lampe, D., Thess, A. & Dotzauer, C. (1998) MRF – Clutch – Design Considerations and Performance. Conference contribution ACTUATOR. Bremen. Germany.

Nováček, V. (2011) Konstrukce MR spojky, master's thesis, VUT Brno, Czech republic.

Saito, T. & Ikeda, H. (2007) Development of Normally Closed Type of Magnetorheological Clutch and its Application to Safe Torque Control System of Human-Collaborative Robot. *Journal of Intelligent Material Systems and Structures*, pp.1181-1185.

19th International Conference
ENGINEERING MECHANICS 2013
Svratka, Czech Republic, May 13 – 16, 2013

EXPERIMENTAL DETERMINATION OF POLYMER MATERIAL CHARACTERISTICS HAVING REGARD TO THE FEM COMPUTATIONAL ANALYSIS

M. Dobeš[*], J. Vrbka[**]

Abstract: *Unfilled polymer materials exhibit a high ductility, which is moreover located in small neck area. Material producers deliver usually the yield strain and break (ultimate) strain values calculated on the basis of material tensile tests for normalized active sample length. Application of so defined material characteristic in the case of Finite Element Method (FEM) analyses of real constructions made of TSCP (typical semi-crystal polymer) led to significantly conservative (smaller) values of limit (ultimate) loads compared with the measured ones. To obtain more precise results the material characteristics used should be in correlation with the size of finite elements. A special experimental method making use of high-speed camera has been developed to determine the strain in defined small area of local strain concentration (neck area) on the specimen during tensile test. The true stress-strain curve till the sample rupture is here calculated and break strain is determined. Application of more realistic (higher) break strain value by the FEM analyses of real TSCP constructions led to the much better agreement between the calculated and measured construction stiffness and limit (ultimate) load.*

Keywords: ***polymer, experiment, stress-strain curve, break strain, FEM analysis***

1. Introduction

The article deals with the problem to determine properly selected material characteristics of the unfilled polymer material, like semi-crystalline plastic (TSCP) with regard to the following FEM analysis of construction to be in better agreement with reality. Some material data (esp. break strain) obtained from TSCP material producer are not suitable for correct FEM analysis, because they were determined as average values for measured standard sample length of 50 mm. A method of experimental detection of real break strain ε_u in the neck area has been developed based on the extension measurement of the defined sample part during the tensile test.

2. Experimental detection of the real TSCP break (ultimate) strain used for FEM analysis

The break strain value delivered by TSCP material producer (Material characteristics of the TSCP) - ε_u = 0,30 does not correspond to the real break strain which occurs in the neck area and leads to the break of the construction made of this material. The FEM analysis of real constructions led to very conservative results (much smaller) especially for construction limit (ultimate) load and ultimate displacement.

The sample deformation during tensile test was recorded making use of the high-speed camera with sampling of 100 pictures/sec, see Fig. 1a. Time course of the sample deformation during the loading is illustrated in following Fig. 1b. The length of sample measured area (10 mm) corresponds to the neck size.

[*] Ing. Martin Dobeš: Institute of Solid Mechanics, Mechatronics and Biomechanics, Faculty of Mechanical Engineering, Brno University of Technology, Technická 2, 616 69 Brno, CZ, e-mail: martin.dobes@cz.bosch.com

[**] Prof. RNDr. Ing. Jan Vrbka, DrSc.: Institute of Solid Mechanics, Mechatronics and Biomechanics, Faculty of Mechanical Engineering, Brno University of Technology, Technická 2, 616 69 Brno, CZ, e-mail: vrbka@fme.vutbr.cz

Fig. 1: a) The measured system with fast-cam, b) The behavior of the tensile sample during by test

The sample part extension is determined with the help of stationary grid. For more exact measurement it is possible to apply some graphic software utilizing the movement monitoring of selected points on the sample surface and evaluating the displacement and strain during the loading process. The calculated engineering as well as true stress-strain curves are presented in Fig. 2 for measured sample part of standard length 50 mm (short curves) and length of 10mm, corresponding to the neck area (long curve).

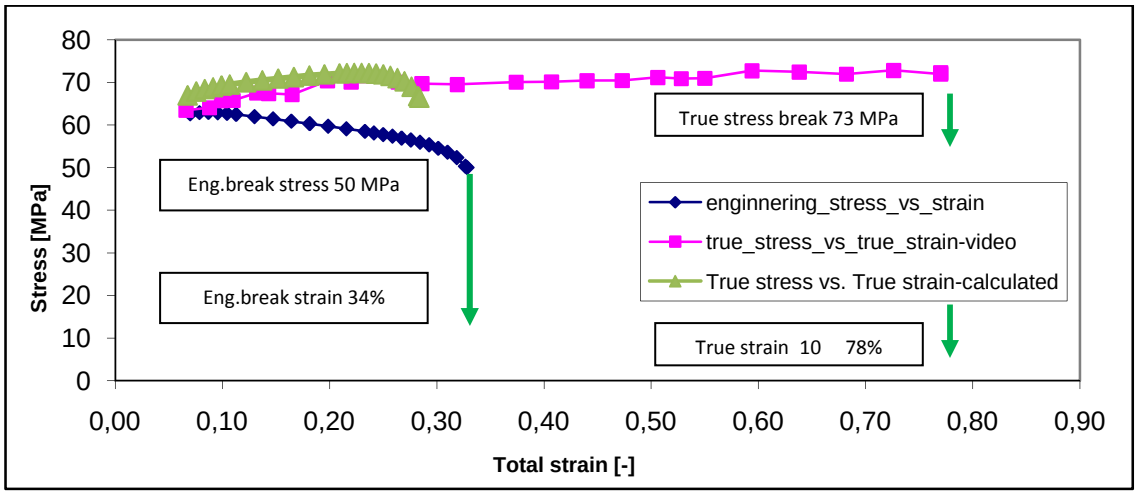

Fig. 2: Comparison of the stress-strain curves from experiment

3. Conclusion

In the article a new experimental method specially proposed for plastic materials has been presented to determine the strain in defined small area of local strain concentration (neck area) during the tensile test, making use of the high-speed camera deformation record. The true stress-strain curve till the sample rupture is then calculated and the break (ultimate) strain ε_u is determined. For investigated strain concentration area (neck area) of length 10 mm on the plastic material TSCP sample the calculated break (ultimate) strain ε_u was about 2,3 times higher than the data from material producer (0,78 versus 0,34 – see Fig.2). Application of the more realistic material values for FEM analysis of real hydraulic connectors made of TSCP material led to the much better agreement between calculated and measured limit loads and limit displacement values.

Acknowledgement

This study was supported by the grant project FSI-S-11-11/1190.

References

Material characteristics of the TSCP, http://www.basf.com/group/corporate/en/

Intern specification of Robert BOSCH s.r.o., *(Construction and design of the plastic parts)*

ANSYS 14.5-help (2012), http://www.ansys.com/Support/Documentation

Theory of the large deformation and strain, http://old.uk.fme.vutbr.cz/kestazeni/MKP/prednaska11_mkp.pdf

19th International Conference
ENGINEERING MECHANICS 2013
Svratka, Czech Republic, May 13 – 16, 2013

LOAD-BEARING CAPACITY OF MASONRY ARCH BRIDGES

M. Drahorád*

Abstract: *The paper is focused on development of new engineering method for determination of load-bearing capacity of buried masonry-arch bridges. This new method is based on assumptions of European standards.*

Keywords: ***Masonry arch bridges, load-bearing capacity.***

1. Introduction

Masonry arch bridges are one of the oldest kinds of bridges. There are many buried masonry arch bridges on the roads in the Czech Republic (estimate is 10.000 pcs.) and many of them are in a rather bad state. As the funds for bridge rehabilitation are limited nowadays, the correct evaluation of maximum service loading of such bridges gains in importance.

Only the European standards (or other consistent standards) should be used for structural check in present days. However, the European standards (EN 1996) do not define any method for assessment of arch structures like masonry arch bridges. Therefore, a new version of the corresponding Czech national standard ČSN 73 6213 was published recently. In this national standard the basic requirements for structural analysis and verification of masonry arch bridges are defined.

This work is focused on the development and verification of a "simple" and credible method for evaluation of the maximum service loading of buried masonry arch bridges. The method is based on the theory of materially non-linear beam.. For calculations of internal forces and determination of load-bearing capacity, a common spreadsheet program is used.

2. Structural model

2.1 Masonry arch

A beam model of unit width which assumes the non-linear material is used for structural analysis. The material (masonry) non-linearity is based on elimination of tensional stresses in the cross-section. In the compression zone, the linear distribution of stresses is assumed. The modulus of elasticity E of masonry is determined by tests or (in common cases) is based on experience.

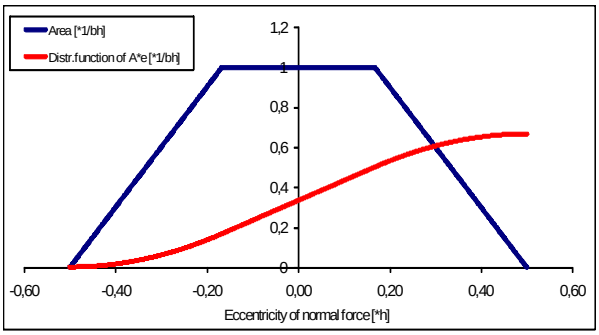

Fig. 1: The dependence of the cross-section area on the eccentricity of the normal force and the distribution function ƒA de

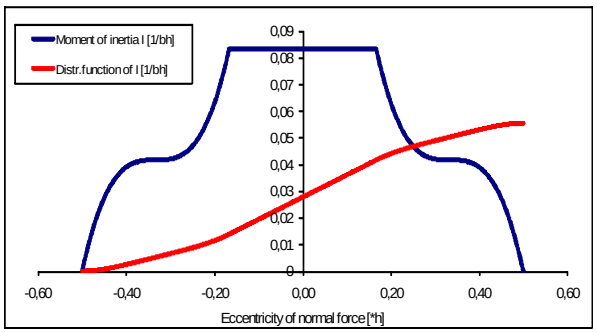

Fig. 2: The dependence of the moment of inertia on the eccentricity of the normal force and the distribution function ƒI de

* Ing. Michal Drahorád, Ph.D.: Faculty of Civil Engineering, Czech Technical University in Prague, Thákurova 7; 166 29 Praha 6; CZ; e-mail: michal.drahorad@fsv.cvut.cz

The compression and flexural stiffness (*EA* and *EI*) of the structure (masonry arch) is dependent on the eccentricity e = M/N of the normal force (see Fig.1 and Fig.2). Functions A(e) and I(e) are defined by three different formulas in each of the basic intervals of eccentricity.

In the structural model, the average values of stiffness *EA* and *EI* are used. The stiffness of the beam elements is calculated from the values of eccentricity in each step of the structural analysis. The average value of the cross-sectional area A_{av} of the beam of length L and variable eccentricity $e(x)$ is derived from formula (1).

$$A_{av} = \frac{\int_0^L A(L)\cdot dL}{L} = \frac{L\cdot \int_{e(0)}^{e(L)} A(e)\cdot de}{L\cdot |e(L)-e(0)|} = \frac{\int_{e(0)}^{e(L)} A(e)\cdot de}{|e(L)-e(0)|} \qquad (1)$$

For average value of the moment of inertia I_{av}, similar formula can be derived. The distribution functions shown in Fig.1 and Fig.2 are used for calculation of the average values A_{av} and I_{av} in case of general course of eccentricity e on the structural member (beam). Distribution functions $\int A$ and $\int I$ are composed of parts according to basic functions for A and I.

2.2 Backfill of the bridge

The backfill is not just a passive part of the structure and therefore its behavior can be divided into two basic parts. The effects of both the parts are related to unit width of the masonry arch. The first part represents the effect of dead load in vertical direction and traffic loading (in vertical and horizontal directions) and is independent on the deformation of arch. The second part represents the effect of earth pressure in the horizontal direction. This part is strongly dependent on pushing of the arch into the embankment and pre-consolidation (compaction) of the embankment material during construction. The embankment resistance may be expressed by known terms for earth pressure loading and its dependence on displacements of structure (see ČSN 73 0037).

3. Load-bearing capacity

Determination of the load-bearing capacity is composed of two basic tasks: finding the critical loading position of basic (unit) vehicle and finding the critical loading value (vehicle weight).

The position of critical loading depends on the loading (vehicle) arrangement and can be found by common linear analysis. The usual decisive criterion is achieving the maximum tensional stress in the critical cross-section.

The value of the critical loading is calculated by non-linear analysis in each limit state. The loading of the structure (in the critical position) is increased until one of the conditions defined by the European and national standards for the appropriate limit state is reached.

4. Conclusions

The new non-linear engineering method for load-bearing capacity determination according to the Europian standards was developed. Currently, the method is being verified in engineering practice.

Acknowledgement

The support of the Technology Agency of the Czech Republic, project No. TA03031099 is gratefully acknowledged.

References

Drahorád, M. & Hrdoušek, V. (2012) Stanovení zatížitelnosti zděných mostů v návaznosti na ČSN P 73 6213. *Seminář mostních inženýrů 2012*, pp.85-91

Foglar, M., Kristek, V. (2012) Centre-line optimisation of buried arch bridges. *Proceedings of the Institution of Civil Engineers: Bridge Engineering*, 165 (3), pp. 159-168.

19th International Conference
ENGINEERING MECHANICS 2013
Svratka, Czech Republic, May 13 – 16, 2013

SINGLE-OBJECTIVE SIZING AND TOPOLOGY OPTIMIZATION OF CABLED-TRUSSES USING GENETIC ALGORITHMS

V.C. Finotto [1], M. Valášek [2]

Summary: *This paper demonstrates the application of genetic algorithms to design cabled-truss structures with minimum weight. Optimized lightweight structures are determined through a discrete topology and sizing optimization process which is based on ground structure approach and genetic algorithms. Simulations are presented showing comparisons between obtained cabled-trusses with traditional truss benchmarks. In addition, simulation results highlight the potential benefits of using cables for improving truss structural performance.*

Keywords: ***Cabled-trusses, genetic algorithms, ground structure approach.***

1. Proposed Optimization framework

With the fast development of tension structures, tensile elements, such as, cables and membranes, have been combined with traditional structures to form efficient hybrid structures. Among tensile members, cables are the most used because tensile stresses are distributed uniformly over the cross-sectional areas of members and the material is thereby utilized in the most efficient manner. Due to their flexibility, cables have negligible bending stiffness and can develop tension only. Cabled-trusses, can be classified as a cabled structure and/or a truss-like structure. However, differently from most of the cabled structures, the stability of cabled-trusses relies on the triangular bar formations. In the optimization of cabled-trusses, pre-stressed elements can redistribute stresses along the structure and are dependent on initial strain (sizing) and the length and orientation of the element (topology). Therefore, an efficient way to achieve optimal design of cabled-trusses has to combine both sizing and topology optimization methods.

The presence of discrete variables in optimization problems has led to the successful application of stochastic search methods. In particular, genetic algorithms (GA) have grown in popularity (Richardson et al., 2012). GAs are stochastic adaptive methods that can be used for searching and optimization problems. As schematized in Fig. 1, the proposed optimization framework starts with a set of initial inputs, such as the number and length of the chromosomes, the crossover and mutation rates, the number of generations and, in the particular case of this work, the binary representation scheme. Subsequently, an initial uniformly distributed random binary population is generated.

The objective function is then evaluated by the NFEM procedure described in (Finotto and Valášek, 2012) to produce the vector of objective values. The proposed optimization framework

[1] MSc. Vitor Finotto Cores, CTU in Prague, Faculty of Mechanical Engineering, Department of Mechanics, Biomechanics and Mechatronics, Technická 4, 166 29 Prague, Czech Republic, e-mail: VitorCores.Finotto@fs.cvut.cz
[2] Prof. Michael Valášek, DrSc.,CTU in Prague, Faculty of Mechanical Engineering, Department of Mechanics, Biomechanics and Mechatronics, T echnická 4, 166 29 Prague, Czech Republic, e-mail: valasek@fsik.cvut.cz

was used as a single-objective method for the optimization cabled-truss structures. Examples comprise ground structures with 15 and 66 elements.

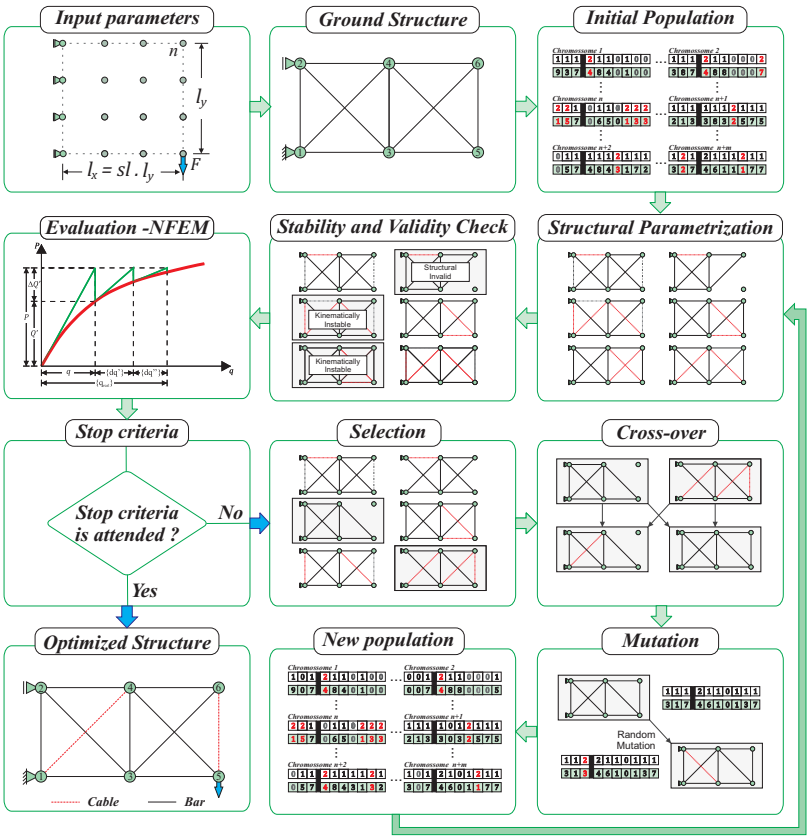

Fig. 1: Cabled-truss optimization based on genetic algorithm.

2. Conclusions

In this work, a single objective optimization framework for discrete topology and sizing optimization of cabled-trusses was presented. The proposed system successfully combined ground structure approach, nonlinear finite element analysis and genetic algorithm. The comparison between optimized trusses and cabled-truss structures shows that optimized cabled-trusses had a significant improvement over trusses in the minimization of the structural mass.

3. Acknowledgment

Our thanks to the research project GACR 101/08/H068.

4. References

Richardson, J.N., Adriaenssens, S., Bouillard, P., Coelho, R.F.. Multiobjective topology optimization of truss structures with kinematic stability repair. Structural and Multidisciplinary Optimization 2012;46:513–532.

Finotto, V.C., Valášek, M.. Discrete topology optimization of planar cable-truss structures based on genetic algorithms. In: Naprstek, J., Fischer, C., editors. Proceedings Engineering Mechanics 2012. Prague: ITAM AS CR, v.v.i.; 2012, p. 245 – 254.

19th International Conference
ENGINEERING MECHANICS 2013
Svratka, Czech Republic, May 13 – 16, 2013

EXPERIMENTAL VERIFICATION OF RESONANCE BEHAVIOUR OF A DAMPED SPHERICAL PENDULUM

C. Fischer, S. Pospíšil, J. Náprstek [1]

Summary: *Theoretical, experimental and numerical analysis of a spherical pendulum is carried out. The stability of the response in a vertical plane is analysed in the theoretically predicted resonance region. Mathematical model respects the non-linear character of the pendulum and allows to introduce asymmetrical damping. Experimental pendulum is hanging from the Cardan joint and placed to carriage. Uni-directional harmonic excitation is applied to the system. The pendulum is damped by two magnetic units. These units are able to reproduce linear viscous damping independently in both principal response components. Response in in-plane and out-of-plane directions is measured and analyzed.*

Keywords: ***non-linear vibration, experimental verification, viscose damping, spherical pendulum, autoparametric system***

1. Introduction

Many civil engineering structures are equipped by tuned mass dampers (TMDs). In case of tall structures the typical TMD has a form of a heavy pendulum placed close to the top of the structure. Such devices are very popular for their reliability and simple maintenance. Dynamic behaviour of such a substructure is however significantly more complex than it is supposed by widely used simple linear single degree-of-freedom (SDOF) models working in a vertical plane only. Moreover, the typical installation differs significantly of the idealized planar model of a pendulum. The bob can be suspended on chains, sometimes from several hinges. Damping of the bob is usually realized by installing oil dampers in certain directions only. The presented theoretical and experimental models comprise such properties up to certain level.

The presented work is an extension of the article which has been published by the authors recently (Fischer et al., 2012) with the focus put upon the experimental verification of the influence of uneven damping in individual directions on the overall stability. Movement of the pendulum is described analytically using the approach introduced in previous works, the derived equations are treated analytically and numerically.

The problem is examined using a specially developed experimental rig. It contains pendulum suspended at a Cardan joint which is excited by an uni-directional harmonic movement. The response components are measured by the rotation sensors. The key parameter, damping, can be adjusted for each response component by means of two independent magnetic units attached to the frame and to the supporting axes of rotation. These units are able to reproduce the linear viscous damping.

[1] RNDr. Cyril Fischer, Ph.D., doc. ing. Stanislav Pospíšil, Ph.D., Ing. Jiří Náprstek, DrSc., Institute of Theoretical and Applied Mechanics, Prosecká 76, 190 00 Prague 9, tel. +420 286 88 21 21, e-mail FischerC@itam.cas.cz

2. Experimental results and discussion

Length of the experimental pendulum is 0.41 m, its fundamental eigenfrequency was measured as $f_0 = 0.76$ Hz. Base of the pendulum was forced to move harmonically direction ξ. Response of the pendulum was measured for excitation frequencies ranging from $f_l = 0.7$ Hz to $f_u = 1.1$ Hz with increments $\Delta f = 0.01$ Hz. Each sweep was started for excitation frequency $f_e = 0.78$ Hz and a small initial disturbance was given to the bob. Then was the excitation frequency gradually changed in small increments up or down to cover the whole frequency range. Each frequency was kept constant for three minutes.

Figure 1 summarizes the maximal amplitudes of the measured response in both directions and for individual configurations of damping coefficients β_ξ and β_ζ. It is clear from the left figure that the maximal in-plane response ξ depends mainly on the value β_ξ and influence of β_ζ is negligible. On the other hand, maximal amplitude of the out-of-plane motion depends on both damping coefficients approximately equally.

3. Conclusions

The results of the experimental and numerical investigation have exhibited a good agreement. It has been shown, that initiation of the spatial response is more sensitive to damping in the in-plane direction (β_ξ). The maximal amplitude of the in-plane response exhibits almost no sensitivity to value of the out-of-plane damping (β_ζ). Increasing of the both components β_ξ and β_ζ shorten the resonance interval and diminish the maximal amplitude of the out-of-plane component of the response.

4. Acknowledgment

The kind support of the Czech Scientific Foundation No. 103/09/0094, Grant Agency of the ASCR No. A200710902 as well as the support of RVO 68378297 are gratefully acknowledged.

5. References

Fischer, C., Náprstek, J., Pospíšil (2012) Resonance behaviour of spherical pendulum – influence of damping. *Engineering Mechanics 2012*, Náprstek and Fischer (eds), ITAM AS CR, v.v.i., Prague, pp. 255–261

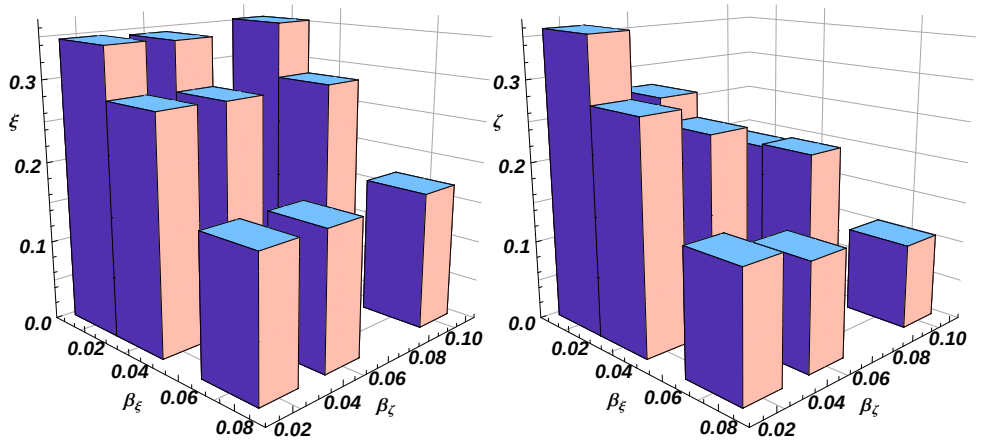

Figure 1: The maximal amplitude of the measured response in in-plane (ξ, left) and out-of-plane (ζ, right) direction for various damping coefficients β_ξ and β_ζ.

19th International Conference
ENGINEERING MECHANICS 2013
Svratka, Czech Republic, May 13 – 16, 2013

THE INFLUENCE OF THE BRIDGE STRUCTURAL ARRANGEMENT ON THE DISTRIBUTION OF THE NOISE IMPACT INDUCED BY TRAFFIC

M. Foglar*, J. Göringer**

Abstract: *Many articles and papers about mitigating the impacts of the transport infrastructure on the environment have pointed out that one of the factors influencing the usage of underbridges for mammal migration is the noise induced by traffic. However, this phenomenon has not yet been properly investigated and verified. This paper describes the influence of the structural arrangement of bridges on the noise induced by traffic. The findings come from noise measurements on several structures on the D1 motorway and the R35 expressway in the Czech Republic.*

Keywords: ***bridge, expansion joint, traffic noise, noise measurement***

Many articles and papers about mitigating the impacts of the transport infrastructure on the environment have pointed out that one of the factors influencing the usage of underbridges for mammal migration is the noise induced by traffic. However, this phenomenon has not yet been properly investigated and verified. To verify this assumption, a noise measurement program was designed and undertaken on highway bridges on selected sections of the D1 motorway and the R35 expressway in the Czech Republic. Simultaneous measurements were made of the noise level and of the use of the bridges for mammal migration. The noise measurements were carried out in summer 2010 and summer 2011. Special attention was paid to the influence of expansion joints and bearings on the noise impact caused by heavy traffic entering the bridge.

For the reasons suggested above, the measurements must be designed in such a way that they produce data both on the noise level in the vicinity of the underbridge and on the impact of the noise below and/or close to the bridge. The arrangement of the noise measurements is explained in Figure 1.

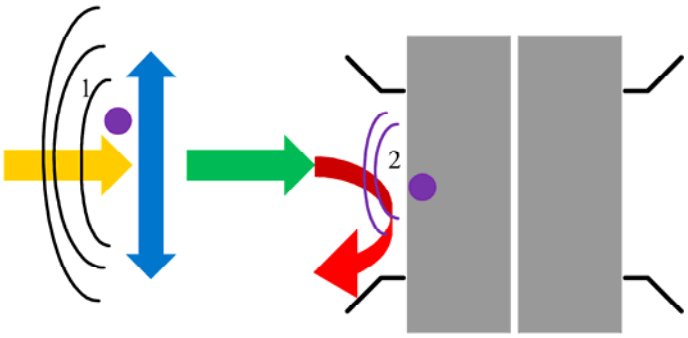

Fig. 1 – The measurement arrangement scheme

The noise measurements were limited to the newly opened part of the D1 motorway (sections D4704 and D4705) and the connecting expressway R35, so that the results would not be influenced by the effect of material deterioration of the bridges themselves and of their expansion joints, see Figure 2.

* Ing. Marek Foglar, Ph.D.: Faculty of Civil Engineering, Czech Technical University in Prague, Thakurova 7; 166 29, Prague; CZ, e-mail: marek.foglar@fsv.cvut.cz

** Ing. Jakub Göringer: Faculty of Civil Engineering, Czech Technical University in Prague, Thakurova 7; 166 29, Prague; CZ, e-mail: jakub.goringer@fsv.cvut.cz

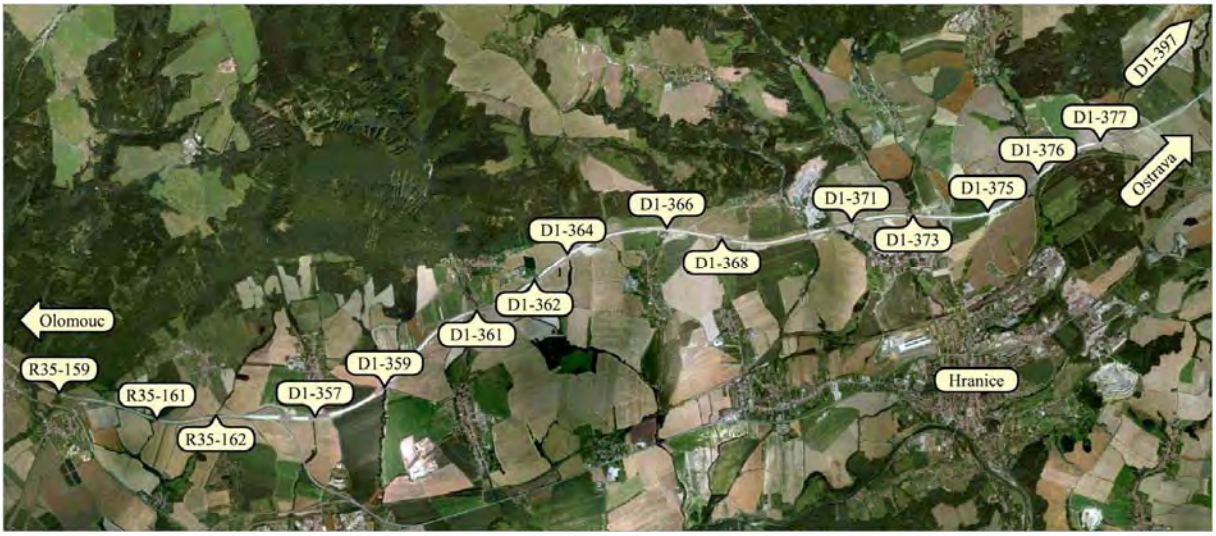

Fig. 2 – Location of the measurement sites

The bridges on the studied section of the motorway were divided into groups (families) according to the length and the number of spans, the position of the bridge (underbridge as a part of the motorway, overbridge crossing the motorway) and the structural arrangement.

Fig. 3 presents the average traffic noise frequency distribution for the different families of bridges, together with the common traffic noise spectrum.

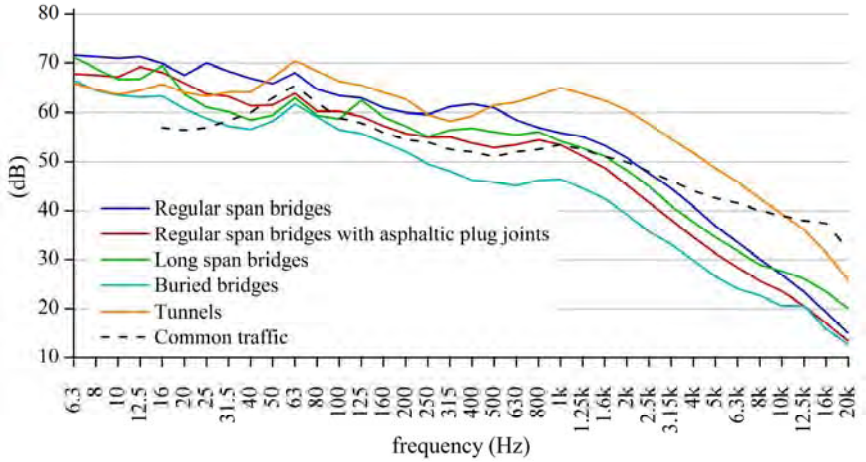

Fig. 3 – The average traffic noise frequency distribution for different families of bridges

The lowest noise levels were observed for buried structures. Long span bridges experienced smaller noise levels than regular span bridges. Structures with less free height above the terrain and an expansion gap experience higher noise impact than structures with more free height.

The noise levels for bridges with no expansion gap (buried structures, structures with a subsurface of asphaltic plug joints) are lower than for structures with an expansion gap (modular expansion joints, strip seal expansion joints). The presence of an expansion gap increases the noise level by up to 12dB.

The measurements show that the most favourable structural arrangement of underbridges for mammal migration are buried bridges and structures without surface expansion joints.

Acknowledgement

Financial support from Technology Agency of the Czech Republic grant project No. TA03031099 is gratefully acknowledged.

References

Foglar, M. & Göringer, J. (2012) Vliv konstrukčního řešení mostu na šíření hluku od dopravy (in Czech), *Silnice železnice*. 7, 4, pp. 73-84.

19th International Conference
ENGINEERING MECHANICS 2013
Svratka, Czech Republic, May 13 – 16, 2013

BASIN BOUNDARIES OF PLANE MODEL OF IMPACTING COIN

P. Frantík, M. Štafa [1]

Summary: *The paper is focused on numerical plane model of a rigid coin with rectangular cross-section impacting to an elastic foundation.*

1. Introduction

Behavior of a rigid object repeatedly impacting to a surface of an elastic body is strongly dependent on properties of the contact and could present chaotic motion, e.g. see Peterka and Tondl (2002). There are several phenomena influencing direction and size of contact forces between the object and the body: Resistance of the surface against penetration of a shape, energy dissipation due to elastic properties of the body and friction between contact surfaces.

In this paper we will concentrate on a problem, which can be interpreted as a typical cylindrical coin restrained to move only in a plane with three degrees of freedom such as the cut by the plane will be a rectangle.

2. Model

The coin of diameter $d = 2$ cm, thickness $t = 2$ mm, weight $m = 3.14$ g, moment of inertia $I = 7.06 \cdot 10^{-8}$ kg m^2, is assumed as a rigid rectangle moving in the plane as shown on fig. 1. Its state is represented by three coordinates x, y, φ and their velocities v_x, v_y, v_φ.

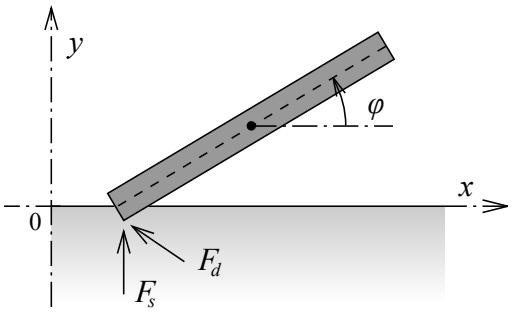

Obrázek 1: Model of a coin

The coin is moving in gravity of size $g = 9.81$ m s^{-2}. The contact between the coin and the body is reduced on the penetration of corner points. Each corner point is loaded by contact force F composed of two forces: statical component F_s and damping component F_d acting only if

[1] Ing. Petr Frantík, Ph.D., Ing. Michal Štafa, Institute of Structural Mechanics, Faculty of Civil Engineering, Brno University of Technology, Veveří 331/95, 602 00 Brno, e-mail: kitnarf@centrum.cz

the corner is under the body surface. The statical component is considered simply as reaction of linear Winkler foundation.

Each simulation starts with specific initial conditions and is terminated after two seconds of the motion of the coin. The values of initial conditions are taken from ranges which ensures that after two seconds a stable state will be achieved. On fig. 2 two simulation results are shown. One for typical solution where the coin lay at the end (on the left) and second where the coin stands (on the right).

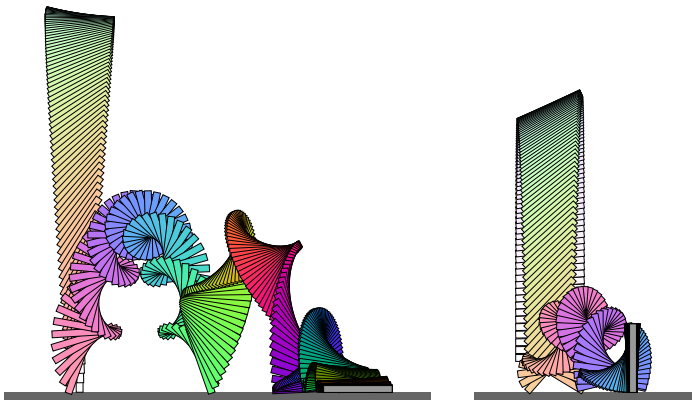

Obrázek 2: Phases of two simulations; the colors are darker as time runs out

The coin has six initial conditions: $x_0, y_0, \varphi_0, v_{x0}, v_{y0}, v_{\varphi 0}$. For the basin boundaries the initial horizontal position x_0 is obviously irrelevant. Fig. 3 enlarges an expressive area from which the coin stands. Initial conditions from this area leads to seven $\pi/2$ rotations as shown on fig. 2 on right side.

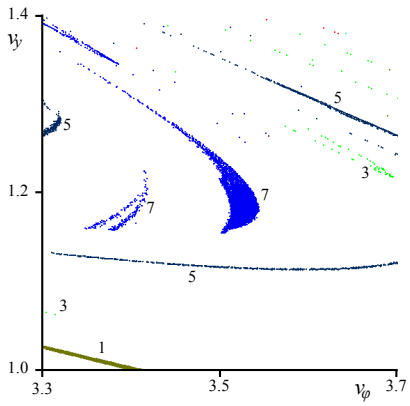

Obrázek 3: Basins where the coin stands

3. Acknowledgment

This outcome has been achieved with the financial support of the project No. FAST-S-12-34.

4. Reference

Peterka, F., Tondl, A. 2002: Subharmonic motions of the oscillator with soft impacts, national conference *Engineering mechanics 2002* Svratka, Czech republic.

19th International Conference
ENGINEERING MECHANICS 2013
Svratka, Czech Republic, May 13 – 16, 2013

SPAN-WISE DISTRIBUTION OF LOSSES IN PRISMATIC TURBINE CASCADE

J. Fürst[1], M. Luxa[2], D. Šimurda[2]

Summary: *The paper deals with the experimental and numerical research of flows through prismatic turbine cascade in transonic regimes. The primary goal is to evaluate the influence of the non-uniformity of the inlet velocity profile to the span-wise distribution of energy losses. The numerical simulation with inlet velocity profile corresponding to the parameters of the flow in high speed wind tunnel in Nový Knín is compared to the experimental data. Next, the simulation assuming different inlet velocity profiles are used to evaluate the effect of the boundary layer in front of the cascade to the span-wise distribution of energy losses.*

1. Introduction

The flow through a turbine cascade is influenced by the interaction with end walls. The secondary flows comming from the development of the end-wall boundary layers cause an aditional losses which affects the overall performance of the turbine cascade. The problem of secondary flows is discussed in the literature, for a review see Lampart (2009a), Sieverding (1985). The complex flow structure of the secondary flows leads to non-trivial distribution of energy losses past the turbine blades. The pitch-averaged loss distribution posses usually a local maxima at certain distance from the end-walls. Moreover, the non-uniformity of the flow field causes also the changes in the exit flow angle.

The effects of blade geometry and some flow parameters on the losses in subsonic axial turbines were investigated e.g. in Lampart (2009b). In the case of flows with supersonic exit velocities one has to account for the additional 3D effects originating form the interaction of the shock waves with the non-uniform flow field in the vicinity of end-walls.

Present contribution is focused on the secondary flow structure and the distribution of energy losses and flow angles in the transonic turbine blade cascade SE1050. The flow fields are calculated for different inlet velocity profiles and the effect of the inlet boundary layer thickness is discussed.

2. Test Blade Cascade

The turbine cascade SE1050 is a freely available test case for transonic flows in turbomachinery Kozel and Příhoda (2004). 8 blades with aspect ratio (blade length/chord) were mounted in the

[1] Doc. Ing. Jiří Fürst, PhD.: Fac. of Mech. Eng., Czech Technical University in Prague, Karlovo nám. 13; 121 35, Prague; CZ, e-mail: Jiri.Furst@fs.cvut.cz
[2] Ing. Martin Luxa, PhD., Ing. David Šimurda, PhD.: Institute of Thermomechanics AS CR, v. v. i., Dolejškova 1402/5, 182 00 Praha 8; CZ, e-mail: luxa@it.cas.cz

high speed wind tunnel and detailed pneumatic measurements of the outlet flow field parameters were carried out. The inlet velocity profiles caused by the long inlet channel were measured by the special shaped Pitot probe. The measurements were carried out for transonic regime characterized by outlet Mach numbers $M_{2i} = 1.2$ and Reynolds number $Re = 1.5 \cdot 10^6$.

3. Numerical Simulations

Numerical solution of both cases was obtained using finite volume method in segregated formulation, Ferziger and Peric (1999). The in-house modification of `rhoSimpleFoam` from freely available software package `OpenFOAM` was used to solve the system of time averaged Navier-Stokes equations for compressible gas completed with the two-equation $k - \omega$ SST turbulence model, Menter (1994).

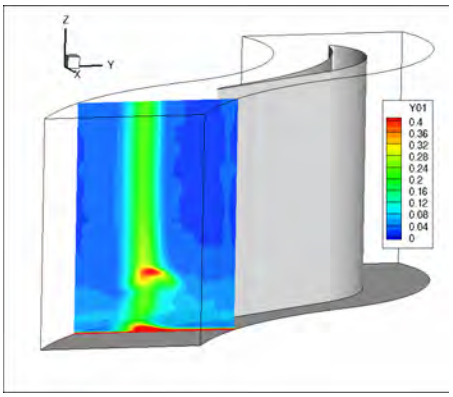

Figure 1: The numerically predicted total pressure loss ($M_{2i} = 1.2$).

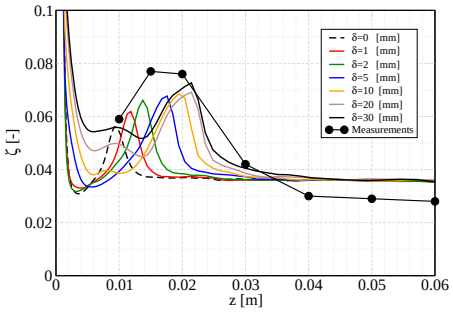

Figure 2: The span-wise distribution of loss coefficent ζ, ($M_{2i} = 1.2$).

4. Acknowledgment

The work was supported by the Grant no. P101/10/1329 of the Grant Agency of Czech Republic.

References

Ferziger, J. H. and M. Peric (1999). *Computational Methods for Fluid Dynamics*. Springer.

Kozel, K. and J. Příhoda (2004). *ERCOFTAC QNET-CFD*. URL: `http://qnet-ercoftac.cfms.org.uk/w/index.php/Silver:AC_6-12_Description`.

Lampart, P. (2009a). "Investigation of Endwall Flows and Losses in Axial Turbines. Part I. Formation of Endwall Flows and Losses". In: *J. of Theoretical and Applied Mechanics* 47.2, pp. 321–342.

– (2009b). "Investigation of Endwall Flows and Losses in Axial Turbines. Part II. The Effect of Geometrical and Flow Parameters". In: *J. of Theoretical and Applied Mechanics* 47.4, pp. 829–853.

Menter, F. R. (1994). "Two-Equation Eddy-Viscosity Turbulence Models for Engeenering Applications". In: *AIAA J.* 8.32, pp. 1598–1605.

Sieverding, C. H. (1985). "Recent Progress in the Understanding of Basic Aspects of Secondary Flows in Turbine Blade Passages". In: *ASME J. Turbomach.* 107, pp. 249–257.

19th International Conference
ENGINEERING MECHANICS 2013
Svratka, Czech Republic, May 13 – 16, 2013

INFLUENCE OF THE LONG TERM EXPOSURE TO AGGRESSIVE ENVIRONMENT ON THE FATIGUE PERFORMANCE OF CONCRETE SPECIMENS

J. Göringer*, M. Foglar**

Abstract: *High stress ranges caused by cyclic loading can result into accelerated crack propagation, higher deflection, structural stiffness reduction and consequently into fatigue failure. Aggressive environment (soluble salts, acids etc.) causes a different kind of deterioration. Agents contained in the aggressive environment penetrate into the structure of concrete and reduce its matrix stiffness. The combination of these effects occurs e.g at bridges in urban environment or at crane tracks in chemical plants and leads to higher long-term structural damage. This paper presents outcomes of a long-term experimental program focused on the fatigue performance of reinforced concrete specimens stored in aggressive environment. The specimens are stored in an acidic lotion for more than 5 years.*

Keywords: ***Fatigue, aggressive environment, concrete, deterioration, deflection.***

1. Introduction

Fatigue can be defined as a process of permanent progressive changes in the structure of material subjected to cyclic loading. Strain development due to fatigue loading was already examined. But the effect of fatigue performance on concrete degradation has not been properly quantified yet. The most material models of concrete consider the characteristics of an undamaged material (strength, elastic modulus). The interaction between cyclic loading and the effects of aggressive environment cause deteriorative processes and leads to faster element deterioration and subsequently into its failure.

This paper presents experimental investigation of performance of reinforced concrete specimens exposed to cyclic loading and aggressive environment.

2. Experimental program

Several reinforced concrete specimens were made for the experimental program. The C25/30-X0 strength class of concrete was chosen; the low grade of resistance against the influence of environment was intentionally chosen to increase the effect of the aggressive environment. The dimensions of the specimens are 300x150x1300 mm. Specimens are designed as over-reinforced, thus failure by compressive-zone crushing should occur and the fatigue failure of concrete is assumed.

Firstly, a solution of sodium chloride (*NaCl*) with concentration of 5% corresponding to de-icing salts used for winter maintenance of roads was chosen. To obtain faster deterioration of specimens, the saline lotion was later substituted by hydrochloric acid solution (*HCl*) with pH = 4. Two reference specimens were made. The first specimen stored in dry condition, the second one was placed in water from the day it was cast and during the rest periods.

The arrangement of the cyclic loading is four-point bending with mid-span length 1000 mm and overhangs with the length of 150 mm. Total loading force of 80 or 100 kN was applied in frequency of 5 Hz.

* Ing. Jakub Göringer: Faculty of Civil Engineering, Czech Technical University in Prague, Thakurova 7; 166 29, Prague; CZ, e-mail: jakub.goringer@fsv.cvut.cz

** Ing. Marek Foglar, Ph.D.: Faculty of Civil Engineering, Czech Technical University in Prague, Thakurova 7; 166 29, Prague; CZ, e-mail: marek.foglar@fsv.cvut.cz

Two types of deflection measurement were conducted during the cyclic loading. The first type was static deflection measurement which took place each hour of the cyclic loading (circa 18000 load cycles). The fatigue testing was stopped during the measurement. The second type was dynamic deflection measurement which was carried out during the fatigue testing at least once between two static deflection measurements.

3. Results and discussion

The first four specimens were evaluated. Dry specimen (n_1 = 600 thousand cycles, age 29 days), wet specimen (n_2 = 200 thousand cycles, age 61 days), specimen in saline lotion (n_3 = 400 thousand cycles, age 383 day) and specimen stored in saline lotion and subsequently in acidic solution (n_4 = 250 thousand cycles, age 564 days).

The procedure of evaluation of measured data sets based on fatigue damage function was developed. The results of the experiments can be seen in Fig. 1. Deflections of the dry specimen show bigger scatter of measured values. Also the "healing" effect of the rest periods seems to be higher. This fact can be attributed to decreased shear resistance of the bond between aggregate and the cement paste in wet specimens.

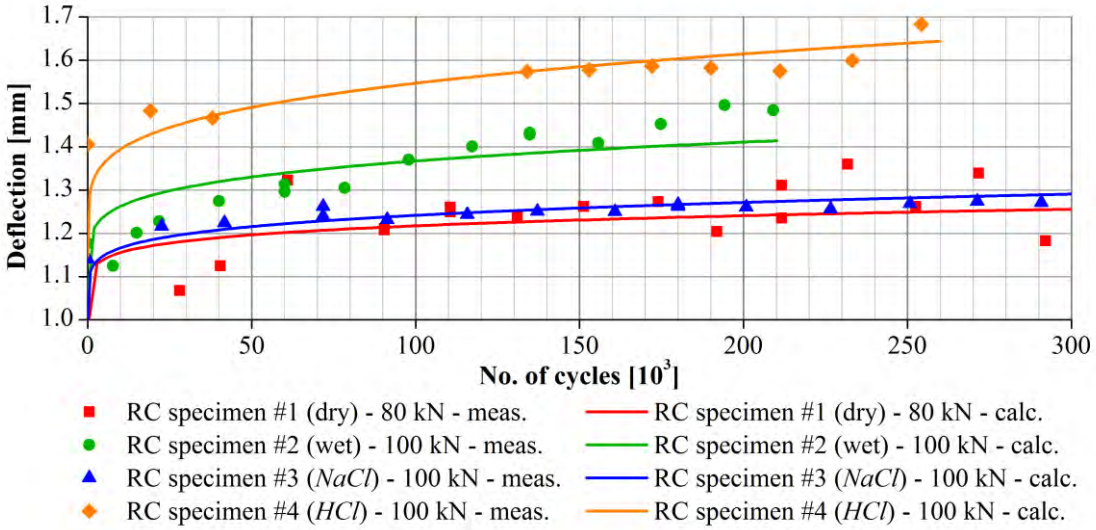

Fig. 1: Measured and calculated deflections of evaluated specimens

When comparing specimens stored in saline lotion and in water it can be observed, that specimen no. 3 show smaller deflection than specimen no. 2. This fact can be attributed to time-dependent increase of compressive strength and elastic modulus with low-rate deteriorative effect of the saline lotion. For specimen stored in acidic solution (no. 4) the increase of the deflections is significant.

4. Conclusion

This paper described long-term experimental programme focused on interaction between aggressive environment and cyclic loading. With regard to the type of examined specimens the influence of material deterioration on deflection and "healing" effect was evaluated.

Acknowledgement

The financial support of the Czech Technical University grant project no. 13/035/OHK1/1T/11, and Czech Science Foundation project no. 13-30441S is gratefully acknowledged.

19th International Conference
ENGINEERING MECHANICS 2013
Svratka, Czech Republic, May 13 – 16, 2013

STRUCTURAL ANALYSIS OF THE TALLEST PURE-BRICK TOWER IN THE WORLD

Ardeshir Guran*

Abstract: *The present paper sets out to study Kavus tower from a structural engineering point of view. To that end we use the finite element method of structural analysis to replace the real building to a discretized physical model. Then, the physical model was replaced by a mathematical model using constitutive equations, properties of material, and loading conditions. Results of static analysis under snow loading and free vibrations of the tower are presented.*

Keywords: ***Retrofit, Finite element analysis, Modal analysis, Static analysis.***

1. History

Kavus tower was built in 1006 AD on the orders of the Ziyarid Amir Shams ol-Ma'āli Kavus.It is located 3 km north of the ancient city of Jorjan (Gorgan), from where the Ziyarid dynasty ruled surrounding Tabarestan. The tower is over 1000 years old (Guran, 2012).

The baked-brick-built tower is an enormous decagon building with a conic roof, which forms the golden ratio 1.618. The interiors contain the earliest examples of Muqarnas decorative styles. The decagon with its 3 meter-thick wall, divided into 10 sides, has a diameter of 17 m. It has a cross section of a ten pointed star, and look like a buttressed brick spaceship.

The tower is so remarkably well preserved that one can scarcely believe it is more than 1000 years old. It is designed to last for ever, and gave Kavus, the ruler of surronding Tabarestan, six years to marvel at his creation before an assassin put him in it permanently. Indeed, not so permanently, actually. His glass coffin, which originally hung from the tower's dome, vanished long ago. Although, it was made to be a tomb tower there is nothing to see inside. Nevertheless, the tower is still the tallest pure-brick tower in the world.

Fig. 1: A photo of Kavus tower

Fig. 2: A photo of Gonbad-e Qābus City

* Professor, Technical University of Munich (Germany), Director, Institute of Structronic, 275 Slater Street, 9th Floor,Ottawa, Canada. Corresponding Author, ardeshir.guran@mcgill.ca

2. SolidWorks. finite element modeling, and structural analysis of the tower

Figure 3 and 4 shows the result of static analysis using Ansys software.

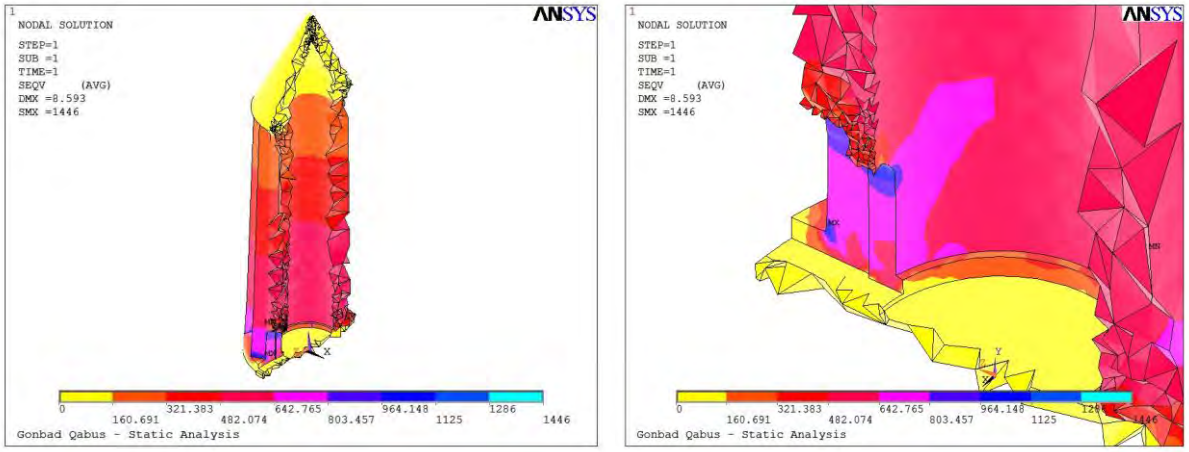

Fig 3: Finite element discretisation of the tower and static analysis under self-weight

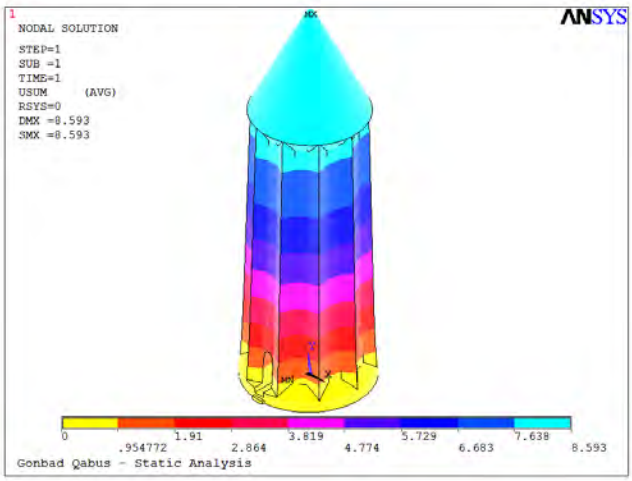

Fig 4: Total displacements under weight and one meter snow

Modal analysis of the tower was performed using ansys. The frequencies of eight modes are given respectively: 1.2852, 1.3005, 4.3229, 5.1819, 5.2085, 6.1596, 10.746, 10.873. Also various mode shapes including bending, torsional, axial and breathing are identified and reported.

3. Conclusions

The In this project we are looking into world's tallest pure-brick tower: Gonbad-e Kavus (Iran) from a structural point of view. It is our hope that the finite element method of structural mechanics can help in the better understanding of design and possibly the preservation of this magnificent monument.

References

Guran, A., (2012) Computational mechanics and modal analysis of Radkan tower (Iran), 28th conference on COMPUTATIONAL MECHANICS, November 12 – 14, 2012, pp. 1-2 , Špičák Czech Republic

19th International Conference
ENGINEERING MECHANICS 2013
Svratka, Czech Republic, May 13 – 16, 2013

NUMERICAL SIMULATION OF TRANSONIC FLOW OF CONDENSING STEAM

J. Halama, J. Fořt [1]

Abstract: *The paper is aimed at a modeling of transonic flow of steam with pressure and temperature range corresponding to conditions in steam turbines. The flow model is based on the model published in (Šejna and Lain, 1994). A possibility of droplet size spectra reconstruction is discussed. Numerical results are compared to experimental data measured for nozzle flow.*

Keywords: ***Wet steam, nucleation, droplet size distribution, condensation***

1. Introduction

Steam during expansion in turbine usually goes from dry to wet region. The condensation of initially dry steam starts later, when the steam temperature decreases sufficiently below the saturation temperature, i.e. it has to be modeled as the non-equilibrium process. The condensation phenomena should not be neglected in the simulations of flow in turbines, since condensation reduces thermal efficiency of turbine, it changes significantly shock wave structure in the transonic flow field and it can initiate pressure pulsations.

Numerical simulations of condensing steam flow started three decades ago, the first simulations (Bakhtar and Tochai Mohammadi, 1980), (Moheban and Young, 1984) were based on the solution of flow field in the Eulerian frame (fixed grid) and condensation was simulated as one-dimensional problem along streamlines in the Lagrangian frame. Recent works are based mainly on full Eulerian approach, i.e. all transport equations for mass, momentum and energy of the mixture and the supplementary transport equations for the parameters of the liquid phase are solved on fixed grid. Some works are based on the mono-dispersed mixture model e.g. (Dykas, 2001) or (Gerber and Kermani, 2004), another, e.g. (Šejna and Lain, 1994) or (Mousavi et al, 2006) use models based on the method of moments (Hill, 1966), which is able to approximate the polydispersity of mixture.

Presented flow model is based on the model published in (Šejna and Lain, 1994). The model is based on the transport equations for mass, momentum and energy of the mixture, mass fraction of liquid phase and three moments for liquid phase. Mass exchange between vapor and liquid is due to homogeneous nucleation and droplet growth. The paper presents two different models of droplet growth. The first one (AVG-P model) is based on the average size of droplet only, the second one (DSDF-P model) is based on the apriori given droplet size distribution function, which is reconstructed from the moments. Numerical method has to cover

[1] Ing. Jan Halama, Ph.D., Prof. Ing. Jaroslav Fořt, CSc., Department of Technical Mathematics, Faculty of Mechanical Engineering, Czech Technical University Prague, Karlovo nám. 13, CZ-12135 Praha 2, Czech Republic, tel. +420-224357549, e-mail Jan.Halama@fs.cvut.cz

very different time scales of convection, nucleation and droplet growth, it is therefore based on the splitting method (Strang, 1968). The paper contains comparison of numerical results obtained by both flow models for the case of flow of condensing steam in the Barschdorff nozzle (Barschdorff, 1971). Details about droplet spectra structure are discussed.

2. Conclusions

Presented results show, that the DSDF-P model could be a good option for more detailed modeling of droplet size spectra. The results also show, that one has to be very careful with the computation of average size of droplet. The original model AVG-P has the average size of droplets nearly independent on definition, it means that AVG-P model yields nearly monodispersed mixture. The average size of droplet for the DSDF-P model strongly depends on the used definition.

Acknowledgment

The support of grants GA ČR 101/11/1593 is gratefully acknowledged.

3. References

Bakhtar, F. & Tochai Mohammadi, M.T. 1980: An investigation of two-dimensional flow of nucleating and wet steam by the time-marching method. *Int. J. Heat Fluid Flow* 2, 5–18

Barschdorff, D. 1971: Verlauf der zustandgroesen und gasdynamische zuammenhaenge der spontanen kondensation reinen wasserdampfes in lavaldüsen. *Forsch. Ing.-Wes.* 37(5)

Dykas, S. 2001: Numerical calculation of the steam condensing flow. *Task Quarterly* 4, 519–535

Gerber, A.G. & Kermani, M.J. 2004: A pressure based eulerian–eulerian multi-phase model for non-equilibrium condensation in transonic steam flow. *International Journal of Heat and Mass Transfer* 47, 2217–2231

Hill, P.G. 1966: Condensation of water vapor during supersonic expansion in nozzles. *Journal of Fluid Mechanics* 3, 593–620

Moheban, M. & Young, J.B. 1984: A time-marching method for the calculation of blade-to-blade non-equilibrium wet steam flows in turbine cascades. *IMechE conference on computational methods in turbomachinery* paper C76/84, 89–99

Mousavi, A. & Gerber, A.G. & Kermani, M.J. 2006: Representing polydispersed droplet behavior in nucleating steam flow with the quadrature - method - of - moments. *2006 ASME Joint U.S.-European Fluids Engineering Summer Meeting*

Šejna, M. & Lain, J. 1994: Numerical modelling of wet steam flow with homogenous condensation on unstructured triangular meshes. *Journal ZAMM* 74(5), 375–378

Strang, G. 1968: On the construction and comparison of difference schemes. *SIAM Journal of Numerical Analysis* 5, 506–517

Wroblewski, W. & Dykas, S. & Chmielniak, T. 2012: Models for water steam condensing flows. *Archives of Thermodynamics* 33(1), 67–86

19th International Conference
ENGINEERING MECHANICS 2013
Svratka, Czech Republic, May 13 – 16, 2013

NUMERICAL MODELING OF GROUNDWATER FLOW IN RANDOM MATERIALS

J. Havelka, A. Kučerová, J. Sýkora [1]

Summary: *The prediction of groundwater flow is strongly influenced by the soil permeability generally varying within the space. Determination of the spatial distribution of the permeability is, however, unfeasible and thus the relevant uncertainties should be taken into account. One possibility is to describe the soil permeability by a random field. The present contribution is devoted to propagation of these uncertainties in permeability into probabilistic description of groundwater flow.*

This paper is focused on the modeling of uncertainties in material properties and investigates the influence of such uncertainties on groundwater flow, described by a steady-state diffusion equation. As a simple example, consider the following (deterministic) elliptic partial differential equation (PDE) for the hydraulic head $u(x)$:

$$-\nabla \cdot (\kappa(x)\nabla u(x)) = f(x), \qquad x \in D, \tag{1}$$

$$u(x) = g(x), \qquad x \in \partial D, \tag{2}$$

where $\kappa(x)$ is the soil permeability (hydraulic conductivity), $f(x)$ is a given source or sink inside the region D ($D \subset \mathbb{R}^2$) and $g(x)$ are prescribed flows and hydraulic heads on the boundary ∂D.

Consider now a system involving material variability. If the input parameter is defined as a random field, the system would be governed by a set of stochastic partial differential equations (SPDE) and the corresponding responses would also be random vectors of nodal displacements, see (Keese and Matthies, 2005; Kučerová and Sýkora, 2013). Let us formulate this for the soil permeability $\kappa(x)$. A random model is obtained by defining $\kappa(x)$ for each $x \in D$ as a random variable $\kappa(x) : \Omega \to \mathbb{R}$ on a suitable probability space $(\Omega, \mathscr{S}, \mathbb{P})$. As a consequence, $\kappa : D \times \Omega \to \mathbb{R}$ is a random field, where any elementary event $\omega \in \Omega$ gives a realization $\kappa(\cdot, \omega) : D \to \mathbb{R}$ of the soil permeability. Alternatively, $\kappa(x, \omega)$ can be seen as a collection of real-valued random variables indexed by $x \in D$, see (Keese and Matthies, 2005; Keese, 2004; Eiermann et al., 2007). Introduction of random system parameters into Eqs. (1) and (2) we obtain the stochastic partial differential equation:

$$-\nabla \cdot (\kappa(x,\omega)\nabla u(x,\omega)) = f(x,\omega), \qquad x \in D, \tag{3}$$

$$u(x,\omega) = g(x,\omega), \qquad x \in \partial D. \tag{4}$$

[1] Bc. Jan Havelka, Ing. Anna Kučerová, Ph.D., Ing. Jan Sýkora, Ph.D., Faculty of Civil Engineering, Czech Technical University in Prague, Thákurova 7/2077, 166 29 Prague 6, tel. +420 224 35 53 26, e-mail jan.havelka.1@fsv.cvut.cz, anicka@cml.fsv.cvut.cz, jan.sykora.1@fsv.cvut.cz

In order to solve this stochastic partial differential equation and obtain the approximate responses of the system, Monte Carlo (MC) method is usually used. The effort of performing Monte Carlo simulations is high, and hence alternative techniques have been developed, such as the spectral stochastic finite element method (SSFEM). The interested reader is referred to (Keese and Matthies, 2005; Kučerová et al., 2012; Chen and Soares, 2008) for further information.

Acknowledgment

This outcome has been achieved with the financial support of the Czech Science Foundation, project No. 105/11/0411 and 105/12/1146, and Grant Agency of the Czech Technical University in Prague, grant No. SGS OHK1-042/13.

1. References

Chen, N.Z. & Soares, C.G. 2008: Spectral stochastic finite element analysis for laminated composite plates. *Computer Methods in Applied Mechanics and Engineering*, vol. 197, 4830–4839

Eiermann, M. & Ernst, O.G. & Ullmann, E. 2008: Computational aspects of the stochastic finite element method. *Computing and Visualization in Science*, vol. 10, 3–15

Keese, A. & Matthies, H.G. 2005: Hierarchical parallelisation for the solution of stochastic finite element equations. *Computers and Structures*, vol. 83, 1033–1047

Keese, A. 2004: *Numerical Solution of Systems with Stochastic Uncertainties.* PhD thesis, TU Braunschweig.

Kučerová, A. & Sýkora, J. & Rosić, B. & Matthies, H.G. 2012: Acceleration of uncertainty updating in the description of transport processes in heterogeneous materials. *Journal of Computational and Applied Mathematics*, vol. 236, 4862–4872

Kučerová, A. & Sýkora, J. 2013: Uncertainty updating in the description of coupled heat and moisture transport in heterogeneous materials. *Journal of Computational and Applied Mathematics*, vol. 219, 7252-7261

Lombardo, M. & Zeman, J. & Šejnoha, M. & Falsone, G. 2010: Stochastic modeling of chaotic masonry via mesostructural characterization. *International Journal for Multiscale Computational Engineering*, vol. 7, 171–185

19th International Conference
ENGINEERING MECHANICS 2013
Svratka, Czech Republic, May 13 – 16, 2013

EFFECT OF SOFTENING FUNCTION TYPE IN THE DOUBLE-*K* FRACTURE MODEL FOR THE EVALUATION OF FRACTURE TESTS ON CONCRETE SPECIMENS WITH AND WITHOUT POLYPROPYLENE FIBRES

I. Havlíková[*], H. Šimonová[**], T. Pail[***], E. Navrátilová[****], R. V. Majtánová[*****], Z. Keršner[******]

Abstract: *Cement-based composites are traditionally a commonly used material in civil engineering structures. The basic representative of this type of material is concrete, a quasi-brittle composite in which crack resistance can be achieved by the addition of fibres. The double-K fracture model can be used to calculate the fracture-mechanical parameter values of structural concrete with and without polypropylene fibres. This model combines the concept of cohesive forces acting on the crack length with a criterion based on the stress intensity factor, using a 'softening function' to determine the cohesive part of fracture toughness. In this paper, authors determine the effect of the type of this softening function on the evaluation of fracture tests performed on sets of concrete specimens with and without polypropylene fibres.*

Keywords: ***Double-K fracture model, softening function, concrete, polypropylene fibre, fracture test.***

1. Introduction

Concrete is a commonly used building material. Its range of applications can be extended using various additives, e.g. polypropylene fibres. Even relatively small volume quantities of these fibres in concrete mixture (1–3 %) can affect the resistance of the composite to crack propagation.

In the study of properties of existing or newly developed cement-based composites the fracture parameters (fracture toughness, fracture energy, tensile strength etc.) have to be quantified. The determination of these parameters is based on standardized fracture experiments on specimens with stress concentrators (typically the three-point bending test, performed on notched beams). Subsequently, the results of these experiments in the form of diagrams showing load versus crack mouth opening displacement are evaluated using one of the many fracture models.

In this paper, the double-*K* fracture model is used. This model can determine the critical crack tip opening displacement and the fracture toughness and is capable of describing levels of crack propagation: an initiation part, which corresponds to the beginning of stable crack growth (at the level where the stress intensity factor, K_{Ic}^{ini}, is reached), and a part featuring unstable crack propagation (after the unstable fracture toughness, K_{Ic}^{un}, has been reached).

An evaluation of three-point bending tests using the double-*K* fracture model is presented in the full paper, with a principal focus on the effect of softening function type in this model: linear, bilinear, and two exponential variants by Reinhardt (exp_R) and Karihaloo (exp_K). Four concretes were made: *OB_REF*, *OB_ FF*19, *OB_FF*38 and *OB_FF*54. The reference mixture (*OB_REF*) was made

[*] Ing. Ivana Havlíková: Brno University of Technology, Faculty of Civil Engineering, Institute of Structural Mechanics, Veveří 331/95; 602 00, Brno; CZ, e-mail: havlikova.i@fce.vutbr.cz

[**] Ing. Hana Šimonová: ditto; e-mail: simonova.h@fce.vutbr.cz

[***] Ing. Tomáš Pail: ditto; e-mail: pail.t@fce.vutbr.cz

[****] Ing. Eva Navrátilová: ditto, Institute of Chemistry; e-mail: navratilova.e@fce.vutbr.cz

[*****] Romana Viktória Majtánová: ditto, Institute of Structural Mechanics; e-mail: majtanovar@study.fce.vutbr.cz

[******] Prof. Ing. Zbyněk Keršner, PhD.: ditto; e-mail: kersner.z@fce.vutbr.cz

without fibres, while the mixtures *OB_FF*19, *OB_FF*38 and *OB_FF*54 included FORTA FERRO polypropylene fibres of 19 mm, 38 mm and 54 mm in length, respectively.

2. Results

The relative mean values of selected material properties (compressive strength, modulus of elasticity, effective crack elongation, and unstable fracture toughness) are introduced in Tab. 1: the 100% value for each material parameter represents the values of those parameters for the reference concrete without fibres *OB_REF*. Relative mean values of ratio K_{Ic}^{ini}/K_{Ic}^{un} are introduced in Tab. 2; 100% represents: (i) the value of ratio K_{Ic}^{ini}/K_{Ic}^{un} for the linear softening curve for the appropriate concrete, (ii) the value of ratio K_{Ic}^{ini}/K_{Ic}^{un} for the reference concrete *OB_REF* for each type of softening curve.

Tab. 1: Relative mean values of selected material parameters in %.

	Concrete			
Parameter	***OB_REF***	***OB_FF*19**	***OB_FF*38**	***OB_FF*54**
f_c	100.0	95.3	78.1	83.4
E	100.0	53.5	57.6	43.1
$a_c - a_0$	100.0	114.4	134.6	117.0
K_{Ic}^{un}	100.0	102.6	107.5	97.4

Tab. 2: Relative mean values of ratio K_{Ic}^{ini}/K_{Ic}^{un} in %.

	Concrete			
Softening function	***OB_REF***	***OB_FF*19**	***OB_FF*38**	***OB_FF*54**
linear	100.0 | 100.0	100.0 | 98.8	100.0 | 106.9	100.0 | 103.3
bilinear	112.0 | 100.0	127.4 | 112.3	127.3 | 121.5	130.3 | 120.2
exp_R	126.6 | 100.0	142.1 | 110.9	140.1 | 118.4	142.7 | 116.4
exp_K	117.6 | 100.0	131.5 | 110.4	130.4 | 118.6	132.9 | 116.7

3. Conclusions

The presence of polypropylene fibres in the composite caused a reduction in the compressive strength values of 5 to 22 percent, and modulus of elasticity values were reduced by 46 to 57 percent. The largest reduction in compressive strength values was exhibited by concrete *OB_FF*38; in the case of elasticity modulus it was composite *OB_FF*54 that showed the largest fall. The effective crack elongation values of composites with fibres were from 14 to 35 percent higher in comparison with the reference concrete, the largest being in the case of concrete *OB_FF*38. The presence of fibres had no significant effect on the unstable fracture toughness values (composite *OB_FF*38 showed the largest relative increase, which was of less than 8 percent). In terms of resistance to stable crack propagation the addition of fibers appears to be a positive step – the highest relative increase in this resistance (over 20 percent) was reported by *OB_FF*38 concrete.

Using the selected softening curve has a significant effect on the determination of the resistance against stable crack growth for all investigated composites. Compared to a linear softening function, using a bilinear softening function leads to an increase in resistance of 12 to 30 percent, Karihaloo's exponential softening curve produced an increase of about 18 to 33 percent, and the highest increase was seen for Reinhardt's exponential softening curve: it was about 27 to 43 percent.

Acknowledgement

This outcome has been achieved with the financial support of the specific research programme at Brno University of Technology, project No. FAST-J-13-2078. The authors greatly thank Dr. Jaromír Laník for providing the results of fracture tests and Ing. Jan Bedáň for providing supports for special calculations; both are members of the Faculty of Civil Engineering at Brno University of Technology.

19th International Conference
ENGINEERING MECHANICS 2013
Svratka, Czech Republic, May 13 – 16, 2013

EXPERIMENTAL INVESTIGATION OF AIR PRESSURE, ACOUSTIC CHARACTERISTICS AND VIBRATIONS OF VOCAL FOLDS ON A COMPLEX PHYSICAL MODEL OF PHONATION IN HUMANS

J. Horáček[*], V. Radolf[*], V. Bula[*], J. Veselý[*], A. M. Laukkanen[**]

Abstract: *The contribution aims to provide material that can be used in development of more realistic physical as well as theoretical models of voice production. The experimental set-up, methodology and the results of measurement of airflow rate, subglottal, oral and generated acoustic air pressures are presented together with the simultaneously measured flow-induced vibrations of a vocal folds replica, made of soft silicon rubber, and recorded by a high speed camera. The data were measured during a 'soft' phonation just above the phonation onset, given by the phonation threshold airflow rate, and during a 'normal' phonation for the airflow rate of about three times higher. A model of the human vocal tract in the position for production of vowel [u:] was used and the flow resistance was raised by phonating into a glass resonance tube either in the air or having the other end of the tube submerged under water, and by phonating into a narrow straw. The results for the pressures presented in time and frequency domain are comparable with the physiological ranges and limits measured in humans for ordinary phonation and for production of vocal exercises used in voice therapy.*

Keywords: ***Biomechanics of voice; subglottal, oral and transglottal pressure; flow resistance***

1. Introduction

Phonation under higher than normal supraglottic impedance is used in voice training and therapy (see e.g. Titze et al., 2002). This contribution compares *in vitro* measurements of phonation on [u:], phonation into a resonance tube and into a narrow straw for a 'normal' phonation and a 'soft' phonation at the phonation onset. The flow resistance of the vocal tract was furthermore increased by phonation through the tube into water making the phonation more difficult due to loading the human phonation system by the hydrodynamic pressure and bubbling.

2. Method

The measurements were carried out with silicon vocal folds replica and with a simplified Plexiglas vocal tract model for which the area cross-sections along its length corresponded to a male vocal tract during phonation on vowel [u:]. The vocal tract was prolonged by a tube or straw, and also tube phonation into water having the other end submerged down to 10 cm below the water surface was studied. Tubes made of glass, e.g., like used here: 27 cm in length, inner diameter 6.8 mm, have been used in Scandinavia for voice training and therapy, similarly like a plastic stirring straw (12.7 cm in length, inner diameter 2.5 mm) considered by Titze et al. (2002). The first set of measurements was performed for a 'normal' sustained phonation at the fixed airflow rate Q=0.4 l/s, and the second set at the phonation threshold defined by the airflow rate measured at a time instant when the flow somehow gradually decreased until the phonation ended. The sound pressure level (*SPL*) inside the model of oral cavity was measured using the B&K special microphone probe designed for measurement of acoustic pressure in small cavities, and the mean oral pressure (P_{oral}) was measured by the digital manometer connected with the oral cavity by a small compliant tube. Generated acoustic signal outside the vocal tract model was recorded using a microphone (B&K sound level meter) installed at a distance of 20 cm from the lips. The recordings were made using 32.8 kHz sampling frequency by the PC controlled measurement system B&K PULSE 10 and synchronized with the high speed camera. The mean (P_{sub}) and peak-to-peak subglottal pressures were measured by special dynamic semiconductor pressure transducers. The fundamental vibration frequencies *F0* of the vocal folds and the formant frequencies (acoustic resonances of the vocal tract) were evaluated from the spectra of the pressure signals.

[*] Ing. Jaromír Horáček, DrSc., Ing. Vojtěch Radolf, PhD., Ing. Vítězslav Bula: Institute of Thermomechanics, Academy of Sciences of the Czech Republic, Dolejškova 5, 182 00 Prague 8; e-mail: jaromirh@it.cas.cz, radolf@it.cas.cz, bula@it.cas.cz

[**] Prof. Anne-Maria Laukkanen: Speech and Voice Research Laboratory, School of Education, University of Tampere, FIN-33014, *Tampere,* Finland; e-mail: anne-maria.laukkanen@uta.fi

3. Results

The flow resistance (P_{sub}/Q) increases with the tube and straw compared to vowel phonation in „normal“ and ‘soft’ phonation, as expected, being higher for tube in air and even more in water, and the highest for straw. Similar tendency was found for the pressures P_{oral} and P_{sub}, especially for ‘normal’ phonation. However, completely different results were obtained for the transglottal pressure. In ‘normal’ phonation it stayed nearly a constant in all cases studied. In ‘soft’ phonation it decreased when flow resistance offered by the tube or straw increased, being lowest for straw. Fundamental frequency *F0* was between 170 and 200 Hz in all cases. The time variation amplitude of the subglottal pressure was comparable in both types of phonation: the smallest for [u:] and the highest for tube phonation into water. A same tendency was found for peak-to-peak variations of the transglottal pressure and of the maximum glottal width, measured at the midpoint of the glottis. The *SPL* values measured outside the vocal tract varied between 60-75 dB for ‘soft’ phonation and between 75-85 dB for ‘normal’ phonation. The *SPL* values measured inside the oral cavity were substantially higher in all cases with the prolonged vocal tract compared to vowel [u:]. In phonation into water a considerably high acoustic energy was generated by bubbling, whose dominant frequency in the spectrum varied between 16-19 Hz in ‘soft’ phonation and increased up to 40 Hz in ‘normal’ phonation.

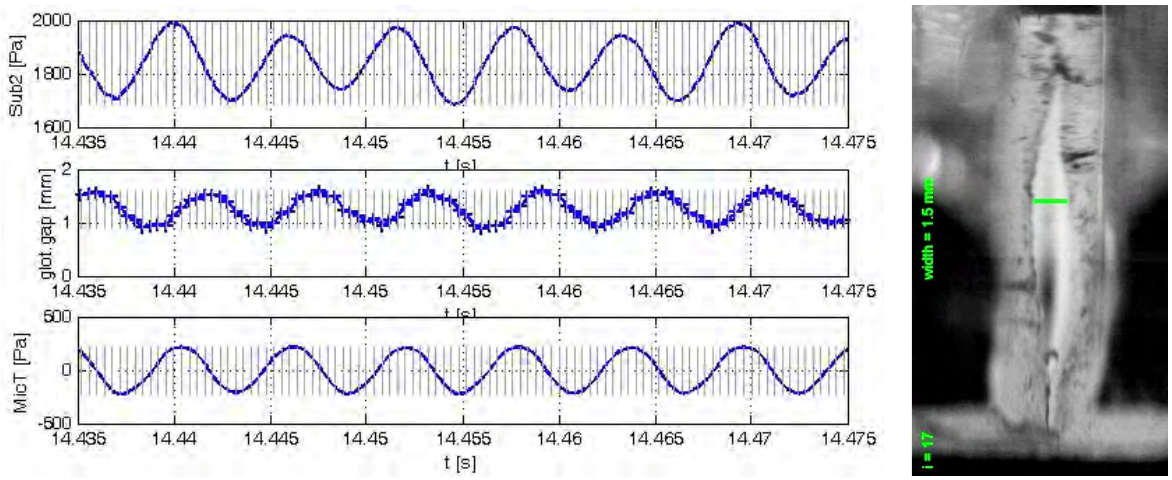

Fig. 1: Example of the measured signals for subglottal pressure (upper panel), glottis opening (middle panel) and oral pressure (lower panel) and the image of vibrating vocal folds at the phase of maximum glottis opening. The maximum glottis opening is delayed after the subglottal pressure whereas between the subglottal and oral pressure there is only a very small phase shift. (‘soft’ phonation, F0=172 Hz, Q=0.12 l/s, speed of the camera 2500 images/s).

4. Conclusions

The vibration amplitudes of the vocal folds perfectly correlate with the peak-to-peak transglottal pressure variation. The results for ‘soft’ phonation show that the phonation onset is given by the airflow rate which was found to be identical for tube, tube in water and straw even if the mean values of the subglottal, oral and transglottal pressures varied considerably. It confirms the theoretical conclusions found in previous studies (Horáček & Švec, 2002) that the fundamental controlling mechanism for phonation onset is given by a critical mass flow rate when the vocal folds start to vibrate due to the loss of aeroelastic stability of the system by flutter. Only exception was found for vowel [u:] where the flutter frequency *F0* was higher than for all other cases studied, which according to the theory resulted in a higher airflow rate needed for the loss of the system stability.

Acknowledgement

The study was supported by the project GAČR P101/12/1306 and the Academy of Finland.

References

Horáček J., Švec J.G. (2002) Aeroelastic model of vocal-fold-shaped vibrating element for studying the phonation, *Journal of Fluids and Structures* 16(7), 931-955, doi:10.1006/jfls.454.

Titze I.R, Finnegan E.M., Laukkanen A-M., Jaiswal S. (2002) Raising lung pressure and pitch in vocal warm-ups: The use of flow-resistance straws. *Journal of Singing* 58, 329-338.

19th International Conference
ENGINEERING MECHANICS 2013
Svratka, Czech Republic, May 13 – 16, 2013

Distance-based and stress-based gradient-enhanced damage models

M. Horák [1] , **M. Jirásek** [2]

Summary: *Damage mechanics is a suitable framework for description of the behavior of quasibrittle materials. However, the classical theory fails after the loss of ellipticity of the governing differential equation. From the numerical point of view, loss of ellipticity is manifested by a pathological dependence of the results on the size and orientation of finite elements. To avoid such an undesired behavior, the model can be regularized by an implicit gradient formulation. However, this enhancement in its usual form leads to excessive energy dissipation near non-convex boundaries (e.g. notches and obtuse corners). This paper describes two modifications of the standard gradient-enhanced damage formulation and their implementation into a finite element code. The difference between the formulations is illustrated by a numerical example.*

1. Introduction

Realistic description of the mechanical behavior of quasibrittle materials such as concrete requires constitutive laws with softening. From the physical point of view, softening can be attributed to the propagation and coalescence of defects, e.g. voids and cracks. It is well known that softening may lead to localization of inelastic strain into narrow process zones. For traditional models formulated within the classical framework of continuum mechanics, such zones have an arbitrarily small thickness, and failure can occur at extremely low energy dissipation, which is not realistic. The mathematical model becomes ill-posed and the numerical solutions suffer by pathological sensitivity to the discretization parameter, e.g. to the size of finite elements. It is therefore necessary to introduce special enhancements acting as localization limiters.

This paper deals with the implicit gradient enhancement. Within this framework, the mathematical model remains well-posed and numerical results are mesh objective. However, the standard implicit gradient enhancement may result in excessive energy dissipation near non-convex boundaries, and its modifications are necessary to reduce this spurious effect.

The paper is organised as follows. In Section 2 the classical isotropic damage mechanics is outlined. In Section 3 the implicit gradient-enhanced formulation is described and its distance-based and stress-based modifications to reduce spurious dissipation near boundaries are introduced. The links to the micromorphic formulation are discussed. In Section 4, implementation of the regularized damage model into a finite element code is described. Finally,

[1] Ing. Martin Horák, Department of Mechanics, Faculty of Civil Engineering, Czech Technical University in Prague, Thákurova 7, 166 27, Prague; CZ, e-mail: martin.horak@fsv.cvut.cz
[2] Prof. Ing. Milan Jirásek, DrSc., Department of Mechanics, Faculty of Civil Engineering, Czech Technical University in Prague, Thákurova 7, 166 27, Prague; CZ, e-mail: milan.jirasek@fsv.cvut.cz

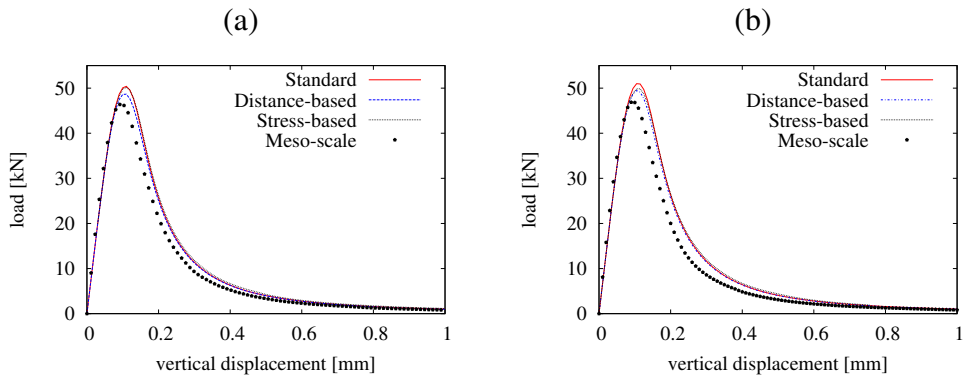

Figure 1: Load-displacement curve: (a) V-notch, (b) sharp notch

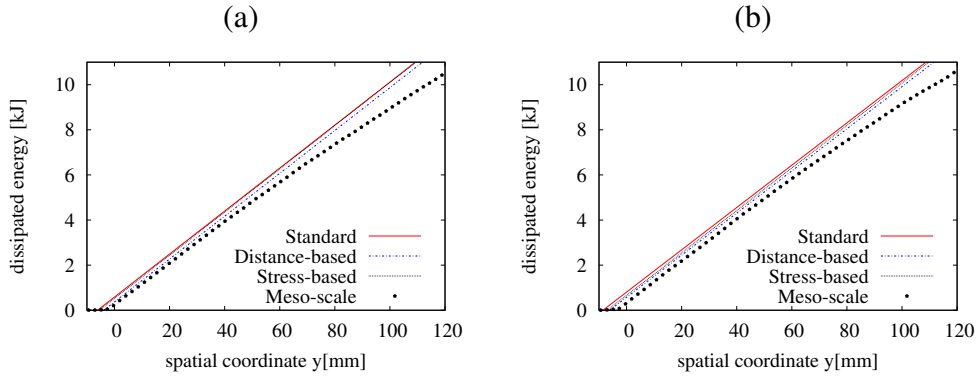

Figure 2: Dissipated energy: (a) V-notch, (b) sharp notch

the performance of the modified regularized models is assessed by simulations of a three-point bending test of concrete specimens with a sharp notch and a V-shaped notch.

2. Numerical examples

In the present simulations, the equivalent strain is based on the Rankine condition of maximum principal stress. The present results are shown in the form of the load-displacement curves (Fig. 1) and cumulated dissipated energy along the height of the beam (Fig. 2). The peak load and dissipated energy of the meso-scale model are overestimated by the standard and also by the modified models for both beam geometries. The distance-based formulation leads to a somewhat better agreement with the meso-scale model. The stress-based model provides slightly better results for the beam with a sharp crack, while for the V-notched specimen the results remain surprisingly close to the standard approach.

3. Acknowledgment

Financial support received from the Czech Technical University in Prague under grant SGS13/034/OHK1/1T/11 is gratefully acknowledged.

19th International Conference
ENGINEERING MECHANICS 2013
Svratka, Czech Republic, May 13 – 16, 2013

SEPARATION OF THE LIQUID PHASE FROM THE STATOR BLADES OF THE LAST STAGE OF A 1000MW STEAM TURBINE

M. Hoznedl, L. Tajč, L. Bednář*

Abstract: *The paper describes measurements of water film separation from the surfaces of hollow stator blades in the last stage of a large steam turbine for a nuclear power plant. Results are presented of the separation of the liquid phase, the efficiency of suction and the distribution of pressure at selected locations in the last stage during starting-up of the turbine. Attention is also paid to water extraction from the casing end wall. The main purpose of the paper is to find the efficiency of the water film separation and to provide general information about the wet steam flow in the last stage of the 1000 MW turbine.*

Keywords: ***Steam turbine, water film separation, experimental measurement.***

1. Introduction

Extensive experimental verification of the efficiency of suction removal of the liquid phase has been conducted by the present authors on a nuclear power plant 1000 MW turbine. In this case the liquid phase was exhausted together with the steam phase, which thus supported the transport of water. The exhausted steam was routed to the chamber above the rotor blade and the steam was then injected into the boundary layer on the wall of the diffuser in the exhaust hood. In this way, separation of the steam flow from the diffuser wall was prevented and its efficiency was improved. The expansion line of the last stage was extended and the output increased to compensate for the loss caused by steam suction from the last stage.

2. Amount of water on the surface of the hollow blades

Changes of steam conditions on the blade slot are shown in Fig. 1. The external steam wetness y_{sb} changes to y_t after throttling to the internal pressure p_{hb} but the measured water mass flow rate G_{vm} corresponds to wetness y_m. By reverse conversion to the conditions at pressure p_{sb} we obtain the water mass flow rate G_{vsm} and wetness y_{sm}. We always consider the theoretical maximum steam mass flow rate G_{max} corresponding to wetness y_{sb}. The mass flow rate of water in the form of coarse droplets G_F is given by $G_F = G_{vsm} - G_{vs}$. The efficiency of water removal is given by $\eta_s = G_{vsm}/G_{vt}$ where G_{vt} is the theoretical mass flow rate of the liquid phase in the rotor passage at the slot location. The extraction efficiency η_F represents the share of the water film in the removed sample. The coefficient of liquid phase concentration k_{sb} represents the actual measured wetness divided by the theoretical one. Steam wetness at the slots is shown in Fig. 2.

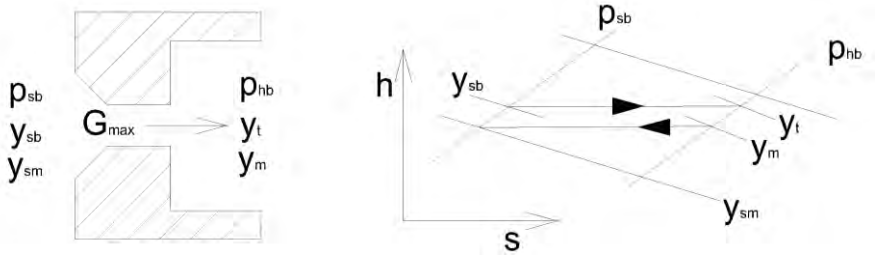

*Ing. Michal Hoznedl, Ph.D.: Doosan Škoda Power, Tylova 1/57; 301 28, Plzeň; CZ, e-mail: michal.hoznedl@doosan.com
Ing. Ladislav Tajč, CSc.: Doosan Škoda Power, s.r.o., Tylova 1/57, 301 28 Plzeň; CZ, e-mail: ladislav.tajc@doosan.com
Ing. Lukáš Bednář: Doosan Škoda Power, s.r.o., Tylova 1/57, 301 28 Plzeň; CZ, e-mail: lukas.bednar@doosan.com

Fig. 1: Changes of pressure and wetness on the blade.

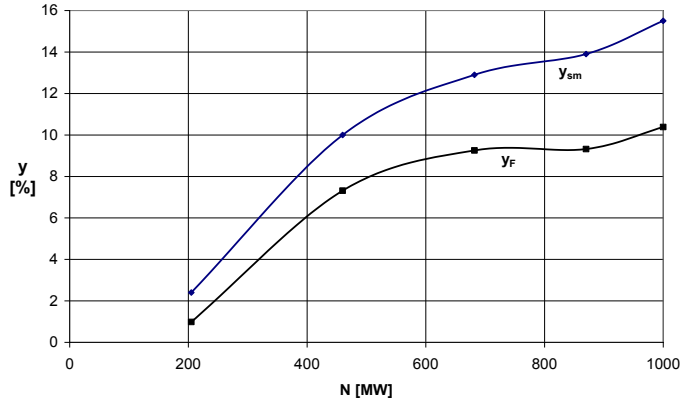

Fig. 2: Steam wetness at the slots.

The water removal efficiency is shown in Fig. 3 where it can be seen that it rises to a level of about 10%. The results correspond to other available information by Dejc et al. (1987) and Tanuma et al. (1991). Thanks to the water film separation, the steam is drier by about 10% for all wetness. About 70% of the separated water fraction corresponds to the water films on the blade surfaces.

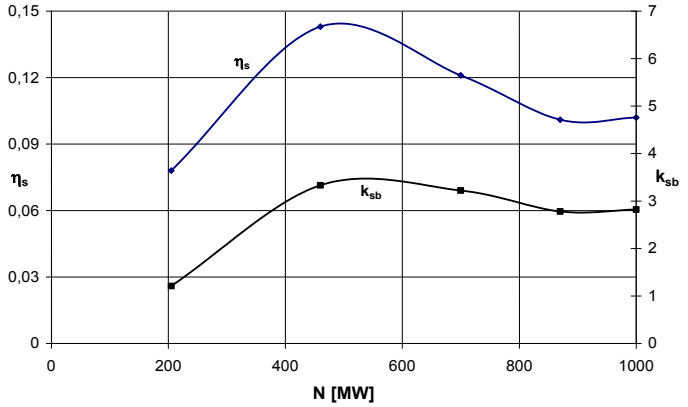

Fig. 3: Efficiency of water film separation.

3. Conclusions

Water separation slots support the extraction of the water film from the surface of hollow blades; about 70% of the removed water comes from the water film. The overall efficiency of water separation is about 10%.

Extraction of the water films is possible in all operational modes of the turbine. The extraction of the water film should contribute to reduced erosion wear of the leading edges of the rotor blades in the last stage.

The pressure conditions in the last stage are effective for water extraction at all operational modes of the turbine.

References

Filippov, G.A. & Povarov, O.A. (1980) Сепарация влагы в турбинах АЕГ (in Russian). *Bibliography.* MPEI Moscow.

Dejc, M.E. & Filippov G.A. (1987) Двухфазные течение в елементах теплоенергетическово оборудования (in Russian). *Bibliography.* MPEI Moscow.

Tanuma, T. & Sakamoto, T. (1991) The removal of water from steam turbine stationary blades by suction slots. *Proc. Instn. Mech. Engnrs. Part C (J. Mech. Eng. Sci.*), Paper 423/022.

Sakamoto, T., Nagao, S. & Tanuma, T. (1992) Investigation of wet steam flow for steam turbine repowering. *Proc. Int. Point Power Generation Conference,* Paper 10/18-22/92, pp. 33-40.

19th International Conference
ENGINEERING MECHANICS 2013
Svratka, Czech Republic, May 13 – 16, 2013

MODAL ANALYSIS OF TALL SLENDER STRUCTURES USING SOFTWARE GMAST

S. Hračov, S. Pospíšil, T. Brůna*

Abstract: *The paper is concerned with a verification of modal properties of tall slender structures determined by recently developed software GMAST. The applicability of the applied numerical model in practice is presented on examples of existing structures, for which the numerically and experimentally identified modal properties are compared.*

Keywords: ***modal analysis, tall slender structures, guyed masts, towers, software.***

1. Introduction

Tall slender structures are commonly used in the telecommunication industry to carry broadcasting antennas, microwave link dishes, telephone arrays as well as various meteorological monitoring aerials at substantial heights. Due to their slenderness, flexibility and low structural damping they are usually very sensitive to the dynamic component of the wind. The response spectrum analysis used for the calculation of the dynamic response requires the knowledge of the modal properties of the structures. In the last decades many authors proposed different models and methods for evaluating of the natural modes, frequencies and the dynamic response, see e.g. Nielsen (1995). In this paper the model presented in the book Koloušek et.al. (1983) and used in recently developed software GMAST (Hračov & Pospíšil (2012)) has been analyzed. The accuracy of the model from the point of view of modal properties has been verified for several cases of real experimentally tested structures.

2. Modal analysis of existing structures

A numerical model applied in software GMAST is based on an idealization of the structure as a continuous 2D beam with continuously distributed parameters on elastic supports. Shaft of structure is divided into sections which could be considered as prismatic i.e. with constant unit mass, bending stiffness and static axial force. Cabins, platforms, wireless and TV antennas and other important equipment are modelled as concentrated masses placed into the nodes between prismatic sections. The effect of guy ropes is introduced in a form of elastic supports with a frequency dependent stiffness. The influence of initial shaft displacements on tension forces in guy ropes is implemented into the program. Only planar displacements are assumed. The change of the structural geometry and other effects associated with initial displacements are neglected. The modal properties are determined using slope-deflection method. The determinant of the complex dynamic stiffness matrix of the structure is calculated for a set of user defined excitation frequencies. Consequently, the zeros of a characteristics polynomial identify eigen-frequencies of the structure. The graphical user interface (GUI) of software GMAST with typical results is presented in Figure 1.

Three guyed masts and one tower have been analysed in order to obtain modal properties and compare them with the experimentally measured counterparts. The dynamic measurements on existing structures consisted in determining the resonant frequencies (eigen-frequencies) of the structures based on the analysis of the vibration due to the wind load. The resonant frequencies and energy participation of respective eigen-modes on total response were determined from the power spectral density of measured

*Ing. Stanislav Hračov, Ph.D., doc. Stanislav Pospíšil, Ph.D., Tomáš Brůna, Institute of Theoretical and Applied Mechanics AS CR, v.v.i., Prosecká 76, 190 00 Prague 9, tel. +420 286 882 121, e-mail: hracov@itam.cas.cz

accelerations. To determine the accuracy of numerical eigen-solution using software GMAST the relative error between experimental and theoretical eigen-frequencies was investigated. The calculated errors together with determined natural frequencies are given for selected structures in Table 1. The low relative errors below 7 % show on good agreement between the numerical and experimental results.

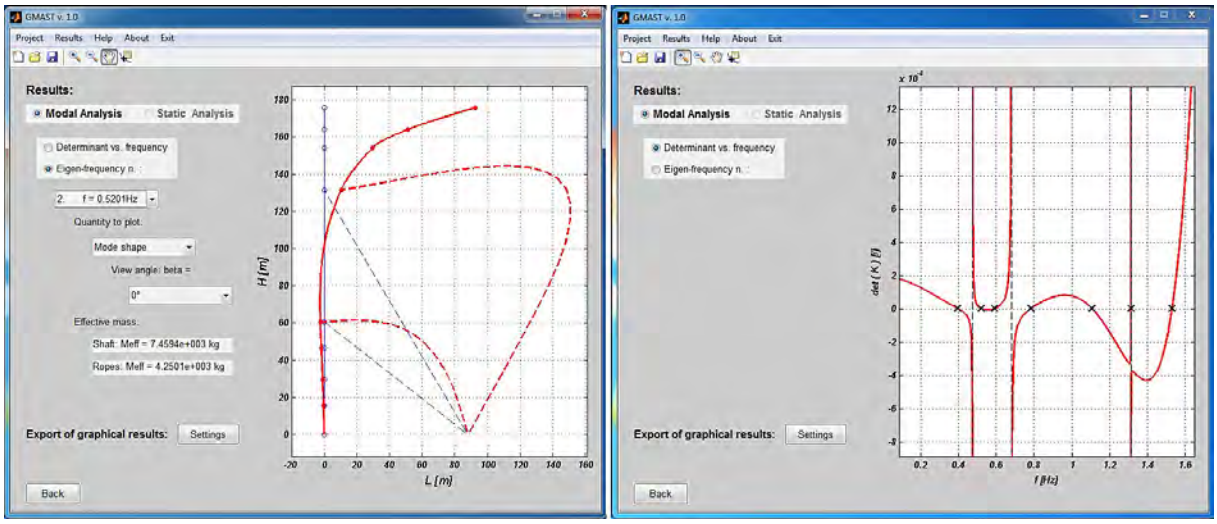

Fig. 1: GUI of software GMAST - Panels with typical results

Tab. 1: Calculated and measured natural frequencies and corresponding relative error Δf

Structure	Klet'			Hošťálkovice		
n.	$f_n[Hz]$		Δf	$f_n[Hz]$		Δf
[/]	GMAST	Measur.	[%]	GMAST	Measur.	[%]
1	0,396	0,408	-3,03	0,368	0,370	-0,54
2	0,520	0,544	-4,62	0,915	0,891	2,62
3	0,590	0,618	-4,24	1,394	1,360	2,44
4	0,783	0,813	-3,83	2,165	2,120	2,08
5	1,106	1,08	0,24	3,883	3,790	2,40

3. Conclusions

The analysis of numerical model used in software GMAST has been carried out in order to determine the accuracy of computed modal properties of tall slender structures. The model has been analyzed in cases of four different existing structures theoretically as well as experimentally. The comparison between theoretically and experimentally obtained results of three guyed masts and one tower has shown good agreement and acceptable accuracy. The comparison reveals that the model is entitled to use for modal analysis of tall slender structures and to assess their dynamic behaviour.

Acknowledgments

The kind support of the project of the Ministry of Industry and Trade No. MPO TIP FR-TI3/654, Czech Science Foundation project No. 13-41574P and of the RVO 68378297 are gratefully acknowledged.

References

Hračov, S. & Pospíšil, S. (2012), *GMAST v. 1.0*, Software for modal analysis of tall slender structures, ITAM AS CR, v.v.i., Prague, Czech Republic, Download: http://www.itam.cas.cz.

Koloušek, V., et al. (1983), *Wind effects on Civil Engineering Structures*, Academia, Prague, Czech Republic.

Nielsen, M.G. (1995), *Comparison of Maximum Dynamic Response for Guyed Masts using four different Methods of Analysis*, IASS WG4, Winchester.

19th International Conference
ENGINEERING MECHANICS 2013
Svratka, Czech Republic, May 13 – 16, 2013

SIMULATION OF INFRARED HEATING FOR INDUSTRIAL PRACTICE

M. Hušek*, J. Loufek**

Abstract: *The content of the upcoming article will be a presentation of the results achieved in the issue of numerical simulations of radiative heating shell moulds for the production of artificial leather. These artificial leathers have become common interior accessories in the automotive. The process of virtual heating starts with design and simulation of suitable types of reflectors of infrared emitters and their location above the model of mould. Followed by the simulation of nonstationary temperature fields containing components of temperature control. Part of simulation is also the calculation of temperature-mechanical loads of mould during the heating process.*

Keywords: ***Radiative heat transfer, simulation, artificial leather, optimization.***

1. Introduction

Heating shell moulds for artificial leather manufacturing process are realized in various ways. The forms can be heated for example by means of hot sand, oil or air. All these methods require some medium for heat up the shell mould, which could be very difficult to handle with.

Another utilizable method of heating-up the mould is based on the using a set of infrared heat emitters located above the shell mould. This paper concerns on two points of view in simulation radiative heat transfer model. First model is aimed on single emitter. This type of simulation is useful to study of heat flow distribution and for appropriate flow optimization. Second model is utilizable for concrete industrial situations. Second model includes shape of shell moulds and set of emitters with measured values of heat flow under each emitter. The aim of this model is to determine temperature on each point of shell moulds.

2. Numerical model of infrared emitter

Model of infrared emitter is designed to be able to figure heat flux distribution over any surface in two-dimensional space. Model is composed of set of straight particle surfaces, whereas every particle surface has given particular properties (location, emittance and temperature). The model was implemented in simulation tool named IRE Designer. In this tool the concrete simulated system is divided into two logical parts. The first part is the irradiated surface. The second part supplies emitters functionality. The numerical model supposes partition both these parts into a set of straight partial surfaces i.e. segments. Fig. 1 shows sample screen of IRE Designer user interface. Numerical model is able to use for example for new emitter configuration design. In general, it is not possible to solve the problem analytically. So it is appropriate to use automated optimization. For the purpose, the tool implements gradient descent algorithm. Fig. 2 shows four different model situations. The four presented cases differ only in reflector shapes, the properties of all surfaces are the same for all configurations.

* Ing. Martin Hušek: Faculty of Mechatronics, Informatics and Interdisciplinary Studies, Technical University of Liberec; Studentská 1402/2; 461 17, Liberec; CZ, e-mail: martin.husek@tul.cz

** Ing. Jan Loufek: Faculty of Mechatronics, Informatics and Interdisciplinary Studies, Technical University of Liberec; Studentská 1402/2; 461 17, Liberec; CZ, e-mail: jan.loufek@tul.cz

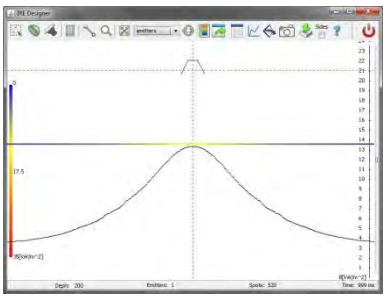

Fig. 1: IRE Designer tool

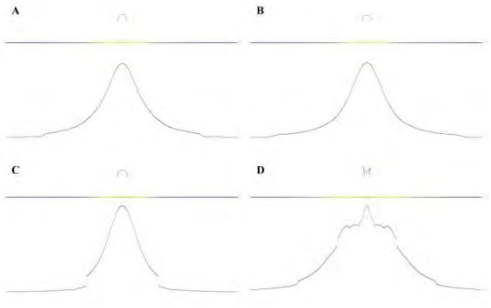

Fig. 2: Comparison of four different reflector shapes

3. Simulation of shell mould heating

The simulation phase of heating begins in simulation tool named IREview Blender. Application was created in Blender software. With the use of the appropriate functions, the emitters are placed around a model of the mould and heat flux loading of the surface is simulated. Heat flux is obtained from the database of the characteristics of emitters created by means of experimental measurements in the laboratory. Fig. 3 shows complete model contains shell mould, infrared emitters and frame for fixing of special holders of emitters. Final temperature of the mould surface is possible to calculate in the CAE software, see fig. 4. Suitable combination CAE software and IREview Blender tool allows to realize regulated heating which is necessary for real heating on the production line.

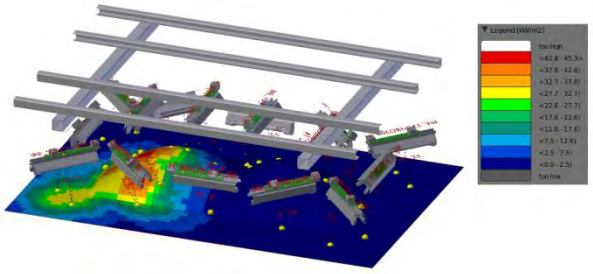

Fig. 3:IREview Blender - heat flux [2]

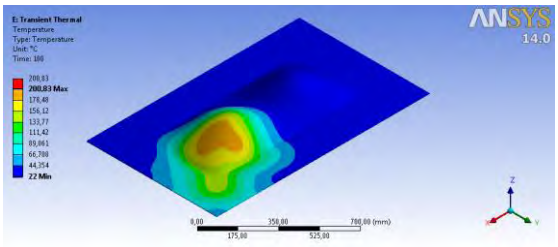

Fig. 4. ANSYS – temperature [2]

4. Conclusions

Numerical model implemented in IRE Designer tool can be used as tool for a design of demanded reflector configuration. For heating of shell moulds is used IREview Blender tool and CAE software for temperature calculation. Further development is focused on linking IRE Designer tool with IREview Blender tool to simulate infrared heating using new emitters types with various shaped reflectors. With suitable virtual model of emitter with reflector will not be necessary the experimental measurements of infrared emitters for simulation of temperature field.

Acknowledgement

The work of J. Loufek was supported by the Ministry of Education of the Czech Republic within the SGS project no. 2013/78000 at the Technical University of Liberec. The work of M. Hušek was supported by the Ministry of Education of the Czech Republic within the SGS project no. 78001/115 at the Technical University of Liberec.

References

Composite authors. Ohřevy radiací – teorie a průmyslová praxe. Editor Jaroslav Mlýnek, Antonín Potěšil 2012, Liberec: Technická univerzita v Liberci, 2012, ISBN 978-80-7372-884-7.

Hušek, M. Model of radiation heating of sluch tehnology. 20th SVSFEM ANSYS Users' Group Meeting and Conference 2012, ISBN 978-80-260-2722-5.

Loufek, J. Simulations of radiation heat transfer in design of alternative infrared emitters. In: XI. International Conference on the Theory of Machines and Mechanisms 2012. Liberec: Technická univerzita v Liberci, 2012.

19th International Conference
ENGINEERING MECHANICS 2013
Svratka, Czech Republic, May 13 – 16, 2013

NUMERICAL MODELLING OF HEAT AND MASS TRANSFER IN THE COUNTERFLOW WET-COOLING TOWER FILL

T. Hyhlík *

Abstract: *The article deals with the numerical modelling of heat and mass transfer in the counterflow wet-cooling tower fill. Due to the complexity of this phenomenon the simplified model based on the set of four ODEs was chosen. Boundary condition for outlet water temperature are based on experimentally obtained Merkel number correlation. The numerical solution of chosen model was performed using Runge-Kutta method combined with shooting method. The results are compared with data available in the literature.*

Keyworlds: ***evaporative cooling, wet cooling tower, Merkel number***

1. Introduction

In the counterflow wet-cooling tower fill of film type water flows vertically down through the fill as a liquid film. Air is driven by a tower draft or fan and flows vertically in the opposite direction. Heat and mass transfer occurs at the water and air interface. Evaporation and convective heat transfer cool the water, what leads to increase of air humidity and temperature.

2. Mathematical models

Due to the complexity of two phase flow occurring in the wet-cooling tower fill the one dimensional models of heat and mass transfer are used (e.g. Kröger (2004); Williamson (2008); Klimanek and Białecky (2009)). These models are based on few assumptions which allow to create simplified one dimensional models. The first assumption talks about neglecting the effects of horizontal temperature gradient in the liquid film, horizontal temperature gradient in air temperature and humidity (e.g. Williamson (2008)). The second one states that temperatures and humidity are represented only by averaged value for each vertical position. We are also assuming that at the interface of two phases, there is a thin vapour film of saturated air at the water temperature (e.g. Williamson (2008)).

3. Conclusions

The results of the numerical solution was discussed in the full text for three test cases. The first two test cases was chosen to compare results with data from references by Klimanek and Białecky (2009) and Kloppers (2003). Figure 1 show results of the numerical simulation for the first test case. The results presented in this article exhibit slight differences from the reference solutions. The main difference is presented in the second case where it seams that supersaturation exhibits little bit later. The differences are probably caused by different choice of saturated vapour pressure equation in references and in this article. The difference is also connected with using the more precise equation for the calculation of specific humidity in this article. The previous two sentences are based on assumption that the work of Klimanek and Białecky (2009) is based on the same thermodynamics equations as are presented in the book of Kröger (2004) and this is not possible to recognize from their article. The third test case is shown in the full text because of the problematic presence of the discontinuity on the distribution of

* Ing. T. Hyhlík, Ph.D., Department of Fluid Dynamics and Thermodynamics, Faculty of Mechanical Engineering, Czech Technical University in Prague, Technická 4, 166 07 Prague 6, e-mail tomas.hyhlik@fs.cvut.cz

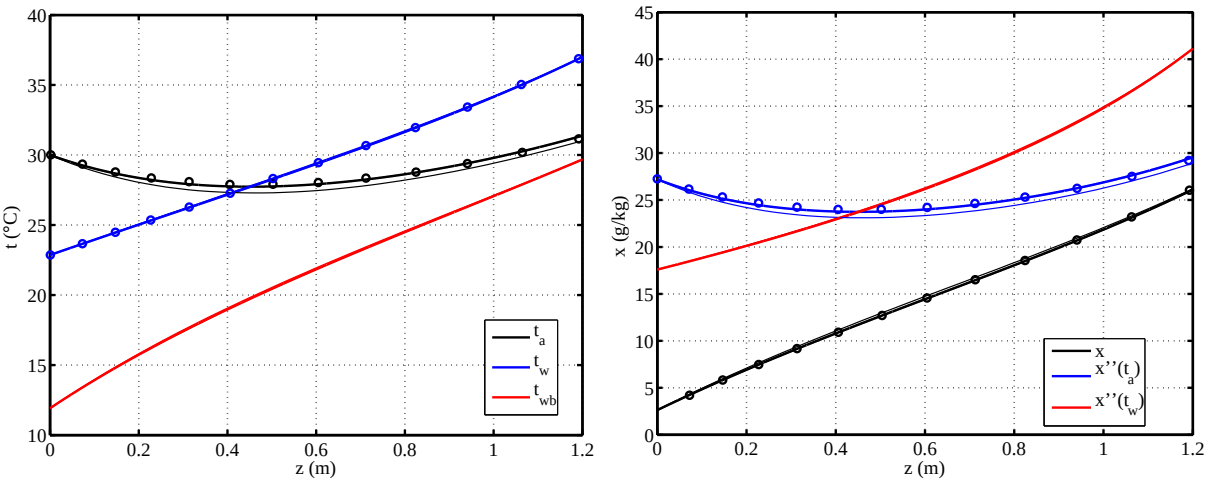

(a) Air temperature t_a, water temperature t_w, adiabatic saturation temperature t_{wb}

(b) Specific humidity x, saturation humidity at the air temperature $x''(t_a)$, saturation humidity at the water temperature $x''(t_w)$

Figure 1: The first test case - distribution of temperature and specific humidity compared with data taken from (Klimanek and Białecky (2009)); solid lines correspond to calculation and circles to data from the reference; thin lines correspond to calculation on coarse grid and thick lines on finest grid.

convective part of the density of heat source. It has been shown that the discontinuity is vanishing with the grid refinement. The presence of discontinuity does not correspond with the increase of error norm. Unfortunatelly, the article by Klimanek and Białecky (2009) does not mention the distribution of the density of convective part of heat source for the case where supersaturation occurs. They have mentioned only general fact that adaptive step size control technique can increase accuracy of the integration with small additional computational effort.

4. Acknowledgement

This work has been supported by *Technology Agency of the Czech Republic* under the project *Advanced Technologies for Heat and Electricity Production - TE01020036*.

5. References

Bosnjakovic, F. (1965): Perry L. Blackshear Jr. (Ed.), *Technical Thermodynamics*, Holt, Rinehart and Winston, New York

Dormand, J. R. & Prince, P. J. (1980): A family of embedded Runge-Kutta formulae. *Journal of Computational and Applied Mathematics* 6(1)

Klimanek, A. & Białecky, R. A. 2009: Solution of Heat and Mass Transfer in Counterflow Wet-Cooling Tower Fills. *International Communications in Heat and Mass Transfer* 36

Kloppers, J. C. 2003: *A Critical Evaluation and Refinement of the Performance Prediction of Wet-Cooling Towers.* Ph.D. thesis, University of Stellenbosch

Kloppers, J. C. & Kröger, D. G. 2005: The Lewis Factor and its Influence on the Performance Prediction of Wet-Cooling Towers. *International Journal of Thermal Sciences* 44

Kröger, D. G. 2004: *Air-Cooled Heat Exchangers and Cooling Towers.* Penn Well Corporation, Tulsa

Williamson, N. J. 2008: *Numerical Modelling of Heat and Mass Transfer and Optimisation of a Natural Draft Wet Cooling Tower.* Ph.D. thesis, University of Sydney

Zúñiga-González, I. 2005: *Modelling Heat and Mass Transfer in Cooling Towers with Natural Convection.* Ph.D. thesis, Czech Technical University in Prague

19th International Conference
ENGINEERING MECHANICS 2013
Svratka, Czech Republic, May 13 – 16, 2013

SIMULATION OF VEHICLE TRACK RUNNING

M. Chalupa[1], R. Vlach[2]

Abstract: *The article describes design of the vehicle track computational model and testing procedure of the track dynamic loading simulation. The proposed approach leads to an improvement of safety of running achieved by improvement of track vehicle course stability. The computational model is meant for MSC. ADAMS, TVT computational system. Computational model, which is intended for MSC computational system, is formed from two basic parts. The first part is represented by geometrical part, while the second one by contact computational part of the model. The aim of the simulating calculation consist in determination of change influence of specific vehicle track constructive parameters on changes of examined qualities of the vehicle track link and changes of track vehicle course stability. The work quantifies the influence of changes of track preloading values on the demanded torque changes of driving sprocket. Further research possibilities and potential directions of next research are also presented on the end of article.*

Keywords: tracked vehicles, track, computational simulation, dynamic loading simulation

1. Introduction

General objective of the work is to define main possibilities of track vehicle directional improvement by simultaneous increase of vehicle maximum speed. It is used now for collecting of undercarriage design parameters with whatsoever influence on vehicle directional improvement.

The aim of the work is to carry out the composition of a computational model. But not only model of the vehicle track but also for the dynamic properties of the complete vehicle and to suggest ways of other use of this mathematic model for computational simulation experiments. It is possible to find out the essential information about individual undercarriage parts behaviour during the vehicle drive. The mathematical model is built for computational simulating system MSC.ADAMS.TVT, that can be used for the computational modelling and dynamic loading simulation.

2. Used methods

The computational system MSC.ADAMS.TVT is used for the computational modelling and simulation. This system can be used for the analysis of kinetic and dynamic characteristics of the modelling mechanic system and its animation also. The computational model consists of geometrical and contact parts of model.

The geometrical part of computational model consists of basic parts of vehicle undercarriage movable organs (road wheels, supporting rollers, driving sprocket, idle wheel). Main part is track line, on which individual track links are connected by a couplings.

The contact part of computational model consist of impact and frictional forces system. To guarantee the highest accuracy and practically, the impact and frictional forces of individual undercarriage parts are defined in such a way, that the whole model resembles the reality as much as possible.

[1] doc.Ing. Milan Chalupa, CSc.: UO Brno, Kounicova 65, 612 00 Brno, tel.+fax: +420 973 44 3 420, E-mail: milan.chalupa@unob.cz.

[2] doc. Ing. Radek Vlach, Ph.D. : Ústav mechaniky těles, FSI VUT Brno; Technická 2, 619 69 Brno; tel.: +420.541 142 757, fax: +420.541 142 876; E-mail: vlach@feec.vutbr.cz.

3. Results and discussion

This article describes the suggestions of the way and using of simulation calculation of the track behaviour results during various undercarriage geometry changes and operational setting-up, which are done for the examination of individual selected parameters of the construction track links and track dynamic and hanging properties on general track behaviour.

The aim of the simulating calculation is the determination of change influence of specific constructive parameters of the vehicle track (track preloading) on changes of examined qualities of the vehicle track link (reaction forces against motion) which are determined especially by intensity changes of required torque moment on driving wheel. It is evident that the results of simulation computations have proved the assumption that changing the constructional parameters of undercarriage parts it is possible to improve dynamical behaviour of some parts of track vehicle undercarriage and to optimise dynamic properties of the vehicle in motion.

After obtaining of sufficient quantity simulation results of different parameter influence, it will possible to determine the universal relation dependence of different construction parameters on dynamic loading of the track.

4. Conclusion

The presented article describes one of the possible ways of real track vehicle movement mechanism computational model setting in MSC.ADAMS.TVT. It is computation system with emphasis on vehicle track design and recommendation for upgrading mathematical model with a view to make the computation simulation attempts for the purpose of finding basic information on track component parts and undercarriage performance of the moving vehicle.

On the grounds of the analysis outcome it will be possible to state which constructional changes or changes of operational setting-up will lead to objective accomplishment. This objective can be defined as track vehicle directional improvement at simultaneous maximum speed increase, limited, apart from other things, not only by track construction, but also by the whole track kinetic and suspension track vehicle undercarriage mechanism.

Acknowledgement

The paper was written with the support of Research plan 0000401 of Faculty of Military Technologies of University of defence in Brno.

References

Chalupa,M., Kotek, V., Vlach, R.(2001) Track construction research for high speed. POV MO 03171100014 final report. Military Academy Brno 2001.

Chalupa, M, Veverka, J, (2007) Dynamic Loading Simulation of Vehicle Track . In: : The book of extended abstracts of National conference with International Participations *„Engineering mechanics 2007“*, CD- 8 lists CD-ROM, Svratka, ČR, 2007. ISBN 978-80-87012-06-2.

Vlach, R., Grepl, R., Chalupa, M., Ondrůšek, Č., (2003) Computational modelling of vehicle track dynamic properties. In: Proceedings of the National conference „Computational mechanics 2003“ 3.-5. 11. 2003, Nečtiny, CR.

Koucký, M. and Vališ, D. (2011) „Some aspects of sequential systems design.“ In Proceedings 17th ISSAT International Conference on Reliability and Quality in Design. Piscataway : International Society of Science and Applied Technologies,. ISBN 978-0-9763486-7-2, ,pp. 62-66.

Rolc, S., Adamík, L., Buchar, J., Severa, L. (2008) Plate response to buried charge explosion, Material Science Forum, Vol 566, pp 83-88, 2008, ISBN 0-87849-465-0.

19th International Conference
ENGINEERING MECHANICS 2013
Svratka, Czech Republic, May 13 – 16, 2013

OBLIQUE COLLISIONS OF NON-ROTATING SPHERICAL PARTICLES WITH A WALL

Z. Chára[*], P. Vlasák[**], B. Kysela[***]

Abstract: *In the present paper non-rotating particle-wall collisions were experimentally investigated. By means of the PIV method a velocity field around falling spheres was analyzed. It was shown that the wake behind the particle which approached a bed in non-normal direction was no more asymmetrical and after the impact the wake passed the particle only along one side. This non-symmetrical velocity field resulted in an additional force which pushed the particle to an opposite direction than was the direction of the particle motion just after the impact.*

Keywords: ***Wake, particle trajectory, velocity field***

1. Experimental arrangements

In our study we have focused on a rebounding of spherical, non-rotating particles from the wall when the particles approached the wall in non-normal direction. The experiments were realized in a water tank of dimensions 400 x 200 x 280 mm. We used two types of spherical particles: - plastic sphere of diameter 37.5 mm and density 1028 kg/m^3 and golf ball of diameter 42.8 mm and density 1120 kg/m^3. The particle movements in water were recorded using a digital video camera NanoSence III+ with a frequency of 700 frames per second (plastic particle) and a frequency of 1000 frames per second for the golf ball. To perform a PIV analysis we used the Time-resolved digital particle image velocimetry tool developed for Matlab. The Reynolds numbers varied from 5000 to 13000.

2. Discussion of the results

Fig. 1 shows non-dimensional trajectories of freely falling plastic particle and golf ball. Since the ratios of densities of both particles to water density were close to one, the particles had tendency to fall not along a straight line but rather along a curved line. The particle strikes the wall at an oblique angle and after the impact the particle seems to follow a path resulting from the law of reflection. But after a short time the particle is suddenly moved to an opposite direction. To explain this behavior we analyze the wake formation during the falling and the rebounding period. The wake behind the particles is shifted to the left during the falling period. When the particle touches the wall the wake moves towards the wall mainly along the left side of the particles and the velocity field around the particle is no more axisymmetrical. The velocities in the wake before the impact are practically the same as is the falling velocity of the particle. After the impact the particle moves up but the wake moves still towards the wall and the relative velocities are about two times the falling velocity (if the restitution coefficient is close to one). According to the Bernoulli equation an increase in the speed of the fluid occurs simultaneously with a decrease in pressure. It means that the pressure on the left side of the particle is lower than the pressure on the right. Therefore this pressure difference probably results in an additional force that pushes the particle to the left. If time series of the velocities are known, it is

[*] Ing. Zdeněk Chára, CSc.: Institute of Hydrodynamics AS CR, v. v. i., Pod Paťankou 30/5; 166 12, Prague; CZ, e-mail: chara@ih.cas.cz

[**] prof. Pavel Vlasák, DrSc.: Institute of Hydrodynamics AS CR, v. v. i., Pod Paťankou 30/5; 166 12, Prague; CZ, e-mail: vlasak@ih.cas.cz

[***] Ing. Bohuš Kysela, PhD.: Institute of Hydrodynamics AS CR, v. v. i., Pod Paťankou 30/5; 166 12, Prague; CZ, e-mail: kysela@ih.cas.cz

possible to determine time derivations of the velocities which are related to total forces acting on the particles. Examples of the time derivations of the vertical as well as the horizontal particle velocities are shown in Fig. 2 for the golf ball. Negative maximum of time derivation of the horizontal velocity occurs approximately at time 0.279 sec (from beginning of the image capturing), negative maximum of time derivation of the vertical velocity occurs at time 0.379 sec. It means that the maximum forces that affect the golf ball in the horizontal and the vertical direction just after the impact do not act simultaneously. It is due to the fact that the velocity field in a vicinity of the rebounding particle is changing. Firstly the wake formed behind the particle during the falling period moves towards the bed even after the particle impact and passes the rebounding particle vertically along the left side. After that a part of the wake moves to a gap between the particle and the bed passes the particle horizontally and forms a non-symmetrical velocity field in the vertical direction. This can be clarified in Fig. 3 for the golf ball.

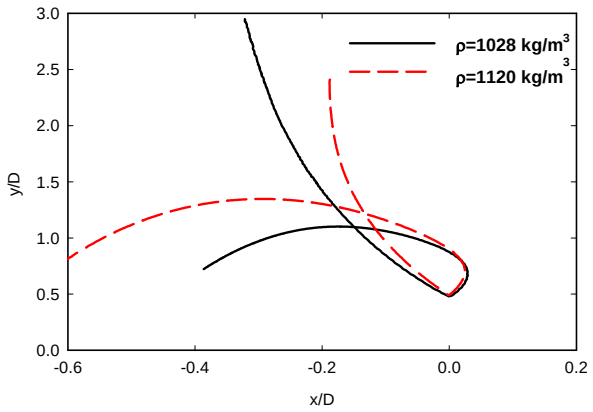

Fig.1: Non-dimensional particle trajectories

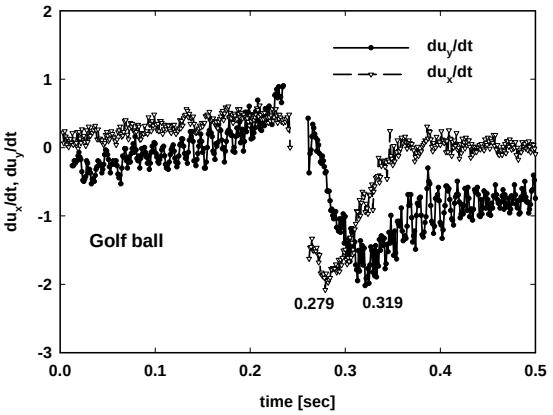

Fig.2: Time derivations of the velocity components

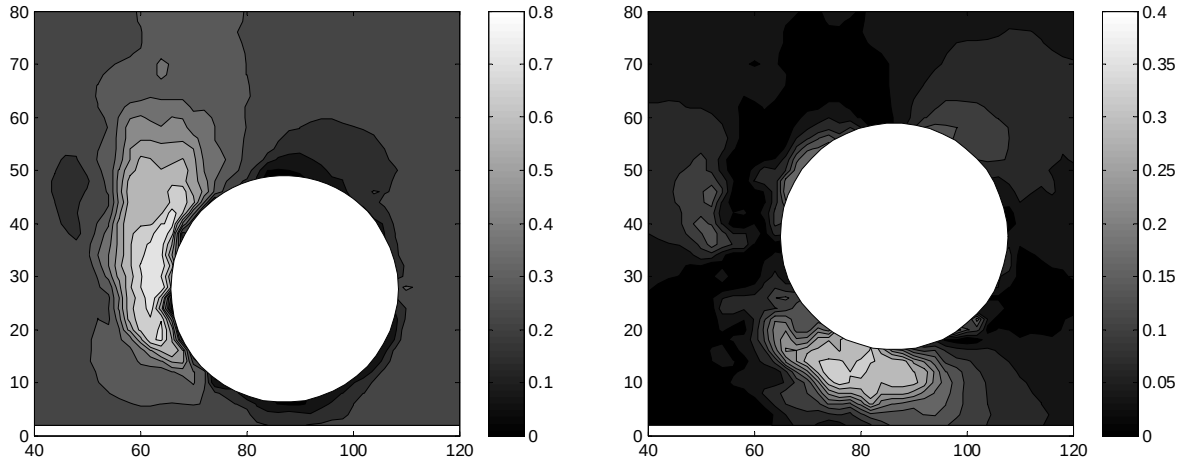

Fig.3: Contours of the vertical velocities captured in time 0.279 sec(left), contours of the horizontal velocities captured in time 0.319 sec (right) for golf ball

3. Conclusions

The movement and the impact of non-rotating spherical particles were analyzed. It was shown that there exist additional forces which act for a short time on the particles both in the horizontal and the vertical directions. These forces result from the Bernoulli principle and from a non-symmetrical motion of the wake formed behind the particles.

Acknowledgement

The supports under project No. 103/09/1718 of the Grant Agency of the Czech Republic and RVO: 67985874 are gratefully acknowledged.

19th International Conference
ENGINEERING MECHANICS 2013
Svratka, Czech Republic, May 13 – 16, 2013

COMPARISON OF NUMERICAL METHODS FOR UNCERTAINTY QUANTIFICATION

E. Janouchová, A. Kučerová, J. Sýkora [1]

Summary:
An extensive development of efficient methods for stochastic modelling enabled uncertainty propagation through complex models. In this contribution, we present a review and comparison of several approaches such as stochastic Galerkin method, stochastic collocation method or polynomial regression based on Latin Hypercube Sampling. The advantages and disadvantages of these methods are demonstrated within the comparison with the traditional Monte Carlo method on a simple illustrative example of a frame structure.

There are many important factors limiting the service life of buildings. An appropriate reliability analysis needs to take account uncertainties in the environmental conditions as well as in structural properties. Thanks to the growth of powerful computing resources and technology, recently developed procedures in the field of stochastic mechanics have become applicable to realistic engineering systems. Methods quantifying uncertainties can be classified into two groups: (i) reliability analysis methods, such as the first- and second-order reliability method (FORM/SORM (Ditlevsen, 1996)) computing the probability of failure related to limit states; (ii) the higher moment analysis focused on estimation of the higher-order statistical moments of structural response as stochastic finite element methods (SFEM), see (Matthies, 2007; Stefanou, 2009) for a review. SFEM is a powerful tool in computational stochastic mechanics extending the classical deterministic finite element method (FEM) to the stochastic framework involving finite elements whose properties are random (Ghanem, 1991).

In this contribution we concentrate on the SFEM based on polynomial chaos expasion (PCE) used for approximation of the model response in the stochastic space. Uncertainty in the model output can be then quantified using Markov chain Monte Carlo method employed for sampling model parameters and evaluating the PCE instead of full numerical model. The efficiency of SFEM thus depends on computational requirements of the PCE construction and its consequent accuracy.

There are several methods for construction of PCE-based approximation of a model response: stochastic Galerkin method (Babuska et al., 2004; Matthies and Keese, 2005), stochastic collocation methods (Babuska et al., 2007; Xiu, 2009) and linear regression (Blatman and Sudret, 2010). The principal differences among these methods are follows. Stochastic Galerkin method is purely deterministic, but leads to solution of large system of equation and needs an

[1] Bc. Eliška Janouchová, Ing. Anna Kučerová, Ph.D., Ing. Jan Sýkora, Ph.D., Faculty of Civil Engineering, Czech Technical University in Prague, Thákurova 7/2077, 166 29 Prague 6, tel. +420 224 35 53 26, e-mail eliska.janouchova@fsv.cvut.cz, anicka@cml.fsv.cvut.cz, jan.sykora.1@fsv.cvut.cz

intrusive modification of the numerical model itself. Stochastic collocation methods is also a deterministic method, does not require intrusive modification of a model, but uses a set of model simulations on a sparse grid constructed for a chosen level of accuracy. The computation of PCE coefficients is based on explicit formula. The linear regression is based again on a set of model simulations performed for a stochastic design of experiments, usually obtained by Latin Hypercube Sampling. The PCE coefficients are then obtained by regression of a model results at the design points, which leads to a solution of a system of equations. The aim of this paper is to compare these methods in terms of computational requirements and resulting accuracy on a simple illustrative example of a frame structure.

Acknowledgment

This outcome has been achieved with the financial support of the Czech Science Foundation, projects No. 105/11/0411 and 105/12/1146, and Grant Agency of the Czech Technical University in Prague, grant No. SGS OHK1-042/13.

1. References

Babuska, I. & Tempone, R. & Zouraris, G. E. 2004: Galerkin Finite Element Approximations of Stochastic Elliptic Partial Differential Equations. *SIAM Journal on Numerical Analysis* 42(2), 800–825.

Babuska, I. & Nobile F. & Tempone, R. 2007: A Stochastic Collocation Method for Elliptic Partial Differential Equations with Random Input Data. *SIAM Journal on Numerical Analysis* 45(3), 1005–1034.

Blatman, G. & Sudret, B. 2010: An adaptive algorithm to build up sparse polynomial chaos expansions for stochastic finite element analysis *Probabilistic Engineering Mechanics* 25(2), 183–197.

Ditlevsen, O. & Madsen, H. O. 1996: *Structural Reliability Methods*, John Wiley & Sons Ltd, Chichester, England.

Ghanem, R. G. & Spanos, P. D. 1991 *Stochastic finite elements: A spectral approach*, Springer-Verlag New York, Inc.

Matthies, H. G. & Keese, A. 2005: Galerkin methods for linear and nonlinear elliptic stochastic partial differential equations. *Computer Methods in Applied Mechanics and Engineering* 194(12–16), 1295–1331.

Matthies, H. G. 2007: Uncertainty quantification with stochastic finite elements. In Erwin Stein, René de Borst, and Thomas J. R. Hughes, editors, *Encyclopaedia of Computational Mechanics*. John Wiley & Sons, Chichester.

Stefanou, G. 2009: The stochastic finite element method: Past, present and future. *Computer Methods in Applied Mechanics and Engineering* 198(9–12), 1031–1051.

Xiu, D. 2009: Fast Numerical Methods for Stochastic Computations: A Review. *Communications in Computational Physics* 5(2–4), 242–272.

19th International Conference
ENGINEERING MECHANICS 2013
Svratka, Czech Republic, May 13 – 16, 2013

INFLUENCE OF THE REINFORCEMENT ON THE IMPACT RESISTANCE OF A BRIGDE PIER

P. Jiříček*, M. Foglar**

Abstract: *The paper presents results of a numerical study focused on the influence of different types of reinforcement arrangement of a bridge pier on its impact resistance. Four types of reinforcement arrangement are evaluated. The vehicle impact at the bridge pier is modeled with the use of ANSYS Autodyn. A nonlinear material model of concrete with damage and strain-rate effect was chosen. The paper concludes the topic introduced at the EMM2012.*

Keywords: ***concrete, RHT concrete model, impact.***

1. Introduction

Traffic intensity increase leads to higher risk of traffic accidents. In 2010 and 2011 about 1250 accidents involving bridges and tunnels happened in the Czech Republic. Heavy trucks (above 30t) hitting the bridge substructure can lead into progressive collapse of the bridge superstructure thus causing severe fatalities, therefore this loading case should be considered especially at the motorways.

The European design standard EN 1991-1-7 prescribes two methods for determination of vehicle impact loading. The first simplified method is based on an equivalent static force. The second method is based on accurate input data and requires a special dynamic analysis for evaluation of the impact loading.

The bridge pier truck impact is considered according to EN 1991-1-7 (vehicle - 30tonnes; 90kph). The whole vehicle impact is modeled with the use of ANSYS Autodyn software. Four options of reinforcement arrangement are compared and evaluated within the paper.

2. Description of the analyzed bridge pier

The dimensions of the bridge pier are 1000 x 4800 x 6700 mm (width x length x height) and concrete class is C30/37. Deflection in bottom and head of pier are restricted.

Main bending reinforcement is formed by vertical bars Ø20/200mm (Fig. 1), shear reinforcement is formed by bars Ø10/300mm. In the case of the second layer of reinforcement, the distance of this layer to the first on is 100mm.

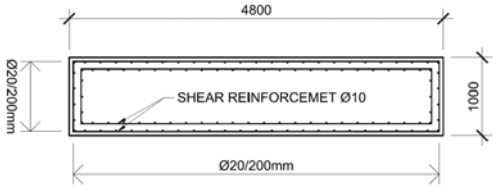

Fig. 1: Scheme of the reinforcement arrangement (section).

* Ing. Pavel Jiříček: Faculty of Civil Engineering, Czech Technical University in Prague, Thákurova 7; 166 29, Prague 6; CZ, e-mail:pavel.jiricek@fsv.cvut.cz

Ing. Pavel Jiříček: Faculty of Civil Engineering, Czech Technical University in Prague, Thákurova 7; 166 29, Prague 6; CZ, e-mail:pavel.jiricek@fsv.cvut.cz

** Ing. Marek Foglar, Ph.D.: Faculty of Civil Engineering, Czech Technical University in Prague, Thákurova 7; 166 29, Prague 6; CZ, e-mail: marek.foglar@fsv.cvut.cz

2.1 The pier without reinforcement

This option is chosen from the previous steps of the research, mainly considered for evaluation of the force of the vehicle impact. In this paper it has only comparative purpose (Fig. 2a).

2.2 The pier with longitudinal reinforcement

Only bending reinforcement is considered. Reinforcement is formed by longitudinal bars Ø20/200mm. The damage is shown in Fig. 2b.

2.3 The pier with vertical and shear reinforcement

In this case, the reinforcement is formed by longitudinal bars Ø20/200mm, the shear force is added (bars Ø10 over 300mm). The damage is shown in Fig. 2c.

2.4 The pier with vertical and shear reinforcement in two layers

This arrangement of reinforcement is recommended by German design standards (DIN-Fachbericht 102), which considers bending and shear reinforcement in two layers. The damage is shown in Fig. 2d.

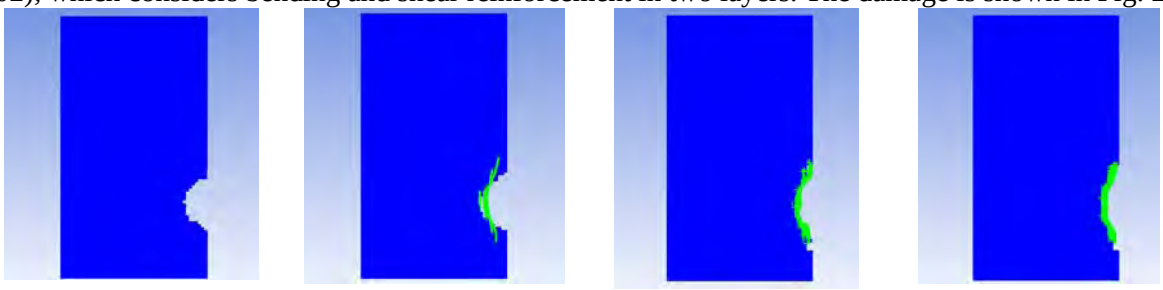

a – The pier without reinforcement

b – The pier with vertical reinforcement

c – The pier with vertical and shear reinforcement

d – The pier with longitudinal and shear reinforcement in two layers

Fig. 2: Damage of the pier.

3. Conclusions

The four types of pier reinforcement were evaluated in this paper. It's obvious that fully anchored longitudinal bending reinforcement transmits some impact force and therefore enlarges impact area in comparison to the plain concrete. The shear reinforcement confines the concrete surrounded by the longitudinal bars and limits the erosion of concrete. In case of placing reinforcement in two layers, the main damage and erosion of concrete takes place in the area of the first layer. The concrete behind the second layer remains mainly uneroded. In general, the increase of reinforcement area in the spot of the impact enhances the resistance of the pier to impact loading.

Acknowledgement

The financial support of CTU grant 13/035/OHK1/1T/11, the Ministry of Interior of the Czech Republic project VG20132015114 and Czech the Republic Grant Agency project No. 13-30441S are kindly acknowledged.

19th International Conference
ENGINEERING MECHANICS 2013
Svratka, Czech Republic, May 13 – 16, 2013

IDENTIFICATION OF DAMPING PARAMETERS OF BLADED DISKS

J. Kellner, V. Zeman, J. Šašek, Z. Kubín [1]

Abstract: *Regarding steam turbine blade vibrations, damping of blades as well as whole bladed disk vibrations are one of the most important parameters in terms of steam turbine operation. Values of the damping parameters depend on properties of material used for blades and disc as well as on geometric parameters of blade shroud contact areas with friction elements. The in-house made software enables fast parametric optimization using a multi-criteria function, for example angle of contact planes or mass of friction elements. The real bladed disk was excited in vacuum machine to provide material and construction damping. The measured modal properties and damping parameters identification are used for model correction as well as detailed meshed model in commercial software.*

Keywords: ***steam turbine blades, damping, friction element, parameter identification.***

The need for higher efficiency leads to thinner blades profile on one hand but the requirement of higher stage power output leads to higher bending stress and blade vibrations on other hand. This higher bending stress in blade is resulting in smaller dynamic load which can be applied on blades. One of the most usual approaches to the suppression of undesirable blade vibrations is application of the friction elements or connection blades to continuous coupled set of blades. In order to increase stiffness and damping of turbine blades a new type of shrouds with friction contacts was developed. However the effect of the friction in contact cannot be determined during design process without deeper knowledge of this type friction and without identification of other damping parameters.

That is why the first goal of this article is a damping identification of new type of shrouded blades depending on excitation amplitude. The damping phenomena is very complex. Damping in real bladed disks usually includes material damping, unwanted root construction damping, friction damping and other issues, for example the air resistance. In order to uncover all aspects of the real blade damping, we will proceed step by step.

From measurement point of view, the good agreement will be presented between the damping ratio of beams specimens and free blades as well as the issues of identification of coupled blades damping. Damping dependence on the amplitude of blade vibration or on the number of nodal diameters will also be discussed.

The real bladed disk was made with 56 high pressure blades. After first measurement with free standing blades, the friction elements were placed between shrouds (i.e. the tops of blades) to increase the total damping as well as stiffness of system. Each friction element has two contact areas with different slope angle, that's why there are two different contacts in the sense of behaviour.

[1] Ing. Josef Kellner, Ph.D., Prof. Ing. Vladimír Zeman, DrSc., Ing. Jakub Šašek, Ph.D., Ing. Zdeněk Kubín, Faculty of Applied Sciences, Univerzitní 22, 326 00 Pilsen, e-mail kkenny@seznam.cz

For dynamic measurements under rotation, vacuum high speed stand was constructed in Doosan Skoda Power. In order to enable dynamic excitation the stand was equipped by a set of alternate electromagnets placed on the duraluminum plates. Boards with 7 electromagnets were placed above and below the blades in the middle distance of 7 mm. This distance was chosen to provide the highest power possible with respect to security. The measurement includes material damping, damping of blade-root connection with disk and the damping caused by energy dissipation in contact areas between friction elements and blade shrouds for several mode shapes.

In theoretical part of this article, the FEM results of in-house code are compared with results obtained by commercial software as well as with measurement. For real-time design process, the methodology for quick and reliable model creation is included. The methodology involves modal condensation in the sense of degree of freedom reduction (for example, disk can be condensed from 13 000 DOF to 320 DOF with minimal error in natural frequencies). This part is important for damping element parameters identification and than for optimization of friction element parameters.

The blades are modelled as one dimensional continuum linked with rigid shroud body in its centre of gravity of last blade profile (Zeman et al., (2009)). Disk is clamped on inner radius to rigid shaft rotating with constant angular velocity ω around its y axis. According to the derivation presented in Rao (1989) the disk can be discretized in the rotating $x\ y\ z$ coordinate system using linear isoparametric hexahedral finite elements (Šašek et al., (2006)). The disk nodes are classified into free nodes and coupled nodes on the outer and inner surface of the blade roots. The mathematical model of the disk was derived in the paper Šašek et al., (2006) using Lagrange's equations.

The detailed methodology for global model creation of the bladed disk with friction elements is introduced and the model behaviours are compared with real measured data. This methodology allows fast model computation. The modal condensation of the bladed disk model is prepared to identification and optimization of friction element parameters.

1. Acknowledgment

This work was supported by the GA CR project No. 101/09/1166 "Research of dynamic behaviour and optimization of complex rotating systems with non-linear couplings and high damping materials".

2. References

Rao, S., S. (1989): *The finite element method of engineering*. Pergamon Press, Oxford.

Šašek, J., Zeman, V. & Hajžman, M. 2006: Modal properties of rotating disks, in *Proceedings of the 22nd Computational Mechanicss 2006* (J. Vimmr ed.), Nečtiny, pp. 593-600.

Zeman, V., Šašek, J. & Byrtus, M. (2009): Modelling of rotating disk vibration with fixed blades. *Modelling and optimization of physical systems, 8* , Gliwice, pp125-130.

Kellner, J. (2009): *Vibration of turbine blades and bladed disks (in Czech)*, Doctoral thesis, UWB, Pilsen.

19th International Conference
ENGINEERING MECHANICS 2013
Svratka, Czech Republic, May 13 – 16, 2013

SALTATION OF SAND IN VICINITY OF CYLINDRICAL COLUMN

I. S. Kharlamova*, A. Kharlamov, P. Vlasák

Abstract: *The paper presents a model of sand sediment transport in water stream in vicinity of a high cylindrical column. It is assumed that an averaged turbulent flow is horizontally layered in vicinity of the cylinder. In each layer the flow around the cylinder is modelled as a potential flow generated by a vertical dipole line. Flow in viscous sub-layer on the surface of the cylinder is neglected. The presented flow model is approximate; however it is simple for use. Trajectories of saltating particles near the cylinder were calculated. Further investigation of such flow will allow a determination of zones where solid particles will collide with the column. That might be useful for prevention of its damage or destruction.*

Keywords: ***Saltation of sand, flow around cylinder, logarithmic profile, dipole line, averaged turbulent flow.***

1. Model of averaged turbulent flow around cylinder

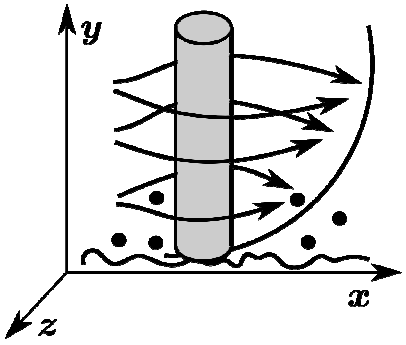

Figure 1. Scheme of average turbulent flow around cylindrical column with sand particles saltating above rough bed.

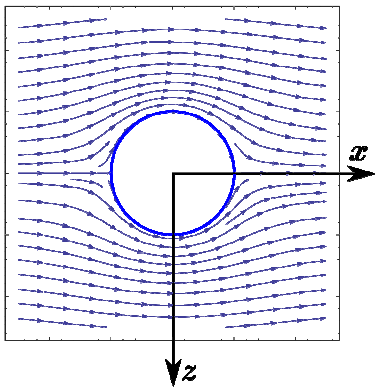

Figure 2. Potential flow in a horizontal plane around a vertical cylinder.

An averaged turbulent flow around a cylindrical column with sand particles saltating above rough bed is consider here, Fig. 1. A uniform turbulent flow above rough plane described by logarithmic law $u_{tx} = u_* / \kappa \ln\left(y / y_0\right)$, where u_* is shear velocity, κ – Karman's constant, y - distance from the bed, y_0 - a constant depending on hydraulic roughness.

It is assumed that the averaged turbulent flow around the cylinder is horizontally layered. All turbulent fluctuations in each layer are neglected; and there is no mixing of layers neither in front of nor past cylinder. The assumption might be true for a high enough cylinder.

For description of two-dimensional flow in each horizontal layer the flow is approximate as potential flow of ideal fluid around cylinder, Fig. 2. Thus, a tree-dimensional problem of turbulent flow above bed and around a cylindrical column is reduced to a two-dimensional problem of flow around a cylinder in each layer.

Potential flow of ideal fluid around a cylinder of radius R_c is the same as a uniform potential flow around a dipole located at the centre of the cylinder at point with radius vector $\vec{r}_c$, Milne-Thomson,

* Mgr. Irina Kharlamova, Mgr. Alexander Kharlamov, Prof. Ing. Pavel Vlasák, DrSc., Institute of Hydrodynamics ASCR, v. v. i.; Pod Pat'ankou 30/5, 166 12, Prague 6, Czech Republic; e-mails: kharlamova@ih.cas.cz, kharlamov@ih.cas.cz, vlasak@ih.cas.cz.

(1960). If the magnitude of unperturbed fluid velocity far from cylinder is u_{tx}, the potential of the dipole is $\varphi(\vec{r}) = -\frac{R_c^2 \vec{u}_{tx}(\vec{r} - \vec{r}_c)}{|\vec{r} - \vec{r}_c|^2}$. Velocity field generated by cylinder in averaged turbulent flow is $\vec{u} = \vec{u}_{tx} + \vec{\nabla}\varphi$. According to the Prandtl's theory, the flow of viscous incompressible fluid around a cylinder can be approximately represented as a combination of a potential flow of ideal fluid around cylinder and a flow in viscous sub-layer on cylinder surface. For saltation purposes, if the thickness of viscous sub-layer is less than diameter of saltating particle, then the flow in viscous sub-layer can be neglected, as saltating particle remains in the sub-layer near cylinder surface relatively short time.

2. Results

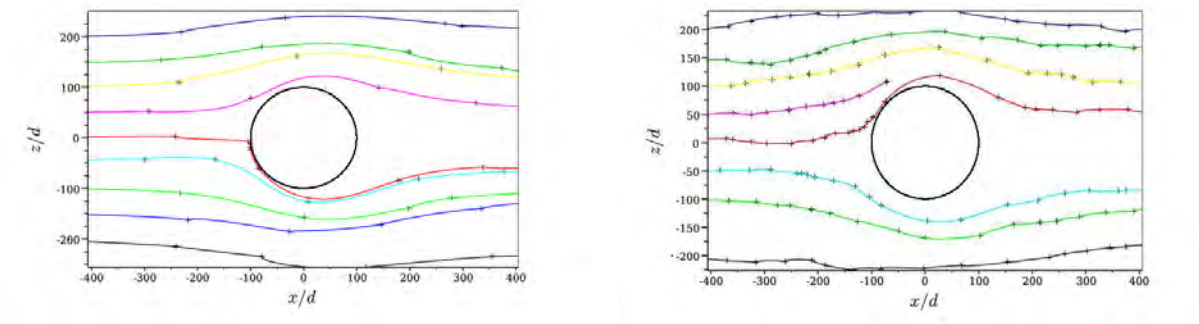

a) *b)*

Figure 3. Examples of saltation trajectories in water in vicinity of vertical cylinder. Diameter of saltating and bed particles is d = 0.001 m. Diameter of the cylinder is $2R_c$ = 0.2 m. shear velocity in a) is $u_* = 0.1$ m/s, $Re = 2R_c u_* /\nu = 20000$; in b) is $u_* = 0.05$ m/s, Re = 10000.

In Kharlamova et al. (2012) there was offered a model of saltation in turbulent flow in wide open channel with rough bed. Now this model is modified for new conditions: for turbulent flow around cylinder in semi-infinite space, where the height of flow is indefinite.

Figure 3 shows trajectories of saltating particles in water. By "+"-signs denote points of collision of saltating particles with bed. At lower shear velocity the particles collide with bed more frequently than at higher shear velocity. The saltating particles collide with the cylinder only on its front side. It's worth noting that at the conditions used for simulation of Fig. 3 the saltating particles move mostly round the cylinder and do not touch it. The trajectories of the particles replicate the streamlines; and particles avoid the zone past cylinder, where turbulent wake should take place.

This model presents a first approximation of the problem, a verification of the model is needed; however, it has its advantages. It allows study of sediment transport in new type of flow geometry. The model can be used for fast estimation of sand movement around cylindrical obstacle and can be extended to the flow past several cylinders, located in a row perpendicular to the flow. It also can be used for determination of zones where solid particles collide with columns most frequently, and thereby, it can help prevent damage of such constructions.

Acknowledgement

Support under the project No. 103/09/1718 of the Grant Agency of the Czech Republic and the Institutional Research Plan No. AV0Z20600510 of the Academy of Sciences of the Czech Republic are gratefully acknowledged.

References

Kharlamova I.S., Kharlamov A.A., Chára Z., Vlasak P. (2012) Numerical study of transition between rolling and saltation movement of spherical particles, *Acta Technica* 57, p. 211–226.

Milne-Thomson L.M. (1960) *Theoretical hydrodynamics*, Macmillan & Co LTD, London.

19th International Conference
ENGINEERING MECHANICS 2013
Svratka, Czech Republic, May 13 – 16, 2013

MODELING OF FIBER ORIENTATION IN FIBER-REINFORCED FRESH CONCRETE FLOW

F. Kolařík [1] **, B. Patzák** [2]

In recent years, popularity of unconventional reinforcing of concrete is growing. Especially fiber reinforcement has very wide usage in high performance concretes like "Self Compacting Concrete" (SCC). Desinging of structures made of fiber-reinforced concrete assumes uniform distribution of the fibers through the structure. Unfulfilling of that assumption can lead to over-estimated design and potentially to collapse of the structure. Therefore, tools for prediction of the distribution and orientation of the fibers in the specimen are needed. This paper deals with developing and implementing suitable tool for prediction of the orientation of fibres in a fluid based on the knowledge of the velocity field. Statistical approach to the topic is employed, where orientation of a fiber is described by probability distribution of the fiber angle.

Keywords: ***Flow, concrete, fibre orientation, probability***

1. Introduction

This paper presents a probabilistic based approach for predicting fiber orientation induced by fluid (SCC) flow. The fluid is considered as a single homogeneous continuous medium. Its motion is governed by the Navier-Stokes equations. Numerical scheme is based on the Finite Element Method. See Donea & Huerta (2003) and Belytschko & Chessa (2003) for further information.

Model of the fiber orientation evolution is based on the probabilistic approach. It assumes that the orientation state of the fiber can be completely described by the probability distribution function of the angle of the fiber. Than, the evolution of the probability distribution evolves due to Fokker-Planck equation, see Olson et al. (2004), Advani & Tucker (1987), Folgar &Tucker (1984).

2. Description of the flow

Problem is described by Navier-Stokes equations. In this work, only 2D flow is considered. The problem formulation can be found in Tezduyar (1991). Constitutive law can be considered as one-parameter (viscosity μ) Newtonian fluid. However, fresh concrete flow has to be described by at least two parameters. Suitable choice is then Bingham model.

[1] Ing. Filip Kolařík, Department of Mechanics, Faculty of Civil Engineering, CTU in Prague, Thákurova 7, 166 27, Prague; CZ, e-mail: filip.kolarik@fsv.cvut.cz
[2] Prof. Dr. Ing. Bořek Patzák, Department of Mechanics, Faculty of Civil Engineering, CTU in Prague, Thákurova 7, 166 27, Prague; CZ, e-mail: borek.patzak@fsv.cvut.cz

3. Description of the fibres

The fibres are assumed to rigid cylinders, uniform in length and diameter. The fibres are distributed uniformly in the specimen. The orientation of a fiber is considered as a random variable. The orientation state at a point in space is described by a probability distribution function, see for examle Advani & Tucker (1987), Folgar &Tucker (1984), Olson et al. (2004). Fokker-Planck type of equation for evolution of distribution function can be formulated for evolution of probability distribution function.

4. Numerical examples

A simple shear flow problem was chosen as a numerical benchmark. At first, the flow inducing the orientation of the fibres is prescribed directly through the fixed value of a strain rate tensor. The same flow problem is modeled via FEM on the rectangular grid. The results are then compared to the first (ideal) case, where the strain rate tensor is prescribed.

5. Conclusion

In this paper, we have shown probabilistic approach to description of a fibre orienation in the fibre-reinforced concrete flow. It was shown that employed approach is useful and computationally manageable.

6. Acknowledgment

The research was carried out within the New Industrial Technologies for Tailor-made Concrete Structures at Mass Customized Prices TailorCrete project, no. 7E10055, suported by the European Community's Seventh Framework Programme.

7. References

J. Donea & A. Huerta (2003) *Finite Element Methods for Flow Problems*, John Wiley & Sons.

J. Chessa & T. Belytschko (2003) An extended finite element method for two phase flow, *ASME J. Appl. Mech.*, Vol 70, 10-17.

J. A. Olson et al. (2004) Modeling a turbulent fibre suspension flowing in a planar contraction: The one-dimensional headbox, *International Journal of Multiphase Flow* 30, 5166.

F. Folgar & C.L. Tucker (1984) Orientation behavior of fibers in concentrated suspension, *J. Reinf. Plast. Compos.*.

S. Advani & C.L. Tucker (1987) The use of tensors to describe and predict fibre orientation in short fiber composites, *J. Rheol.*

T. E. Tezduyar (1991) Stabilized Finite Element Formulations for Incompressible Flow Computations, *Advances in Applied Mechanics*, Volume 28, Pages 1-44.

19th International Conference
ENGINEERING MECHANICS 2013
Svratka, Czech Republic, May 13 – 16, 2013

WEB GIRDER RESISTANCE TO TRANSVERSE FORCES

Y. Koleková[*], I. Baláž[**]

Abstract: *Transverse force denotes the load which is applied perpendicular to the flange in the plane of the web. The loading is usually free and transient, as for crane runway girders or bridge girders during launching, so that in this case transverse stiffeners are not appropriate. A concentrated transverse loading is often referred to as patch loading. The collapse behaviour of girders subjected to transverse loading is characterized by web yielding, buckling or crippling. A separation of these three phenomena accepted in the former standards is not reasonable. The paper describes the design procedure used in the current Eurocodes, shows its application in numerical example and informs about new improvements.*

Keywords: ***Patch loading, design resistance, Eurocodes, numerical example.***

1. Introduction

The design resistance of the webs of rolled beams and welded girders may be determined according to EN 1993-1-5 (2006) in accordance with the clause 6.2 (or cl. 6.7.5 in EN 1999-1-1 (2007)), provided that the compression flange is adequately restrained in the lateral direction.

The load is applied as follows:

a) through the flange and resisted by shear forces in the web, see *Fig. 1(a)*;
b) through one flange and transferred through the web directly to the other flange, see *Fig. 1(b)*;
c) through one flange adjacent to an unstiffened end, see *Fig. 1(c)*.

The interaction of the transverse force F_{Ed}, bending moment M_{Ed} and axial force N_{Ed} may be verified according to sections 3. The interaction of the bending moment M_{Ed}, shear force V_{Ed} and axial force N_{Ed} may be verified using the cl. 7.1 of EN 1993-1-5 (2006) or cl. 6.7.6 in EN 1999-1-1 (2007)). The formulae enabling of the verification of the interaction F_{Ed} and V_{Ed} are investigated in the Evolution Group EG EN 1993-1-5 and they will be available in the next generation of EN 1993-1-5.

The design rules concerning the resistance to transverse force in the standards for steel structures EN 1993-1-5 (2006) and for aluminium alloys structures EN 1999-1-1 (2007) are practically identical.

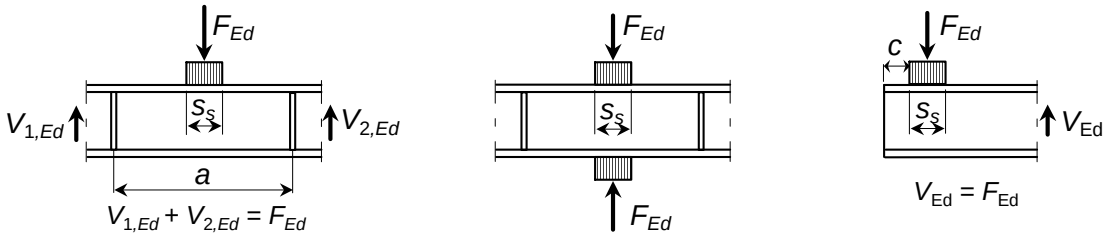

$$k_F = 6 + 2\left(\frac{b_w}{a}\right)^2 \qquad k_F = 3{,}5 + 2\left(\frac{b_w}{a}\right)^2 \qquad k_F = 2 + 6\frac{s_s + c}{b_w} \le 6$$

Type (a) Type (b) Type (c)

Fig. 1: Buckling coefficients k_F for different types of load application

[*] Assoc. Prof. Ing. Yvona Koleková, PhD.: Department of Structural Mechanics, Faculty of Civil Engineering, Slovak University of Technology, Radlinského 11; 813 68, Bratislava; SK, e-mail: yvona.kolekova@stuba.sk

[**] Prof. Ing. Ivan Baláž, PhD.: Department of Metal and Timber Structures, Faculty of Civil Engineering, Slovak University of Technology, Radlinského 11; 813 68, Bratislava; SK, e-mail: ivan.baláž@stuba.sk

2. Verification of resistance F_{Rd} to transverse force F_{Ed}

For unstiffened or stiffened webs the design resistance to local buckling under transverse forces should be taken as

$$F_{Rd} = L_{eff}\ t_w \frac{f_{yw}}{\gamma_{M1}} \tag{1}$$

where the effective length $L_{eff} = \chi_F\ \ell_y$ (2)

The effective loaded length ℓ_y should be calculated as follows:

$$m_1 = \frac{f_{yf} b_f}{f_{yw} t_w} \tag{3}$$

$$\begin{aligned} m_2 &= 0{,}02 \left(\frac{h_w}{t_f}\right)^2 \quad if\ \overline{\lambda}_F > 0{,}5 \\ m_2 &= 0 \qquad\qquad\quad if\ \overline{\lambda}_F \le 0{,}5 \end{aligned} \tag{4}$$

For types a) and b) in *Fig. 1*, ℓ_y should be obtained using:

$$\ell_y = s_s + 2\, t_f \left(1 + \sqrt{m_1 + m_2}\right) \text{ , but } \ell_y \le \text{ distance between adjacent transverse stiffeners} \tag{5}$$

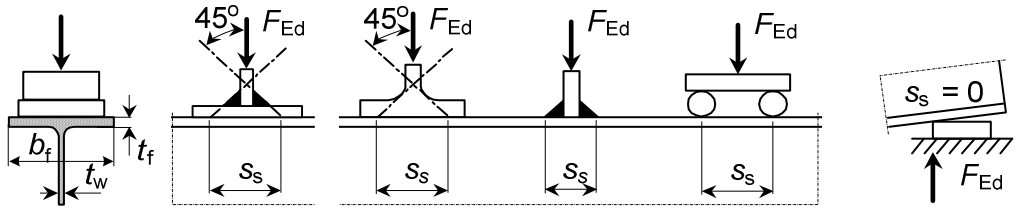

Fig. 2: Length of stiff bearing s_s

The reduction factor χ_F should be obtained from $\chi_F = \frac{0{,}5}{\overline{\lambda}_F} \le 1{,}0$ (6)

where the slenderness $\overline{\lambda}_F = \sqrt{\frac{\ell_y t_w f_{yw}}{F_{cr}}}$ (7)

critical force $F_{cr} = \sigma_{cr} h_w t_w = k_F \sigma_E h_w t_w = k_F \frac{\pi^2 E}{12(1-\nu^2)} h_w t_w = 0.904 k_F E \frac{t_w^3}{h_w} \approx 0{,}9\, k_F E \frac{t_w^3}{h_w}$ (8)

The verification should be performed as follows:

$$\eta_2 = \frac{F_{Ed}}{L_{eff}\ t_w \frac{f_{yw}}{\gamma_{M1}}} \le 1{,}0 \tag{9}$$

Acknowledgements

Project No. 1/0748/13 was supported by the Slovak Grant Agency VEGA.

References

Baláž, I., Koleková, Y. (2013) *Elastic critical buckling stress of the web girder subjected to transverse force.* Proceedings of 19th International conference Engineering Mechanics 2013. May 13 – 16, 2013, Svratka, CR.

EN 1993-1-1 (2005) *Eurocode 3 - Design of steel structures. Part 1-1: General rules and rules for*

EN 1999-1-1 (2007) Eurocode 9 - Design of aluminium structures. Part 1-1: General structural

19th International Conference
ENGINEERING MECHANICS 2013
Svratka, Czech Republic, May 13 – 16, 2013

EXPERIMENT E5/0,1 WITH LATERAL PASSIVE PRESSURE DURING ROTATION ABOUT THE TOE – GRANULAR MASS DEFORMATIONS

P. Koudelka*, J. Bryscejn**

Abstract: *A basic physical experimental research of lateral passive pressure is in progress at the Institute. The research is composed of three doubles of the same experiments with three basic retaining wall movements: rotations about the toe and top and translative motion. The experiment E5/0,1 with passive pressure and pressure at rest during wall rotation about the toe was carried out in 1st half 2012 and it was the first of the same experiment double (the 2nd one was the experiment E6/0,1 finished in the early 2013. Both experiments together should prove a real behaviour of non-cohesive mass acting on moving wall. The behaviour appears distinct from a theory of EUROCODE 7-1 contemporaneously used. Each of experiments has brought a huge data quantity. The paper shows mass deformations and slip surfaces of the experimental sandy mass.*

Keywords: ***Lateral earth pressure, pressure at rest, passive pressure, physical experiments, ideally non-cohesive sand, mass deformation, slip surface, bi-component pressure sensor.***

1. Introduction

A basic research of earth/lateral pressure based on physical and numerical experiments has begun in 1998 at the institute of the authors and it has continued. The physical research should prove behaviour of ideally non-cohesive granular mass during three basic types of structure movement towards active and passive directions The first research period in 1998-2000 aimed on active pressure and in 2001-2002 on the first long/term experiment with passive pressure (E3/0.2). In the course of the second period was developed experimental equipment on an advanced contemporary level. The first experiment with passive pressure E3/0,2 (2001-2) during wall *rotation about the top* was repeated like experiment E5/0,2 (2010) such as a long-term operation test of the new experimental equipment. It brought similar results to E3/0,2 however, with lower pressure values. The experiment E5/0,2 had to be repeated (2011) and a new one was denoted E6/0,2. The second experimental double (E5/0,1 and E6/0,1) searching *rotation about the toe* followed in 2012 and early 2013. Results of a visual mass monitoring of the earlier carried out experiment E5/0,1 are presented in the paper.

2. Experimental equipment

The actual advanced equipment was described in detail formerly (Koudelka & Bryscejn, 2010; Koudelka & Valach & Bryscejn, 2011, 2012). It can be briefly said the equipment has the same sample size (length of 3.0 m, width of 1.0 m, height of 1.2 m) and it is fully controlled by two computers (for front wall movement and data registration, for visual monitoring and photo registration) and reaches up very suitable characterizations: arbitrarily *slow* front wall movement of velocity from of 3.684 to of >0 mm/min. i.e. arbitrarily slow movement, max. pressing force cca 2870 kN, 5 bi-component pressure sensors in front moved wall, 1 three-component sensor and 5 bi-component pressure sensors in back solid wall, 2 +2 movement sensors, 1 impulse summer, max. record frequency of 1000 Hz. The equipment can afford a huge quantity of data of 803 MB/day.

Deformation of the sample and displacements into it are monitored visually. Slip surfaces and uplifts of the sample mass are monitored through the right transparent side due to red strips into the

* Ing. Petr Koudelka, DrSc.: Institute of Theoretical and Applied Mechanics, Czech Academy of Sciences, Prosecká 76; 190 00 Prague 9; CZ, e-mail: koudelka@itam.cas.cz

** Ing. Jan Bryscejn: Institute of Theoretical and Applied Mechanics, Czech Academy of Sciences, Prosecká 76; 190 00 Prague 9; CZ, e-mail: bryscejn@itam.cas.cz

mass (see Fig.1a). Displacements of black little globes located in front sample part in net of 50/50 mm are monitored by camera through the transparent left side. Upper surface of the sample is monitored by two cameras located above both front walls (moved and solid). Visual registration data of cameras are stored separately in the second separate computer.

3 Experiment E5/0,1

All experiments with passive pressure are in progress a motional phase by a reconsolidation phase, altogether of 3motional phases and 4 reconsolidation phases in an area of *pressure at rest* (movements in order 0.1 mm). Then 3 motional phases and 3 reconsolidation phases follow in an area of *passive* pressure according to movement values supposed by EUROCODE 7-1 (Annex C) for: a half of top passive pressure (4^{th} phase – p1a), top passive pressure (5^{th} phase – p1b) and the maximal possible wall movement cca of 150 – 220 mm (the last 6^{th} phase (p2). The first three motional phases of pressure at rest are not measured (invisible changes). The experiments (all) have been begun using a velocity of wall movement of 0.0049 mm/min. The presented experiment E5/0,1 with passive pressure during rotation about the toe was entered 28.2.2012 on and finished successfully on 26.6.2012. The equipment attained the maximal top movement at the experiment end of 152.00 mm (wall height 1.0 m). The experiments (all) use the same dried non-cohesive sand.

4 Results

The experiments bring an extreme data quantity (E5/0,1 of *1.027.GB* in (lfx) or of *30.3 GB* in (ASCII). The paper deals with changes of the sample both inside and outside (deformation, slip surfaces, displacements) regarding wall movement. Data of pressure sensors are mentioned only but not analyzed. The front wall rotation about the toe influences the maximal movement of the top. The wall is very rigid and it behaves like solid structure.

Amplitude and extend of sample deformation is shown through uplift (or stability) and failures (due to slip surfaces) of the red strips on the sample right side and also through uplift and slip surface openings on upper surface of the sample. The figures in the paper can give a good imagine on behaviour of sandy masse during retaining wall rotation about the toe. The maximal final top movement was reached of 152.00 mm. An actual uplift of the red strips and four visible slip surfaces can be seen in Fig. 2b and in detail according measured data in Fig. 3b. An actual uplift of the red strips and four visible slip surfaces can be seen in Fig. 2b and in detail according measured data in Fig. 3b. Not all slip surfaces crosscut through adjacent strip: two slip surfaces nearer to the moved wall were continuous but the other surfaces (farer from the wall) were not continuous what is obvious in Fig. 3b. The surface did not get deep into the sample, e.g. the first two surfaces got in a depth of 0.2 m, the deepest single strip failure was registered in depth of 0.4 m.

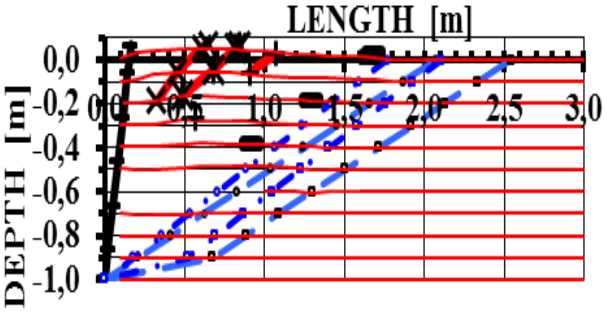

Fig. 2a (left): View on deformation of the sample (especially of front part left) according to the red strips after front wall rotation about the toe. The moved wall is left and the back solid wall is right. Deformation of the sample after the final top movement of 152.00 mm with four slip surfaces in sample front part into depth of about 0.3 m (in detail see Fig. 3b).

Fig. 3b (right): Deformation of the sample after the final top movement of 152.00 mm Measured uplifts of red strips and slip surfaces of the sample. Blue dashed lines are theoretically considered shear surfaces for analysis of passive earth pressure according to ČSN 73 0037 and EUROCODE 7-1.

19th International Conference
ENGINEERING MECHANICS 2013
Svratka, Czech Republic, May 13 – 16, 2013

MECHANICAL PROPERTIES OF FRC WITH VARIOUS FIBER TYPE AND CONTENT

M. Kovář*, M. Foglar**

Abstract: *The paper presents results of a study focused on the mechanical properties of fiber reinforced concrete with different fiber type and content. Original experiments are compared to results available from the literature. Conclusions on the dependence of the fracture energy on the fiber type and content are drawn.*

Keywords: ***Fiber reinforced concrete, fracture energy, strain-rate effect***

Fiber reinforced concrete (FRC) is because of its mechanical properties much more suitable for the use in structures subjected to higher strain rates, e.g. blast or impact loading. The value of fracture energy is the decisive material characteristics for assessment of the damage of concrete structures by loadings with higher strain rates. This paper summarizes the results of the tests focused on fracture energy of fiber reinforced concrete of different strength classes, different fiber types and fiber contents subjected to different loading rates.

The fracture characteristics of FRC are usually tested on beams subjected to three-point bending or on specimens subjected to uniaxial tension. The value of the fracture energy is equal to the area under the force-deflection diagram (F-δ):

$$G_f = \frac{W}{B.H} \tag{1}$$

$$W = \int F.d\delta \tag{2}$$

where W is the area of under the force-deflection diagram and $B.H$ [m] are the cross-sectional dimensions of the crack of the specimen, F [N] is the force which loads the specimen and δ [m] is the deflection the force is causing in the middle of the span of the specimen. The area under the force-deflection diagram is taken for a limited deflection. When the loading of the specimen continues until the collapse, the value B.H is equal to the area of the concrete specimen.

The tests described in this paper were not performed according to the RILEM recommendations. The specimens are beams, 150x150x700mm with the span of 600mm. No notch is used for the definition of the position of the macro-crack. The specimen is loaded by four-point bending, the forces divide the span into thirds. The benefit of this test arrangement is the constant value of the bending moment in the middle third of the specimen and elimination of the effect of the shear force.

The experiments were performed on two different strength classes of concrete and varying fiber type and content. The strength classes of concrete were chosen C30/37 and C55/67. For both types of concrete, two different materials of fibers with two different fiber contents were tested. The poly propylene (PP) 54mm long fibers were used in dosages of 4,5 and 9 kg/m3 (0.5% and 1%), the steel fibers were used in dosages of 40 and 80 kg/m3 (0.5% and 1%). In total, 8 options were used. Every material option was tested at three speeds of deformation to verify the dynamic increase factor and the

* Ing. Martin Kovář: Department of concrete and masonry structures, Czech Technical University, Thákurova 7; 166 29, Prague; CZ, e-mail: martin.kovar@fsv.cvut.cz

** Ing. Marek Foglar, Ph.D.: Department of concrete and masonry structures, Czech Technical University, Thákurova 7; 166 29, Prague; CZ, e-mail: marek.foglar@fsv.cvut.cz

influence of the loading rate on the fracture energy. The speeds of deformation were chosen 0.2 mm/min (approximately static loading), 2mm/min and 6 mm/min. The results of the experiments and corresponding strain rates are summarized in Table 1.

Tab. 1: Comparison of the fracture properties of FRC specimens (material of the fibers, fiber content and strength class)

Influence of the fiber content	**F_{CLS}**		**G_f**	
C30/37, 0,2mm/min	0,5% PP	1% PP	0,5% PP	1% PP
	1,00	**0,97**	1,00	**1,91**
	0,5% FE	1% FE	0,5% FE	1% FE
	1,00	**1,26**	1,00	**1,73**
C55/67, 0,2mm/min	0,5% PP	1% PP	0,5% PP	1% PP
	1,00	**1,08**	1,00	**2,92**
	0,5% FE	1% FE	0,5% FE	1% FE
	1,00	**1,01**	1,00	**1,67**
Influence of the material of the fibers	**F_{CLS}**		**G_f**	
C30/37, 0,2mm/min	0,5% PP	0,5% FE	0,5% PP	0,5%FE
	1,00	**0,92**	1,00	**2,53**
	1% PP	1% FE	1% PP	1% FE
	1,00	**1,18**	1,00	**2,29**
C55/67, 0,2mm/min	0,5% PP	0,5% FE	0,5% PP	0,5%FE
	1,00	**1,16**	1,00	**2,17**
	1% PP	1% FE	1% PP	1% FE
	1,00	**1,09**	1,00	**1,24**

The experiments showed great influence of the fiber type and content on the fracture energy of FRC.

The fracture energy rises with the increasing fiber content.

The increase of the speed of deformation from 0.2 mm/min to 2 mm/min caused an increase of the fracture energy. Yet, the further increase of the speed of deformation to 6 mm/min did not cause further increase of the fracture energy.

The increase of the strength class of concrete causes increase of the fracture energy of the PP-fiber FRC. The increase of the strength of concrete did not cause increase of the fracture energy of the FRC.

The increase of the concrete tensile strength was shown with the increased speed of deformation.

Fiber reinforced concrete (FRC) is because of its bigger ductility much more suitable for the use in structures subjected to higher strain rates, e.g. blast or impact loading. The value of fracture energy is the decisive material characteristics for assessment of the damage of concrete structures by loadings with higher strain rates and is used for calibration of material models.

Acknowledgement

This paper was supported by the Czech Ministry of Interior project MVČR VG20132015114, the Grant Agency of the Czech Republic Grant Projects No. GAČR13-30441S and the CTU project No. SGS13/077/OHK1/1T.

19th International Conference
ENGINEERING MECHANICS 2013
Svratka, Czech Republic, May 13 – 16, 2013

CLIMATIC WIND TUNNEL FOR MATERIAL AND STRUCTURES INVESTIGATION

R. Král, S. Pospíšil [1]

Summary: *The paper deals with a description of the new climatic wind tunnel laboratory built in historical city Telč. The tunnel will be used for fundamental research in engineering problems within civil engineering, architecture, heritage care and in other fields where wind effects appear along with further factors.*

Keywords: Climatic Tunnel; Flow Resistance; Aerodynamics; Tunnel Testing.

1. Introduction

New climatic wind tunnel laboratory was founded in spring 2012 within the project "Centrum Excelence Telč" (CET). This facility will serve basically for investigation of climatic effects on historical buildings and monuments. Because of unique combination of the aerodynamic working section and climatic chamber, the tunnel offers investigation of mutual interaction of several physical phenomenon at the same time ever at constant laboratory conditions.

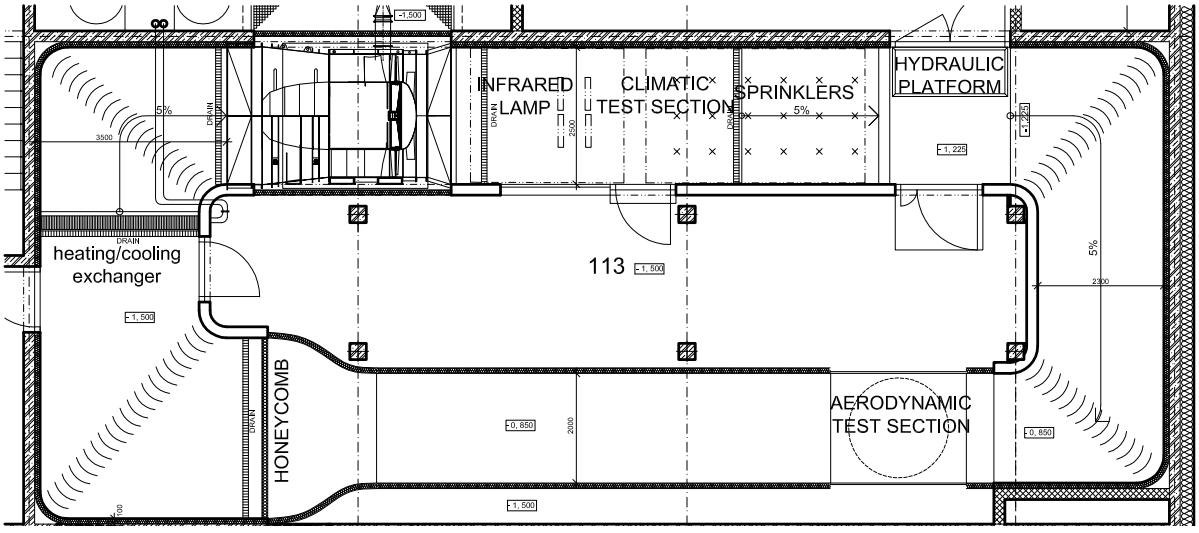

Fig. 1: Ground plan of the wind tunnel laboratory. It is designed in oval closed shape adapted for aerodynamic and climatic testing.

[1] Ing. Radomil Král, Ph.D., Doc.Ing. Stanislav Pospíšil, Ph.D, Institute of Theoretical and Applied Mechanics, Prosecká 76, 190 00 Prague 9, tel. +420 286 88 21 21, e-mail kral@itam.cas.cz

2. Facility description and pressure losesses estimation

From the operating point of view, the climatic wind tunnel consists of two fundamental parts - (i) aerodynamic part and (ii) climatic part, see Fig. 1. While the aerodynamic part provides well-fitted conditions to study wind effects on scaled model of prototypes, an equipment of the climatic part is suited for investigation of influences of weather including the wind, temperature, rain and radiant heat. This arrangement takes an advantage in wide universality and adaptability to experimental demands.

The fan is fundamental part of the tunnel. Powered by 200kW motor, it delivers a possibility to reach the wind velocity of more than 30 m/s. Using the cooling/heating exchanger cycle temperature changing of the airflow is available within the range of -5 to 30 °C in raletively short time. Furthermore, the laboratory provides rain simulators and infrared lamps that allow loading the structures by rain and heat radiation, respectively. Integral part of the tunnel equipment consists of instruments for airflow diagnostic, data acquisition system, direct pressure surface measurement, precise thermometry, etc.

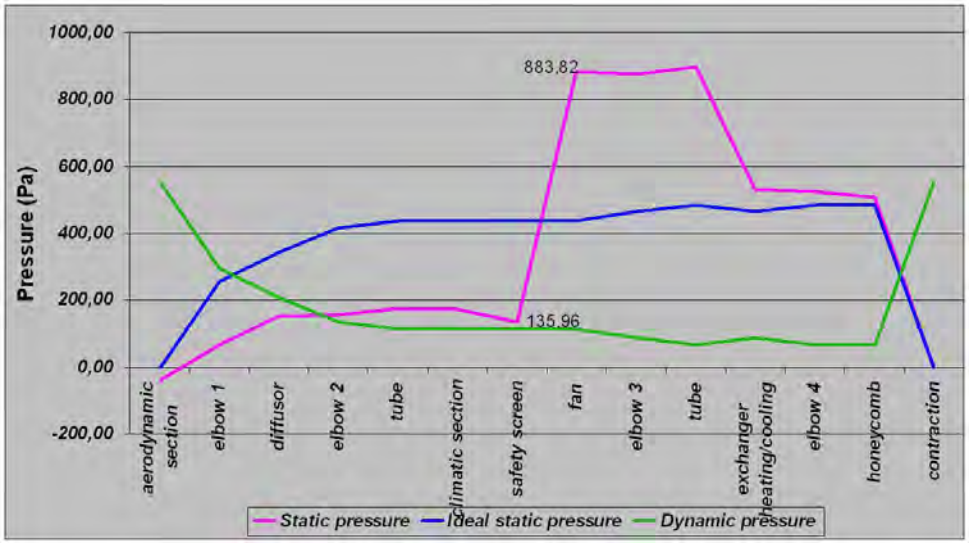

Fig. 2: Pressure development along the longitudinal centerline. The magenta line represents an estimation of static pressure including flow resistance of tunnel elements.

Using two-dimensional computational fluid dynamic model, see (Tezduyar T.E. , 1992), and design guide of flow resistance, see (Fried and Idelchik , 1989), the principal parts of the tunnel are designed taking into account both the optimal flow characteristics and flow resistance. In Fig. 2, pressure development along the longitudinal tunnel centerline is displayed. The strong discontinuity of the magenta line clearly shows the required pressure gain of the fan to overcome windage losses emerging when the maximal wind speed requirement is met.

Acknowledgment

The support of the project CZ.1.05/1.1.00/02.0060 is gratefully acknowledged.

Reference

Fried, E. & Idelchik, I.E. 1989: *Flow Resistance: A Design Guied for Engineers.* Taylor&Francis, London.

Tezduyar T.E. 1992: Stabilised Finite Element Formulations for Incompressible Flow Computations. *Advances in Applied Mechanics, volume 28*, 1–44.

19th International Conference
ENGINEERING MECHANICS 2013
Svratka, Czech Republic, May 13 – 16, 2013

SPHERICAL NANOINDENTATION APPLIED TO ALUMINIUM FOAM

V. Králík*, J. Němeček**

Abstract: *Nanoindentation is widely used for the assessment of micromechanical behavior of multiple phases within the material microstructure. Evaluation is often restricted to isotropic linearly elastic solids compared to engineering macroscopic tests in which stress–strain curves are analyzed to find variety of constitutive parameters (e.g. viscous, plastic). In this paper, we identify, in addition to the elastic properties, also inelastic properties that can be directly deduced from the load–depth curve of a spherical indentation test through formulations of the effective indentation strain and stress. The accuracy of the determined material properties derived from spherical indentation depends on the accurate knowledge of the indenter shape. Therefore, calibration and determining the exact geometry of the spherical tip compared with a conical tip is described in details.*

Keywords: ***aluminium foam, porous system, spherical nanoindentation, micromechanical properties, plastic properties.***

1. Introduction and theory

Instrumented indentation with spherical indenter is widely used for characterization of local mechanical properties of various materials and offers several advantages comparing to the indentation with sharp indenters. Using spherical indenter, the contact pressure and strains under the indenter are gradually changed as the indentation depth increases while the deformation remains constant in the case of sharp indenters (Menčík, 2011).

For elastic–plastic behavior of metals, Tabor (1951) proposed definitions of indentation stress and representative strain which can be used instead of true stress and strain measured in a conventional tensile or compression test. Indentation (or representative) stress is given by:

$$\sigma_{repr} = \frac{P_m}{C} = \frac{P}{C\pi a^2}, \tag{1}$$

where P_m is the mean contact pressure, P is the load and a is the contact radius. The parameter C is reffered to as "constraint factor" which equals approximately to 3 for most of the engineering materials. This factor is actually the degree by which the resistance to plastic flow is higher than the uniaxial flow stress. The increase in this resistance arises mainly from the fact that the plastic zone beneath the indeter is confined by a large volume of material which is elastic. Representative (or average indentation) strain is given by Tabor (1951):

$$\varepsilon_{repr} = 0.2\frac{a}{R}, \tag{2}$$

where a is the contact radius, R is the radius of the spherical indenter.

2. Results

Partial unloading indentation with increasing load were performed up to maximum load of 3 mN for 10 μm indenter radius and 5 mN for 5 μm indenter radius. The correct determination of material

* Ing. Vlastimil Králík: Faculty of Civil Engineering, Department of Mechanics, Czech Technical University in Prague, Thákurova 2077/7; 166 29, Prague; CZ, e-mail: vlastimil.kralik@fsv.cvut.cz

** Doc. Ing. Jiří Němeček, Ph.D.: Faculty of Civil Engineering, Department of Mechanics, Czech Technical University in Prague, Thákurova 2077/7; 166 29, Prague; CZ, e-mail: jiri.nemecek@fsv.cvut.cz

properties by spherical indenter depends on the exact knowledge of its radius. Therefore, the calibration curve R_{eff} (h_c) for spherical indenters of nominal radius 5 and 10 μm (Fig. 1) was used instead of nominal radius of the tip R (Menčík, 2011). Indentation load and depth data from individual cycles were used for the construction of the true stress-strain diagram as shown in Fig. 2 (using Eqs. (1) and (2)). As a first approximation, an elasto-plastic material model with isotropic linear hardening can be assumed. Then, the plastic parameters are described by two constants, the yield point (σ_y) and tangent modulus (E_{tan}) as depicted in Fig. 2. The elastic modulus was evaluated for individual indents at each unloading cycle using standard Oliver and Pharr methodology. Resulting elastic modulus E_{Al} = 57.1 ± 4.4 GPa was obtained by averaging results from all cycles of selected curves (n=7). The tangent modulus was obtained by least square fitting of the measured points (Fig. 2) using linear approximation. The yield point was found as an intersection of elastic and plastic branches in the diagram (Fig. 2). The evaluated elastic and plastic parameters of Al-rich phase of the material are listed in Tab. 1.

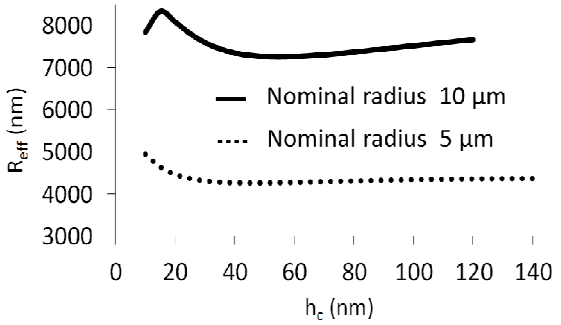

Fig. 1. Effective radius R_{eff} as a function of contact depth h_c. Nominal radius R = 5 μm and R = 10 μm.

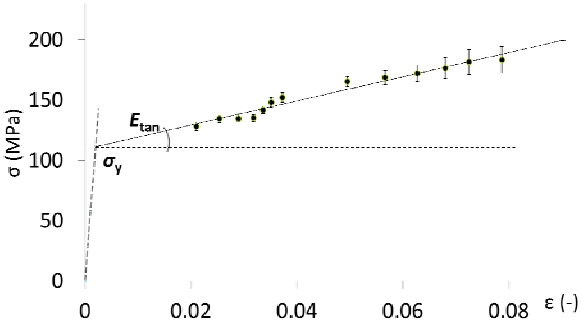

Fig. 2. Stress–strain relations obtained by nanoindentation with different indenter radii (Alporas cell wall, Al-rich phase)

Tab. 1: Resulting material constants for Alporas cell wall, Al-rich phase.

Elastic modulus	E [GPa]	57.1 ± 4.4
Yield point	σ_y [MPa]	111.1 ± 0.6
Tangent modulus	E_{tan} [MPa]	1001.6 ± 112.7

3. Conclusions

The partial unloading indentation technique with two different indenter radii was used for the prediction of the local mechanical behavior of prevailing phase in the aluminium foam cell wall. Stress–strain relations were constructed from nanoindentation experiment using Tabor's formulae. Plastic parameters were assessed assuming elasto-plastic material model with linear isotropic hardening. The values of yield point and elastic modulus are in good agreement with the range of values based on FEM model reported for Alporas® by Zlámal et al. (2012).

Acknowledgement

Support of the Czech Science Foundation (GAČR P105/12/0824) and the Grant Agency of the Czech Technical University in Prague (SGS12/116/OHK1/2T/11) is gratefully acknowledged.

References

Menčík J. (2011) Opportunities and problems in nanoindentation with spherical indenters, *Chemické Listy*, 105, pp. 680-683.

Tabor D. (1951) *Hardness of Metals*. Clarendon Press, Oxford.

Zlámal P., Jiroušek O., Králík V. (2012) Identification of elasto-visco-plastic constitutive material model with damage for porous material based on the indirect finite element simulation of the nanoindentation test, in: *Proceedings of the 13th Bilateral Czech/German Symposium* (CTU in Prague, Faculty of Transportation Sciences), pp. 107-110.

19th International Conference
ENGINEERING MECHANICS 2013
Svratka, Czech Republic, May 13 – 16, 2013

THE ANALYSIS OF THE BOUNDARY CONDITIONS FOR THE COMPRESSIBLE GAS FLOW AS A MODIFICATION OF THE RIEMANN PROBLEM

M. Kyncl, J. Pelant [1]

ABSTRACT

Keywords: compressible gas flow, the Riemann problem, boundary conditions.

The correct design of the boundary conditions plays an important role in the computational fluid dynamics (CFD). We present a special construction of the boundary conditions in order to match the experimental data. We work with the system of equations describing non-stationary compressible turbulent fluid flow (2D,3D), i.e. the Reynolds-Averaged Navier-Stokes (RANS) equations, and we focus on the numerical solution of these equations and on the boundary conditions. The boundary values (for the density, velocity, pressure) must satisfy the considered system of equations. Many boundary conditions (i.e. fixed, linearized) don't satisfy this eligible demand, and bring non-physical errors into the solution, slow down convergent process, and may even ruin the solution in the whole domain. In our general approach we seek the boundary values as the solution of the incomplete initial-value problem complemented with various given data. This approach can be used within various methods in CFD.

We choose the well-known finite volume method to discretize the analytical problem, represented by the system of the equations in generalized (integral) form. To apply this method we split the area of the interest into the elements, and we construct a piecewise constant solution in time. The crucial problem of this method lies in the evaluation of the so-called fluxes through the edges/faces Γ_{ij} of the particular elements. The values in the vicinity of the edge Γ_{ij} at time instant t_k are known, and form the initial conditions (LIC - left-hand side, and RIC - right-hand side) for the so-called Riemann problem for the 2D/3D split Euler equations. The exact (entropy weak) solution of this problem cannot be expressed in a closed form, and has to be computed by an iterative process (to given accuracy). Therefore various approximations of this solution are used. We decided to use the analysis of the exact solution also for the discretization of the fluxes through the boundary edges/faces. At the boundary faces we deal with the local modified Riemann problem, where the LIC is given, while the RIC is not known. In some cases (far field boundary) it is wise to choose the RIC here as the solution of the local Riemann problem with given far field values, which gives better results than the solution of the linearized Riemann problem, see Dolejsi (2006). Another boundary condition based on the exact Riemann problem solution, simulating the impermeable wall on move, was shown in (TORO, 1997, pages

[1] RNDr. Martin Kyncl, Ph.D., RNDr. Jaroslav Pelant, CSc., Výzkumný a zkušební letecký ústav, VZLÚ, Beranových 130, 199 05 Praha - Letňany, Czech Republic, tel. +420 225 115 521, e-mail kyncl@vzlu.cz, pelant@vzlu.cz

221-225), where the RIC is constructed in a special way, in order to obtain the desired solution. Using the analysis of the Riemann problem we show, that the RIC for the local problem can be partially replaced by the suitable complementary condition. We suggest such complementary conditions (by preference of pressure, temperature, velocity, total quantities,...) to yield physically relevant data, see Kyncl (2011) . On the contrary to the initial-value Riemann problem, the solution of such boundary problems can be written in the closed form.

We construct own algorithms for the solution of the boundary problem. We emphasize that the computed boundary values are chosen such a way that the local modified Riemann problem has a solution. Algorithms were coded and used within our own developed code for the solution of the compressible gas flow (the Euler, NS, and RANS equations). Numerical examples show superior behavior of the suggested boundary conditions. Constructed boundary conditions are robust and accelerate the convergence of the method. This is the original result of our work.

Acknowledgment
This result originated with the support of Ministry of Industry and Trade of Czech Republic for the long-term strategic development of the research organisation. The authors acknowledge this support.

References

E. F. Toro 1997: *Riemann Solvers and Numerical Methods for Fluid Dynamics*. Springer, Berlin.

V. Dolejší 2006: Discontinuous Galerkin method for the numerical simulation of unsteady compressible flow. *W*SEAS Transactions on Systems,5(5):1083-1090.

M. Kyncl 2011: Numerical solution of the three-dimensional compressible flow. Doctoral Thesis, Charles University, Prague.

19th International Conference
ENGINEERING MECHANICS 2013
Svratka, Czech Republic, May 13 – 16, 2013

CARRYING CAPACITY OF ROUND TIMBER BOLTED JOINTS WITH STEEL PLATES UNDER STATIC AND CYCLIC LOADING

A. Lokaj[*], K. Klajmonová[**], D. Mikolášek[***]

Abstract: *Aim of this article is in presentation of results of static and dynamic tests of round timber bolted connections with slotted – in steel plates. Round timber joints static tests in tension were made on pressure machine EU100 in laboratory of the Faculty of Civil Engineering VSB-TU Ostrava. Results of laboratory tests have been statistically evaluated and completed by graphical records of deformation response on loading. Round timber joints multicyclic dynamic (fatigue) tests in tension were made on pulsator INSTRON in laboratory of ITAM CAS Prague.*

Keywords: ***Round timber, bolt, joint, carrying capacity, static, dynamic, multicycle, fatigue.***

1. Introduction

Nowadays timber constructions made of round timber become increasingly popular. It concerns footbridges, bridges, watchtowers or playground equipment. If these constructions are designed with truss supporting system, elements connections are often made of bolts with slotted-in steel plates (gusset plates). Connections from round timber don`t have sufficient support in existing Eurocodes. Problem is also in determination of cyclically loaded round timber joints (fatigue loading in wood e.g. (Malo, K. A. et al., 2002) and (Smith, I. et al., 2003).

Fig. 1-A/B: Tested sample in the press EU 100 (A - left), dynamic test - Pulsator INSTRON (B - right)

2. Description of the static tests

Samples of round timber bolt connections with slotted - in steel plates were tested for carrying capacity and deformation of a single tension – up to the failure of connection. Carrying capacity and

[*] Doc. Ing. Antonín Lokaj, Ph.D.: Faculty of Civil Engineering, VŠB-Technical University of Ostrava, L. Podéště 1875; 708 33 Ostrava-Poruba; CZ, e-mail: antonin.lokaj@vsb.cz

[**] Ing. Kristýna Klajmonová: Faculty of Civil Engineering, VŠB-Technical University of Ostrava, L. Podéště 1875; 708 33 Ostrava-Poruba; CZ, e-mail: kristyna.klajmonova.st@vsb.cz

[***] Ing. David Mikolášek, Ph.D.: Faculty of Civil Engineering, VŠB-Technical University of Ostrava, L. Podéště 1875; 708 33 Ostrava-Poruba; CZ, e-mail: david.mikolasek@vsb.cz

deformation of connections under static loading was measured in this test, results were compared with the calculation of carrying capacity according to current applicable European standard for design of timber structures – Eurocode 5. Spruce round timber with diameter 120 *mm* and sample length 450 *mm* was used. The bolts made of HS (High Strength Steel) steel category 8.8 with diameter 20 *mm* were used. Connection plates made of steel S235 with thickness 8 *mm* were used. Nine test samples were produced reasonably (Figure 1-A). Tensile tests were conducted on the press EU100 with a recording system.

3. Dynamic multicyclic tests of bolted joints

Dynamic tests on similar testing samples had been prepared on the base of results of static tests of bolted joints carrying capacity. The dynamic tests were carried out on pulsator device – INSTRON (Fig. 1-B) in laboratory of ITAM CAS Prague. Length of samples was 700 *mm*, diameter of round timber was 120 *mm*, diameter of bolts was 20 *mm*. Pulsator INSTRON allows loading test samples by tension forces 0 to max. 100 *kN* with frequency up to 5 *Hz*. Only 14 samples there were tested due to limited financial and time possibilities. Magnitude of tension forces was between 80 % and 140 % of average static carrying capacity of the joints. Frequency was 3 or 4 *Hz*. There were achieved various number of loading cycles (3 – 120000).

4. Conclusion

The results of static testing of round timber bolted joints with slotted-in steel plates indicate well corresponding with calculated values according to Eurocode 5, in spite of relatively large dispersion of measured values. During dynamic testing (by multicycling passing loading) smaller part (one third) of tested samples failed in different way in opposite to static tests – by block shear. In several first cycles small plastic zone in timber element under bolt can be observed and it protected round timber element from rapid development of initial crack.

Acknowledgement

This outcome has been achieved with funds of conceptual development of science, research and innovation assigned to VŠB-TU Ostrava by Ministry of Education Youth and Sports of the Czech Republic.

References

Eurocode 5: Design of timber structures - Part 1-1: General – Common rules and rules for buildings. 2004.

Krejsa, M., Janas, P. and Čajka, R. (2013) Using DOProC Method in Structural Reliability Assessment. *Applied Mechanics and Materials: Mechatronics and Applied Mechanics II*. Editors: Ching Kuo Wang and Jing Guo. Zurich, Switzerland: Trans Tech Publications, 2013, Vols. 300 - 301, p. 860-869 (10 p). ISSN 1662-7482. DOI: 10.4028/www.scientific.net/AMM.300-301.860.

Kuklík, P., Kuklíková, A. (2000) Nondestructive Testing of Solid Timber, in: *Proceedings of International Conference on Wood and Wood Fiber Composites*, Stuttgart, pp. 303-312.

Kuklík, P. (2005) *Timber Structures (in Czech)*, Prague, ISBN 80-86769-72-0.

Lokaj, A. et al.. (2010) *Timber buildings and timber structures, chapter I. and II. (in Czech).* CERM Akademické nakladatelství Brno, ISBN 978-80-7204-732-1.

Lokaj, A., Marek, P. (2009) Simulation-based reliability assessment of timber structures, in: *Proceedings of the 12th International Conference on Civil Structural and Environmental Engineering Computing*. Funchal, Madeira, ISBN 978-190508830-0.

Lokaj, A., Vavrušová, K. (2011) Contribution to the probabilistic approach of the impact strength of wood, in: *Engineering Mechanics 2011*, Svratka, pp. 363 - 366, ISBN: 978-80-87012-33-8.

Malo, K. A. et al. (2002) Fatigue Tests of Dowel Joints in Timber Structures, Part II: Fatigue Strength of Dowel Joints in Timber Structures. *Nordic Timber Bridge Project*, ISBN 82-7120-035-6. Nordic Timber Council AB, Stockholm, Sweden.

Smith, I. et al. (2003) *Fracture and Fatigue in Wood*. John Wiley & Sons, England.

Vavrušová, K., Lokaj, A. and Žídek, L. (2012) Reliance of embedment strength on dowel diameter in joinst of cement-splinter boards, in: *Applied Mechanics and Materials, Vol. 188 (2012), pp 242-246.*

19th International Conference
ENGINEERING MECHANICS 2013
Svratka, Czech Republic, May 13 – 16, 2013

ASSESSMENT OF BUILDING STRUCTURE LOADED BY TERRORIST EXTERNAL EXPLOSION

D. Makovička[*], D. Makovička[**]

Abstract: *An example of dynamic analysis of a new reinforced concrete structure, loaded with a terrorist charge explosion of 90 kg TNT located in a car in the distance of 18.3 m from the threatened structure, was used to apply the principles of simplified engineering analysis of an explosion-loaded structure based on time courses of calculated internal forces and displacements of individual structure elements. The criteria of structural elements failure due to explosion load effects were determined as a part of the dynamic structure response assessment.*

Keywords: ***explosion, blast wave, building, dynamic response, assessment.***

1. Introduction

In the process of evaluating the building structure response to the effects of an explosion, specific conditions of the given locality and of the building structure should be considered, based on which the structure response to explosion load can be estimated, either more accurately by a calculation or approximately based on empiric formulas and criteria (Makovička & Makovička, 2012 and Makovička & Janovský, 2008). In particular, this applies to the type and location of the pressure wave source compared to the structure under evaluation, characteristics of the pressure wave at the source, and especially the course of explosion pressure in time.

2. Evaluation of the structure response

The magnitudes of the internal forces in the structure are considered as a part of the evaluation of the limit bearing capacity conditions, based on load combinations when they are reduced using ductility factor q. The resulting internal forces are then evaluated on the basis of design standards for the appropriate structure material type, or as a variant, also according to its increased strength using factor k_1. However, this procedure entails two important uncertainties in the case of bent structures, i.e. a suitable choice of the ductility factor, on the one hand, and the material strengthening factor, on the other. During very rapid reshaping of the structure, which is typical for explosion loads, both factors may achieve numeric values of the order of tens, and not only of units, as mentioned above. Thus they may lead to considerable overdesigning of the structure. Evaluations of structures loaded by an explosion based on dynamic displacement and rotation round the central line of plate, wall or beam systems during the action of a dynamic load of this type have been of very topical interest in recent times, as regards the process of evaluating the effects of an explosion on a structure.

The dynamic rotation round the central line of an appropriate structure element is therefore the criterion used to evaluate the response occurring at the following angle

$$\psi = \text{arctg}\,(x_m / (0.5\, h_{span})) \qquad (1)$$

where x_m is the maximum achieved dynamic displacement caused by the explosion load and h_{span} is the span of the plate ceiling structure or the height of the wall structure within one storey, or the span of any beam, the height of a column, etc.

[*] Doc. Ing. Daniel Makovička, DrSc.: Klokner Institute, Czech Technical University in Prague, Šolínova 7; 166 08, Prague 6; CZ, e-mail: daniel.makovicka@klok.cvut.cz

[**] Ing. Daniel Makovička, Jr.: Static and Dynamic Consulting, Šultysova 170; 284 01 Kutná Hora; CZ, e-mail: d.makovicka@makovicka.cz

Tab. 1: Limit failure angle ψ_{max} [°] upon breaking of the material (Makovička 1998, 1999)

Type	*Structure material*	ψ_{max} [°]
1	*Concrete C16/20 to C40/50*	*6.5*
2	*Masonry, full bricks 10, mortar 4 or mortar 10*	*5.0*
3	*Masonry, cement bricks, mortar 4*	*4.5*
4	*Masonry, cellular concrete or perforated precise blocks, mortar 4*	*4.0*
5	*Steel S235*	*10.5*
6	*Wood, hard and soft*	*12*
7	*Window glass, thickness 3 mm*	*6*

The mean occurrence of damage corresponds to the damage to reinforced concrete or masonry elements, e.g. spalling, or the occurrence of tiny cracks in the structure elements, which pose no threat to their stability and can be repaired, e.g. by grouting. However, hazardous occurrence of damage approaches emergency level damage, and its failure angle is found at the lower limit, below the maximum failure angle value ψ_{max}, see Tab. 1.

3. Conclusion

The structure response based on the results of a 3D dynamic computation according to the magnitude of internal forces and displacements, and partial rotation of the central line of beam or slab cross-sections of the structure. It corresponds to the most recent research trends. The authors used limit values determined experimentally upon explosion load of brick-layered, reinforced concrete and window glass boards based on comparing their own and other published results (Henrych, 1979 and MC Cann & Smith, 2007).

Acknowledgement

This research was supported as a part of the research projects in GAČR P105/11/1580 Transient response of structure under short-term dynamic or impact load due to seismic effects and explosions, for which the authors would like to thank the Agency.

References

Henrych, J. (1979) *The dynamics of explosion and its use*, Academia Prague.

Makovička, D. (1998) Shock wave load of window glass plate structure and hypothesis of its failure. In: *Structures Under Shock and Impact '98. Computational Mechanics Publications*, WIT Press Southampton, pp. 43-52.

Makovička, D. (1999) Failure of masonry under impact load generated by an explosion. *Acta Polytechnica*, Vol. 39, No. 1, pp. 63-91.

Makovička, D. & Janovský, B. (2008) *Příručka protivýbuchové ochrany staveb*, Česká technika – nakladatelství ČVUT v Praze.

Makovička, D. & Makovička, D. (2012) Blast resistant design and limits of the response of a structure to an external explosion, In: Schleyer, G. & Brebbia, C.A (Eds.): *Structures Under Shock and Impact XII*, WIT Press Southampton, pp. 229-239.

McCann, D.M. & Smith, S.J. (2007) Blast resistant design of reinforced concrete structures, *STRUCTURE magazine*, pp. 22-26.

19th International Conference
ENGINEERING MECHANICS 2013
Svratka, Czech Republic, May 13 – 16, 2013

HARMFUL GAS DISPERSION IN COMPLEX TERRAIN

P. Michálek*, D. Zacho**

Abstract: *Experiments on gas dispersion modeling in boundary layer wind tunnel were and will be performed in order to verify a software for modeling of gas dispersion in urban area and complex terrain, which is being developed in VZLU.*

Keywords: ***Gas dispersion, wind tunnel modeling***

1. Introduction

Expansion of human society has negative impacts on the environment. Atmospheric boundary layer is one of the most endangered spheres. People living in cities are threatened with different types of gas pollution, i.e. transport emissions, local furnaces and industrial emissions. Probably most dangerous case is an industrial accident or terrorist attack with massive harmful gas leakage into the atmosphere. Prediction of gas dispersion and concentration in nearby area of possible sources of harmful gases is therefore important and may save lives, health and material values.

2. Physical modeling

Physical modeling is an experimental technique, which uses building models and wind tunnel in order to simulate flow in Earth boundary layer as precise as possible. This technique is often used for verification and comparison of results from mathematical modeling. Mathematical modeling by the means of CFD (Computational fluid dynamics) is nowadays a primary tool for gas dispersion research. However, computer modeling requires real initial and boundary conditions in order to create valid results. These conditions can be provided using measurements in wind tunnel. Afterwards, physical modeling with same models as in computer modeling is used to compare the results of both methods and verify that computer calculations are correct and as precise as possible.

2.1. Similarity conditions and simulation tools

Physical modeling is based on a principle of similarity between flow in atmospheric boundary layer and flow in so-called boundary layer wind tunnel (BLWT). BLWT in VZLU is able to simulate geometric and dynamic flow similarity. Guidelines for gas emission modeling were proposed by Snyder (1981).

The BLWT in VZLU is an open circuit wind tunnel with 55 kW fan and 1,8 x 1,5 m cross section. The test section where boundary layer develops is 13,6 m long. Maximum flow velocity above the boundary layer is 25 $m.s^{-1}$. Model section is 2 m long and contains a turntable, where wind direction impacting the model can be changed. Velocity above the boundary layer is monitored by Pitot-static tube and hot-wire transducer probe. Static pressures along the entire wind tunnel are monitored as well using pressure transducers.

The used boundary layer simulates suburban areas according to Eurocode 1 (2007). Its mean velocity profile is described with logarithmic distribution (Jirsák & Ulman, 2001). Velocities in boundary layer were measured by means of hot-wire anemometer with dual-sensor probe.

* Ing. Petr Michálek, Ph.D.: Department of Aerodynamics , Aerospace Research and Test Establishment (VZLU), Beranových 130; 199 05, Praha 9; CZ, e-mail: michalek@vzlu.cz

** Mgr. David Zacho, Ph.D.: Department of Aerodynamics , Aerospace Research and Test Establishment (VZLU), Beranových 130; 199 05, Praha 9; CZ, e-mail: zacho@vzlu.cz

3. Experimental setup and results

In order to simulate gas leakage near ground level, small chamber sized 30x30x15 mm with filtration fabric on top was placed in the turntable centre in tunnel floor. This point source can simulate continuous leakage of gases into the atmosphere. Its flow properties were published in Michálek and Zacho (2012). Used tracer gas dosaged into source was ethane. For simulation of non-buoyant gas emission compressed air is used, for heavier-than-air gas emission sulfur hexafluoride is used. These gases were dosaged by electronic flow controller and then mixed together and released into the source.

Tracer gas concentration was measured on a simple rectangular building sized 170x170x60 mm made of duralumin and equipped with eight taps placed on model vertical centerline (see Fig.1). These taps were connected via capillary tubes to flame ionization detectors, which measure tracer gas concentration and convert it into an electric signal, which can be recorded in computer. Fig.2 presents measured concentration on model with taps oriented on windward side for different initial concentration emitted from the source.

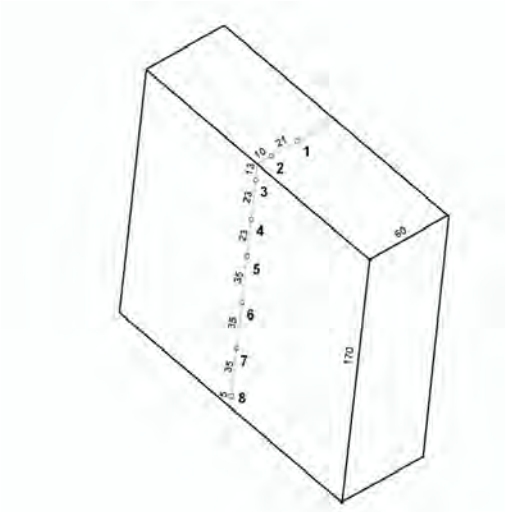

Figure 1: Experimental building model

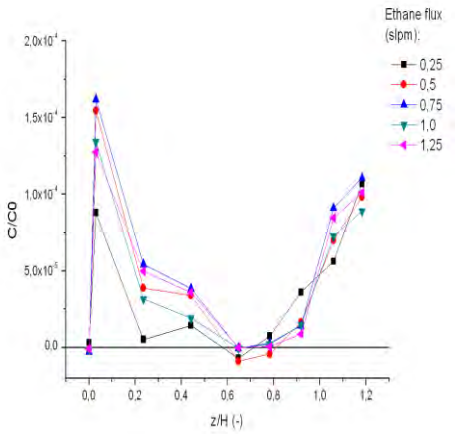

Figure 2: Windward side concentration

4. Conclusions

Gas concentrations on a rectangular building model were measured in a boundary layer wind tunnel. These measurements will serve as boundary conditions and verification for newly developed software calculating gas dispersion in chosen urban areas including complex terrain configuration.

Acknowledgement

This work has been supported by research project "SCENT" granted to VZLU, a.s. by Ministry of the Interior of the Czech Republic.

References

Eurocode 1 (2007): ČSN EN 1991-1-4 Eurocode 1: Actions on structures – Part 1-4: General action – Wind loads. *Český normalizační institut, 2007*

Jirsák M., Ulman R. (2001) Boundary Layer Simulation and its lower velocity limit. *Proc. Of the 3rd European & African Conference on Wind Engineering*, Eindhoven University of Technology, pp. 237-240

Michálek P., Zacho D. (2012) Effect of surface roughness on neutral and dense gas dispersion in the BLWT. *Air Pollution 2012 Proceedings, Wessex Institute of Technology, A Coruña, Spain, 2012*

Snyder W.H. (1981) Guideline for fluid modeling of atmospheric diffusion. *Environmental Protection Agency, Research triangle park, NC 27711, Report No.600/8-81-009, 1981*

19th International Conference
ENGINEERING MECHANICS 2013
Svratka, Czech Republic, May 13 – 16, 2013

MULTIOBJECTIVE MINIMAX DESIGNS OF EXPERIMENTS

E. Myšáková[1], M. Lepš[2]

Summary: *Space-Filling Design Strategies known as Design of (Computer) Experiments (DoE) create an essential part of a surrogate modeling. One of the space-filling metrics is miniMax – the radius of the biggest sphere with its center inside the hypercube that does not contain any point of the set. In this contribution, a multiobjective procedure is proposed to take into account not only miniMax, but also the positions of the spheres with respect to the domains center.*

Keywords: ***Design of Experiments, space-filling, miniMax, Voronoi diagram, largest empty sphere problem, multiobjective optimization, adaptive sampling***

1. Introduction

The design of experiments (DoE) is an essential part of the development of any meta-model (surrogate) (Simpson et al., 2001). The aim is to gain maximum knowledge from a given system with a minimum number of designs. Since we assume that the final meta-model is *a priori* unknown, the design should be spread over the domain as uniformly as possible. The effectiveness of such DoE can be measured by several metrics aiming mainly at orthogonality or space-filling properties.

For our work, we have selected the *miniMax* (*mM*) for its simplicity and easiness in visualization. Given a set of n points in a d-dimensional hypercube, the miniMax is the radius of the biggest sphere with its center inside the hypercube that does not contain any point of the set. This problem is also known as *the largest empty sphere problem (LES)* (Dickerson and Eppstein, 1995). One possible solution is to inspect all vertices forming Voronoi diagram of the given points. However, for the unbounded case the number of vertices grows as $O(n^{\lceil d/2 \rceil})$ and for bounded case, i.e. the case of points inside a hypercube, the number is even higher.

2. Proposed methodology

Recently, we have implemented a parallel evolutionary approach (Myšáková and Lepš, 2013) that is able to guess an approximate value of the miniMax in a reasonable time. A parallel evolution strategy has been used to find the center of the biggest empty sphere. This algorithm

[1] Bc. Eva Myšáková: Faculty of Civil Engineering, Czech Technical University in Prague, Thákurova 7, 166 29 Prague 6; CZ, e-mail:eva.mysakova@fsv.cvut.cz
[2] doc. Ing. Matěj Lepš, Ph.D., Faculty of Civil Engineering, Czech Technical University in Prague, Thákurova 7, 166 29 Prague 6; CZ, e-mail:leps@cml.fsv.cvut.cz

can produce a reliable estimates of miniMax in several minutes even for a problem consisting of few dozens of variables.

The availability of the miniMax value, although approximate, enables to explore properties of a particular DoE. Since the miniMax is the radius of the biggest sphere that does not contain any other point of the set, an interesting information can be the position of such a sphere. Although our experience shows that majority of these spheres are located at the border of the admissible domain, the most dangerous situation is that such spheres are inside the domain, especially in the center of the design space.

One of the drawbacks is that the number of potential points that should be inspected is relatively huge. Therefore, we propose in this paper a multiobjective procedure that finds a trade-off between miniMax value and the distance of centers of the spheres to the domains center. Similar procedure can be found within reliability analyses or Reliability-Based Design Optimization (RBDO) area (Sudret, 2007) where the distance to the Limit State Function (LSF) can be applied instead as the second objective. Then, the points forming Pareto front represents ideal candidates for adaptive sampling of the LSF. Presented results show that the number of points of the Pareto set grows only linearly with the number of dimensions, and therefore, the proposed methodology can be efficiently used even for multidimensional spaces.

3. Acknowledgment

The authors gratefully acknowledge the financial support from the Grant Agency of the Czech Republic through the project GAČR P105/12/1146 and from the Grant Agency of the Czech Technical University in Prague, the grant SGS13/034/OHK1/1T/11.

4. References

Dickerson, M. and Eppstein, D. (1995). Algorithms for proximity problems in higher dimensions. *Comput. Geom.*, 5:277–291.

Myšáková, E. and Lepš, M. (2013). Searching for minimax designs of experiments: A parallel evolutionary approach. In Topping, B. H. V. and Iványi, P., editors, *Proceedings of the Third International Conference on Parallel, Distributed, Grid and Cloud Computing for Engineering*, Stirlingshire, United Kingdom. Civil-Comp Press. paper 18.

Simpson, T. W., Peplinski, J. D., Koch, P. N., and Allen, J. K. (2001). Metamodels for computer-based engineering design: Survey and recommendations. *Engineering with Computers*, 17:129–150.

Sudret, B. (2007). *Uncertainty propagation and sensitivity analysis in mechanical models – Contributions to structural reliability and stochastic spectral methods*. Habilitation à diriger des recherches, Universitè Blaise Pascal, Clermont-Ferrand, France.

19th International Conference
ENGINEERING MECHANICS 2013
Svratka, Czech Republic, May 13 – 16, 2013

MULTIOBJECTIVE ADAPTIVE UPDATING OF SURROGATE MODELS

E. Myšáková, A. Pospíšilová, M. Lepš [1]

Summary: *A meta-model (or a surrogate) is a modern name for what was traditionally called a response surface. Our contribution presents an adaptive updating procedure to improve the quality of the surrogate. It is based on the minimax metric as an objective coming from the space-filling domain of the Design of Experiments. The second objective is aimed at an approximation quality in the region of interest. The final goal of the surrogate usage is to fit structural reliability problems.*

Keywords: ***Multiobjective optimization, Design of Experiments, miniMax, Maximin, Adaptive, Surrogate, Radial Basis Function Models, Limit State Function***

1. Introduction

Reliability-based design optimization (RBDO) is a research area that tries to optimize structures under assumption of uncertainties. Usually, an objective function (e.g. a structure weight, a maximal displacement etc.) is to be minimized with respect to constraints in which a probabilistic approach is included (Kang, 2005). It is hard or nearly impossible to create an analytical probabilistic approach on real structures thus some alternative method should be used. Our planned goal is to utilize a surrogate-based Monte Carlo approach (Dubourg, 2011) enhanced by an adaptive Design of (Computer) Experiments (DoE) (Sudret, 2007). This contribution presents the adaptive part shown on a simple example.

2. Methodology

Radial Basis Function Networks (RBFN) (Kučerová et al., 2005) is a very popular meta-model that is applied in our work. For generating meta-models, an appropriate number of sampling points is needed. Moreover, to improve the quality of the surrogate, an adaptive updating procedure is proposed. It is based on the miniMax metric as an objective coming from the space-filling domain of the Design of Experiments. Overall, there are two criteria that have to be optimized. The first criterion (i.e. miniMax) is to maximize the nearest distance of the added point from already sampled points. The second criterion is to be as close as possible to the approximate Limit State Function, i.e. we are not concentrated on the whole domain, but only

[1] Bc. Eva Myšáková, Ing. Adéla Pospíšilová, doc. Ing. Matěj Lepš, Ph.D., Faculty of Civil Engineering, Czech Technical University in Prague, Thákurova 7, 166 29 Prague 6, tel. +420 224 355 326, e-mail leps@cml.fsv.cvut.cz

on the border between the failure and safe region. These two criteria lead to multi-objective optimization. In our work, a modified Nondominated Sorting Genetic Algorithm II (NSGA-II) is used.

A Nondominated Sorting Genetic Algorithm II (NSGA-II) (Deb et al., 2000) is a method based on evolutionary principles. To create a new generation, only a mutation operator is used to support an exploration part of the algorithm. A selection from several consecutive Pareto fronts is followed by the computation of the crowding distances. Selected individuals with the greatest crowding distance are then used as a new generation. After a predetermined number of generations, only Pareto front is added as an adaptive update.

To evaluate the difference between the original and the approximate model an error function has to be defined. Since we are interested in the quality of the description of the LSF, i.e. in the division of the design domain into a positive and a negative part, our error function counts a number of times the signs of these two models differ. The overall methodology is then shown on an simple academic example.

3. Future application

The future application of the proposed procedure is to solve the Reliability Based Design Optimization (RBDO) problem consisting of minimization of the weight of the structure as the first objective and minimization of the probability of failure characterized by a reliability index as the second objective. The latter can be evaluated by Monte Carlo-based Sampling algorithms utilizing the presented surrogate model. And again, this problem is multiobjective and the presented NSGA-based algorithm can be used.

4. Acknowledgment

The authors gratefully acknowledge the financial support from the Grant Agency of the Czech Republic through the project GAČR P105/12/1146 and from the Grant Agency of the Czech Technical University in Prague, the grant SGS13/034/OHK1/1T/11.

5. References

Deb, K., Agrawal, S., Pratap, A., and Meyarivan, T. (2000). A fast elitist non-dominated sorting genetic algorithm for multi-objective optimization: NSGA-II. pages 849–858. Springer.

Dubourg, V. (2011). *Adaptive surrogate models for reliability analysis and reliability-based design optimization*. PhD thesis, Blaise Pascal University - Clermont II.

Kang, Z. (2005). *Robust Design Optimization of Structures under Uncertainties*. PhD thesis, Institut für Statik und Dynamik der Luft- ind Raumfahrkonstruktionen Univesität Stuttgart.

Kučerová, A., Lepš, M., and Skoček, J. (2005). Large Black-box Functions Optimization Using Radial Basis Function Networks. In *Proceedings of the Tenth International Conference on Civil, Structural and Environmental Engineering Computing*, Stirling. Civil-Comp Press Ltd.

Sudret, B. (2007). *Uncertainty propagation and sensitivity analysis in mechanical models – Contributions to structural reliability and stochastic spectral methods*. Habilitation à diriger des recherches, Universitè Blaise Pascal, Clermont-Ferrand, France.

19th International Conference
ENGINEERING MECHANICS 2013
Svratka, Czech Republic, May 13 – 16, 2013

DYNAMIC RESPONSE OF A HEAVY BALL ROLLING INSIDE A SPHERICAL DISH UNDER EXTERNAL EXCITATION

J. Náprstek, C. Fischer [1]

Summary: *The set of a heavy metallic ball which is rolling freely inside a semi-spherical dish with larger diameter, being fixed to structure, is frequently used as tuned mass damper of vibration. Ratio of both diameters, mass of the rolling ball, quality of contact surfaces and other parameters should correspond with characteristics of the structure. The ball damper is modelled as a non-holonomic system. Hamiltonian functional including an adequate form of the Rayleigh function is formulated in moving coordinates using Euler angles and completed by ancillary constraints via Lagrangian multipliers. Subsequently Lagrangian differential system is carried out. Together with rolling conditions the governing system of seven equations is formulated. Later Lagrangian multipliers character is analysed and redundant motion components are eliminated. First integrals are derived and main energy balances evaluated together with their physical interpretation. Discussion of basic dynamic properties of the system is provided.*

Keywords: ***Non-holonomic systems, Hamilton functional with constrains, Moving coordinates, Non-linear vibration, Vibration ball absorber***

1. Introduction

Passive vibration absorbers of various types are very widely used in civil engineering, especially when wind induced vibration should be suppressed. TV towers, masts and other slender structures exposed to wind excitation are usually equipped by such devices. Conventional passive absorbers are of the pendulum type. Although they are very effective and reliable, they have several disadvantages limiting their application.

Most of the shortcomings can be avoided using the absorber of ball type. The basic principle comes out of a rolling movement of a metallic ball of a radius r inside of a metallic rubber coated spherical dish of a radius $R > r$. This system is closed in an airtight case. Such a device is practically maintenance free. Its vertical dimension is relatively very small and can be used also in such cases where a pendulum absorber is inapplicable due to lack of vertical space or difficult maintenance.

Dynamics of the real ball absorber is more complicated in comparison with the pendulum one. Its movement can be hardly described in a linear state although for the first view its behaviour is similar to the pendulum absorber type. The ball moving inside the spherical dish is

[1] Ing. Jiří Náprstek, DrSc., RNDr. Cyril Fischer, Ph.D., Institute of Theoretical and Applied Mechanics, Prosecká 76, 190 00 Prague 9, tel. +420 286 88 21 21, e-mail naprstek@itam.cas.cz

very sensitive to the stability loss of the semi-trivial state representing the movement in a vertical plane. However this type of the ball motion is requested, as it provides the optimal efficiency of any damper. Therefore any stability loss of the semi-trivial state deteriorates or invalidates any effect of the device. Due to probability of the stability loss, which is much higher than of the spherical pendulum, semi-trivial states should be carefully analysed including a large variety of post-critical processes.

2. Mathematical model formulation

The slipping-less movement of a ball on a surface is a non-holonomic problem. So constraints relating mutual movement of a ball and a surface include velocity components of their movement. Putting together expression for kinetic and potential energies T, V, Rayleigh function Υ and external forces $\mathbf{Q}$, the final expressions results from the relevant Lagrangian equations.

Basic formulae for kinetic and potential energies as well as the Rayleigh function are introduced in moving coordinates fixed to the moving dish. As regards damping, only the rolling resistance and rotation friction proportional to relevant velocity components are respected. No axial damping forces proportional to air flow velocity are taken into account. Projections of the velocity vector components are formulated using the Euler angles. Taking into account the contact condition, an algebro-differential system for vertical angle, horizontal angle and three Euler angles describing system response are formulated.

3. Conclusions

The mathematical model of the ball type vibration absorber has been outlined. Preliminary theoretical and mainly experimental investigation revealed that the non-linear character of this device is an important factor influencing significantly its dynamic properties and practical efficiency. Simplification leading to various types of linearised models is hardly acceptable. Moreover, it seems that the non-linear character making the form of resonance curves dependent on the excitation amplitude leads to better efficiency in comparison with linear mechanism.

The model has been approached as non-holonomic with five degrees of freedom completed by two non-trivial reaction components in a form of Lagrange multipliers. Energy dissipation has been introduced via Rayleigh function considering linear dependence of damping forces on angular velocity components of the ball in moving coordinates. Several special cases have been investigated in order to compare the presented model with conventional partial models investigated earlier.

4. Acknowledgement

The kind support of the Czech Scientific Foundation No. 103/09/0094, Grant Agency of the ASCR No. A200710902 and RVO 68378297 institutional support are gratefully acknowledged.

19th International Conference
ENGINEERING MECHANICS 2013
Svratka, Czech Republic, May 13 – 16, 2013

STUDY OF THE NUCLEAR POWER PLANT CONTAINMENT DAMAGE CAUSED BY IMPACT OF A PLANE

I. Němec[*], Š. Sychrová [**]

Abstract: *The article is a contribution to the discussion concerning nuclear safety which has intensified after the Fukushima Daiichi nuclear disaster. The parametric study presented here is focused on the containment damage evaluation for various materials, containment wall thicknesses and different aircraft speeds before impact. A detailed analysis of plane impact is also included. The solution was obtained by the explicit finite element method utilizing the RFEM program. The knowledge gained from this study might also be applied to the detailed impact analysis of a plane on other particular nuclear power plant containment structures as needed. The purpose of this study was also to foster experiential suggestions for improving the explicit method in the RFEM program in order to release it for RFEM users.*

Keywords: ***Damage extent, explicit method, finite element method, impact, nuclear safety.***

1. Introduction

Following the accident in Fukushima, every country generating nuclear energy launched assessing of the response of the nuclear power plant to severe external events in order to verify safety. The presented article is a contribution to this process. The paper investigates the effects of the impact of an airliner on the containment structure of a nuclear power plant. A parametric study was performed and some its results are presented in the sections below.

The shape and dimensions of the containment structure correspond with the Bushehr nuclear power plant containment. The choice of dimensions of the structure model was based on data found in technical literature. A Boeing 737 was chosen as the impacting body. A parametric study was performed for various materials, wall thicknesses and different plane speeds before impact. Solution of the problem was obtained by the explicit finite element method

2. Containment damage

The study focused on two types of containments: steel and reinforced concrete containment structures. In the case of the steel containments common structural steel was used and the von Mises yield criterion was applied.

A series of calculations of varying thicknesses of the steel and reinforced concrete containments were performed. The resulting containment damage was for purposes of this study assessed by means of the value of permanent deformation and extent of plastic strain. Comparing the reinforced concrete and steel containments, qualitatively different deformation shapes could be observed. The permanent displacement shapes of reinforced concrete containments are approximately circular and the permanent displacement shapes of steel containments are rather irregular. This qualitative difference in deformation and plastic yielding patterns is caused by the fact that these two materials (reinforced concrete and steel) have different ratios between bending and membrane stiffnesses. Membrane stiffness increases linearly with thickness whereas bending stiffness increases with the third power of thickness.

[*] doc. Ing., CSc, Institute of Structural Mechanics, Faculty of Civil Engineering, Brno University of Technology, Veveří 95; 602 00, Brno; Czech Republic, tel. (+420) 541 147 373, e-mail: nemec@fem.cz

[**] Ing., Institute of Structural Mechanics, Faculty of Civil Engineering, Brno University of Technology, Veveří 95; 602 00, Brno; Czech Republic, tel. (+420) 541 147 373, e-mail: sychrova@fem.cz

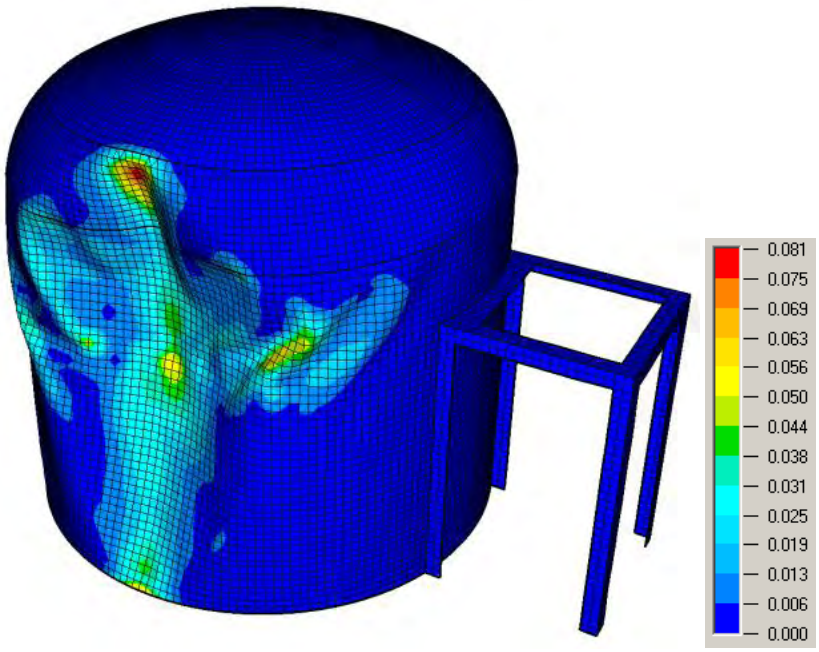

Fig. 2 *Steel containment, wall thickness 0.05m – maximum plane speed*

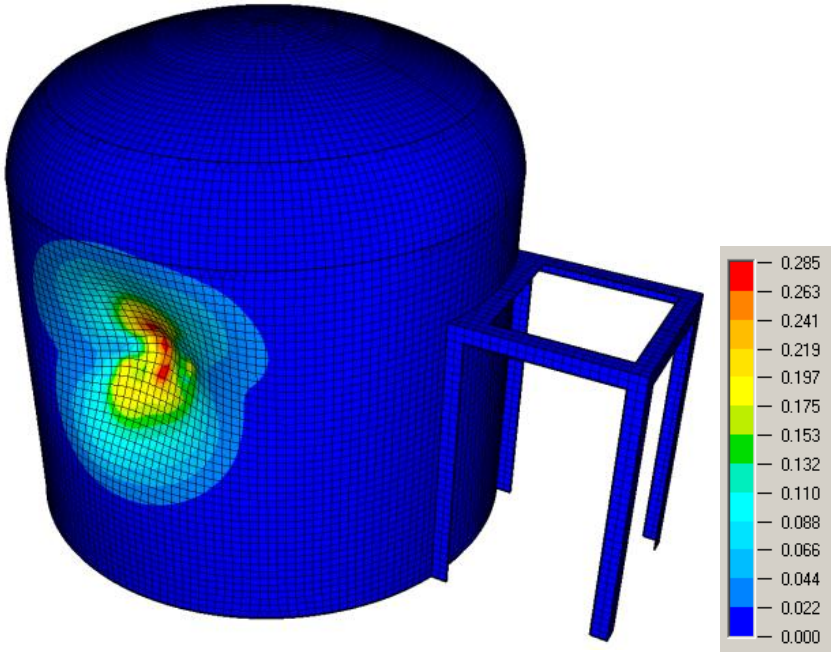

Fig. 3 *Reinforced concrete containment wall thickness 0.6m – maximum plane speed*

3. Conclusions

The study proves the capability of the RFEM program to analyze nonlinear transient dynamic effects. The results of the study can also serve in estimating the damage caused by the impact of a plane into any similar nuclear power plant containment. The study also indicates that there is low probability of radioactive material leakage from the analyzed containments during such an event despite extensive damage to the structures.

References

Wu, S. R., Gu, L., (2012), *Introduction to the Explicit Finite Element Method for Nonlinear Transient Dynamics*, John Wiley & Sons, Inc., page 3-35.

19th International Conference
ENGINEERING MECHANICS 2013
Svratka, Czech Republic, May 13 – 16, 2013

2D FINITE ELEMENT ANALYSIS OF AGGREGATE INFLUENCE ON MECHANICAL PROPERTIES OF MORTAR SAMPLES

V. Nežerka, J. Vorel, J. Zeman [1]

Abstract: *Virtual testing of composite materials is, compared to a conventional experimental analysis, less time consuming, and it can very clearly reveal the failure mode. Therefore, it can be used for an optimization of the shape and amount of aggregates. Unlike the basic analytical homogenization methods, numerical modeling can predict the strength of the material and energy needed for the crack propagation. In our study three-point bending and splitting tests, by means of 2D plane-stress nonlinear finite element analysis utilizing isotropic damage model, were simulated. The results of the analysis indicate that angular aggregates of bigger size contribute to an increased fracture energy of the mortars, while the mortars containing fine round aggregates exhibit higher strength due to absence of stress concentrations around the grains.*

Keywords: ***FEM, damage model, mortar, influence of aggregates***

It has been observed by many researchers (e.g. Stefanidou and Papayianni (2005); Tasong et al. (1998)) that the material properties of mortars and concrete are dependent on the amount, type and geometry of aggregates in the mix. The purpose of this work was to investigate the influence of aggregates on flexural strength of the tested mortar, determined from a three-point bending test simulations, and on fracture energy evaluated from simulations of a splitting test.

The aggregates of round, ellipsoidal and angular shape were placed only in the area of expected crack propagation in a relative volume $c^{\text{agg}} = 0.4$. Each aggregate shape configuration was represented by the fine (F) (passing the sieve opening d_0 = 1.0 mm) and coarse (C) (d_0 = 2.5 mm) monodisperse particles.

The plane-stress numerical simulations were carried out in the OOFEM finite element code with the object oriented architecture (Patzák and Bittnar (2001)). An isotropic damage model with linear softening (Jirásek (2004)) was assumed for the matrix phase, while the aggregates were modeled as isotropic and elastic. The equivalent strain, $\tilde{\varepsilon}$, was determined based on Mazars norm, accounting only for the positive part of the strain tensor. The interfacial transition zone was not modeled. Figure 1 depicts the crack propagation through the material.

The following conclusions can be made from the results of the analysis:

- 2D plane-stress finite element simulations and isotropic damage model can successfully simulate the crack propagation through a microstructure in a realistic way,
- simulation of splitting test can be used for the evaluation of fracture energy in brittle materials without snap-back response in load-displacement diagram,

[1] Ing. Václav Nežerka, Doc. Ing. Jan Zeman, Ph.D., Ing. Jan Vorel, Ph.D., Faculty of Civil Engineering, Czech Technical University in Prague, Thákurova 7, 166 29 Praha 6, Czech Republic; e-mail: vaclav.nezerka@fsv.cvut.cz

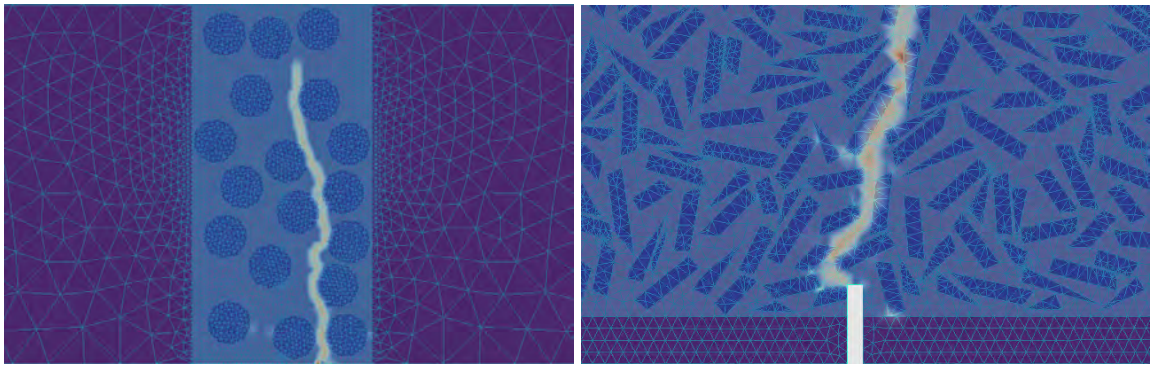

(a) bending test (configuration R(C)) (b) splitting test (configuration A(C))

Figure 1: Detail of FE mesh and crack pattern

- the bending strength is enhanced by the addition of fine spherical sand particles into mortars, since they do not introduce excessive stress concentrations around their tips,
- the fracture energy of mortars can be enhanced by the addition of coarse angular aggregates, since these create an efficient obstacle against the crack propagation.

The study was not supposed to yield exact values, it only revealed the trends. Three-dimensional model, incorporating shrinkage microcracking and interfacial zone around aggregates, would probably give more accurate data at significantly higher computational cost.

Acknowledgment

The authors would like to thank for the financial support by the grant no. SGS13/034/OHK1/1T/11.

References

Jirásek, M. (2004). Non-local damage mechanics with application to concrete. *Revue Europeaenne de Génie Civil*, 8:683–707.

Patzák, B. and Bittnar, Z. (2001). Design of object oriented finite element code. *Advances in Engineering Software*, 32:759–767.

Stefanidou, M. and Papayianni, I. (2005). The role of aggregates on the structure and properties of lime mortars. *Cement & Concrete Composites*, 27:914–919.

Tasong, W., Lynsdale, C., and Cripps, J. (1998). Aggregate-cement paste interface: influence of aggregate physical properties. *Cement and Concrete Research*, 28(10):1453–1465.

19th International Conference
ENGINEERING MECHANICS 2013
Svratka, Czech Republic, May 13 – 16, 2013

BOINC FOR VOLUNTEER COMPUTING

J. Nosek

Abstract: *GRID is a utilization of heterogeneous computing facilities interconnected with the fast Ethernet. The main advantage is GRID availability, since all offices are nowadays equipped with powerful PCs. There is no need for so-called volunteer computing like the famous SETI@home project which uses a computing power offered by anonymous users on internet. Any project can be implemented in a framework of a scientific group through the BOINC middleware which was developed during the SETI@home project. Our contribution shows the possibilities of such computing environment on an example of structural sizing optimization that needs an enormous computational power.*

Keywords: ***GRID, BOINC, parallel computing, volunteer computing.***

1. Introduction

Many tasks (for our purpose structural size optimization) need enormous computing time. Enormous means many months or years if you use a common computer. But there exist many ways of grid computing. Our paper focused on volunteer computing using (BOINC). It is a simple open source middleware based on server – client technology. BOINC offers image of server virtual machine. It is an easy way to start building your own BOINC server in a few minutes. It looks attractive but there are several problems. On the internet you can find many step-by-step manuals as (VmServer). I offer you other point of view. I want to show a possible breakpoint during the first installation of a server and application.

First, consider the potentials of volunteer computing. During the last year, there was sold more than three hundred and fifty million units of PC (Gartner). In the world there are in use approx 1.4 billion computers (answers.com). Approximately, the same number of computers not being used. Now we are still talking about PCs. There are other devices such as a mobile phone or a tablet containing good processors, often with multi-core and hyper threading. For instance, Samsung has sold 30 million pieces of Galaxy S III, containing Exynos 4412 processor, 2 cores, each running at 1.2 GHz. And still we are talking only about counting on processors, not GPU.

We have to mention other options of volunteer computing, such as the storage potential of volunteer computing (Anderson a David).

2. Volunteer versus grid and HPC computing

I would like to clarify the grid computing versus volunteer computing. Both are a form of distributed computing. Grid computing is a group of computers to achieve a common goal. Grid computing is between HPC and volunteer computing. Grid computing are symmetrical institution that can provide and access resources simultaneously. Volunteer computing, in contrast, is asymmetric. Volunteers supply CPU time and not getting anything back. You can give them credit, but it is not monetary.

3. Use BOINC

(BOINC) middleware we can use for both computational models. If BOINC client run on our computers, it is grid computing. But it is more efficient to use general public PCs. Now we speak about volunteer computing. Main advantage is the low running cost. What is the catch? Is necessary to do a few steps, such as promote project, communicate with volunteers, run application on a wide range of computes type. Doing the promotion is an essential part of the project and can determine a success or a failure of the project.

4. Main parameter of application

As a user (not a volunteer) and an author of an application, keep in mind several fundamental differences between the grid and volunteer computing. If you use grid computing, you push jobs to the computers. On the other hands, volunteer computers request (pull) job from server. You must determine who, when and how to give jobs to volunteers. For each job you determine boundaries of volunteer computers (also called host). BOINC-client send to the server the information about computer resources, such as CPU benchmark (whetstone and Dhrystone), size of RAM, size of HDD, free space of HDD, OS and several others. These are very important and useful information for job creator. You must also define how to make the application job-failure resistant. How to secure the job from hackers. The most common method is to send the job to multiple volunteers and validate whether I got the same results.

5. First application

For easy start-up BOINC provide (wrapper) which enables converting a stand-alone application to BOINC. When you have stand-alone application, just divide task to small jobs and add new application to BOINC project. Wrapper handles all communication with BOINC client.

6. Conclusions

Using volunteer computing for academic purpose is very suitable. Usually at the university it is easy to get a large number of volunteers. You can get a high-performance computational tool. By the beginning of the project, you need only a standard computer and a few days of free time. You do not need a budget, money is useful but not necessary. Another advantage of it is to raise the awareness of the scientific tasks between other colleagues and students. Volunteer computing is also a form of social network.

Acknowledgement
This work was supported by the Grant Agency of the Czech Technical University in Prague, grant No. SGS OHK1-042/13

References

Anderson, U.C and P. David. “The Computational and Storage Potential of Volunteer Computing.” *CCGRID '06 Proceedings of the Sixth IEEE International Symposium on Cluster Computing and the Grid*. 2006.

answers.com. *How many computers are in the world?* n.d. <http://wiki.answers.com/Q/How_many_computers_are_in_the_world>.

BOINC. *BOINC, Open-source software for volunteer computing and grid computing*. n.d. <http://boinc.berkeley.edu/>.

Gartner. *Gartner Says Declining Worldwide PC Shipments in Fourth Quarter of 2012 Signal Structural Shift of PC Market*. n.d. <http://www.gartner.com/newsroom/id/2301715>.

VmServer. <http://boinc.berkeley.edu/trac/wiki/VmServer>.

wrapper. <http://boinc.berkeley.edu/trac/wiki/WrapperApp>.

19th International Conference
ENGINEERING MECHANICS 2013
Svratka, Czech Republic, May 13 – 16, 2013

EXTENSION OF SEMI-ANALYTICAL FRACTURE MODEL BASED ON THE COHESIVE CRACK APPROACH

T. Pail*, P. Frantík**

Abstract: *The paper presents the description of the developed JAVA implementation of the semi-analytical fracture model based on cracked hinge approach by Ulfkjær et al (1995) and introduces generalization of the model formulation to enable using the tensile softening function with an arbitrary shape for the nonlinear part of the model assumed as cohesive crack. Performed simulations of an adopted wedge-splitting test show consistency of the new formulation with reference data. A comparison with FEM solution is also presented to demonstrate a dependency of a load-crack mouth opening curve obtained by FEM and the implemented hinge model on its band width for different choices of softening function.*

Keywords: ***hinge model, fracture, concrete, tensile softening, fracture energy.***

1. Introduction

Nowadays, one of main approaches commonly applied for a description of fracture behavior is the cohesive crack approach, further generalized by Hillerborg et al. (1976) for quasi-brittle materials (typically concrete) as the fictitious crack model (FCM). This model recognizes experimentally observed cohesive character of crack propagation which these materials exhibit due to microcracking and other related processes (e.g. crack bridging). This phenomenon takes place within the extensive fracture process zone (FPZ) developed ahead of the tip of a real traction-free crack. The cohesive (fictitious) crack concept considered the fracture energy dissipated in the process zone via certain closing cohesive stress applied to the fracture surface of a fictitious extension of a real crack (called fictitious crack) approximating the FPZ. The corresponding tensile softening function $\sigma(w)$ is introduced as the crack evolution property of the model describing the relationship between the magnitude of applied cohesive stress and crack opening displacement.

The popularity and prevalence of models based on the cohesive crack approach is generally given by their simple implementation within the framework of the finite element method (FEM). Some well-known complex numerical tools for modelling both elastic (or elastic-plastic) behavior and the quasi-brittle fracture process have been developed on this basis, e.g. (ATENA or DIANA). However, the practical using of such tools is limited by a trustworthy knowledge of the stress-crack opening relationship $\sigma(w)$ considered as the key material input. Application of indirect methods is most widely used procedure to estimate softening curve from standardized fracture tests—the three-point bending test (TPBT) or the wedge splitting test (WST)—either using evaluation methods, e.g. the work of fracture method, or increasingly used inverse analysis with the possible employment of advanced optimization techniques. In the present paper, the own JAVA implementation of the semi-analytical model based on the cracked hinge concept is introduced with some extensions as the example of effective numerical tool suitable for purposes of the inverse analysis.

2. The cracked hinge model

The idea of a cracked hinge was presented originally by Ulfkjær et al. (1995) as the analytical model for calculation of load–displacement curves of notched and un-notched beams, further developed by

* Ing. Tomáš Pail: Institute of Structural Mechanics, Brno University of Technology, Veveří 331/95; 602 00, Brno; CZ, e-mail: pail.t@fce.vutbr.cz

** Ing. Petr Frantík, Ph.D.: Institute of Structural Mechanics, Brno University of Technology, Veveří 331/95; 602 00, Brno; CZ; e-mail: kitnarf@centrum.cz

other authors. The basic assumption of the model is that presence of a crack influences overall stress and strain field of a structure only in a local manner and this discontinuity is expected to vanish outside the certain bandwidth, *s*. Within this band a crack propagation is modelled as the fictitious crack, while outside, the rest of the structure is considered in terms of the classical elastic theory. Thus, the cracked hinge model can be viewed as a set of independent nonlinear spring elements which are formed by incremental horizontal strips of the predetermined area of the structure surrounding a propagating crack, see Fig. 1 (left). Some additional improvements of the crack hinge formulation have been developed by authors. Main reason for this modifications was to allow using an arbitrary softening curve without any significant increase in the computation costs in the global iterative scheme.

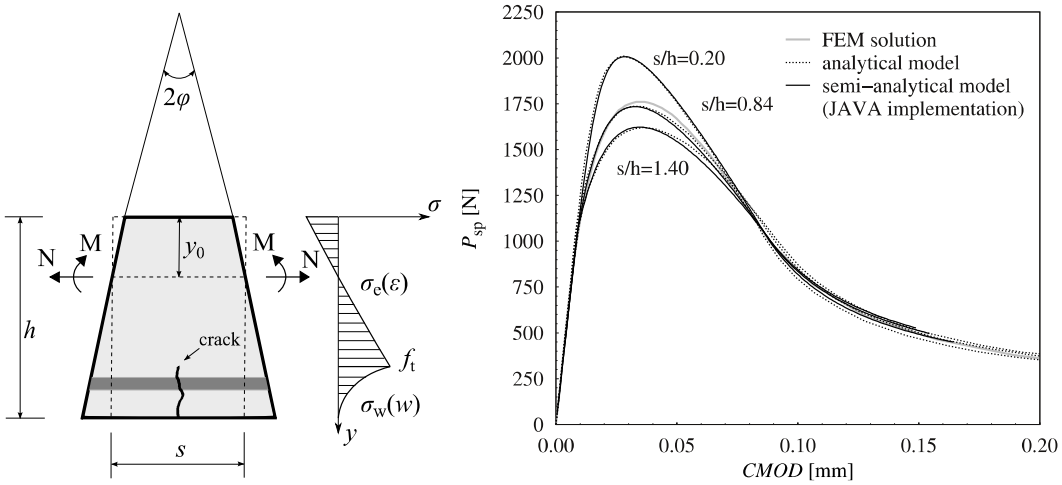

Fig. 1: Loading and deformation of the cracked hinge element with stress distribution (left); comparison of the P–CMOD response of the implemented semi-analytical model with data of FEM and analytical solution originally published by Østergaard (2003)

3. Conclusion

The paper presents the description of the own implementation (in JAVA programming language) of semi-analytical fracture model based on the cracked hinge approach introduced by Ulfkjær et al. (1995). Generalized formulation of this model was adopted which enables to use for the cracked part of a structure described as the fictitious (cohesive) crack the tensile softening function with an arbitrary shape. The implemented procedures were validated by data published by Ostergaard (2003) where a wedge splitting test had been simulated. The obtaining results correspond nicely with origin data and confirm the applicability of the implemented model. The general dependency of band width of the hinge element incorporated to the WS specimen was also presented in the numerical study involving FEM modelling. There, the influence of the change of a tensile softening function shape and increasing value of fracture energy was investigate and indicates that this dependency is not strong but implies the necessity to calibrate the hinge model when we required optimal agreement with a FEM solution.

Acknowledgements

The financial support received from the Czech Science Foundation under Project No. P105/11/1551 and specific research program of Brno University of Technology under Project No. FAST/J/13/1938 is gratefully acknowledged.

References

Hillerborg, A., Modeer, M. & Petersson, P. E. (1976). Analysis of crack formation and crack growth in concrete by means of fracture mechanics and finite elements. *Cem. Concr. Res*., Vol. 6, pp. 773–782.

Østergaard L. (2003). Early-age fracture mechanics and cracking of concrete. *PhD Thesis*, Department of Civil Engineering, Technical University of Denmark, Lyngby, Denmark.

Ulfkjær, J. P., Krenk, S. & Brincker, R. (1995) Analytical model for fictitious crack propagation in concrete beams. *ASCE Journal of Engineering Mechanics*, Vol. 121, pp.7-15.

19th International Conference
ENGINEERING MECHANICS 2013
Svratka, Czech Republic, May 13 – 16, 2013

Identification of Parameters of the Feigenbaum-Dafalias Directional Distortional Hardening Model

S. Parma, J. Plešek, Z. Hrubý, R. Marek,[1] H. P. Feigenbaum[2], Y. F. Dafalias[3,4]

1. Introduction

Distortion of yield surface due to strain hardening was observed in numerous experiments with various types of metals. The distorted surface shows high curvature in the load direction and flattening in the opposite direction, see Fig. 1, Wu and Yeh (1987). This phenomena is referred to as the directional distortional hardening (DDH). Recently, Feigenbaum and Dafalias (2008) proposed a phenomenological model to capture this phenomena. The model is a generalization of isotropic and kinematic hardening, one more parameter is added to isotropic and kinematic model to model the distortion. In sum, Feigenbaum-Dafalias DDH model therefore includes six independent material parameters.

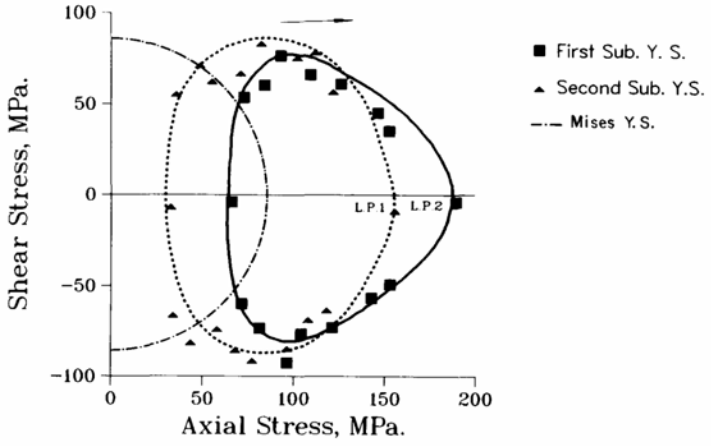

Figure 1: *Distorted yield surface, Wu and Yeh (1987).*

Practical application of any parametric model is associated with the identification algorithm. In the past, identification algorithm for model parameters was proposed, but this takes into

[1] Ing. Slavomír Parma, Ing. Jiří Plešek, CSc., Ing. Zbyněk Hrubý, Ph.D., Ing. René Marek, Institute of Thermomechanics Academy of Sciences of the Czech Republic, v. v. i., Dolejškova 1402/5, 182 00 Prague 8, Czech Republic, e-mail plesek@it.cas.cz, parma@it.cas.cz, zbynek@it.cas.cz, marek@it.cas.cz
[2] Department of Mechanical Engineering, Northern Arizona University, PO Box 15600, Flagstaff, AZ 86011, USA, e-mail heidi.feigenbaum@nau.edu
[3] Department of Civil and Environmental Engineering, University of California at Davis, Davis, CA 95616, USA, e-mail jfdafalias@ucdavis.edu
[4] Department of Mechanics, Faculty of Applied Mathematical and Physical Science, National Technical University of Athens, Zographou, 15780, Hellas, e-mail yfdafalias@central.ntua.gr

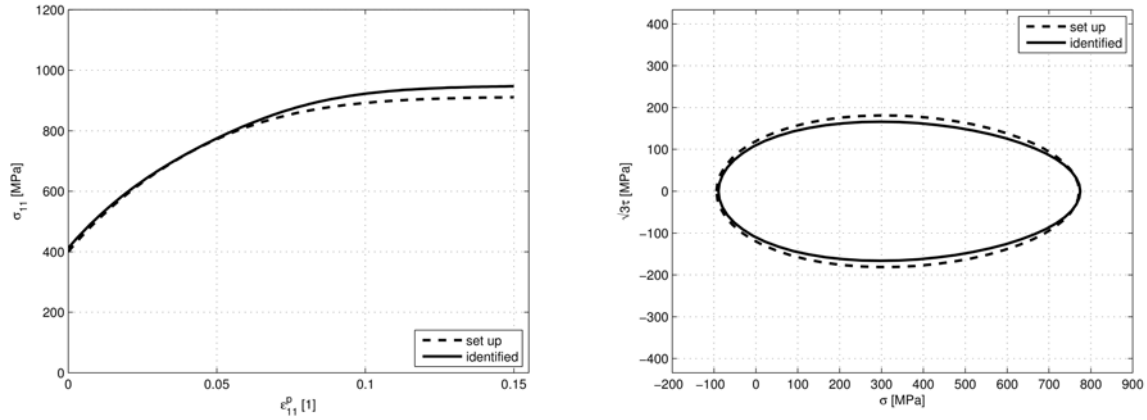

Figure 2: *Comparison of stress-strain diagram and distorted yield surface of set up and identified models.*

account an experimental response in the stress space only. In this paper, different identification algorithm for model parameters is developed as the stress-strain curve and the distorted yield surface are assumed as input data.

First, Feigenbaum and Dafalias DDH model is analyzed. Model equations are simplified to uniaxial and biaxial form in order to model the stress-strain curve and the distorted yield surface, respectively. In simplified form, equations represent one-dimensional initial value problem with possibility of analytical solution. The problem is therefore solved leading to a model of the stress-strain curve and the distorted yield surface.

For identification, some significant features of discussed curves, e.g., initial point, initial slope, are chosen to be compared with experimental data. This comparison takes form of the system of ten nonlinear equations for six unknown parameters with possibility of analytical solution.

Since no komplex experimental data are available, the identification algorithm is tested on virtual experiments. Tests show good agreement of original model and identified one, see Fig. 2.

2. References

Feigenbaum, H. P. & Dafalias, Y. F. (2007). Directional distortional hardening in metal plasticity within thermodynamics. *Int.J. Solids Struct.*, 44, 7526–7542.

Feigenbaum, H. P. & Dafalias, Y. F. (2008). Simple model for directional distortional hardening in metal plasticity within thermodynamics. *J. Eng. Mech.*, 134, 730–738.

Plešek, J. & Feigenbaum, H. P. & Dafalias, Y. F. (2010). Convexity of yield surface with directional distortional hardening rules. *J. Eng. Mech.*, 136, 477–484.

Wu, H. C. & Yeh, W. (1991). On the experimental determination of yield and some results of annealed 304 stainless steel. *Int. J. Plast.*, 7, 803–826.

19th International Conference
ENGINEERING MECHANICS 2013
Svratka, Czech Republic, May 13 – 16, 2013

A STUDY OF FUEL ROD VIBRATION INDUCED BY COOLANT CROSS FLOW IN THE REACTOR CORE

L.Pečínka*, M.Švrček**

Abstract: *An analysis model has been drived on the vibrations of fuel rod induced by coolant cross flow in the reactor core. The force on the fuel rod was fitted out using parameters that describe rod position. The amount of energy a fuel rod receives from the coolant through one cycle of its vibration was calculated as a positional integration of the fluid force. The vibration mode of the fuel rod and the effective momentum flux of the fluid were calculated using the energy.*

Keywords: ***fuel rod, the vibration mode, external force, amount of work, Connor´s equation, critical flow speed .***

1. Introduction

The dynamical behaviour of a nuclear reactor core is very difficult to calculate because of the large numbers of fuel elements and different type of exciting force. In normal reactor operation mode this ones may be divided in two basic groups. The first group represents kinematic excitation of the fuel assemblies headpieces and the tailpieces (Zeman 2012) induced by vibrations of reactor internals. The second group represent force excitation represented by turbulent pressure pulsations in boundary layer on the surface of fuel rods (Pečínka 2012) and transversal coolant flows in the lower part of fuel assembly. Theoretical solution of this task is presented in this paper.

2. Analysis model for effective momentum flux

The first three eigenfrequencies of fuel rod of fuel assembly TVSA-T are as follows: f_1=33.86 Hz, f_2=37.87 Hz, f_3=43.92 Hz. A transversal flow induced vibrational mode of fuel rod is not a proper mode, however, but it varies depending on the fluid force distribution. The vibrational mode of a fuel rod is expressed in the following equations using superimposition of the proper vibratory response modes in the form

$$y(z) = \sum_{n=1}^{3} \beta_n \emptyset_n(z,t) = \sum_{n=1}^{3} y_{n,max} \emptyset_{n,(z)} cos(\omega_n t + \psi) \quad (1)$$

Transversal flow act on the element of length by the force

$$dF_n = \frac{1}{2} c_L \rho(z) V^2(z) \pi D \, dz \, cos(\omega_n t + \psi) \quad (2)$$

The amount of work ΔL by this external force in one cycle of a fuel rod vibration is

$$\Delta L = \int_0^L \int_0^{2\pi/\omega_n} dF_n \dot{y}_n(z,t) dz \, dt = \frac{\pi}{2} c_L \sum_{n=1}^{3} \int_0^L D\rho(z) V^2(z) \phi_n^2(z) sin\psi \, dz \quad (3)$$

The amount of energy ΔE dissipated in the damping mechanism in one cycle is

$$\Delta W = \sum_{n=1}^{3} \int_0^L \int_0^{2\pi/\omega_n} K\omega_L^2 \beta_n^2 \phi_n^2(z) \, sin^2 \omega_n L \, dz \, dt = \sum_{n=1}^{3} 4\xi\pi y_{max}^2 \int_0^L \frac{1}{2} k(z) \phi_n^2(z) \, dz \quad (4)$$

where k(z) is the stiffness of fuel rod at position z and ξ is the attenuation factor of the fuel rod.

The integration

* Ing. Ladislav Pečínka, CSc._ÚJV Řež, a. s., Hlavní 130, Řež, 250 68 Husinec, CZ; e-mail: pel@ujv.cz
** Ing. Miroslav Švrček : ÚJV Řež, a. s., Hlavní 130, Řež, 250 68 Husinec, CZ; e-mail: smi@ujv.cz

$$\int_0^L \frac{1}{2} k(z) \phi_n^2(z) dz$$

means stress energy of the fuel rod in its whole length, which is expressed in an alternate formula

$$U_n = \frac{1}{2} \int_0^L E\ I\ \left[\frac{\delta^2 \phi_n(z)}{\delta z^2}\right]^2\ dz \tag{5}$$

Substituting Eq. (5) into Eq. (4) we obtain

$$\Delta E_n = 2\xi\pi y_{max}^2\ \int_0^L E\ I\ \left[\frac{\delta^2 \phi_n(z)}{\delta z^2}\right]^2\ dz \tag{6}$$

The balance formula of energy in a cycle is ΔL=ΔE. Then

$$\frac{\pi}{2} c\ y_{max}^2\ \int_0^L \rho\ (z) \phi_n^2(z) V^2(z) \sin\psi(z) dz \tag{7}$$

$$= 2\pi\xi y_{max}^2 \int_0^L E\ I\ \left[\frac{\delta^2 \phi_n(z)}{\delta z^2}\right]^2\ dz$$

After some rearrangement as the result we obtain

$$\frac{m_0 \omega_n^2 \int_0^L \frac{\rho(z)}{\rho_0} \phi_n^2(z) V^2(z) \sin\psi(z) dz}{\int_0^L E\ I \left[\frac{\delta^2 \phi_n(z)}{\delta z^2}\right]^2 dz} = \frac{8\pi}{\bar{c}}\ f_n^2\ \frac{m_0 \delta}{\rho_0} = V_{crit}^2 \tag{8}$$

where V_{crit}^2 represents critical flow speed at which unstable vibrations begin. Right side of Eq. (8) may be expressed in the form of the well known Connor´s relation

$$\frac{V_{crit}}{f_n D_0} = K\ \left(\frac{m_0 \delta}{\rho_0 D_0^2}\right)^{1/2} \tag{9}$$

where K represents experimentally obtained coefficient. Using Eqs. (8) and (9) one can after some arrangement obtain the theoretical expression of the coefficient K in the form

$$K^2 = \frac{4\pi^2 \int_0^L \rho(z) \phi_n^2(z) V^2(z) \sin\psi(z) dz}{\delta\ \int_0^L E\ I \left[\frac{\delta^2 \phi_n(z)}{\delta z^2}\right]^2 dz} \tag{10}$$

This equation partly explain that some of the “spread” in the experimental data is due to very different ways in defining the instability threshold, measurement and definition of δ, excited form of vibration etc. The experimentally obtained values of K are 15.4, 9.1, 3.3 and as ultraconservative value 0.8. The value of K obtained from Eq (10) is 0.57.

Assessment of the V_{crit} represents only first step of the problem solution. In the second step the exciting force shall be calculated. The following equation is valid

$$F = \frac{1}{2} \rho V^2 D_0\ L c_L \tag{11}$$

where c_L represents lift coefficient.

References

Zeman Vl., Hlaváč Zd.: Dynamic response of nuclear fuel assembly excited by pressure pulsations, Computional mechanics 2012

Pečínka L., Švrček M.: Vibrations of the splender rod induced by the turbulence in the coolant flow. Engineering Mechanics 2012

Connors H.S.: Fluid elastic Vibraton of Tube Arrays Excited by Cross Flow. Proc. ASME Annual Winter Meeting, December 1970

19th International Conference
ENGINEERING MECHANICS 2013
Svratka, Czech Republic, May 13 – 16, 2013

NEW MATHEMATICAL MODEL OF CONTINUUM MECHANICS

F. Pochylý [*], S. Fialová [**] J. Krutil [***]

Abstract: *This paper presents a variant of a mathematical model of continuum mechanics. Adaptation of the model is focused on unsteady term. The solution is based on the assumption of zero value of the divergence vector, which can have a different physical meaning.*

Keywords: ***operator equation, momentum equation, continuum mechanics, Maxwell equations.***

1. Introduction

Solution of many problems of continuum mechanics is based on the method of control volumes. Formulation of the task is often complicated by the unsteady term on which in the classic formulation cannot be used Gauss Ostrogradsky theorem.

The above mentioned unsteady term often complicates the problematic of the solid-liquid interaction. Major complications occur even in dealing with the interactions of fields of different physical nature; for example the interaction of the fluid and electromagnetic fields.

2. Mathematical model

Considering multiple contiguous region V bounded by the surface *S*. The boundary orientation is defined by a unit vector outward normal $\boldsymbol{n}$ to the surface *S*.

The mathematical model is defined by the Cartesian coordinate system, the Euler approach, where each independent variable, generally designated $\boldsymbol{E}$ depends on the spatial coordinate *x* and time *t*. Thus $\mathrm{E} = \mathrm{E}(\mathbf{x}, \mathrm{t})$, $\mathbf{x} = (\mathrm{x_j})$. On the *V* there is defined the variable field $\boldsymbol{E}$.

The mentioned area is defined by a mathematical model of continuum using the summation convention in the form:

$$\frac{\partial A_i}{\partial t} + \frac{\partial B_{ij}}{\partial x_j} = C_i \tag{1}$$

$$\frac{\partial A_i}{\partial x_i} = 0 \tag{2}$$

In the equations (1), (2), we assume:

$$A_i = A_i(\boldsymbol{x}, t)\,; \qquad B_{ij} = B_{ij}[\boldsymbol{A}(\boldsymbol{x}, t)]\,; \qquad A_i = A_i(\boldsymbol{x}, t) \tag{3}$$

$$C_i = C_i(\boldsymbol{x}, t)\,; \tag{4}$$

$$div\boldsymbol{C} = 0$$

[*] Prof. Ing. František Pochylý, CSc.: Institute of Power Engineering, Brno University of Technology, Technická 2896/2; 616 69, Brno; CZ, e-mail: pochyly@fme.vutbr.cz

[**] Ing. Simona Fialová, Ph.D.: Institute of Power Engineering, Brno University of Technology; Technická 2896/2; 616 69, *Brno*; CZ, e-mail: fialova@fme.vutbr.cz

[***] Ing. Jaroslav Krutil, Ph.D.: Institute of Power Engineering, Brno University of Technology; Technická 2896/2; 616 69, Brno; CZ, e-mail: jkrutil@seznam.cz

On the given assumptions is the new mathematical model written in shape:

$$\frac{\partial}{\partial x_j}\left[\left(\frac{\partial A_j}{\partial t} - C_i\right)x_i + B_{ij}\right] = 0 \tag{5}$$

Additionally it holds following identity:

$$\int_V \frac{\partial \boldsymbol{A}}{\partial t} dV = \int_S \left(\frac{\partial \boldsymbol{A}}{\partial t}\boldsymbol{n}\right)\boldsymbol{x} dS \tag{6}$$

Examples:

- Momentum equations – Navier- Stokes equations

$$\frac{\partial v_i}{\partial t} + \frac{\partial}{\partial x_j}\left(v_i v_j - \frac{\sigma_{ij}}{\rho}\right) = g_i \tag{7}$$

$$\frac{\partial v_i}{\partial x_i} = 0 \tag{8}$$

Comparing with (1) , (2) holds:

$$A_i = v_i\,; \quad B_{ij} = v_i v_j - \frac{\sigma_{ij}}{\rho}\,; \quad C_i = g_i \tag{9}$$

- Homogenous conductor with constant conductivity and permeability

$$\frac{\partial \mathbf{H}}{\partial t} + rot(\mathbf{H} \times \boldsymbol{v}) - \alpha \Delta \boldsymbol{H} = 0 \tag{10}$$

$$div\boldsymbol{H} = 0 \tag{11}$$

$$\boldsymbol{A} = \mathbf{H}\,; \quad B_{ij} = \varepsilon_{ijk}\varepsilon_{kmn}\mathrm{H}_m v_n - \alpha\frac{\partial H_i}{\partial x_j} \quad ; \quad C_i = 0 \tag{12}$$

Acknowledgement

This work was gratefully acknowledged by grant projects: GAČR P101/13-20031S, CZ.1.07/2.3.00/30.0005

References:

Brdička,M., Samek, L., Sopko, B.: Mechanika kontinua. In Czech Academia, Prague, 2000, ISBN 80-200-0772-5.(in Czech)

LD Landau, EM Lifshitz: Elektrodynamika splošnych Sred. Série "Teoretická fyzika VIII", Moskva, 2003, p 656, ISBN 5-9221-0123-4 (T. VIII) (in Russian)

Sedov, L. I.:Mechanika splošnych sred. TOM 1. Nauka, Moskava, 1976, p.536 (in Russian)

Pochylý, F.; Fialová, S.; Krausová, H. Variants of Navier-Stokes Equations. In Engineering Mechanics 2012; Book of extended abstracts. Svratka, CZ, Association for Engineering Mechanics. 2012. p. 1011 - 1016. ISBN 978-80-86246-40-6.

Pochylý, F.; Fialová, S.; Kozubková, M.; Bojko, M. Tensors of added damping, stiffness and mass in a thin gap of hydrodynamic machine. IOP Conference Series: Earth and Environmental Science. 2012. 15(7). p. 1 - 8. ISSN\~1755-1315.

19th International Conference
ENGINEERING MECHANICS 2013
Svratka, Czech Republic, May 13 – 16, 2013

EXPERIMENTAL AND COMPUTATIONAL INVESTIGATION OF A SIMPLE FIBRE-MASS SYSTEM

P. Polach[*], M. Hajžman[**], J. Václavík[***]

Abstract: *Experimental measurement is performed on a simple fibre-mass system: moving mass coupled with a frame by a fibre. Dynamic response of the mass is measured. The same system is numerically investigated by means of a simple multibody model. The influence of the model parameters on the coincidence of results of experimental measurements and the simulations are evaluated. The simulations aim is to create a phenomenological model of a fibre, which will be utilizable in fibre modelling in the case of more complicated mechanical or mechatronic systems.*

Keywords: ***Fibre-mass system, vibration, experiment, simulation.***

1. Introduction

The replacement of the chosen rigid elements of manipulators or mechanisms by fibres or cables is advantageous especially due to the achievement of a lower moving inertia, which can lead to a higher machine speed. Drawbacks of using the flexible elements like that can be associated with the fact that cables should be only in tension (e.g. Valášek & Karásek, 2009) in the course of a motion.

Experimental measurements focused on the investigation of the fibre behaviour were performed. The simple fibre-mass system consists of moving weight coupled with a frame by a fibre (see Fig. 1a). The same system is numerically investigated using a simple multibody model created in the **alaska** simulation tool. The influence of the model parameters on the coincidence of results of experimental measurements and simulations are evaluated. The simulation aim is to create a phenomenological model of a fibre, which will be utilizable in fibre modelling in the case of more complicated mechanical or mechatronic systems.

2. Experimental stand, measurements and simulations

In the chosen mechanical system for the experimental measurement the fibre is driven with one drive and is led over a pulley. On its other end there is a prism-shaped steel weight, which moves on an inclined plane (see Fig. 1b). Drive exciting signals can be of a rectangular, a trapezoidal and a quasi-sinusoidal shape and there is a possibility of variation of a signal rate. Displacement of the weight, displacement of the drive and the force acting in the fibre will be the measured quantities. Angle of inclination of the inclined plane can be changed.

Investigation of the single fibre properties eliminating the influence of the drive and of the pulley (see Fig. 1a) was an intermediate stage before the measurement on this stand. Fibre was fixed on a force gauge. In the other end of the fibre the already mentioned prism-shaped steel weight was fastened. The weight was lifted to a certain height (from 5 to 20 millimetres) and then let to fall in the vertical direction or to slide down the inclined plane. The weight moved in prismatic linkage. The time histories of the weight position and of the force acting in the fibre were recorded.

The fibre model is considered to be phenomenological. It is modelled by the forces which comprise e.g. influences of fibre transversal vibration, etc. The weight is considered to be a rigid body.

[*] Dr. Ing. Pavel Polach: Section of Materials and Mechanical Engineering Research, Výzkumný a zkušební ústav Plzeň s.r.o., Tylova 1581/46; 301 00, Plzeň; CZ, e-mail: polach@vzuplzen.cz

[**] Ing. Michal Hajžman, Ph.D.: Department of Computer-Aided Modelling, Výzkumný a zkušební ústav Plzeň s.r.o., Tylova 1581/46; 301 00, Plzeň; CZ, e-mail: hajzman@vzuplzen.cz

[***] Ing. Jaroslav Václavík: Dynamic Testing Laboratory, Výzkumný a zkušební ústav Plzeň s.r.o., Tylova 1581/46; 301 00, Plzeň; CZ, e-mail: vaclavik@vzuplzen.cz

Two models of the fibre are considered: the massless model and the point-mass model (Polach et al., 2013). Behaviour of these nonlinear systems is investigated using the **alaska** simulation tool.

When looking for compliance of the results of experimental measurement with the simulation results influences of the following system parameters are considered: the fibre damping coefficient, the fibre stiffness and the frictional force between the weight and the prismatic linkage. Results of experimental measurements and simulations of six tested situations are presented in the paper.

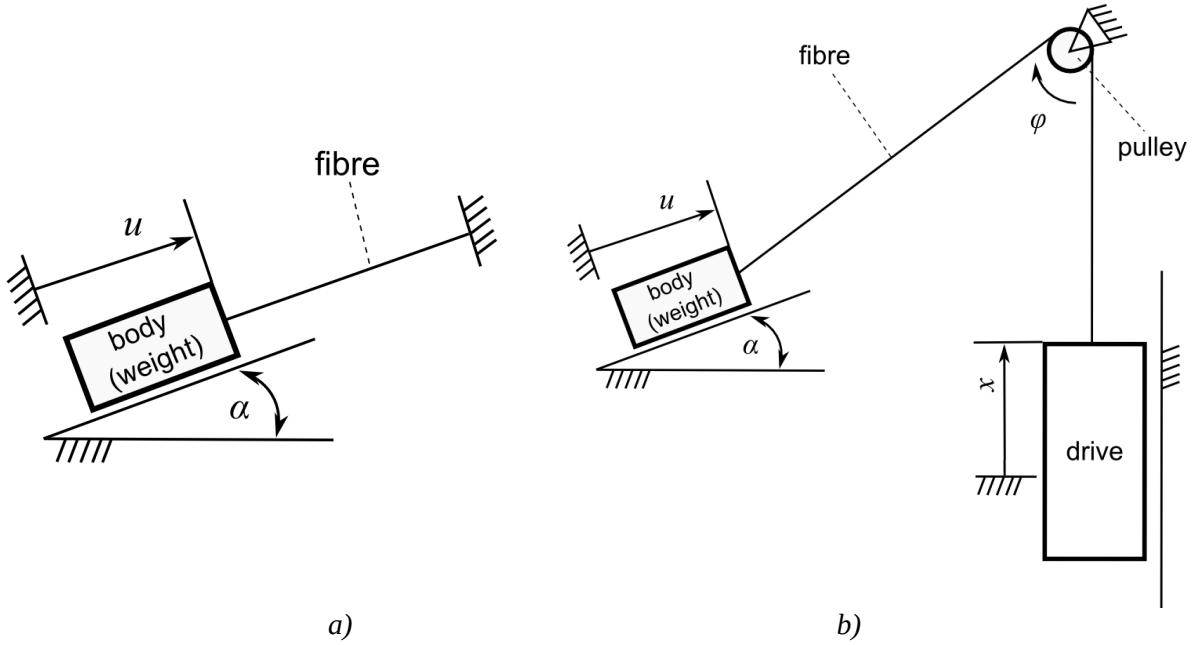

a) *b)*

Fig. 1: a) Weight-fibre mechanical system, b) weight-fibre-pulley-drive mechanical system.

3. Conclusions

From the achieved results it is evident that the general phenomenological model of the fibre was not determined. General influences of the individual parameters on the system behaviour, which are usable for all systems containing fibre-mass subsystem(s), were assessed. Suitable fibre models, but only in dependence on the definite simulated test situation, were determined. In the case of the investigated simple fibre-mass mechanical system the created models are dependent on the angle of inclination of the (inclined) plane on which the weight moves. It is obvious that it would not be possible to generalize the created models either for the weight-fibre-pulley-drive mechanical system, which will be experimentally investigated, or for the other similar systems. Naturally, the cause of problems can also be in the experimental measurements.

Development of the fibre phenomenological model will continue. It can be supposed that in more sophisticated phenomenological model of a fibre more complicated dependencies of the fibre stiffness and of the fibre damping coefficient than currently used constant values will be considered and the usability of the functions of higher orders for the model of the friction force will be verified. The question is if it is possible to create the phenomenological model like this.

Acknowledgement

The paper has originated in the framework of solving No. P101/11/1627 project of the Czech Science Foundation entitled “Tilting Mechanisms Based on Fiber Parallel Kinematical Structure with Antibacklash Control”.

References

Polach, P., Hajžman, M. & Václavík, J. (2013) Simple fibre-mass model and experimental investigation, in: *Proc. National Colloquium with International Participation Dynamics of Machines 2013* (L. Pešek ed.), Institute of Thermomechanics Academy of Sciences of the Czech Republic, Prague, pp. 79-84.

Valášek, M. & Karásek, M. (2009) HexaSphere with Cable Actuation. *Recent Advances in Mechatronics: 2008-2009*, Springer-Verlag, Berlin, pp. 239-244.

19th International Conference
ENGINEERING MECHANICS 2013
Svratka, Czech Republic, May 13 – 16, 2013

BRANCH AND BOUND METHOD FOR OPTIMIZATION OF CABLE-TRUSS STRUCTURES

A. Pospíšilová, M. Lepš [1]

Summary: *This contribution introduces a new formulation of a classical Branch and Bound method to find global optima of truss sizing optimization problems enhanced with cables. Our paper shows that the problem is solvable as a binary version of the mixed integer programming problem. The text presents the derivation and the implementation details.*

Keywords: ***Size Optimization, Cable-Truss Structures, Benchmarks, Global Optima, Mixed-Integer Linear Problem, Big-M Problem, Cables***

1. Introduction

This contribution presents steps that are needed to solve the global optima of the Cable-Truss Structures. The different behavior of cables in compression must be taken into account. The topology of the structure is unchanging and the goal is to find minimal weight with the best combination of cross-section areas. Prescribed constraints are minimal and maximal possible values of displacements as well as stresses.

This optimization problem is nonlinear in constraints

$$\min_{\mathbf{x}\in\mathbb{B}^{na\cdot nr},\mathbf{u}\in\mathbb{R}^{nd}} \quad \rho\sum_{j=1}^{nr}\ell_j\sum_{i=1}^{na}a_i x_{i,j} \quad \text{(weight)} \tag{1}$$

$$\text{subject to} \quad \mathbf{K}(\mathbf{x})\mathbf{u}=\mathbf{f} \quad \text{(force equilibrium)}, \tag{2}$$

$$\sum_{i=1}^{na}x_{i,j}=1 \quad \forall j \quad \text{(one area per bar)} \tag{3}$$

$$\mathbf{u}^{\min}\le\mathbf{u}\le\mathbf{u}^{\max} \quad \text{(displacement constraint)} \tag{4}$$

$$x_{i,j}\in 0,1 \quad \forall(i,j). \tag{5}$$

however it can be transformed into pure linear one.

We limit our attention only to prescribed topology, i.e. to the pre-defined positions of bars and cables. A vector $\mathscr{M}$ differentiates whether the truss-member is a cable or a bar. Vector $\neg\mathscr{M}$

[1] Ing. Adéla Pospíšilová, doc. Ing. Matěj Lepš, Ph.D., Faculty of Civil Engineering, Czech Technical University in Prague, Thákurova 7, 166 29 Prague 6, tel. +420 224 355 417, e-mail adela.pospisilova@fsv.cvut.cz

is a logical complement to vector $\mathscr{M}$. Then, the final derivation reads

$$\min_{\mathbf{x},\mathbf{u},\mathbf{s}} \quad \rho\Big((\boldsymbol{\ell}\otimes\mathbf{1}_{[na]})^T\odot(\mathbf{1}_{[nr]}\otimes\mathbf{a})^T\Big)\,\mathbf{x} \tag{6}$$

$$\text{s.t.} \quad \mathbf{B}\mathbf{s}=\mathbf{f}, \tag{7}$$

$$\sigma^{\min}\,\mathrm{diag}\big(\mathbf{1}_{[nr]}\otimes\mathbf{a}\big)\,\mathbf{x}\le\mathbf{s}\le\sigma^{\max}\,\mathrm{diag}\big(\mathbf{1}_{[nr]}\otimes\mathbf{a}\big)\,\mathbf{x}, \tag{8}$$

$$\Big(\big(\xi\otimes\mathbf{a}\otimes\mathbf{1}^T_{[nd]}\big)\odot\mathbf{B}^T\Big)\mathbf{u}-\mathbf{s}\ge\mathrm{diag}\big(\mathscr{M}\otimes\mathbf{1}_{[na]}\big)\cdot(-\infty)+\ldots \tag{9}$$

$$+\mathrm{diag}\big(\neg\mathscr{M}\otimes\mathbf{1}_{[na]}\big)\odot\big(\mathbf{1}_{[na\cdot nr]}-\mathbf{x}\big)\odot\mathbf{C}^{\min},$$

$$\Big(\big(\xi\otimes\mathbf{a}\otimes\mathbf{1}^T_{[nd]}\big)\odot\mathbf{B}^T\Big)\mathbf{u}-\mathbf{s}\le\big(\mathbf{1}_{[na\cdot nr]}-\mathbf{x}\big)\odot\mathbf{C}^{\max}, \tag{10}$$

$$\mathbf{I}_{[nr]}\otimes\mathbf{1}_{[na]}\cdot\mathbf{x}=\mathbf{1}_{[nr]}. \tag{11}$$

This problem is linear in design variables $\mathbf{x}$, $\mathbf{u}$ and $\mathbf{s}$. All other symbols are constant vectors and matrices. All symbols are described in the full paper.

2. Conclusions

The presented contribution shows major steps needed for the relaxation of the cable-truss sizing optimization problem. At this point, a Branch and Bound method can be used. However, two issues remain unsolved. The first one is a free selection of a cross-sectional type, i.e. whether the rod will be a cable or a truss. This is a domain of topology optimization and therefore was not taken into account in our work. For more details, inspect e.g. a work on tensegrity structures Kanno (2011), which are a special part of cable-truss structures. Note, that the inclusion of the cross-sectional type needs additional binary variable for each rod which can dramatically complicate computational demands of the optimization task. The second issue deals with the prestressing of the cables. At this point, the procedure is relatively simple and is also presented in Kanno (2011).

3. Acknowledgment

The authors gratefully acknowledge the financial support from the Grant Agency of the Czech Republic through the project GAČR P105/12/1146 and from the Grant Agency of the Czech Technical University in Prague, the grant SGS13/034/OHK1/1T/11.

4. References

Kanno, Y. 2011: Topology optimization of tensegrity structures under compliance constraint: a mixed integer linear programming approach. *Optimization and Engineering*, pages 1–36, 2011.

Pospíšilová, A. & Lepš, M. 2013: Parallel Branch and Bound Method for Size Optimization Benchmarks- In B. H. V. Topping and P. Iványi, editors, *Proceedings of the Third International Conference on Parallel, Distributed, Grid and Cloud Computing for Engineering*, Stirlingshire, United Kingdom, 2013. Civil-Comp Press. paper 20.

Rasmussen, M. H. & Stolpe, M. 2008: Global optimization of discrete truss topology design problems using a parallel cut-and-branch method. *Computers & Structures*, 86:1527–1538.

19th International Conference
ENGINEERING MECHANICS 2013
Svratka, Czech Republic, May 13 – 16, 2013

NUMERICAL SIMULATIONS OF EFFECTS OF SPECIMEN PREPARATION METHOD ON PROPERTIES OF FIBER COMPOSITES

M. Přinosil*, P. Kabele**

Abstract: *The correct determination of mechanical properties of construction materials has a major impact on the design and reliability of structures. Strength and deformation characteristics are evaluated based on data from experiments. The determined parameters can be largely affected also by fabrication of experimental specimens. Either by nature of production, storage conditions before experiment itself, or by testing set-up (equipment, boundary conditions, etc.). This article deals with influence of specimen preparation method on the strength of reinforcement in fiber composites. To clarify this phenomenon we performed numerical calculation based on randomly generated fibers.*

Keywords: ***fiber-reinforced composites, fiber bridging, cohesive law, specimen preparation method***

1. Introduction

In our research, we are developing new high performance mortar for restoration works on historical structures. It is a composite material made from fine-grained lime matrix, which is reinforced with short randomly oriented fibers in a small volume fraction ($V_f \leq 2\%$). For the material design we use a methodology, which has been developed for design of quasi-brittle composites reinforced with short fibers (Li, 2003). This methodology was successfully used, for example, for design of Engineered Cementitious Composites – ECC (Li, 2003). As part of the research of cementitious composites, several comparative tests were carried out. A comprehensive round-robin study was performed to compare the experimental data from tensile and bending tests on specimens with different shape and size (Kanakubo, 2006). Another comparative study was organized by RILEM Technical Committee 208 – HFC in 2007 (not published yet) and involved only tensile experiments. All specimens were prepared from identical commercially available dry mix (ECC-crete, produced by Kajima corp. and Futase corp., Japan), but in different laboratories according to local convention with different equipment. The results of these studies indicate that obtained material characteristics are largely influenced by the particular set up of the experiments, such as boundary conditions, size of a specimen and the method of specimen preparation. The aim of our work is to clarify some differences in behavior between experimental specimens that were prepared either by casting into appropriate mold or by cutting from a large body of material. For the purpose of this work we performed numerical simulations to predict cohesive behavior of a single crack for specimens prepared by different methods.

2. Numerical simulations

Numerical simulations were performed for lime mortar reinforced with polyvinyl-alcohol fibers (PVA – type REC 15, made by Kuraray Company) in volume fraction 2% with variable length (4 ÷ 12 mm) to predict cohesive behavior of a single crack (cohesive law) – relation between crack opening displacement δ and bridging stress σ_b. From calculated relations the most important was maximum bridging stress σ_{mb} at each point of the cross-sectional area of the specimen. Therefore the cross section was divided into a regular grid and the maximum bridging stress was calculated in every part.

* Ing. Michal Přinosil: Czech Technical University in Prague, Faculty of Civil Engineering, Department of Mechanics, Thákurova 7; 166 29, Prague; CZ, e-mail: michal.prinosil@fsv.cvut.cz

** prof. Ing. Petr Kabele, Ph.D.: Czech Technical University in Prague, Faculty of Civil Engineering, Department of Mechanics, Thákurova 7; 166 29, Prague; CZ, e-mail: petr.kabele@fsv.cvut.cz

3. Effects of specimen preparation method

Figure 1 shows the maximum bridging stress σ_{mb} for both types of preparation method. In the case of casted specimen, surface layer has a higher maximum bridging stress than the inner part. The highest strength is calculated in corner sections where the fibers are aligned with two surfaces and their direction nearly corresponds to the longitudinal axis. In the case of sawed specimen, it is just the opposite. Damaged fibers are able to transfer reduced force and therefore the surface layer is weakened. It is particularly evident in the corners where the fibers are sawed by two surfaces.

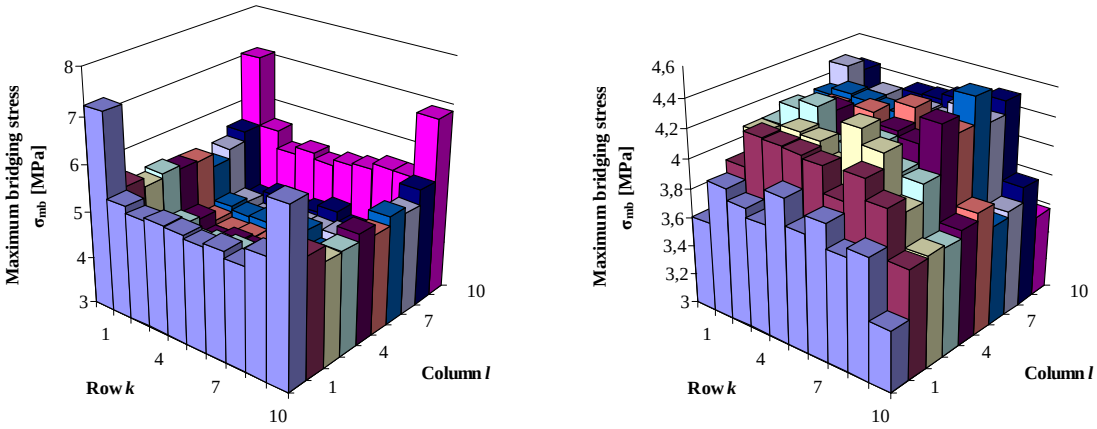

Fig. 1: Maximum bridging stress σ_{mb} at particular points of the cross-section of casted (left) and sawed (right) specimen

4. Conclusion

The results of numerical calculations confirmed the assumption that material parameters of fiber composites evaluated from experiments depend on the preparation method of the specimen. It has been demonstrated that in the case of sawed specimens, the fibers in surface layer are damaged and thus their ability to transfer the load is reduced. In the case of casted specimens, fibers tended to align with mold surface and thus the maximum bridging stress in surface layer increases. According to the results, the depth of weakened surface layer doesn't depend on the fiber length compared to the depth of the reinforced layer in the case of casted specimens.

Acknowledgement

The presented research has been carried out with financial support of the Czech Technical University in Prague under project SGS13/034/OHK1/1T/11.

References

Kanakubo, T. (2006) Tensile characteristics evaluation method for ductile fiber-reinforced cementitious composites. *Journal of Advanced Concrete Technology*, 4, 1, pp.3-17.

Li, V. C. (2003) On Engineered Cementitious Composites (ECC) – A review of the material and its applications. *Journal of Advanced Concrete Technology*, 1, 3, pp.215-230.

Li, V. C. & Leung, C.K.Y. (1992) Steady state and multiple cracking of short random fiber composites. *Journal of Engineering Mechanic*, 188, 11, pp.2246-2264.

Přinosil, M. (2010) Modeling of Fiber Reinforced Cementitious Composites using Stochastic Finite Elements. Master's thesis, Czech Technical University in Prague.

Přinosil, M. & Kabele, P. (2012) Prediction of the behavior of lime mortar reinforced with fibers based on their micromechanical parameters, in*: Proc. 8th Int.Conf. on Structural Analysis of Historical Constructions* (Jerzy Jasieńko eds), Wroclaw University of Technology, Wroclaw, pp.883-889.

Přinosil, M. (2012) FiberBridging: User's manual. http://mech.fsv.cvut.cz/~prinosil/index.php?id=FiberBridging.

Yang, E.-H., Wang, S., Yang, Y. & Li, V.C. (2008) Fiber-Bridging Constitutive Law of Engineered Cementitious Composites. *Journal of Advanced Concrete Technology*, 6, 1, pp.181-193.

19th International Conference
ENGINEERING MECHANICS 2013
Svratka, Czech Republic, May 13 – 16, 2013

MODEL OF TURBINE BLADES BUNDLES

L. Půst[1], L. Pešek[1]

1. Introduction

An effective way against undesirable vibrations of turbine blades vibrations is introducing additional damping elements into blade shroud. A lot of theoretical, numerical and experimental studies in this field were done also in Institute of Thermomechanics ASCR, where the measurements on the experimental physical model of five-blades bundles is now prepared.

The presented theoretical study is oriented particularly on the elaboration of a theoretical background for analysis of data gained by measurement.

2. Vibrations of blades bundle –experimental model

Laboratory measurements of blade bundle will be realized on the experimental set consisting of five models of blades with shroud heads, which were rigidly fastened to a steel plate basement, Fig.1.

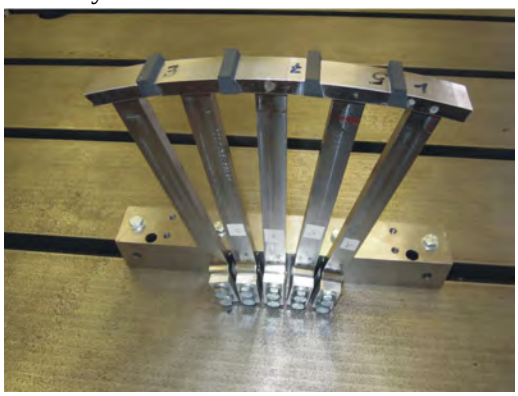

Fig. 1

Inserted damping elements are made of special rubber FKM with a trade mark VITON of hardness 70 ShA, having high resistance against high temperatures, against majority of aggressive chemicals, synthetic and mineral oils, etc. It has very strong dependence of its mechanical behavior on the temperature and frequency and therefore the mathematical modeling of the dynamic properties of systems containing these elements need a special treatment.

Experimental system can be modeled by a five masses system Fig. 2, where the blades are replaced by 1 DOF systems, the eigenfrequencies of which corresponds to the first bending eigenfrequency of the real blades. Masses m are loaded by forces$F_i(t) = F_{0i}\cos(\omega t)$, i =1,..5. the linkage forces among masses are described by the linear Kelvin Voigt viscous-elastic model.

Differential equations of motion for the excitation by given vector of force amplitudes and for free vibrations were derived for stiffness k_1 = 2000 N/m. All five calculated eigenfrequencies are in the range 120 – 125 Hz and the corresponding eigenmodes are plotted in Fig. 3.

The responses of 5 DOF system on the various combinations of external harmonic forces were investigated. Response curves calculated at sweep excitation with angular acceleration $\varepsilon = 0.20\ rad/s^2$ and for the force vector consisting of only one force F_{01} = 1 N, (i.e. [1,0,0,0,0]), are

[1] Ing. L. Půst, DrSc., Ing. L. Pešek, CSc., Institute of Thermomechanics AS CR, v.v.i., Dolejškova 5, 18200 Praha 8, e-mail: pust@it.cas.cz, pesek@it.cas.cz,

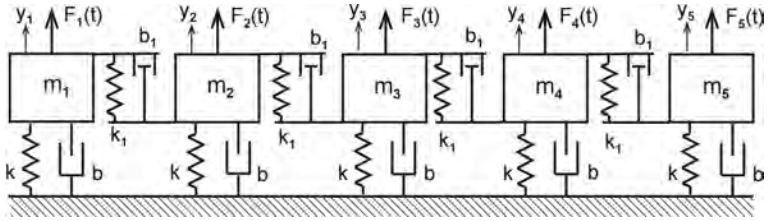

Fig.2

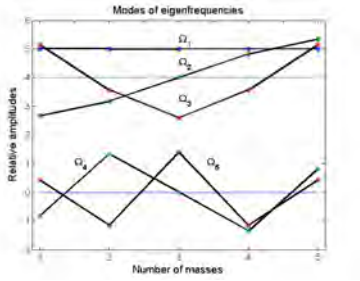

Fig.3

plotted in Fig. 4. The second resonance causes small distortion of response curves, the other resonances cannot be excited by the one-force action. The multi-point excitation with appropriate forces distribution enables to isolate higher modes, as it is shown e.g. in Fig. 5 for the forth resonance of 5-blades bundle.

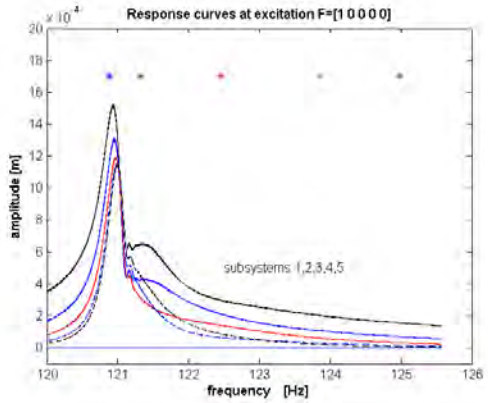

Fig. 4

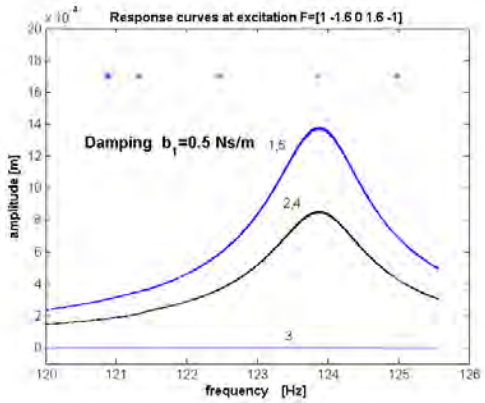

Fig. 5

3. Conclusions

- A mathematical model of five blades bundle connected in the heads slots by damping elements made of special rubber has been developed and applied for the ascertaining of dynamic behavior of blades bundle at different external excitation.
- Properties of rubber FKM with a trade mark VITON of hardness 70 ShA, which was selected as material for the damping elements for the prepared experimental research in laboratory IT AVCR, were discussed particularly in view of the dependence on frequency of oscillations.
- Detail analysis of frequency and temperature effect on this material showed that the eigenfrequency spectrum varies mainly in the temperature range under 50 ^{o}C and in the range 50 – 120 ^{o}C the influence of temperature is negligible. The variability of stiffness and damping properties on frequency is similar.
- Effect of the temperature and frequency on the forms of eigenmodes in the whole investigated area is negligible.
- The analysis of influence of different force distribution on the response curves of blades bundle was realized at the lower stiffness k_1 = 2000 N/m.
- It was proved that due to the more complicated forms at higher eigenmodes the mode's damping increases with frequency even at the constant material viscous damping coefficient
- The application of orthogonality of excitation forces distribution to the other eigenmodes of blades bundle is necessary for analysis and isolation of selected resonance.

19th International Conference
ENGINEERING MECHANICS 2013
Svratka, Czech Republic, May 13 – 16, 2013

IN VIVO MEASUREMENTS OF AIR PRESSURE, VOCAL FOLDS VIBRATION AND ACOUSTIC CHARACTERISTICS OF PHONATION INTO A STRAW AND A RESONANCE TUBE USED IN VOCAL EXERCISING

V. Radolf[*], A. M. Laukkanen[**], J. Horáček[*], J. Veselý[Ŧ], D. Liu[***]

Abstract: *The study investigates the differences between three most widely used methods in voice training and therapy: Phonation into a glass resonance tube (1) the outer end in the air, (2) the outer end submerged 2-10 cm below water surface in a bowl ('water resistance therapy' with bubbling effect), and (3) phonation into a very thin straw. One female speech trainer served as subject. Acoustic samples, electroglottographic signals and both mean and dynamic airpressures in the mouth cavity were registered for repetitions of [pu:pu], and for phonation into the tubes, while the outer end was randomly shuttered, in order to get an estimate of subglottic pressure. Both phonation threshold and ordinary, most comfortable phonation were recorded.*

Keywords: ***Biomechanics of voice; subglottal, oral and transglottal pressure; phonation into tubes.***

1. Introduction

Phonation into straws and tubes is widely used in vocal exercising and voice therapy (see e.g. Titze et al., 2002). The present study aims to compare the most common tube training methods: resonance tube in air, resonance tube 2 cm under water and 10 cm under water, and stirring straw from the point of view of phonation threshold pressure, and subglottal pressure as well as electroglottographic parameters for the most comfortable phonation at habitual speaking pitch.

2. Method

One female voice trainer, phonated (in speech mode) at comfortable pitch on [pu:] both at comfortable loudness and phonation threshold, and similarly at two loudness levels into a straw (12.7 cm in length, 2.5 mm in inner diameter) in the air, into a resonance tube (made of glass, 27 cm in length, 6.8 mm in inner diameter) in the air and with the other end submerged 2 cm and 10 cm below water surface.

The sound pressure level (*SPL*) inside the oral cavity was measured using the B&K special microphone probe and the mean oral pressure (P_{oral}) was measured by the digital manometer connected with the oral cavity by a small compliant tube. Pressure during [pu:] and manual shuttering of the other end of the tube gave an estimate of subglottic pressure (P_{sub}). The nose was closed with a clip to prevent any leakage of air through the nose. Generated acoustic signal outside the vocal tract model was recorded using the microphone (B&K sound level meter) installed at a distance of 20 cm from the lips. Electroglottographic signal was registered using a dual channel EGG device (Glottal Enterprises). The recording was made using 32.8 kHz sampling frequency by the PC controlled measurement system B&K PULSE 10. The fundamental vibration frequencies *F0* and the formant frequencies (acoustic resonances) were evaluated from the spectra of the pressure signals.

[*] Ing. Vojtěch Radolf, PhD., Ing. Jaromír Horáček, DrSc.: Institute of Thermomechanics, Academy of Sciences of the Czech Republic, Dolejškova 5, 182 00 Prague 8; e-mail: radolf@it.cas.cz, jaromirh@it.cas.cz

[**] Prof. Anne-Maria Laukkanen: Speech and Voice Research Laboratory, School of Education, University of Tampere, FIN-33014, *Tampere,* Finland; e-mail: anne-maria.laukkanen@uta.fi

[***] Dr. Dong Liu: Inverse Problems Group, Department of Applied Physics, University of Eastern Finland, Kuopio, Finland; e-mail: dong.liu@uef.fi

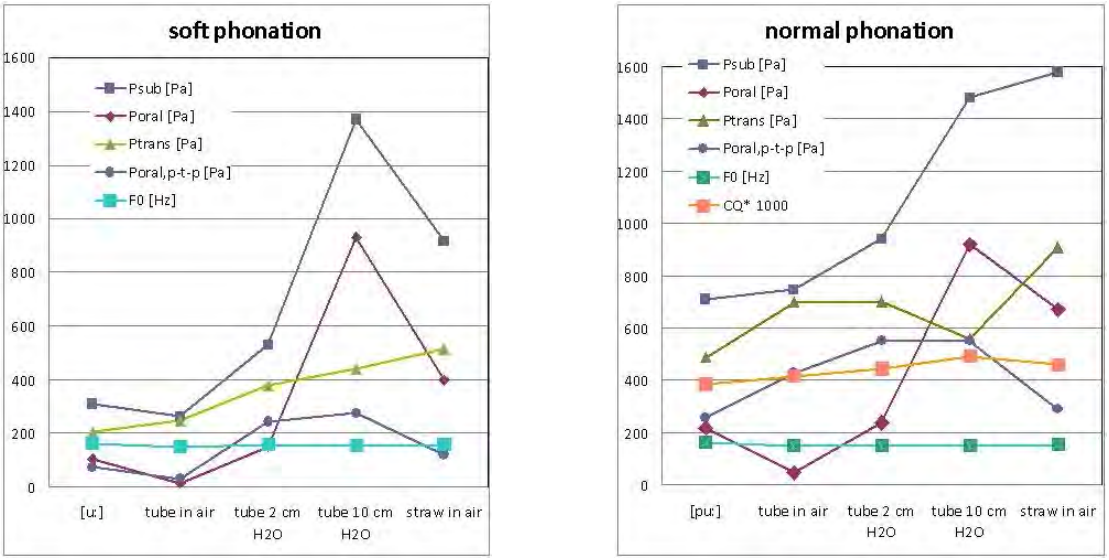

Fig. 1: Mean values of the measured subglottal, oral and transglottal pressures, peak-to-peak values of oral pressures and fundamental frequency for soft phonation (left) and normal phonation (right) on vowel [u:], into the resonance tube in air, into the tube submerged in water and into the narrow straw.

3. Results

Compared to vowel phonation and the other vocal exercises, phonation into resonance tube in air brought about the lowest phonation threshold pressure PTP (P_{sub} = 310 Pa), tube 10 cm under water the highest (1.37 kPa) and straw second highest (910 Pa), see Fig. 1 (left). The lower PTP for straw than tube 10 cm in water may be due to some over blowing from the lips. Oral pressure P_{oral} was surprisingly lower for tube in air than for vowel [u:]. It may be caused by a reduced lip opening during the vowel phonation. Thus a very closed vowel seems to be an effective exercise, increasing oral pressure compared to more open vowels.

Oral pressure oscillation was highest for tube 10 cm in water (270 Pa peak-to-peak for soft phonation), which may offer strongest massage effect on the vocal tract and vocal folds. Transglottal pressure ($P_{trans} = P_{sub} - P_{oral}$) was larger for all exercises, being largest in those exercises which seem to offer highest supraglottic impedance. Thus, the subject of the present study seems to overcompensate for an increase in oral pressure by increasing $P_{sub.}$

In EGG signal the closed quotient CQ was higher for the tubes compared to vowel phonation. The largest change was observed for tube 10 cm in water, see Fig. 1 (right). It was also possible to see the effect of water bubbling on the EGG signal. That causes a baseline shift of the signal, due to variation in vertical laryngeal position caused by water bubbling, at a frequency of 15 Hz and also a decrease in the vocal fold contact. It may be either due to increased intraglottal airpressure or an artefact related to changes in vertical position of the larynx.

4. Conclusions

Exercises that increase supraglottic airpressure offer a possibility to train glottal and respiratory adjustments under the influence of increased backpressure which may both assist vocal fold vibration and prevent excessively loading vocal fold collision.

Acknowledgement

The study was supported under the grants of the Czech Science Foundation No P101/12/P579 and by the Academy of Finland (grants No. 1128095 and 134868).

References

Titze, I.R., Finnegan, E.M., Laukkanen, A-M. & Jaiswal, S. (2002) Raising lung pressure and pitch in vocal warm-ups: The use of flow-resistance straws. *Journal of Singing* 58, pp. 329-338.

19th International Conference
ENGINEERING MECHANICS 2013
Svratka, Czech Republic, May 13 – 16, 2013

Meshless local Petrov-Galerkin formulation for analysis of composite plates reinforced by unidirectional fibers

D. Riecky*, A. Sapietová, M. Žmindák****

Abstract: *This paper deals with application of the meshless methods for analysis of composite plates. The main focus is on the implementation of the MLPG formulation for layered plates. The software for homogenization of material properties uses direct homogenization method that is based on volume average of stresses in the representative volume element (RVE). Homogenization is performed by a multisoftware approach, by linking MATLAB and ANSYS software. Data obtained are used in analyses performed in own software, which is based on the MLPG method. Results obtained by MLPG were compared with those obtained by FEM programs ANSYS and ABAQUS.*

Keywords: ***Composite plates, unidirectional composites, Reissner-Mindlin theory, meshless method***

1. Introduction

The finite element method (FEM) is one of the most widely used and most popular numerical methods for analyzing plate structures. Although the method is stable, well developed and has reached extensive development during last decades, it also has some limitations.

In last years an increase of interest in new type of numerical methods known as meshless methods was observed (Soares, et al., 2012). These methods are interesting due to their flexibility and ability of solving boundary value problems without predefined mesh. Computational model in these methods is represented by a set of nodes distributed within global domain and its boundary. These nodes do not have to be connected into explicitly defined elements.

One of the areas where meshless methods are convenient to use is analysis of plate and shell structures. Compared to FEM formulations there are less meshless formulations available for plate and shell structures.

2. Homogenization of composite

There are various homogenization methods. Direct homogenization is based on the volume average of field variables, such as stress, strain and energy density. Effective properties can be calculated from effective properties definitions. The mean and calculation of field variables can be performed numerically, for example by FEM, BEM and the geometry and microstructural properties can be generalized. Indirect homogenization is based on the Eshelby solution of self-deformation for one inclusion in an infinite matrix – the equivalent inclusion method (Eshelby, 1957). This method does not use averaging of the field variables and the effective properties can be obtained by deducing from the volume fractions and the inclusion geometry as well as the component properties. An alternate approach to direct and indirect homogenization is the variational method, which can determine the upper and lower limits of the elasticity modulus (Hashin & Shtrikman, 1962).A relatively new approach a homogenization of microstructures consist of mathematical homogenization based on a two-scale extension of the displacement field.

This part describes the procedure of homogenization of material properties of composites using the method of representative volume element (RVE). For the analysis of the material properties an own software was programmed in MATLAB language and a part of the solution was carried out in ANSYS software. Homogenized lamina RVE consists of a fibers and epoxy matrix. The fibers are from three

* Ing. Daniel Riecky, PhD.: Plastic Omnium Auto Exteriorx, LtD. 900 55 Lozorno, Slovakia, e-mail: riecky@plasticomnium.com

** doc. Ing Alžbeta Sapietová, PhD., University of Žilina, Faculty of Mechanical Engineering, Department of Applied Mechanics, Univerzitná 1, 010 26 Žilina, Slovak Republic, e-mail:alzbeta.sapietova@fstroj.uniza.sk

** prof. Ing. Milan Žmindák, CSc.: University of Žilina, Faculty of Mechanical Engineering, Department of Applied Mechanics, Univerzitná 1, 010 26 Žilina, Slovak Republic, e-mail:milan.zmindak@fstroj.uniza.sk

material types: carbon, glass, polyaramid. Used carbon fibers have an industrial labeling T300 and M40J. The glass fiber label is EGlass and S2Glass. Polyaramide fibers have the label K49.

3. Governing equations

Classical laminated plate theory was formulated by deriving classical plate theory for composite plates. In this theory the plate composes of N orthotropic layers with total thickness h. The midsurface of layered plate is located in the region Ω, in plane (x_1, x_2). Axis $x_3 \equiv z$ is perpendicular to the midsurface.

4. Numerical implementation MLPG for composite plate

In the present paper we will present a meshless method based on the local Petrov-Galerkin weak-form to solve static problems for laminated plate bending described by the Reissner-Mindlin theory. The derived meshless method uses a local interpolation to represent the trial function with the values (or the fictitious values) of the unknown variable at some randomly located nodes.

5. Numerical example

Clamped and simply supported square plates are analysed. We consider composite plates with the dimensions $L_x = 0.24$ *m* and $L_y = 0.2$ *m*. Is composed from six lamina with thickness $\Delta_z = 0.00025$ *m*, total thickness of plate is $h = 0.0015$ *m*. Material of the analyzed plate is EGlass_vf06. Comparison of stresses course of stresses σ_{11} a σ_{22} at given point of plate from center of corresponding layer and values are given in Tab. 1.

Tab. 1: Comparison of stresses σ_{11} a σ_{22} from MLPG and FEM, Eglass_vf04

layer	1	2	3	4	5	6
σ_1^{MLPG} [-]	7.76e+6	3.14e+6	3.43e+6	-3.43e+6	-3.14e+6	-7.76e+6
σ_1^{REF} [-]	7.57e+6	3.07e+6	3.35e+6	-3.35e+6	-3.07e+6	-7.57e+6
|err| [%]	2.58	2.52	2.37	2.37	2.52	2.58
σ_{22}^{MLPG} [-]	10.20e+6	17.91e+6	1.50e+6	-1.50e+6	17.91e+6	-10.20e+6
σ_{22}^{REF} [-]	9.92e+6	17.4e+6	1.46e+6	-1.46e+6	-17.4e+6	-9.92e6
|err| [%]	2.85	2.94	2.88	2.88	2.94	2.85

6. Conclusions

The MLPG method was applied to analysis of laminated composite plates under static loadings. The numerical results confirm the fact that MLPG method is a good tool for analysis of composite structures. It is a reliable method after sufficient setting of parameters such as order of numerical integration, size of the integration domain, support domain for weight function, etc.

Acknowledgement

The authors gratefully acknowledge for support the Slovak and technology Assistance Agency registered under number APVV-0169-07, Slovak Grant Agency VEGA 1/1226/12.

References

Eshelby, J. D. (1957) The determination of elastic field of an ellipsoidal inclusion and related problems. in:*Proc. R. Soc. Londýn*, pp. 276- 396.

Hashin, Z.- Shtrikman, S. (1962) On some variational principles in anisotropic and nonhomogeneous elasticity, J. *Mech. Phys. Solids*, vol. 10, p.335-342.

Soares, D. Jr., Sladek, J., Sladek, V., Zmindak, M., Medvecky, S (2012): Porous Media Analysis by Modified MLPG Formulations. CMC: Computers, Materials,& Continua, 27,2, pp. 101-127.

19th International Conference
ENGINEERING MECHANICS 2013
Svratka, Czech Republic, May 13 – 16, 2013

PARALLEL NUMERICAL SIMULATION OF AIRFLOW PAST AN OSCILLATING NACA0015 AIRFOIL

V. Řidký*, P. Šidlof and V. Vlček*****

Abstract: *This paper focuses on parallel computation of pressure fields around an elastically supported airfoil self-oscillating due to interaction with the airflow vibrating airfoil. The results of numerical simulations are compared with data measured in a wind tunnel, where physical model of a NACA0015 airfoil was mounted and tuned to exhibit the flutter instability. The numerical solution is implemented in OpenFOAM, an open-source software package based on finite volume method. In the numerical solution is prescribed displacement of the airfoil, which corresponds to the experiment.*

Keywords: ***Airfoil, CFD, parallel computing, OpenFOAM.***

1. Introduction

The main focus is on a parallel numerical solution of incompressible airflow past a NACA0015 airfoil using 2D and 3D computational meshes, and comparison of the numerical results with experimental data measured in aerodynamic tunnel of the Institute of Thermomechanics in Nový Knín. Specifically, the simulated distribution of pressure on the surface of the wing vibrating in the channel due to flutter instability is compared to the experimental surface pressures. In the experiment, the pressures are evaluated from interferograms obtained using Mach-Zehnder interferograms. [Vlček 2010].

2. Mathematical model, geometry and boundary conditions

Geometry of the computational domain corresponds to experimental setup, where the airfoil is placed in a channel with a cross-section of 210 x 80 mm. The length of the computational domain is set to 580 mm.

The flow pas the moving airfoil is described by incompressible Navier-Stokes equations

$$\nabla \cdot \boldsymbol{u} = 0 \tag{1}$$

$$\frac{\partial \boldsymbol{u}}{\partial t} + \nabla \cdot (\boldsymbol{u}\boldsymbol{u}) - \nabla \cdot \nu \Delta \boldsymbol{u} + \frac{1}{\rho} \nabla p = 0\,, \tag{2}$$

where $\boldsymbol{u}$ is flow velocity, p is dynamic pressure, ν is kinematic viscosity and ρ is density. These equations are in strong conservative form, suitable for finite volume discretization.

Boundary conditions for the pressure and velocity fields are specified as follows: on fixed walls, the flow velocity $\boldsymbol{u}$ is zero, on the moving wing surface the flow velocity is equal to the velocity of the airfoil. At the inlet a flat velocity profile u_x = 147 m/s is prescribed. At the outlet, the pressure is set to zero. Due to large intensity of vorticity resulting from flow separation downstream of the wing, a stabilized boundary condition for the velocity is prescribed at outlet $\partial \boldsymbol{u}/\partial n = 0$ when velocity direction points outward of the domain, u_x = 0 m / s otherwise, for pressure p = 0 Pa.

* Ing. Václav Řidký: Institute of Thermomechanics AS CR, v. v. i., Dolejškova 1402/5; 182 00, Praha 8; CZ, e-mail: vaclav.ridky@tul.cz

** Ing. Petr Šidlof, Ph.D.: Institute of Thermomechanics AS CR, v. v. i., Dolejškova 1402/5; 182 00, Praha 8; CZ, e-mail: sidlof@it.cas.cz

*** Ing. Václav Vlček, Csc.: Institute of Thermomechanics AS CR, v. v. i., Dolejškova 1402/5; 182 00, Praha 8; CZ, e-mail: vlcek@it.cas.cz

3. Results

During the experiment, the airfoil was placed on elastic support allowing vibration with two degrees of freedom: pitch (rotation about the elastic axis, located in 1/3 of the chord length) and plunge (vertical motion). The amplitude of the rotational movement was ± 17 °, and the amplitude of the plunging movement was ± 7 mm. The motion of the airfoil in the numerical simulation was prescribed according to vibratory patterns identified from the experiment [Vlček 2011]. The frequency of vibration of the airfoil was 19,5 Hz.

Simulated pressure fields on the airfoil surface, averaged over five periods of vibration, are compared with experimental data in Figs. 1. The figure in the left show the normalized pressure field around the airfoil in a selected phase of the vibration period (more phases can are shown in the full paper on the CD-ROM). The reference pressure p_0 is taken as the pressure at inlet. The graph on the right shows the normalized pressure distribution along the bottom surface of the airfoil. On the top surface of the airfoil where massive flow separation occurs, the numerical results and experimental data differ significantly (the results are not shown here). This is mainly because the current numerical simulation is run without turbulence model and with insufficiently fine mesh in the boundary layer.

The values of p/p_0 in the range 1,02 up to 1,04, found in the numerical simulations near the stagnation point, are physically incorrect. This is probably caused by minor inconsistency between the model and the experiment, mainly by the simplified velocity boundary condition at the inlet, which inevitably differs from the real inflow conditions.

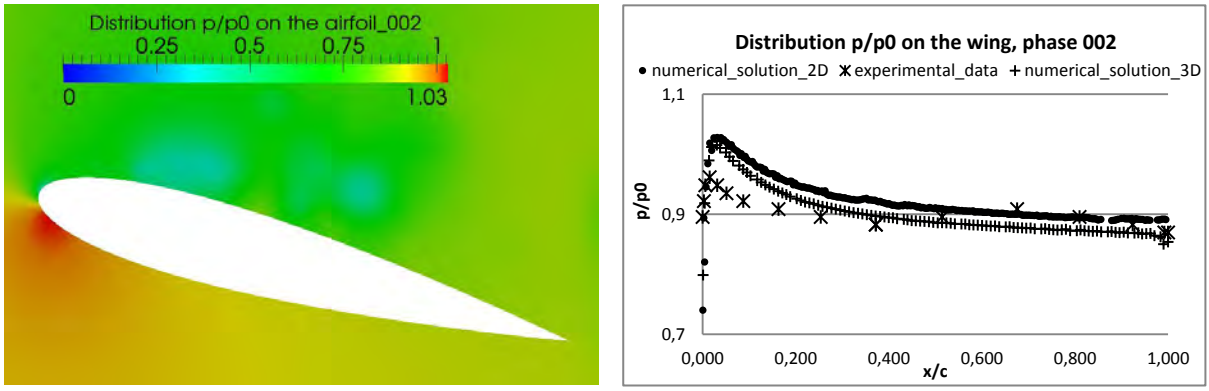

Fig. 1: Normalized pressure field from the numerical simulation (left), normalized pressure distribution p/p_0 on the bottom surface from experiment, 2D and 3D simulation (right), phase 002.

4. Conclusions

3D and 2D numerical simulations of airflow past a vibrating airfoil were performed and compared with experimental data. The current numerical model provides good match with the experimental data only in the regions, where there is no flow separation. In the separated regions, the results of numerical simulation and experimental data are very different. This is probably caused by the fact that for the purpose of this preliminary study, a simple incompressible model without any turbulence modelling was chosen. The evaluation of the interferographic images, on the other hand, is also problematic, especially in the regions of high density gradients. In the future, it will be appropriate to switch to the compressible flow model and possibly incorporate a suitable turbulence model.

Acknowledgement

The research has been supported by the Czech Science Foundation, project P101/11/0207

References

Vlček V., Kozánek J. (2010) Preliminary interferometry measurements of flow field around a fluttering NACA0015 profile. Engineering Mechanics 2010, pp. 540–550.

Vlček V., Kozánek J., Zolotarev I. (2011) Forces acting on the fluttering profile in the wind tunnel. Vibration problems ICOVP 2011 - Supplement, 2011, pp. 516–522.

19th International Conference
ENGINEERING MECHANICS 2013
Svratka, Czech Republic, May 13 – 16, 2013

ON ADVANCE IN LEVELING PROCESS OF LONG PRODUCTS

F. Sebek*, J. Petruska, T. Navrat*****

Abstract: *This paper is concerned with numerical simulation of long products' leveling. The main goal is estimating useful setting of leveling machine to minimize curvature of particular material which is determined by measured geometrical data and given material characteristics as input information to the algorithm. The program is compiled with software MATLAB. Suggested algorithm which is fast is based on the Finite Element Method (FEM) and its fundamental equation. The curved bar passes through laterally offset rollers with cyclic elasto-plastic deformation resulting in convenient redistribution of residual stress which brings down curvature of long product. Solving of this problem is complicated due to high inherent nonlinearity, instability or sensitivity caused by cyclic plasticity of leveled material. The useful setting is found by iterative process applying Newton-Raphson method for solving nonlinear problems.*

Keywords: ***leveling, FEM, elasto-plastic bending, residual stress.***

Nowadays development of manufacturing technology places the emphasis on quality of used material. When we are talking about long products the feature of quality can be its curvature. So there is a necessity of straightening of curved long products.

The basic idea of leveling process is based on elasto-plastic bending as it is published in Petruska et al. (2012), Sebek (2012) and others. In our case we work with seven roller leveling machine illustrated in Fig. 1. Each of rollers in the top row is individually adjustable. Rollers in the bottom row are fixed. The curved product moves through leveling machine with constant velocity respecting the Eulerian approach. We are starting from intermeshing of adjustable rollers.

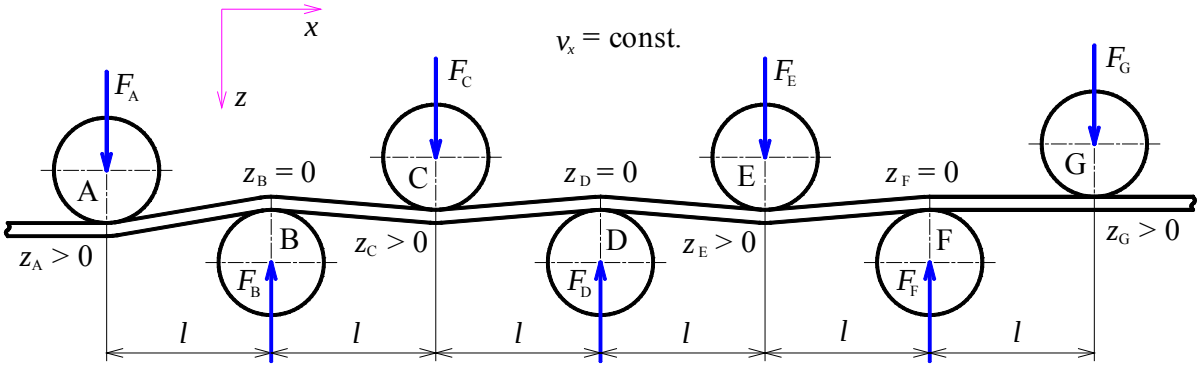

Fig. 1: Scheme of seven roller leveling machine (Petruska, 2012 and Sebek, 2012)

The main assumptions are uniaxial stress state, circular cross section, linear progress of hardening and kinematic hardening rule which is the necessary prerequisite (Schleinzer, 2001). The algorithm is based on the fundamental equation of FEM in Eq. (1) solved by Newton-Raphson method.

$$\mathbf{K}_{T,i-1} \cdot \Delta\mathbf{U}_i = \mathbf{R}_{i-1} \quad (1)$$

* Ing. Frantisek Sebek: Institute of Solid Mechanics, Mechatronics and Biomechanics, Faculty of Mechanical Engineering, Brno University of Technology, Technicka 2896/2; 616 69, Brno; CZ, e-mail: y107598@stud.fme.vutbr.cz

** prof. Ing. Jindrich Petruska, CSc.: Institute of Solid Mechanics, Mechatronics and Biomechanics, Faculty of Mechanical Engineering, Brno University of Technology, Technicka 2896/2; 616 69, Brno; CZ, e-mail: petruska@fme.vutbr.cz

*** Ing. Tomas Navrat, Ph.D.: Institute of Solid Mechanics, Mechatronics and Biomechanics, Faculty of Mechanical Engineering, Brno University of Technology, Technicka 2896/2; 616 69, Brno; CZ, e-mail: navrat@fme.vutbr.cz

The verification of our algorithm is realized by using results published in Nastran & Kuzman (2002). We performed a comparison of deflection, slope, curvature (Fig. 2) and bending moment along the bar length with satisfactory results.

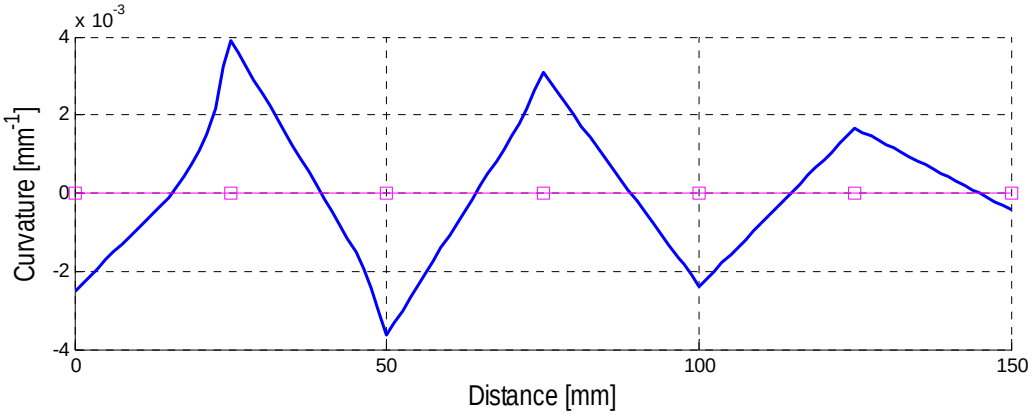

Fig. 2: Progress of curvature along the leveled material

The user friendly program for solving the leveling processes has been developed. The usage of our program is faster than the application of multipurpose FEM software where the solution is complicated. It is possible to include more improvements due to modular structure of the algorithm. We are really aimed to direct applicability of our results in the industry and further progress and advances will be presented in a future.

Acknowledgement

Financial help of the grant projects FSI-J-13-2020 and European Regional Development Fund project CZ.1.05/2.1.00/01.0002 is gratefully acknowledged.

References

Petruska, J., Navrat, T. & Sebek, F. (2012) A New Model for Fast Analysis of Leveling Process. *Advance Materials Research*, 586, pp. 389-393.

Nastran, M. & Kuzman, K. (2003) Some comments on cold forming process stability analysis. *Journal of Materials Processing Technology*, 133, pp. 166-173.

Sebek, F. (2012) *Computational analysis of leveling of square cross section rods*. Master's thesis. Brno University of Technology, Brno.

Mutrux, A., Berisha, B. & Hora, P. (2011) Prediction of cyclic softening in a medium carbon steel during cross roll straightening. *Journal of Materials Processing Technology*, 211, pp. 1448-1456.

Tokunaga, H. (1961) On the Rolled Straightener. *Japan Society of Mechanical Engineers*, 4, 15, pp. 605-611.

Schleinzer, G. & Fischer, F. D. (2001) Residual stress formation during the roller straightening of railway rails. *International Journal of Mechanical Sciences*, 43, pp. 2281-2295.

Biempica, C. B., Díaz, J. J. C., Nieto, P. J. G. & Sánchez, I. P. (2009) Nonlinear analysis of residual stresses in a rail manufacturing process by FEM. *Applied Mathematical Modeling*, 33, pp. 34-53.

Zhao, Y., Guo, D. & Hu, F. (2011) Finite element simulation of web falling during heavy rail roller straightening. *Procedia Earth and Planetary Science*, 2, pp. 44-49.

Li, K. Y., Chen, C. K. & Yang, S. C. (1999) Profile determination of a tube-straightening roller by envelope theory. *Journal of Materials Processing Technology*, 94, pp. 157-166.

Wu, B. J., Chan, L. C., Lee, T. C. & Ao, L. W. (2000) A study on the precision modeling of the bars produced in two cross-roll straightening. *Journal of Materials Processing Technology*, 99, pp. 202-206.

Doege, E., Menz, R. & Huinink, S. (2002) Analysis of the levelling process based upon an analytic forming model. *Manufacturing Technology*, 51, 1, pp. 191-194.

Liu, Z., Wang, Y. & Yan, X. (2012) A new model for the plate leveling process based on curvature integration method. *International Journal of Mechanical Sciences*, 54, 1, pp. 213-224.

Nastran, M. & Kuzman, K. (2002) Stabilization of mechanical properties of the wire by roller straightening. *Journal of Materials Processing Technology*, 125-126, pp. 711-719.

Owen, D. R. J. & Hinton, E. (1980) *Finite Elements in Plasticity*. Pineridge Press, Swansea.

19th International Conference
ENGINEERING MECHANICS 2013
Svratka, Czech Republic, May 13 – 16, 2013

PROJECTILE IMPACT MODELS OF COMPOSITE PLATES FOR NUMERICAL SIMULATIONS

V. Sháněl[1], M. Španiel[2]

Summary: *The paper deals with numerical modeling approaches of a steel projectile impact on composite plates. Currently, vehicle ballistic protection is achieved predominantly using metal-based armor which is heavy and thus negatively affects other vehicle parameters, such as maneuverability. Another option is to use a composite or hybrid sandwiches. To speed up the design of such elements for ballistic protection, it is appropriate to use numerical simulations which allow for a reduction of the number of experiments required to select appropriate alternatives for the construction features of ballistic protection. For this reason, different numerical models describing the penetration of composite plate by a steel projectile have been developed. These models are based on different damage criteria. Since there is no universal damage criterion, it is necessary to find suitable options as well as methods to identify parameters for different types of materials. Therefore, different possibilities to adjust these models to experimental data were investigated. The proposed models will be used in the development of high-quality composite sandwiches for ballistic protection.*

1. Introduction

Experimental methods play an essential role in developing new designs or materials, but their applications are demanding in terms of time, cost and realization. Due to the development of knowledge in the field of phenomenological material models and methods themselves, especially numerical analysis methods of mechanical systems, the design process and structure analysis is commonly supported by their usage. As far as conventional construction is concerned, numerical analysis is used routinely in cases when it is necessary to assess the stiffness, durability, frequency characteristics, etc. But also for example in the analysis of breakdown situations or structures that perform their functions through a partial or total destruction, as in our case, the development of ballistic shields protection, it is desirable to carry out experiments and numerical simulations together. We expect a deepening understanding of experiments due to numerical simulations and

[1] Ing. Bc. Vít Sháněl, Department of Mechanics, Biomechanics and Mechatronics, Faculty of Mechanical Engineering, Czech Technical University in Prague, Technická 4, 166 07 Prague 6, tel. +420 224 35 25 19, e-mail Vit.Shanel@fs.cvut.cz
[2] Doc. Ing. Miroslav Španiel, CSc, Department of Mechanics, Biomechanics and Mechatronics, Faculty of Mechanical Engineering, Czech Technical University in Prague, Technická 4, 166 07 Prague 6, tel. +420 224 35 25 61, e-mail Miroslav.Spaniel@fs.cvut.cz

also continuous consequent promotion of rationally designed experiments, thus reducing their number.

For the first calculations, a geometrically simple case was chosen: a projectile impact of a composite plate. Software Abaqus/Explicit by Dassault Systemes was used for the calculation together with Intel Visual Fortran which compiled the material model and integrated it into a solver. Because of the construction of the model which has implemented damage criteria in an external subroutine VUMAT, it is possible to make modifications of these criteria and thus tune the model to a particular type of samples. The described model was tuned according to the results obtained from the DASSAULT SYSTEMES (2007) experiment by selecting which part of the criteria should be taken into account for the element deletion during the simulation because of its damage. The damage model now consists of four parts: Hashin's criteria for fiber tension and compression and Puck's criterion for matrix tension and compression damage. This paper studies the influence of criterion part selection on the results of the simulation. The following table shows the comparison of the simulation results with experimental data.

Table 1. The values of the initial and residual velocity of the projectile compared to the experimental data.

Impact velocity s [m/s]	Residual velocity experimetal [m/s]	Residual velocity simulation [m/s]
150	45	59
180	102	104
250	184	165

2. Conclusions

Initially, the aim of the performed simulations was to test the software possibilities in dealing with composite materials projectile impacts at different impact speeds. Based on the obtained experimental data, a modification of the model damage deformation was made to determine the moment of removing the element from the simulation. The results of the simulation showed a good agreement with the experimental data. This model is ready for impact simulation of composite plates now which will be carried out after selecting the final material. Then model will be adjusted to the experimental data obtained to support the development of elements for vehicle ballistic protection elements.

3. Acknowledgment

This work was supported by Ministry of Industry and Trade of the Czech Republic in the project FR-TI4/317.

4. References

Buchar, J. & Voldřich J. 2003: *Terminální balistika.* Academia, Praha.

DASSAULT SYSTEMES, 2007: *Projectile Impact on a Carbon Fiber Reinforced Plate* [online]. Available at: http://www.3ds.com/products/simulia/resource-center/

19th International Conference
ENGINEERING MECHANICS 2013
Svratka, Czech Republic, May 13 – 16, 2013

ANALYSIS OF THE THERMAL BEHAVIOR OF MASS CONCRETE BASED ON SEMI-ADIABATIC TEMPERATURE MEASUREMENTS

W.R.L. Silva [1], V. Šmilauer [2], P. Štemberk [3]

Abstract: *The prediction of mass concrete thermal behavior is usually based on FEM analysis in combination with adiabatic measurements of cement hydration. Because adiabatic measurements are costly, this work proposes an alternative solution; in particular, a low-cost semi-adiabatic calorimeter. The measurements from this setup are used to adjust a hydration model. The adjusted model is used as basis to predict the thermal behavior of a 511m³ mass concrete foundation block, and the predicted results are compared to real scale measurements for validation.*
Keywords: ***adiabatic calorimeter, hydration, mass concrete***

1. Introduction

The prediction of temperature evolution due to cement hydration can be complex due to the number of phenomena involved in the reactions. Usually, preference is given to hydration models with a few input parameters. Particularly, attention is put on the model proposed by Cervera et al. (1999). A slightly modified formulation is proposed here

$$\frac{\mathrm{d}DoH}{\mathrm{d}t} = \widetilde{A}_{25}(DoH) = B_1\left(\frac{B_2}{DoH_\infty} + DoH\right)(DoH_\infty - DoH)\exp\left(-\bar{\eta}\frac{DoH}{DoH_\infty}\right), \quad (1)$$

where $\widetilde{A}_{25}(DoH)$ is the chemical affinity, B_1 and B_2 the coefficients to be adjusted, DoH_∞ the ultimate hydration degree, and $\bar{\eta}$ the micro-diffusion of free water through formed hydrates. Eq. (1) express isothermal hydration at 25°C. In adiabatic conditions, $\widetilde{A}_{25}(DoH)$ has to be scaled via Arrhenius equation. The parameters from Eq. (1) are adjusted based on adiabatic measurements. To overcome the need for adiabatic calorimeters, which are costly, this work proposes a low-cost semi-adiabatic calorimeter. The measurements from this are used to adjust a hydration model, which is then combined with FEM analysis to predict the thermal behavior of a mass concrete block. Next, the predicted results are validated against real scale measurements.

2. Experimental program and simulations

The semi-adiabatic setup consists of a 240 mm concrete cube covered by a 100 mm thick polystyrene foam. A concrete mixture with the same composition as the one poured in the foundation block was monitored by K-type thermocouples. The foundation block has the dimensions of 19.6×10.1×2.5 m. Continuous casting of concrete was performed for 12 h. The experimental program and simulations are summarized in Fig. 1a.

[1] Ing. Wilson Ricardo Leal da Silva, Ph.D., Faculty of Civil Engineering, CTU in Prague, Thákurova 7, 166 29 Prague 6, tel. +420 224 35 4629, e-mail: wilsonecv@gmail.com
[2] doc. Ing. Vít Šmilauer, Ph.D., Faculty of Civil Engineering, CTU in Prague, Thákurova 7, 166 29 Prague 6, tel. +420 224 35 4483, e-mail: vit.smilauer@fsv.cvut.cz
[3] doc. Ing. Petr Štemberk, Ph.D., Faculty of Civil Engineering, CTU in Prague, Thákurova 7, 166 29 Prague 6, tel. +420 224 35 4364, e-mail: stemberk@fsv.cvut.cz

3. Results and discussion

First, hydration kinetics of cement was calibrated from semi-adiabatic experiment (Fig. 1b), and the results indicate that the hydration kinetics fitted reasonably. The maximum temperature in the cube reached 55.2°C at 16 h, Fig. 1b shows the corresponding temperature field. Next, the foundation block was modeled in OOFEM (Patzák et al., 1993) with the boundary conditions shown in Fig. 1c. The results from simulations (Fig. 1d) validates temperature evolution in the block. Inner gauges 2, 4, and 6 gave practically the same temperature, which was slightly influenced by boundary conditions. The maximum temperature in the block reached 65°C at 74 h, the corresponding temperature field is shown in Fig. 1d.

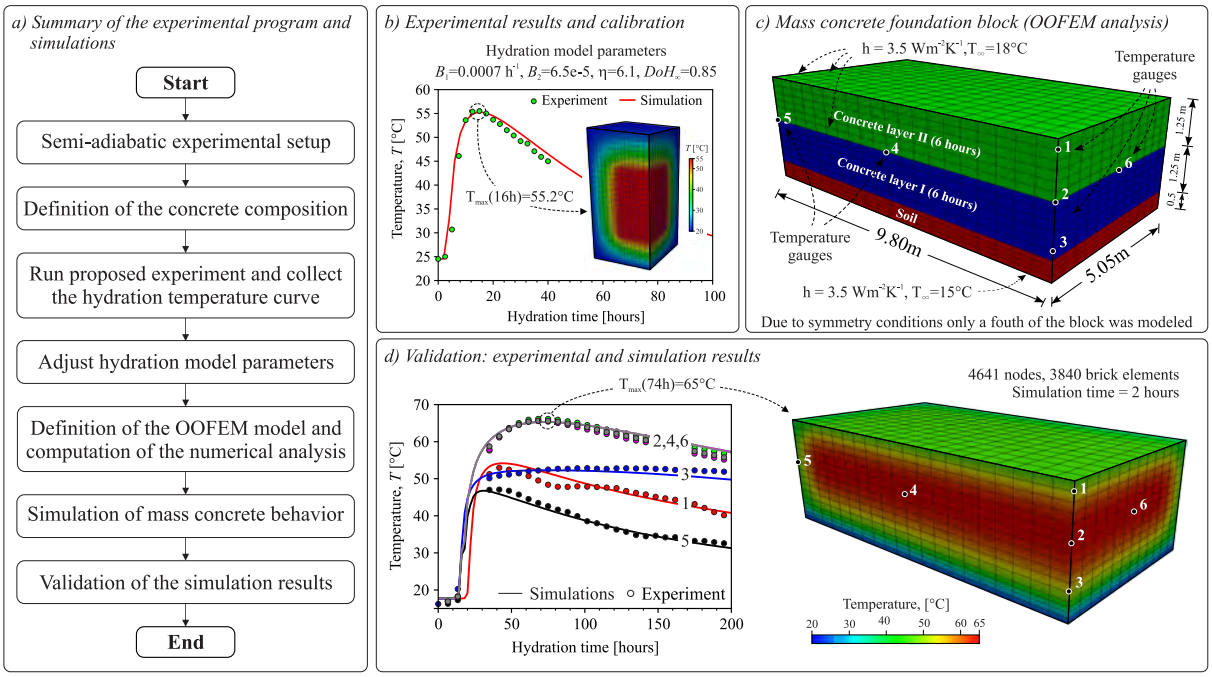

Fig. 1: Summary of results from the experimental program and simulations.

4. Conclusion

The results proved that calibrating an affinity hydration model to a small-size concrete cube under semi-adiabatic conditions can be applied to a large-scale block with different boundary conditions. Hence, the proposed setup can be a suitable alternative to the adiabatic calorimeter. This solution turns out to be highly attractive for the concrete industry due to its low cost.

5. Acknowledgment

The financial support from Czech Science Foundation grant No. 105/10/2400 and from Grant Agency of the CTU in Prague SGS12/116/OHK1/2T/11 and SGS13/039/OHK1/1T/11 are gratefully acknowledged.

6. References

Cervera, M., Oliver, J., Prato, T. (1999) Thermo-chemo-mechanical model for concrete. I: Hydration and aging, *Journal of Engineering Mechanics ASCE*, 125, 9, pp.1018-1027.

Patzák, B., et al., (1993) Object Oriented Finite Element Method - OOFEM. Available at http://www.oofem.org.

19th International Conference
ENGINEERING MECHANICS 2013
Svratka, Czech Republic, May 13 – 16, 2013

FREE VIBRATION ANALYSIS OF EULER-BERNOULLI BEAM WITH DISCONTINUITIES BY MEANS OF DISTRIBUTIONS

J. Sobotka*

Abstract: *The general equation for the transverse vibration of Euler-Bernoulli beam has been used since it was derived by means of classical derivatives of the shear force, the bending moment, the slope and the deflection of the beam. However these derivatives are not defined at such points of center-line between ends of the beam in which there is a concentrated support or a concentrated mass or a concentrated moment of inertia or an internal hinge connecting beam segments. We have applied the distributional derivative for a discontinuous shear force, a discontinuous bending moment, and a discontinuous slope of the beam in order to derive generalized mathematical model for free transverse vibration as a system of partial differential equations. We have computed a general solution to the generalized mathematical model for prismatic beam by means of a symbolic programming approach via Maple. As a result of this approach, computing natural frequencies and modal shapes of a slender beam, it is not necessary for continuity conditions to be put together at discontinuity points mentioned. As an example we have used this approach to obtain a frequency equation of a beam on three pin rigid supports, which would be more complicated if we tried to apply the transfer matrix method.*

Keywords: ***Euler-Bernoulli beam, transverse vibration, discontinuities, Dirac distribution.***

1. Introduction

Classical analytical method of calculating natural frequencies of a beam with discontinuities is based on the following main steps (Timoshenko, 1937). Firstly we divide the beam into segments without discontinuities. Secondly we find a continuous solution to a differential equation of motion for each segment separately. Thirdly we express boundary conditions for each segment, and continuity conditions among adjoining segments leading to a homogeneous system of linear algebraic equations. Finally we derive a frequency equation as a condition of nontrivial solution to the homogeneous system.

Applying the distributional derivative definition for a discontinuous shear force, a discontinuous bending moment, and a discontinuous slope of the beam, we can derive a mathematical model for free transverse vibration of Euler-Bernoulli beam with discontinuities caused by concentrated supports or concentrated masses or concentrated moments of inertia situated between ends of the beam, or hinges connecting beam segments. This mathematical model can be solved like one differential task without dividing the beam into segments where all the continuity conditions among adjoining segments are fulfilled automatically. Using this approach, we always have only four integration constants irrespective of the number of the discontinuities.

2. The classical equation of motion for free transverse vibration of Euler-Bernoulli beam

Neglecting the effects of rotary inertia and shear deformation, and supposing no axial loading of the slender beam, we may express the equation of motion for free transverse vibration of the beam without discontinuities in the shear force, the bending moment, the slope and the deflection (Rao, 2007) as

$$\rho\, \mathrm{A}(x)\left(\frac{\partial^2}{\partial t^2}\,\mathrm{w}(x,t)\right) = -E\left(\frac{\partial^2}{\partial x^2}\left(\mathrm{J}(x)\left(\frac{\partial^2}{\partial x^2}\,\mathrm{w}(x,t)\right)\right)\right) \quad . \tag{1}$$

* Ing. Jiří Sobotka, Ph.D., ČEZ, a.s., 67550 Dukovany; CZ, e-mail: jiri.sobotka@cez.cz

3. A mathema tical model for free t ransverse vibration of Euler-B ernoulli beam with discontinuities

Expressing the first classical derivative of the shear force with respect to x from the equation of motion for an element cut out of the beam (Brepta at al., 1994), and adding discontinuities of this force by using the distributional derivative definition (Kanwal, 2004), we can derive Eq. (2) in which $r_i(t)$ is a reaction at i*th* concentrated support at a point $x=a_i$ ($0< a_i < l$), l is the length of the beam, m_i is a concentrated mass at a point $x=b_i$ ($0< b_i <l$), and Dirac(x-a_i) denotes Dirac distribution.

When a beam carrying concentrated masses with moments of inertia J_i at points $x=b_i$ is vibrating, jump discontinuities in the bending moment may occur at these points. Expressing the first classical derivative of the bending moment from the static equilibrium equation for an element cut out of the beam, and adding discontinuities in this moment multiplied by Dirac distribution, we can obtain Eq. (3).

If a beam contains hinges connecting segments of the beam at points $x=c_i$ ($0< c_i < l$), discontinuities in the slope (ϕ) of magnitude $\psi_i(t)$ may be found at these points. Expressing the first classical derivative of the slope from the relation between the bending moment and the beam centerline curvature, and adding distributional parts containing $\psi_i(t)$ to the classical part of the distributional derivative, we can acquire Eq. (4).

$$\frac{\partial}{\partial x}\mathrm{Q}(x,t)=\rho\,\mathrm{A}(x)\left(\frac{\partial^2}{\partial t^2}\mathrm{w}(x,t)\right)+\left(\sum_{i=1}^{n_1} r_i(t)\,\mathrm{Dirac}(x-a_i)\right)+\left(\sum_{i=1}^{n_2} m_i\left(\frac{\partial^2}{\partial t^2}\mathrm{w}(x,t)\right)\Big|_{x=b_i}\mathrm{Dirac}(x-b_i)\right) \tag{2}$$

$$\frac{\partial}{\partial x}\mathrm{M}(x,t)=\mathrm{Q}(x,t)-\left(\sum_{i=1}^{n_2} J_i\left(\frac{\partial^2}{\partial t^2}\phi(x,t)\right)\Big|_{x=b_i}\mathrm{Dirac}(x-b_i)\right)\quad, \tag{3}$$

$$\frac{\partial}{\partial x}\phi(x,t)=-\frac{\mathrm{M}(x,t)}{E\,\mathrm{J}(x)}+\left(\sum_{i=1}^{n_3}\psi_i(t)\,\mathrm{Dirac}(x-c_i)\right)\quad, \tag{4}$$

$$\frac{\partial}{\partial x}\mathrm{w}(x,t)=\phi(x,t)\quad. \tag{5}$$

4. Conclusions

Contribution of this paper to the modal analysis of slender beams is that the mathematical model for the free transverse vibration, i.e. Eqs. (2)-(5), holds true also for the discontinuous shear force, the discontinuous bending moment and the discontinuous slope. Discontinuities in the shear force are supposed to be owing to idealized concentrated supports or inertia masses between ends of the beam. Likewise, discontinuities in the bending moment are assumed to be due to idealized concentrated moments of inertia situated between ends of the beam. On the contrary, discontinuities in the slope are caused by real hinges connecting beam segments. Jump discontinuities in the unknown dependently variable quantities have been expressed in the corresponding distributional derivatives (2)-(4) where the singular distribution Dirac(x), which is usually denoted as δ(x), is always moved into the point with a discontinuity mentioned, and multiplied by a magnitude of the discontinuity. To be able to find modal shapes of a slender beam analytically with discontinuities mentioned, we have derived a system of ordinary differential equations (SODE) for shapes of the shear force, the bending moment, the slope and the deflection. Using the Laplace transform method, we have computed the general solution to the SODE containing integration constants in the form of initial parameters.

References

Brepta, R., Půst, L., Turek, F. (1994) *Mechanické kmitání*. Sobotáles, Praha.
Juliš, K., Brepta, R. a kol. (1987) *Mechanika II., Dynamika*. SNTL, Praha.
Kanwal, R. P. (2004) *Generalized Functions*. Birkhäuser, Boston.
Rao, S. S. (2007) *Vibration of Continuous Systems*. Wiley, New Jersey.
Schwartz, L., (1972) *Matematické metody ve fyzice*. SNTL, Praha.
Štěpánek, J. (2001) *Distribuce a diferenciální rovnice*. Karolinum, Praha.
Timoshenko, S.P. (1937) *Vibration problems in engineering*. VAN NOSTRAND, New York.
Weaver, W. Jr.,Timoshenko, S.P., Young, D.H. (1990) *Vibration problems in engineering*. Wiley, New York.

19th International Conference
ENGINEERING MECHANICS 2013
Svratka, Czech Republic, May 13 – 16, 2013

SIMULATION OF HOST ROCK CRACKING DUE TO PRESSURE CHANGES IN MAGMA CHAMBER

M. Somr, P. Kabele [1]

Abstract: *Calderas are volcanic structures, which can be dangerous but also beneficial at the same time. Therefore, it is important to understand complex processes leading to a formation of the calderas. For this purpose, numerical simulations using the finite element method can be employed very well. In our paper, we look for a simplified, yet still realistic concept of modeling of a host rock and a magma chamber. Results indicate that our approach is able to capture phenomena, which are described by geologists in field studies. This work shows that it is possible to model a complex volcanological process using a relatively simple concept.*

Keywords: ***numerical modeling, quassibrittle, caldera, host rock, magma chamber***

Calderas are volcanic depressions caused by rupturing of a magma chamber roof as a consequence of a pressure evolution inside a magma chamber. A formation of a caldera is usually accompanied by volcanic eruptions. These eruptions represent a serious risk because even a single eruption can kill thousands of people (e.g. Witham (2005). Scientists also pay attention to calderas because they can partially reveal magmatic processes ongoing under the surface.

In the present study we focus our attention on the fracture of a magma chamber roof that eventually leads to its collapse and formation of a caldera. Therefore, only phenomena essential to this process are taken into account in the proposed model. We consider a magma income in a form of a fresh magma injection from lower stratas of the Earth. An increasing volume of magma causes an overpressure in the magma chamber and when the tensile strength of the surrounding rock is exceeded, cracks occur. An eruption is assumed to take place when the cracks propagating from the chamber reach the Earth surface. The subsequent depletion of the chamber causes a decrease of the magma pressure, which results in the loss of magma chamber roof support and its caving in.

To numerically simulate the above-mentioned phenomena, we construct a finite element model of a magma chamber embedded in a large body of a host rock. As the focus is on the host rock fracture, a model combining quasibrittle approach for fracture in tension and plasticity for compression (Červenka et al. (2012); Červenka and Papanikolaou (2008)) is utilized. The magma is assumed to act on the host rock as a nearly incompressible fluid. However, its flow within the chamber as well as into the formed cracks are not modeled. Instead, magma is represented as a nearly incompressible elastic region, whereas the injection and release of magma is modeled by applying eigenstrain (expansion and contraction, respectively) to it. Furthermore, the interface between the magma and the host rock is assumed to transfer only pressure, but no tension and shear. All these phenomena can be well represented by the material models

[1] Ing. Michael Somr, Prof. Ing. Petr Kabele, Ph.D., Faculty of Civil Engineering, Czech Technical University in Prague, Thákurova 7, 166 29 Praha 6, Czech Republic; e-mail: michael.somr@fsv.cvut.cz,

implemented in the ATENA 2D software (Červenka et al. (2012)), which is thus used for the calculations.

The result of the magma chamber expansion can be seen in Figure 1a. Numerous radial cracks occur, especially in the vicinity of a central vent. This phenomenon can be really observed in the nature.

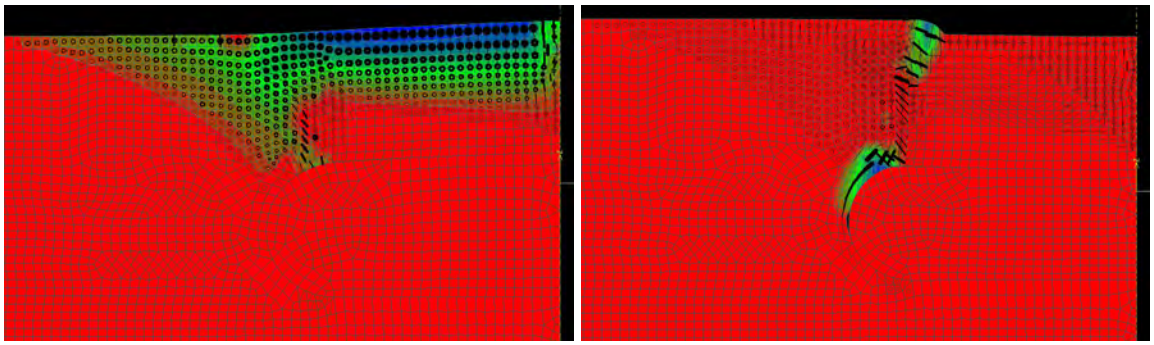

(a) inflation — magma injection (10 × magnified displacements)

(b) deflation — magma eruption (5 × magnified displacements)

Figure 1: Main stages in simulation of caldera formation

The consequent contraction of the chamber leads to a localized zone of the cracks close to a margin of the chamber, Figure 1b. The magma chamber roof then subsides as a coherent block. This type of the collapse is well recognized by the geologists who call it *the piston-like collapse*.

Despite the simplifications, the proposed approach provided very satisfactory results. The analysis was not supposed to predict the exact values, the aim was to reproduce the fracturing and deformation of the magma chamber surroundings, which can be observed in the nature. The further development of the model should include a fluid-solid interaction and thermal-mechanical phenomena. In the future, a study dealing with a relationship between the type of the collapse and the dimensions of the magma chamber (and its position in a crust) will be carried out.

Acknowledgment

The authors would like to thank for the financial support by the grant no. SGS13/034/OHK1/1T/11.

References

Červenka, J. and Papanikolaou, V. K. (2008). Three dimensional combined fracture-plastic material model for concrete. *International Journal of Plasticity*, 24(12):2192–2220.

Červenka, V., Jendele, L., and Červenka, J. (2012). ATENA Program documentation. *Part 1 — Theory*.

Witham, C. (2005). Volcanic disasters and incidents: a new database. *Journal of Volcanology and Geothermal Research*, 148:191–233.

19th International Conference
ENGINEERING MECHANICS 2013
Svratka, Czech Republic, May 13 – 16, 2013

DAMPING OF BEAM TRANSVERSAL VIBRATIONS BY A PERMANENT MAGNET WITH COIL

G. J. Stein [*] and R. Chmúrny [*]

Abstract: In the paper the use of permanent magnet with coil, augmented by an external resistance, for transversal vibration control of a flexible slender beam is analysed. The magnetic circuit properties are varied due to external harmonic excitation by a rotating machine. The so induced alternating voltage drives alternating current through closed electric circuit, which is dissipated in an external resistor. The induced current driven through the coil generates magnetic force, which damps the excitation force and changes the damped natural frequency of the oscillatory system. The internal losses in the coil influence the overall system performance. A lumped parameter model of the combined system is derived in a simplified, linearised form for a particular machine frame, using measured system parameters and accounting for the coil internal losses.

Keywords: ***Vibration control assessment, Electromagnetic actuator, Harmonic excitation, Numerical simulation.***

1. Introduction

In rotating machinery a resonance phenomena can cause severe problems. In order to avoid it, vibration control needs to be implemented. Except of passive means active and semi-active methods of vibration control can be implemented in vibration reduction as well. Electro-dynamic and electro-magnetic actuators are sometimes used, as presented e.g. in (Giurgiutiu & Lyshewski, 2009).

This contribution, based on first author's previous work (Stein et al., 2011 & 2012), analyses the use of a permanent magnet with a coil for vibration attenuation purposes. It has been shown that the controller of interest is capable to introduce damping, as well as alter damped natural frequency of the oscillatory system. In order to model more realistic system, electrical losses are introduced, which were not hitherto considered. Their influence on system behaviour is analysed for a mock-up realistic system by simulation means.

2. The vibration controller

The use of an industrial type of permanent magnet (PM) with coil and corresponding ferromagnetic yoke fixed to a mass-spring-damper system, as shown in Fig. 1, is analyzed. The PM generates a static magnetic field of magnetic induction B_0 in the air gap. The attractive static magnetic force F_{M0} is in equilibrium with the spring elastic force at air gap width d_0. Exposing the yoke to vibration, caused by a harmonic force $F_E(t)$, the air gap width $d(t) = d_0 + w(t)$ changes in time, which causes variation of the air gap reluctance. According to Faraday's law, change in reluctance is responsible for induction of alternating voltage $u_i(t)$ in the coil; where it forces an alternating current $i(t)$ to flow in a closed electrical circuit with total resistance R_T. The alternating magnetic force $F_{MO}(t)$, generated by the alternating current $i(t)$ opposes the excitation force (Lenz's law) and is superimposed onto the static magnetic force F_{M0}. Using a shunt resistance R_S, connected in series with resistances R_C and R_L representing in turn the electrical losses in the winding and in the magnetic material, the control of the system is facilitated. So the total circuit resistance R_T is $R_T = R_C + R_L + R_S$.

[*] Ing. George Juraj Stein, PhD. and Ing. Rudolf Chmúrny, PhD.: Institute of Materials and Machine Mechancis, Slovak Academy of Sciences; Račianska 75; SK-83102 Bratislava; SR, e-mail: stein@savba.sk

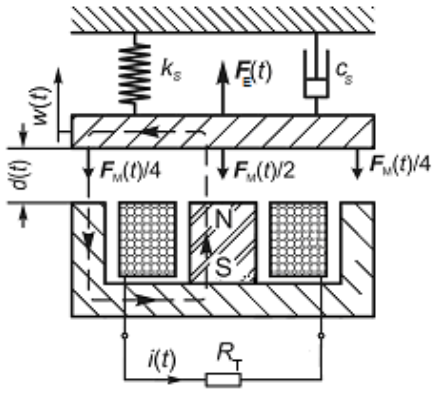

Fig. 1: Schematics of the analyzed electro-mechanical system. (flux line is denoted dashed)

The equation of motion of the equivalent SDOF oscillatory system (Fig. 1) is (Stein, et. al., 2011):

$$m\ddot{w} + c_S\dot{w} + k_S w = F_E(t) - F_M(d_0, i(t)) \ ,$$

where:

- m is the mass of the yoke and mass of the machine,
- c_S is the viscous damping coefficient, modelling the internal damping of the beam,
- k_S is the equivalent beam stiffness at its midpoint,
- w is the midpoint displacement in the upward direction.

The first harmonic of the dynamic magnetic force F_{MO} is derived in the same way as in previous papers (Stein et al., 2011 & 2012); however the electrical losses of the PM with the coil are included.

3. Results

The electrical and magnetic parameters of the specific PM with coil were determined experimentally and introduced into simulation model of the vibration control system. The FRF course was numerically simulated for different values of distance d_0 and shunt resistance R_S. From the simulation results follows, that due to dynamic magnetic force F_{MO} superimposed on static magnetic force F_{M0}:

- Higher harmonics up to the third one are generated,
- Change in oscillatory system natural frequency, i.e. de-tuning of the system can be facilitated,
- Additional damping can be introduced, so attenuating the vibration transmissibility.

The attainable extent of de-tuning and of the additional electro-magnetic damping is influenced by the electrical parameters of the coil and of the shunt resistor R_S, as well as by the air gap width d_0.

Acknowledgement

This contribution is a result of the project No. 2/0083/13 of the Slovak VEGA Grant Agency.

References

Giurgiutiu, V. & Lyshewski, S.E. (2009) *Micromechatronics: Modeling, Analysis and Design*, 2nd ed., CRC Press, Boca Raton.

Stein, G. J., Darula, R. & Sorokin, S. (2011). Control of transversal vibrations of a clamped-clamped beam by a permanent magnet and a shunt circuit. in: *Proc. of the 8th intl. Conference on Structural Dynamics (EuroDyn 2011),* Katholieke Universiteit Leuven, Department of Civil Engineering, 2011, pp. 1735-1741.

Stein, G. J., Darula, R. & Sorokin, S. (2012) Control of forced vibrations of mechanical structures by an electromagnetic controller with a permanent magnet. in: *Proc. of International Conference on Noise and Vibration Engineering (ISMA 2012),* Katholieke Universiteit Leuven, Dept. Werktuigkunde, pp. 385-393.

19th International Conference
ENGINEERING MECHANICS 2013
Svratka, Czech Republic, May 13 – 16, 2013

FEM – DEM COUPLING AND MuPIF FRAMEWORK

J. Stránský [1]

Abstract: *MuPIF is a multi-physics integration tools that faciliates the implementation of multi-physics and multi-level simulations assembled from independently developed applications (Patzák et al. , 2012). Such independently developed applications might be a finite element code and a discrete element code. In this contribution, the design of integration of discrete element method (DEM) into existing continuous based (e.g. FEM) MuPIF components is presented.*

Keywords: ***FEM, DEM, multi-physics, Python***

1. Introduction

Numerical simulations are nowadays an indispensable part of engineering and science development. Usually the simulation is performed by a computer program, which is focused on narrower or wider class of problems (such as solid mechanics, fluid dynamics, heat analysis etc.). If a combination of two classes of problems is required (coupling of mechanical and heat analysis for instance), often it is possible to find a code allowing such approach. However, in some cases, there exists no such program allowing desired problems combination. For instance, it is possible to couple mechanical and heat analysis within the chosen code, but we would like to use a special material model for mechanical analysis, which is not implemented.

One possible approach to solve such situation would be to write a new or extend existing program implementing requested features. Another possible approach would be to use existing independently developed codes, each one focused on specific class of problems, and "glue" them together. The latter approach is a motivation of MuPIF (multi-physics integration framework) tool development. So far, only continuum based methods (finite element method, finite difference method etc.) were considered in the implementation.

There exist several types of FEM – DEM coupling, e.g. surface coupling, see Munjiza (2004); Oñate & Rojek (2004); Villard et al. (2009), volume coupling, see Rousseau at al. (2009); Xu et al. (2002) or multiscale coupling, see Rojek & Oñate (2007); Wellmann & Wriggers (2012). For each type, different implementation approach is presented.

2. Acknowledgment

The financial support of project SGS13/034/OHK1/1T/11 is gratefully acknowledged.

[1] Ing. Jan Stránský, Czech Technical University in Prague, Faculty of Civil Engineering, Thákurova 7, 166 29 Praha 6, tel. +420 224 35 54 17, e-mail jan.stransky@fsv.cvut.cz

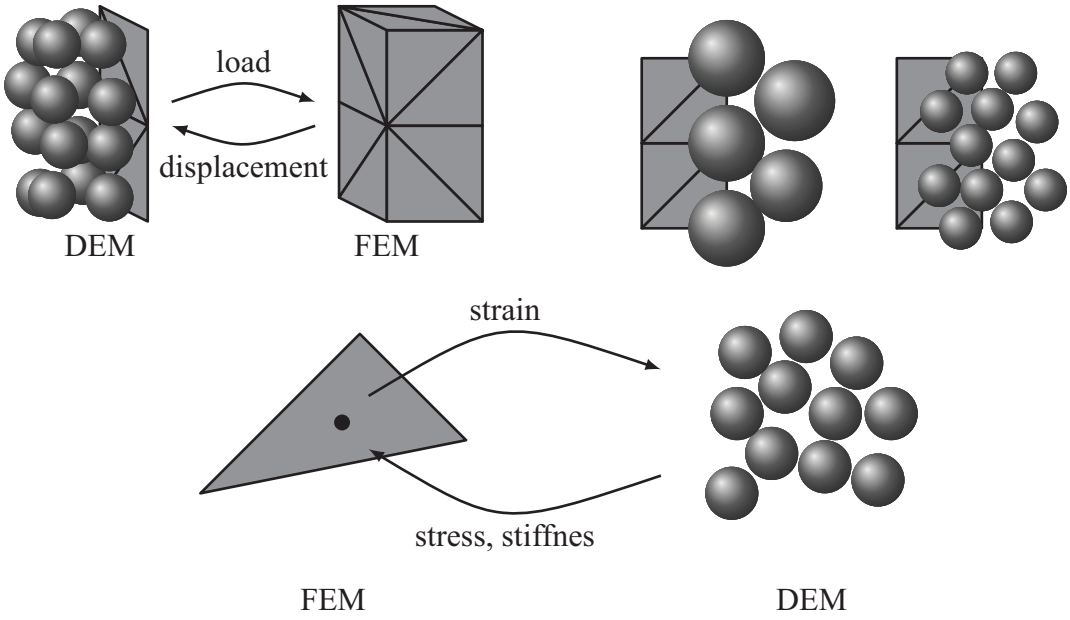

3. References

Munjiza, A. (2004) *The combined finite-discrete element method*. Wiley, Chichester.

Oñate, E. & Rojek, J. (2004) Combination of discrete element and finite element methods for dynamic analysis of geomechanics problems. *Computer Methods in Applied Mechanics and Engineering*, vol. 139, 3087–3128.

Patzák, B., Rypl, D. & Kruis, J. (2012) MuPIF – A distributed multi-physics integration tool. *Advances in Engineering Software*, Available online 3 November 2012, http://www.sciencedirect.com/science/article/pii/S0965997812001329.

Rojek, J. & Oñate, E. (2007) Multiscale analysis using a coupled discrete/finite element model. *Interaction and Multiscale Mechanics*, vol. 1, no. 1, 1–31.

Rousseau, J., Frangin, E., Marin, P. & Daudeville, L. (2009) Multidomain finite and discrete elements method for impact analysis of a concrete structure. *Engineering Structures*, vol. 31, 2735–2743.

Villard, P., Chevalier, B. & Le Hello, B. & Combe, G. (2009) Coupling between finite and discrete element methods for the modelling of earth structures reinforced by geosynthetic. *Computers and Geotechnics*, vol. 36, 709–717.

Wellmann, C. & Wriggers, P. (2012) A two-scale model of granular materials. *Computer Methods in Applied Mechanics and Engineering*, vol. 205–208, 46–58.

Xu, M., Gracie, R. & Belytschko, T. (2002) Multiscale modeling with extended bridging domain method. In: *Bridging the Scales in Science and Engineering* (J. Fish ed.). Oxford University Press.

19th International Conference
ENGINEERING MECHANICS 2013
Svratka, Czech Republic, May 13 – 16, 2013

A CALIBRATION OF GURON-TVERGAARD-NEEDLEMAN MICROMECHANICAL MODEL OF DUCTILE FRACTURE

L. Stratil[*], H. Hadraba[**], F. Šiška[***], I. Dlouhý[****]

Abstract: *Fracture mechanics characteristics of ductile fracture often depend on geometry and size of specimens. A micromechanical modelling of material damage proposes a tool for treatment of geometry and size effects in fracture mechanics. Application of micromechanical model for certain material requires a calibration of model's parameters. This contribution presents the calibration procedure of Gurson-Tvergaard-Needleman model of ductile fracture for Eurofer97 steel. The identification of ductile damage of the steel and its tensile properties at various level of stress triaxiality by testing smooth and notched bars were determined in the previous study. The calibration procedure was performed by hybrid method as a combination of FEA simulations of tensile tests and fractography analyses. The Gurson-Tvergaard-Needleman model performance is greatly influenced by true stress-true strain curve of the material. It was verified that derivation of true stress-true strain curve of the material by using of multiple linear regression model proposed by Mirone is very suitable.*

Keywords: ***ductile fracture, GTN model, void nucleation, MLR model, Eurofer97***

1. Introduction

It is usually observed that R-curves, as fracture mechanics characteristics of resistance against stable crack growth, of tested geometries depend on size, geometry and configuration of specimens without no general trend. One possibility to deal with size and geometry effects offers local approach to fracture, which goes beyond the limits of conventional fracture mechanics. Application of local approach to fracture involves identification of micromechanism of damage of the material, choice and calibration of suitable micromechanical model of damage. One of the most using micromechanical models of ductile fracture in fracture mechanics is the Gurson-Tveergard-Needleman (GTN) model (Tvergaard & Needleman, 1984). In the previous study (Stratil et al., 2012) obtained parameters of GTN model based on smooth tensile specimen results were not sufficiently determined. This contribution continues with determination of micromechanical parameters of GTN model based on both smooth and notched tensile results.

2. Experimental

The results of tensile testing were taken from study Stratil et al., 2012, where testing of smooth and notched tensile bars was performed. In that study also ductile damage identification of the Eurofer97 steel was carried out by fractography and metallography analysis of broken tensile bars. The significant influence on performance of GTN model has the true stress-true strain curve, as void nucleation and growth process is mainly deformation driven. The axisymmetric 2D models of tensile bars were created and used for FEA simulation in ABAQUS Explicit code. The true stress-true strain curve of the steel was obtained by application of MRL model introduced by Mirone, 2004, and next by

[*] Ing. Luděk Stratil: Institute of Physics of Materials, ASCR, Žižkova 22; 616 62, Brno; CZ, e-mail: stratil@ipm.cz and Institute of Material Science and Engineering, Faculty of Mechanical Engineering, Brno University of Technology, Technická 2896/2; 616 69, Brno; CZ, e-mail: ystrat04@stud.fme.vutbr.cz

[**] Ing. Hynek Hadraba, Ph.D.: Institute of Physics of Materials, ASCR, Žižkova 22; 616 62, Brno; CZ, e-mail: hadraba@ipm.cz

[***] Dr. Ing. Filip Šiška, Ph.D.: Institute of Physics of Materials, ASCR, Žižkova 22; 616 62, Brno; CZ, e-mail:siska@ipm.cz

[****] Prof. Ing. Ivo Dlouhý, CSc.: Institute of Physics of Materials, ASCR, Žižkova 22; 616 62, Brno; CZ, e-mail: idlouhy@ipm.cz and Institute of Material Science and Engineering, Faculty of Mechanical Engineering, Brno University of Technology, Technická 2896/2; 616 69, Brno; CZ, email: dlouhy@fme.vutbr.cz

trial-error iteration way according to mechanical response of specimens. Both approaches lead to quite similar determination of true stress-true strain curve. Calibrated values of micromechanical parameters were based on the results of quantitative study of void nucleation and growth from previous study and on the results of parametric studies remaining micromechanical parameters, Fig. 1 and Tab. 1.

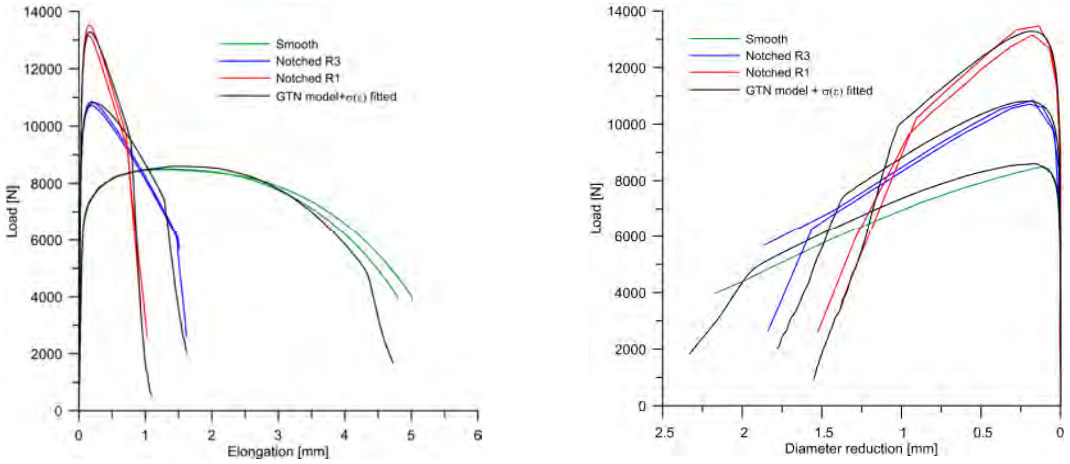

Fig. 1: Comparison of experimental and computed response of tensile specimens.

Tab. 1: The identified parameters of GTN model for Eurofer97 steel.

q_1	q_2	ε_n	s_n	f_n	f_0	f_c	f_f
1.46	0.931	0.3	0.1	0.00055	0	0.0045	0.1

3. Conclusions

The calibration of micromechanical parameters of Gurson-Tvergaard-Needelman model of ductile fracture was performed by combination of tensile bars testing and its numerical simulation. Calibrated values of micromechanical parameters were based on the results of quantitative study of void nucleation and growth from previous study and on the results of parametric studies of chosen micromechanical parameters. The successful calibration of micromechanical parameters requires at least determination of dependence load vs. diameter diameter reduction during tensile test of smooth specimen. It was found that performance of Gurson-Tvergaard-Needelman model depends also on true stress-true strain curve of the material. This curve can be easily derived according to the model proposed by Mirone from results of smooth tensile bar or by its fitting to the results of smooth and notched tensile bars.

Acknowledgement

The authors gratefully thank for the financial support of projects of the Operational Programme "Education for Competitiveness" No. CZ.1.07/2.3.00/20.0197 and the project of specific research FSI-J-12-27/1733.

References

Mirone, G. (2004) A new model for the elastoplastic characterization and the stress-strain determination on the necking section of a tensile specimen. *International Journal of Solids and Structures,* 41, pp. 3545-3564.

Stratil, L., Hadraba, H., Kozák, V., Dlouhý, I. (2012) Modelling of ductile fracture for sub-sized three-point-bend geometry, in*: Proc. 18th Int.Conf. Enginnering Mechanics 2012* (J.Náprstek & C.Fischer eds), Inst. Of Theor. and Applied Mechanics, Prague, pp.1253-1258.

Stratil, L., Hadraba, H., Dlouhý, I. (2012) Ductile damage identification and tensile notch effect for Eurofer97 steel. *Acta Metallurgica Slovaca-Conference,* 3, pp. 185-190.

Tvergaard, V. & Needleman, A. (1984) Analysis of the cup-cone fracture in a round tensile bar. *Acta Metallurgica*, 32, pp.157-169.

19th International Conference
ENGINEERING MECHANICS 2013
Svratka, Czech Republic, May 13 – 16, 2013

TRANSVERSE VIBRATING BEAM LOADED BY MOVING LOAD

V. Šána*, M. Polák**

Abstract: *Simplest model for prediction effects of pedestrians to the structures is the harmonic force, which is fitted in the most efficient point on the pedestrian bridge. This article is focused on alternative modeling of human – structure interaction.*

Keywords: ***Vibrating beam, moving load, Finite Difference Method.***

1. Introduction

In this paper is presented numerical solution of the simply supported transverse vibrating beam with continuous weight per unit length. The beam is exposed to moving force with constant magnitude. It is the simplest model for analyze the human-structure interaction. This load acting at the structure only in the distance d_p, which is the length of human step, and in the time, which corresponds with velocity of moving load and step length. It means, that the structure is loaded by impulses of force moving with velocity v.

2. Equation for the analysis

Transverse vibration of beam with continuous mass distribution is described by fourth order partial hyperbolic differential equation

$$EI\frac{\partial^4}{\partial x^4}w_{(x,t)}+\mu\frac{\partial^2}{\partial t^2}w_{(x,t)}+2\mu\omega_b\frac{\partial}{\partial t}w_{(x,t)}=\delta_{(x-vt)}F \tag{1}$$

where EI is the bending stiffness, μ is the mass per unit length, ω_b is damping angular frequency and δ is the Dirac's (delta) function.

Area of solution is the rectangle $\Psi=[0;L]\times[0;T]$ with boundary and initial conditions. If we consider simply supported beam, the boundary conditions are:

$$w_{(0,t)}=0 \ \wedge \ w_{(L,t)}=0 \tag{2}$$

$$\left.\frac{d^2w_{(x,t)}}{dx^2}\right|_{x=0}=0 \ \wedge \ \left.\frac{d^2w_{(x,t)}}{dx^2}\right|_{x=L}=0 \tag{3}$$

Second condition is expressed as a static condition it means, the bending moment at the both edges of the beam is equal to null. Initial conditions are revolved, that the beam is inactive at the beginning of analysis.

$$w_{(x,0)}=0 \ \wedge \ \left.\frac{\partial w_{(x,t)}}{\partial t}\right|_{t=0}=0 \tag{4}$$

* Ing. Vladimír Šána: Department of Mechanics, Czech Technical University, Thákurova 7; 166 29, Prague; CZ, e-mail: vladimir.sana@fsv.cvut.cz

** Prof. Ing. Michal Polák, CSc.: Department of Mechanics, Czech Technical University, Thákurova 7; 166 29, Prague; CZ, e-mail: e-mail: polak@fsv.cvut.cz

2.1. Solution of differential equation

Numerical solution of equation (1) is realized by Finite Difference Method (FDM), where are the derivations substituted by differences, obtained from Taylor - McLaurin expansion. The differential equation (1) is transformed to the system of algebraic equations corresponding to the difference scheme, which was used.

The displacement at the $(i+1)$ th time layer and on the j th space layer is expressed for example as:

$$w_j^{i+1} = \frac{1}{2\mu(1+\omega_b\tau)} \left\{ \begin{array}{l} 2\mu(\omega_b\tau - 1) w_j^{i-1} + 4\mu w_j^i + \\ + \dfrac{2\tau^2}{\xi^4} EI\left(-w_{j+2}^i + 4w_{j+1}^i - 6w_j^i + 4w_{j-1}^i - w_{j-2}^i\right) \end{array} \right\} \qquad (5)$$

where ξ is the spatial step and τ is the time step

2.2. Numerical example

Parameters for numerical solution were chosen according to numerical stability of FDM, which is dependent on the finite differences used in solution. Parameters, which were used in numerical solution:

$$EI = 3{,}83 \cdot 10^6\, kNm^2\,,\ L = 25m\,,\ \mu = 5{,}3\, t/m\,,\ \omega_b = 0{,}238 s^{-1}\,,\ F = 1{,}8kN$$

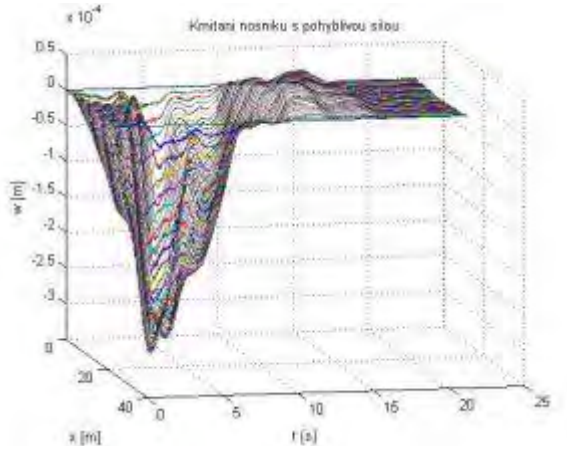

Fig. 1: Transverse vibration of beam in the spatial-time coordinates – deformed mesh

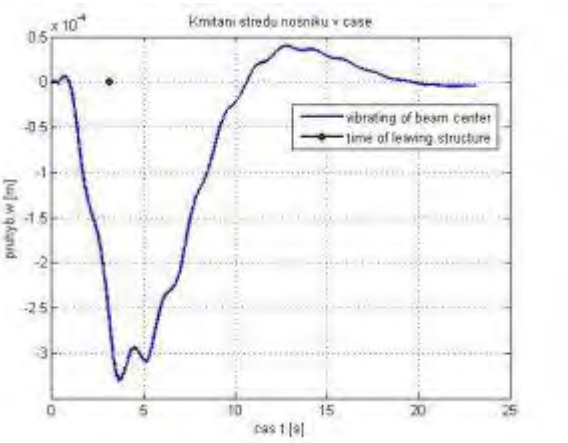

Fig. 2: Vibrating of beam center

3. Conclusion

Stability of Finite Difference Method is dependent on bending stiffness. For increasing EI has to be chosen fine time step τ in contrast to the spatial step ξ. This is the essential reason why this method is not usable for real structures, because computing time increases exponential with decreasing of step in time domain.

Acknowledgement

This paper has been created thanks to the project SGS12/117/OHK1/2T/11 supported by Czech Technical University in Prague.

References

Frýba, L. (1989) Kmitání těles a konstrukcí způsobené pohybujícím se zatížením. *ACADEMIA*, ISBN 80-200 0039-9.

19th International Conference
ENGINEERING MECHANICS 2013
Svratka, Czech Republic, May 13 – 16, 2013

OPTIMIZATION OF DINAMICALLY LOADED CIVIL ENGINEERING STRUCTURES

D. Šedlbauer*

Abstract: *Contribution presents a tool for general optimization on the macro level of civil engineering structures that are subjected to dynamic phenomena. These phenomena are represented mainly by harmonic loads. Optimization process is based on communication between new script and widespread program for structural analysis including FEM solver. Communication is accomplished using Extensible Markup Language (XML). Very robust optimization method Simulated Annealing is used due to the requirement of a general optimization of dynamic problems. In the last part of contribution two optimizations of simple structures of different materials (reinforced concrete, steel) are performed. Long-term task of this work is to put academic knowledge in the field of optimization into common practice of structural analysis.*

Keywords: ***Optimization, civil engineering structures, dynamics, simulated annealing, software.***

1. Introduction

A lot of research work has already been done on the academic field on the topic of optimizing and structure dynamics (Chahande et al., 1994, Park et al., 2005). Unfortunately, this knowledge often cannot be successfully put into practice. Several aspects are to blame. One of them is the absence of supporting software that would quickly and effectively help to engineers with the optimization process. This process leads to optimal design and economical structure. Such software has already found its use in mechanical engineering.

Nowadays, optimization process in practice is perceived only as an iterative computation of one or two steps that fulfills standard requirements. Thus design of optimal shapes and dimensions of structures remains only on designer's knowledge and experiences. Another aspect related to above mentioned problem is the complexity of optimization functions in civil engineering and many restrictive conditions, which are in codes. These are the reasons why to deal with the optimization of structures and make support tools for designers.

2. Optimization process

Presented process of optimization could be divided into two sections according to the program, which is used for that particular part of the process. In the first part software for structural analysis is used for creating model of optimized structure. Than parameters have to be implemented to the model. These parameters will be updated according to optimization method commands and hence will be a change of objective function and constraints. In this section it is necessary to make XML file(s) as well. This file ensures communication between new optimization script and the program with FEM solver.

The second part of the process is provided by new script. Script has to face three main tasks:

- Upload, update and save XML files
- Ensure execution of recalculation in software for structural analysis
- Include the optimization algorithm - Simulated annealing (Kirkpatrick et al., 1983, Černý, 1985)

* Ing. David Šedlbauer: Department of mechanics, Faculty of Civil Engineering, Czech Technical University in Prague, Thákurova 7/2077; 166 29, Prague; CZ, e-mail: david.sedlbauer@fsv.cvut.cz

2.1. XML files operations

Content of the input XML (IN) consists of table with parameters implemented to static structure model. Given that the table can be variously modified depending on the type and number of parameters or the version of static program, so this part of script is "made to measure" XML file. Script has to found position (line), where parameter or its bounds are located. After finding the line, script searches parameter value and change it according to the optimization algorithm commands. The situation is similar with the output (OUT) XML file. Document structure is the same, but the script searches for objective or other functions such as code limits, unit checks etc.

2.2. Recalculation

To avoid complicated programming of FEM principles for calculation and structural analysis, among users-designers widespread software is utilized. It is necessary to update model after changing input parameters. Execution of appropriate type of calculation follows. Thereafter output XML file is updated. All these operations are accomplished by a command with several attributes. The most important attribute is then switch for calculation type. This allows us to run gradually modal analysis and linear calculation.

3. Conclusion

Possible solution of optimization problems with dynamic phenomena (especially harmonic forces) was introduced. Optimization is based on cooperation between widely extended static software including FEM solver and new script in program Matlab. Main tasks of new script are to get data from software for structural analysis, change parameters in model according to the optimization algorithm and ensure recalculation. An important role in this process play XML files, which are mediators of communication between new script and software for structural analysis.

Simulated annealing was used as an optimization algorithm located in the body of the script. For this method exist mathematical proofs of convergence and to its robustness is suitable for wide range of difficult tasks involving a large number of parameters or discrete functions. However, there is a disadvantage – time consumption.

Above mentioned optimization process was used for optimization of two examples involving harmonic loads. The first was optimization of cantilever column made of reinforced concrete. Second one was optimization of hinged steel frame. There were around fifteen percent savings of main materials in both examples compared to initial design.

Acknowledgement

This work was supported by the Grant Agency of the Czech Technical University in Prague, grant No. SGS OHK1-042/13: Advanced algorithms for numerical simulations in civil engineering.

References

CHAHANDE, A. I. & ARRORA, J. S. (1994) Optimization of Large Structures Subjected to Dynamic Loads with the Multiplier Method. *International Journal for Numerical Methods in Engineering*, 37(3), pp. 413-430. ISSN 0029-5981

KIRKPATRICK, S., GELATT, C. D. & VECCHI, M. P. (1983) Optimization by Simulated Annealing. *Science*, 4598, Vol. 220, pp. 671-680.

PARK, K. J., LEE, J. N. & PARK, G. J. (2005) Structural shape optimization using equivalent static loads transformed from dynamic loads. *International Journal for Numerical Methods in Engineering*, 63(4), pp. 589-602. ISSN 0029-5981

ČERNÝ, V. (1985) Thermodynamical approach to the traveling salesman problem: An efficient simulation algorithm. *Journal of Optimization Theory and Applications*, 45(1), pp. 41-51. ISSN 0022-3239

19th International Conference
ENGINEERING MECHANICS 2013
Svratka, Czech Republic, May 13 – 16, 2013

EXPERIMENTAL INVESTIGATION OF THE FIRE RESISTANCE OF MODIFIED CONCRETE

M. Šejnoha*, M. Brouček**

Abstract: *The paper presents results from large scale experiments on reinforced concrete panels obtained during an extensive experimental program aimed at possible application of cement reduced (fly ash replaced) concrete in the production of precast segmental linings for tunnels created by TBM. In particular, this paper is focused on the comparison of fire resistance of enhanced mixtures loaded by the RWS fire curve, which assumes 50 m^3 fuel tanker fire lasting for 120 minutes. The results from the experiments include spalling, overall damage of the surface, deformations during the fire exposure, temperature distribution and residual strength of the tested panels. The possibility of numerically approximate the deformations and time dependent temperature distribution throughout the specimens is evaluated. The paper also presents a description of a method proposed for the evaluation of the extent of spalling during the experiments as due to the extreme temperatures the direct observation of the exposed surface is excluded.*

Keywords: ***Fire resistance, Concrete, Spalling, Fly ash, PP fibres***

Cement producing facilities are responsible for a significant portion of CO2 emissions which together with rising prices of cement leads to increased effort in a search for appropriate replacement. The idea of substituting cement for fly ash and thus reducing the heat from hydration has been successfully used in the past (e.g. Keil J., 1966) for massive concrete structures with low requirements on strength or strength increase rate. However only in past few decades an increased effort in the use of waste material powered by international agreements, increased taxation and subsidy from national and international agencies, and new challenges and improved standards on structural safety enabled incorporation of materials which so far have been used only under specific circumstances.

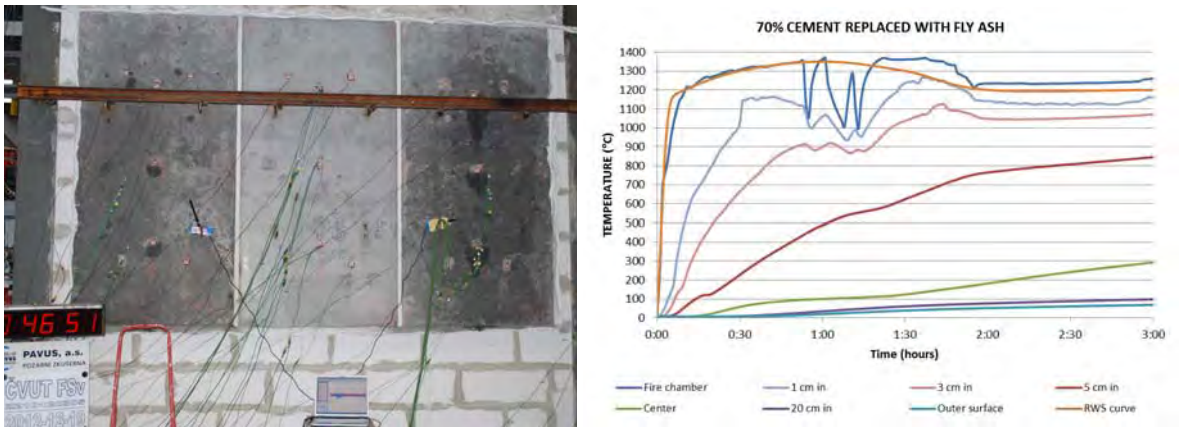

(a) *(b)*

Fig. 1: Full scale experiments: (a) Specimens built-in the fire chamber, (b) Measured temperatures inside the FAC3 specimen

The results presented within this paper are part of an extensive experimental program aimed at possible application of cement free (alkali activated) or cement reduced (fly ash replaced) concrete in the production of precast segmental linings for tunnels created by TBM. The scope of this paper

* Prof. Ing. Michal Šejnoha, Ph.D., DSc.: Czech Technical University in Prague, Faculty of Civil Engineering, Thákurova 7; 166 29, Prague; CZ, e-mail:sejnom@fsv.cvut.cz

** Ing. Miroslav Brouček: Czech Technical University in Prague, Faculty of Civil Engineering, Thákurova 7; 166 29, Prague; CZ, e-mail:miroslav.broucek@fsv.cvut.cz

includes full scale fire resistance experiments of enhanced mixtures including large portion of fly ash, PP fibres and a protective layer. Requirements applied on mechanical parameters of tested mixtures correspond with concrete C45/55 with improved resistance against fire and hostile environment (mainly aggressive sulphate).

Due to very specific conditions are fire outbreaks in tunnels different from others especially in terms of peak temperature and rate of temperature increase which limits chances of survival of any living creature. Therefore unlike in case of fires in buildings the resistance of segmental tunnel lining is assessed in view of repair or replacement costs. In recent years a great deal of research has taken place internationally to ascertain the types of fire which could occur in tunnel and underground spaces. Such research has taken place in laboratory conditions as well as in disused tunnels. In the presented experiments the RWS curve (Ingason and Lönnermark, 2003) which assumes 50 m^3 fuel tanker fire lasting for 120 minutes is modelled.

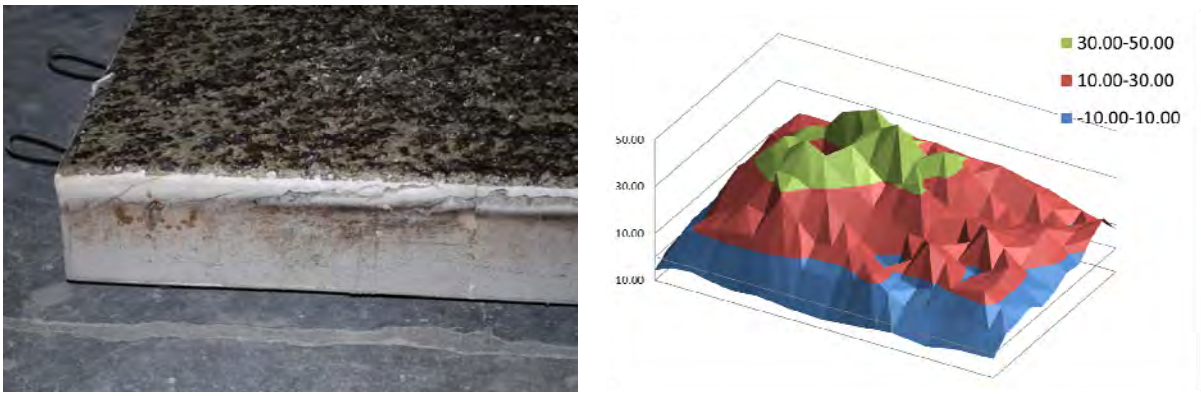

(a) *(b)*

Fig. 2: FiFAC3 specimen after an experiment: (a) photo, (b) measured surface

The paper summarizes results obtained from large scale fire resistance experiment with three models of flat TBM segment linings made of enhanced concrete mixtures. Increased amount of fly ash replacing cement proved to have positive influence on the fire resistance which is, however, still unsatisfying.

Although temperatures inside specimen covered with protection layer made of 25 mm of calcium-silicate material (PROMATEC-T plate) did not exceed generally accepted limit values and no visible damage was observed on the specimen, residual mean compressive strength measured on columns drilled from the specimen was less than 60% of the mean compressive strength after 28 days.

Specimen with added plastic fibres showed better behaviour in terms of spalling and temperature distribution but the compressive strength was smaller by more than 10% when compared to the specimen without fibres.

Proposed method of acoustic pressure measurement proved the capacity to relate spalling which takes place in closed fire chamber with time and temperatures inside the specimen, when combined with appropriate audio or video capturing device, and also to distinguish between several specimens tested within one experiment. Direct observation of the exposed surface is due to extremely high temperatures very limited.

Acknowledgement

The financial support of the project No. TA01030245 provided by the Czech Technology Agency is gratefully acknowledged.

References

Keil J. (1966), *Construction of the Orlik dam* - collection of essays, the national water company, (in Czech).

Ingason, H. and Lönnermark, A (2003) Large Scale Fire Tests in the Runehamar Tunnel – Heat Release Rate (HRR). *Proc. International Seminar on 'Catastrophic Tunel Fires (CTF)'*

19th International Conference
ENGINEERING MECHANICS 2013
Svratka, Czech Republic, May 13 – 16, 2013

INFLUENCE OF THE DESIGN PARAMETERS ON THE RESPONSE OF THE STEP SKEW JOINT WITH A KEY

K. Šobra[*], P. Fajman[**]

Abstract: *Nowadays the numerical and experimental analysis of the splice skew joint with a key is made. The article is focused on influence of some design parameters on the response of this type of joint, especially on geometry of the joint, mainly skew angle and position and material of a key. Some material parameters and results of numerical modeling same as comparison of numerical and experimental analysis will be shown.*

Keywords: ***Historical trusses, vertical step skew joint, numerical modeling, distribution of forces***

1. Introduction

Timber is one of the oldest building materials. It was used mainly for roofing of different types of buildings in Ancient World. One of the oldest well-preserved constructions is the gothic trusses. Considering many fires during the ages there are not many gothic trusses in Czech Republic.

In traditional historical trusses the carpentry joints are used to transfer forces between truss members. Forces are primary transferred by direct contact and by friction. It is necessary to protect initial (historical) shape of construction and conserve originality of members as much as possible during the reconstruction of historical trusses. On the basis of this only damaged part of truss is cut of and replace with a new material. Vertical splice step joint (Fig. 1) is one of the most common carpentry joint which is used for replacing parts of the trusses (adjusting existing undamaged member) (Gerner, 2003).

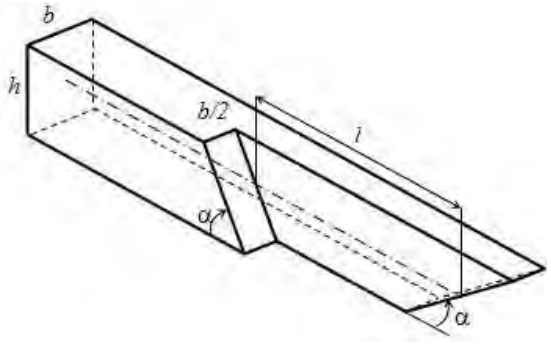

Fig. 1: Half of vertical splice skew joint

2. Forces in the joint

As was mentioned, typical utilization of step joint is in a roof trusses. In truss members is one dimension more than 10times bigger than other two. On the basis of this it is possible to simplify plane stress. It is sufficient to observe normal stress, which is parallel with fibers in a wood (L direction) and shear stresses in a plane of section perpendicular to fibers (T and R direction) (Majano, Hughes & Fernández-Cabo, 2009; Požgaj, 1997) during joint analysis. It is possible to design truss members from the internal forces.

[*] Ing. Karel Šobra: Department of Mechanics, Czech Technical University in Prague - Faculty of Civil Engineering, Thákurova 7; 166 29, Prague 6 - Dejvice; CZ, e-mail: karel.sobra@fsv.cvut.cz

[**] doc. Ing. Petr Fajman, CSc.: Department of Mechanics, Czech Technical University in Prague - Faculty of Civil Engineering, Thákurova 7; 166 29, Prague 6 - Dejvice; CZ, e-mail: fajman@fsv.cvut.cz

Step joint loaded only by bending moment helps to better understanding of distribution of forces in the joint. By Fajman (2013) it is possible to simplify distribution of forces according to fig. 2.

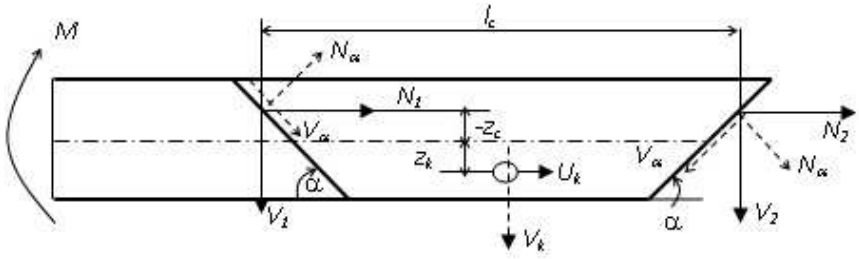

Fig. 2: Force distribution in the joint

Normal force N_α and friction force V_α have their application point on the step end of the joint. These two forces resists to the loading. For the bending moment loaded part of construction it is possible to write two force conditions of equilibrium (1) and one momentum condition of equilibrium (2). Symmetry of construction about vertical axes causes $N_1 = N_2 = N$ and $V_1 = -V_2 = V$.

$$\rightarrow 2N + U_k = 0 \qquad \uparrow 0 = 0 \tag{1}$$

$$-M - 2N \cdot (-z_c) + V \cdot l_c + U_k \cdot z_k = 0 \tag{2}$$

Problem of equations of equilibrium is that a shear force U_k on a key is not known same as forces N_α and V_α on the step end of the joint and size of contact pressed area A_c. Shear force V_α is depended on a coefficient of friction, which can be found in literature or can be determinate by an experiments. After applying some assumption relation between resultant of forces at a compressive area of step end and force in the key is shown in equation (3).

$$z_c = \frac{-M + V \cdot l + U_k \cdot z_k}{-2N + 2V \cot \alpha} = \frac{-M + U_k \cdot C \cdot l + U_k \cdot z_k}{U_k (1 - 2 \cdot C \cdot \cot \alpha)} \tag{3}$$

It is necessary to have numerical model strong enough to observe changes in distribution of forces after changes in design. Experimental tests which are made serves as assurance of these behavior (Šobra, Fajman, 2013). Numerical modeling of the joint is shown in the full text of this paper.

3. Conclusions

The forces in the joint are deeply wedded with coefficient of friction and size of contact pressed area. These parameters can be determinate by experiments. Only range of intensity of forces can be determinate on the basis of these two values. Intensity of internal forces and behavior of step joint is also depended on a many design parameters for example on stiffness of key and skew angle of step end. Lower skew angle causes lower intensity of internal forces shown numerical and experimental analysis of step joint.

Acknowledgement

The results presented in this paper are outputs the Ministry of Culture project NAKI – DF12P01OVV004 - Design and Assessment of Timber Joints of Historical Structures.

References

Fajman, P. (2013) Distribution of forces from bending moment on a step joint. *Stavební obzor* (in Czech, in print)

Gerner, M. (2003) *Carpentry joints*, 1.issue. Grada, Prague (in Czech).

Majano, M.A., Hughes, M., Fernández-Cabo, J.L. (2009) Fracture Characteristics and Properties of Thermally Modified Timber made out of Beech, in: *European Conference on Wood Modification*, SP Technical Research Institute of Sweden, pp. 177-180.

Požgaj. A. (1997) *Composition and properties of wood*, Príroda, Bratislava (in Slovak)

Šobra, K., Fajman, P. (2013) Experimental and numerical analysis of a step joint, *Stavební obzor* (in Czech, in print)

19th International Conference
ENGINEERING MECHANICS 2013
Svratka, Czech Republic, May 13 – 16, 2013

FINITE ELEMENT MODELLING OF SOUND PRESSURE AROUND THE HUMAN HEAD DURING PHONATION

P. Švancara[*], V. Tomeček[*], J. Horáček[**], J. G. Švec[***]

Abstract: *The study presents finite element (FE) model of sound propagation through the vocal tract and around the human head during speech production. Similar experimental studies are not easily realisable. The FE model of the acoustic spaces corresponding to the human vocal tract for Czech vowel [a:] and acoustic space around the human head was created from computer tomography (CT) images. Modal and transient analyses (excitation by a short pulse) are used for analysis of resonant characteristics of the FE model. The production of vowel is then simulated using transient analysis of the FE models excited by Liljencrants-Fant's (LF) glottal signal model. Formant frequencies detected from computed spectra are in good agreement with results of modal analysis and with literature. The results of numerical simulation enable evaluating of the transfer functions between a reference point near the lips and any point in the space around the head.*

Keywords: ***biomechanics of voice, finite element method, sound pressure level, human head model.***

1. Introduction

The sound pressure field around the human head during speech were experimentally studied in several papers (Dunn & Farnsworth, 1939; Halkosaari et al., 2005; Sugiyama, 1991). Knowledge of sound waves transformation during propagation around the head is important for calibration of microphones for speech and singing recordings, and for development of exact voice measurement methods. The aim of this study is to numerically simulate propagation of acoustic waves from vocal folds through the vocal tract and around the human head using the finite element (FE) method. The FE models of the vocal tract for vowel [a:] and the acoustic spaces around the head were developed from CT images taken during the subject phonation. For segmentation of images freeware software ITK-SNAP was used (Švarc, 2012). The geometry was exported to CAD programs CATIA and ATOS where geometry was repaired, smoothed and optimized. Because a top part of the head was missing in the CT images, it was necessary to complete this part manually using the software ATOS. After that a model of acoustic space between the head surface and a sphere of radius one meter around the head was created.

2. Finite element model

The FE meshing was performed by the program package ICEM CFD. The mesh was then exported to the software system ANSYS 14.0 where the acoustic modal and transient analyses were realized similarly as in the paper by Švancara & Horáček (2006). Fig. 1 shows the geometry of the human head created from the CT images and a detail of cross-section through the designed FE model. The complete FE model consists of 674 480 acoustic elements. Created mesh fulfils the requirement of six elements per one wavelength up to the frequency 5 kHz. For modelling the acoustic radiation into an infinite acoustic space a single layer of infinite elements was added onto the outer surface of the sphere.

[*] Ing. Pavel Švancara, PhD.: Institute of Solid Mechanics, Mechatronics and Biomechanics; Brno University of Technology; Technická 2896/2; 616 69; Brno; CZ, e-mail: svancara@fme.vutbr.cz

[*] Bc. Vojtěch Tomeček: Institute of Solid Mechanics, Mechatronics and Biomechanics; Brno University of Technology; Technická 2896/2; 616 69; Brno; CZ, e-mail: y107940@stud.fme.vutbr.cz

[**] Ing. Jaromír Horáček, DrSc.: Institute of Thermomechanics; Academy of Sciences of the Czech Republic; Dolejškova 1402/5; 182 00; Prague; CZ, e-mail: jaromirh@it.cas.cz

[***] RNDr. Jan G. Švec, PhD.: Department of Biophysics; Palacky University Olomouc; 17. listopadu 12; 771 46; Olomouc; CZ, e-mail: svecjang@gmail.com

The infinite elements are based on an infinite geometry mapping and on special shape functions. Boundary walls of the vocal tract, skin of the face and hairs were considered acoustically absorptive. The results could be used for evaluation of the transfer functions between a reference point and points around the head, where the microphones are usually placed (in front of the lips, cheek bone, forehead etc.).

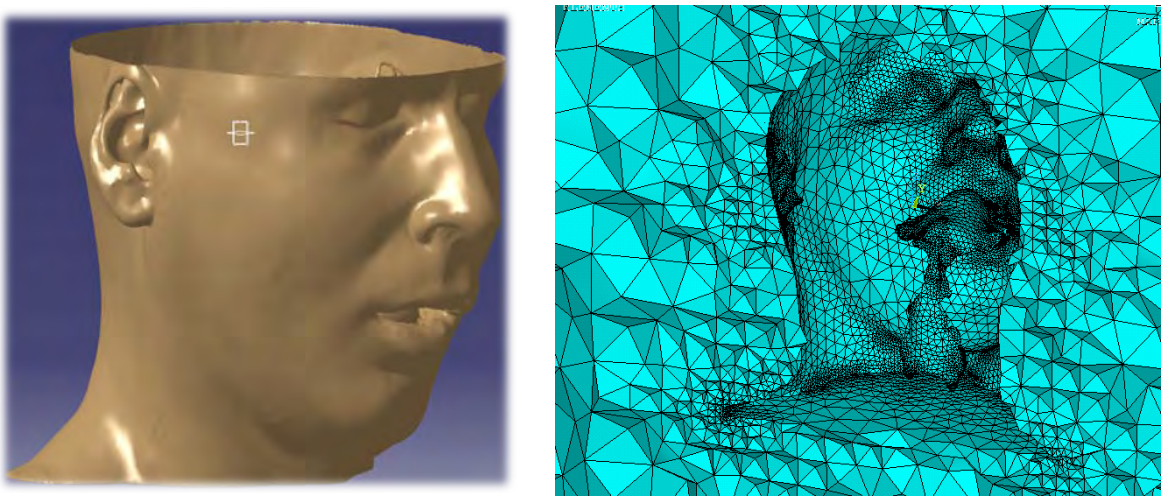

Fig. 1: Geometry of the human head created from CT images (left) and detail of cross-section through the designed FE model (right).

3. Conclusions

The finite element model of the acoustic cavities corresponding to the human supraglottal spaces for vowel [a:] and incorporating the acoustic spaces around the human head was created from the CT images. The formant frequencies of the FE model were evaluated by modal analysis of vocal tract and by excitation of the complete FE model by a short pulse of glottal airflow. Results of both methods are similar and are in good agreement with data in literature. Phonation on vowel [a:] was numerically simulated using the Liljencrants-Fant's glottal source signal model applied at the position of vocal folds and using the transient analysis in time domain.

The transfer functions between a reference point at the lips and any point in the space around the head could be evaluated from the results of numerical simulations, for example in the points where the measurement microphones are usually placed. The time domain solution allows creating sound files for verification of the quality of numerically produced sound at different points around the head by listening. This pilot study should also enable to simulate sound waves propagation around the human head during phonation with applications in modelling the hearing of own voice by the air conduction.

Acknowledgement

This research is supported by the Grant Agency of the Czech Republic by the project No P101/12/1306 and by the European Social Fund Projects OP VK CZ.1.07/2.4.00/17.0009.

References

Dunn, H. K. & Farnsworth, D. W. (1939) Exploration of pressure field around the human head during speech. *Journal of Acoustical Society of America*, 10, pp. 184-199.

Halkosaari, T., Vaalgamaa, M. & Karjalainen, M. (2005) Directivity of artificial and human speech. *Journal of the Audio Engineering Society*, 53, 7/8, pp. 620-631.

Sugiyama, K. (1991) Comparison of the sound pressure radiation from a prolate spheroid and the human mouth. *Acustica*, 73, pp. 271-276.

Švancara, P. & Horáček, J. (2006) Numerical modelling of effect of tonsillectomy on production of Czech vowels. *Acta Acustica united with Acustica*, 92, 5, pp. 681-688.

Švarc, M. (2012) *Development of finite element model of human vocal tract and space around the head based on data from computer tomography.* Bachelor's thesis, Brno University of Technology.

19th International Conference
ENGINEERING MECHANICS 2013
Svratka, Czech Republic, May 13 – 16, 2013

VIBRATION CONTROL OF CARBON BRIDGES

Alexander Tesar

Tuned vibration control in aeroelasticity of slender carbon fiber vs laminated wood composite bridges is treated in present paper. The approach suggested takes into account multiple functions in aeroelastic analysis and flutter of such bridges subjected to laminar and turbulent wind flow. Tuned vibration control approach is presented with application on actual bridge. Ultimate flutter response of slender wood bridge as shown in Fig.1 is studied. The span of the bridge is 100 m. The main girder of the bridge is made of laminated wood. The carbon fiber composites are adopted for the cables.

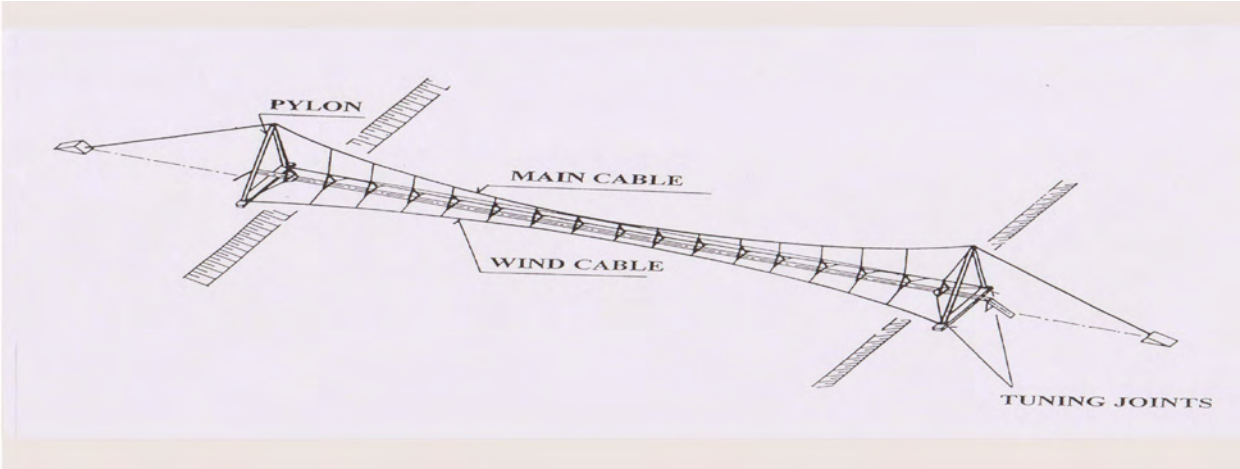

Fig. 1. Slender wood bridge with with TVC-equipment

Advanced bridges are designed in such a way that no traffic or environmental load can decrease their ultimate reliability. However, the experiments sampled up indicate that ultimate behaviour of such bridges occurring due to wind can initiate unpredictable ultimate response influencing their safety. Ultimate flutter behaviour of such bridges occurs by laminar and turbulent air-flow along the surface of the main girder. Linear theory specifies a critical pressure at which the bridge motion becomes unstable. The linear theory specifies the flutter boundary but cannot give information about ultimate flutter response. For large amplitude oscillations the nonlinear effects restrain the motion to a bounded value with growing amplitudes as dynamic pressure increases.

One measure to control such response is the application of tuned vibration control (TVC) in special joints adopted In the bridge. The monitoring and identification of actual parameters, the selection of target reliability and optimal tuning by evaluation of amplification curves are made in tuning joints either automatically for each forcing situation occurring or are set up stationary for the assumed range of forcing. The TVC controls the length of time interval in which the flutter response remains stable with limited amplitudes.

[1)] Prof. Alexander Tesar, Institute of Construction and Architecture, Slovak Academy of Sciences, Dubravska cesta 9, 845 03 Bratislava 45, Slovak Republic, usarate@savba.sk

Slender main girders of bridges studied are made of laminated wood. Carbon fiber composites are adopted for cables. Such bridges, when subjected to laminar or turbulent air flow, can be forced into ultimate flutter response with large amplitudes and unstable aeroelastic behaviour. The monitoring submits all data for the TVC. The forces in wind cables are automatically varied in order to control the response. The TVC-software in tuning joints allows updated identification of all structural and forcing data, their evaluation, monitoring, optimization and consequently the control of structural response.

The treatment and modeling of turbulent air flow in artificial boundary layer around the bridge is a research domain based on advanced scientific technologies. They are imposed by necessity of studying the turbulent air movement in the proximity of slender structures. The models of turbulent air flow are used in the assessments being validated by tunnel testing of parameters integrated in calculation.

The efficiency of the system for tuned vibration control of slender wood bridges, adopting the variability of forces in the wind cables, will be illustrated. The TVC appears there as efficient tool for the reliability of slender wood bridges subjected to laminar and turbulent wind forcing.

REFERENCES

Tesar, A.: Aeroelastic Response of Transporter Shell Bridges in Smooth Air Flow. The Norwegian Institute of Technology, Tapir, Trondheim, 1978

Tesar, A.: Transfer Matrix Method, KLUWER Academic Publishers, Dordrecht, Boston, London, 1988

Tesar, A. and Svolik, J,: Wave distribution in fibre members subjected to kinematic forcing. Int. Journal for Communication in Numerical Mechanics, 9, 1993

Tesar, A. and Tvrda, K.: Energy approach for analysis of nonlinear time response. Building Research Journal, Vol. 54, Nr. 2, 2006, pp. 101-122

19th International Conference
ENGINEERING MECHANICS 2013
Svratka, Czech Republic, May 13 – 16, 2013

ROLE OF MICROFLUIDICS IN DISCOVERING NEW MARKETABLE SUBSTANCES – A SURVEY

V. Tesař*

Abstract: *Paper surveys developments in combinatorial chemistry and related search for new biomedical and other products, characterised by simultaneous testing of many substances (and their mixtures). Attention is focused on advantages offered by small-scale no-moving-part microfluidics. Typical problems and their solution are then demonstrated on author's development of a microfluidic unit for parallel tests of catalyst for Fischer-Tropsch synthesis of liquid fuels from biomass*

Keywords: ***Combinatorial chemistry, pressure-driven microfluoidics***

1. Introduction

Progress in discovering new materials and substances is slow because the process involves synthesising the compounds and testing their properties one by one. An acceleration is achieved by testing simultaneously large number of candidate substances. Paper presents a survey showing how a number of the necessary steps may be performed, with advantage, by devices and circuits of modern no-moving-part fluidics. To accommodate the requested increasingly large numbers of tested samples, attention focuses on low Reynolds number microfluidics – with its typically large numerical density of elements. This may, however, necessitate using unusual operating principles.

2. Testing catalysts

An example described in more detail is testing of catalysts that can make more economical synthesis of liquid fuels and lubricants by the Fritsch-Tropsch process of hydrogenating CO - a gas that together with hydrogen can be obtained by decomposition of biomass. Essential part of the testing facility was sampling unit, taking reaction product samples and delivering them in a sequence into am FT-IR spectrometer analyser for evaluation of catalysts performance.

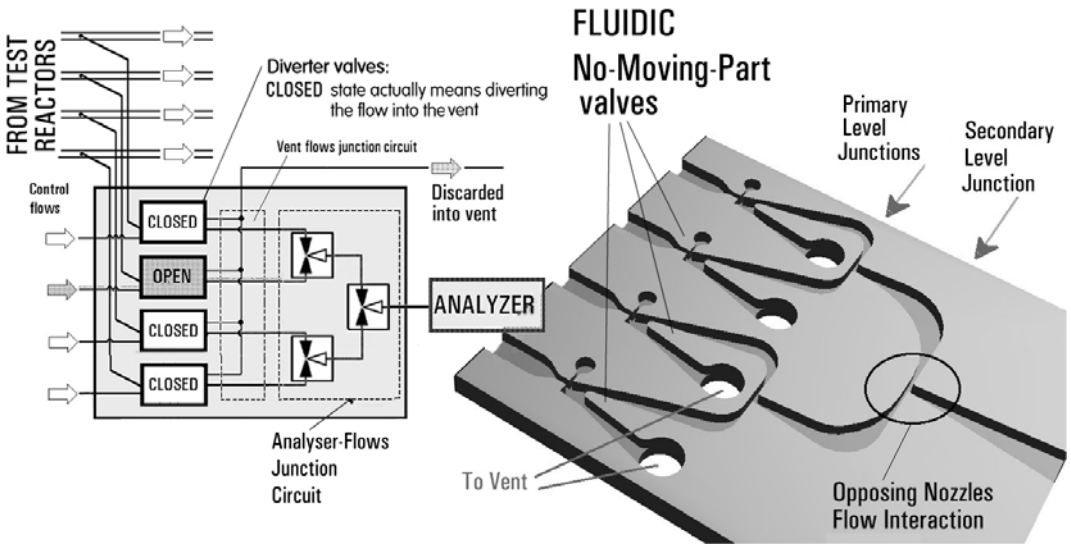

Fig. 1 Author's first unit for taking samples form test reactors and delivering them into an analyser, using fluidic devices operating at sufficiently high Reynolds numbers..

* Prof. Ing. Václav Tesař, Institute of Thermomechanics v.v.v.i., Academy of Sciences of the Czech Republic, Dolejškova 5; 182 00, Prague 8; CZ, e-mail: tesar@it.cas.cz

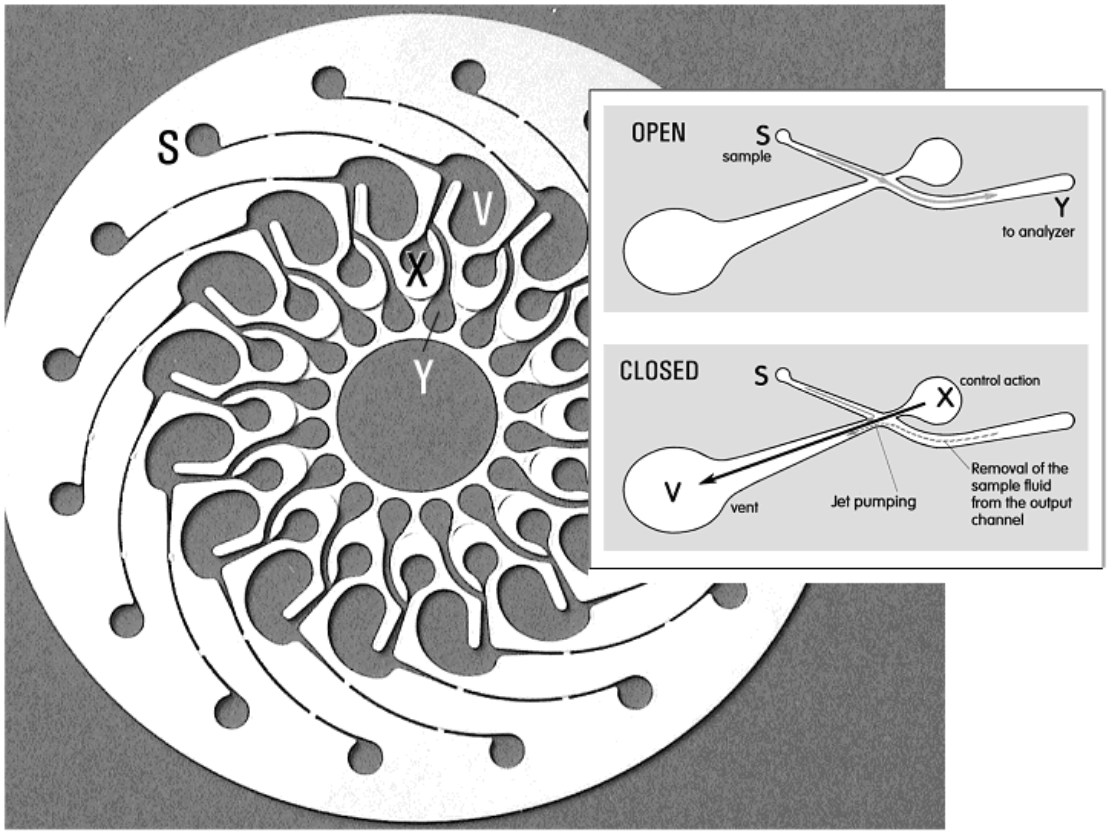

Fig. 2 The operating principle (inset) and a photograph of the later, low Reynolds number version of the sampling unit. An extraordinary feature is the control flow much more powerful than the controlled sample flow – this was needed to generate the jet-pumping effect necessary for cleaning the sample leftovers from "dead" downstream cavities.

The first version (Fig. 1) was based on Coanda-effect switching valves and junction circuits composed of devices using gas-flow inertia and entrainment-based jet pumping. The mutual tuning of valve properties and the actions in the junction circuits were needed to eliminate the possible (although not highly probable) cross-contamination between individual gas samples. This version of the sampling unit did work, but was not up to the gradually increased severity of requirements. Demands of smaller flow rate of gas samples (from smaller reactors) led to lowe flow velovity in the valve. Other aspects were high viscosity (hydrogen in the syngas is a high kinematic viscosity component – and here it was used at high temperatures, further increasing the viscosity value. In addition, there were permanent calls for smaller size. As a result, it became necessary to develop another, microfluidic version, with valves specially designed for low Re operation.

The second version was demonstrated to operate at Re as low as ~30. It was a case of pressure-driven microfluidics. Its design was particularly complicated because of the continuing requirement of eliminating the cross-contamination between the sample flows by small auxiliary flows. On one hand, these flows remove sample leftovers in "dead" spaces downstream from the valves – and, on the other hand, another small "guard" flow prevent a return flow from the common vent into which are discarded all the sample flows flow not entering, at a particular instant, the analyser. Generating these flow necessitated a very special valve design with "fractional" flow gain < 1.0 . For example, the cleaning return flow for removal of previous samples from the "dead" volumes is generated by jet-pumping effect inside the valve, generated by the relatively very powerful control flow (from the terminal X – Fig. 2).

Acknowledgement

Author expresses his gratitude for the support by the grant Nr. 13-23046S received from GAČR — the Czech Science Foundation, and by grant TA02020795 received from the Technological Agency of the Czech Republic, programme ALPHA.

19th International Conference
ENGINEERING MECHANICS 2013
Svratka, Czech Republic, May 13 – 16, 2013

STRUCTURAL AND MATERIAL ANALYSIS OF CERAMIC MATRIX COMPOSITES

S. Urbanová[*], M. Šejnoha[**], J. Vorel[***]

Abstract: *This paper deals with the structural and material analysis of ceramic matrix composites. Especially composite systems with plain weave textile reinforcement, where attention is paid to the design of an idealized geometric model based on a statistically equivalent periodic unit cell and the verification of homogenization procedures used for the determination of effective elastic properties, which were solved by the Mori-Tanaka scheme and the finite element method. The results were then compared with experimental measurements.*

Keywords: ***Textile composite, homogenization, Mori-Tanaka scheme, finite element method.***

1. Introduction

Ceramics shows a significant brittleness which is their main disadvantage. One of the possibilities for the improvement of the resilience is adding of the textile reinforcement. Common textile reinforcements are glass, ceramic, carbon or basalt fibers.

However, a very limited database of construction dates for composites exists. It is a reason for using mathematical models in technical praxis - simulations enabling predictions of properties of the designed composite systems based on the knowledge of properties of reinforcing fibers and polymer matrices, the knowledge of time-temperature modes of matrices curing etc. Numerical evaluation of effective properties also requires information about complex inner geometry of the composite system, which depends on a technology of composite fabrication and on a type of applied textile reinforcement.

2. Evaluation of effective elastic properties

Evaluation of effective elastic properties was performed both experimentally and numerically.

In the framework of experiment, several samples of analyzed composites were fabricated and subsequently cut to obtain their cross-sections. After which were then grinded, polished and finally scanned. In order to acquire geometric parameters of statistically equivalent periodic unit cell - SEPUC (Šejnoha, 2007), optimization in cross-sections of the composites in binary form was performed. Volume fractions of particular phases (yarn, matrix, macroscopic pores) were determined from 2D images by means of the image processing toolbox included in MATLAB software. Because of the low resolution of the images, the volume of pores and cracks incorporated in the yarns (micro-scale) was only estimated. Material parameters of individual phases were performed by nanoindentation (Němeček, 2010) in the Department of Mechanics, Faculty of Civil Engineering, CTU in Prague, by doc. Ing. Jiří Němeček, Ph.D.

Because of fabrication difficulty of ceramic composites, this paper is focused on composites with a polymer matrix in the development of geometric model and testing of homogenization procedures. Therefore, measuring of elastic properties was also performed on these composites. Because of the

[*] Ing. Soňa Urbanová: Faculty of Civil Engineering, CTU in Prague, Thákurova 7, 166 29, Prague; CZ, e-mail: sona.urbanova@fsv.cvut.cz

[**] Prof. Ing. Michal Šejnoha, Ph.D. DSc., Faculty of Civil Engineerig, CTU in Prague, Thákurova 7, 166 29, Prague; CZ, e-mail: sejnom@fsv.cvut.cz

[***] Ing. Jan Vorel, Ph.D.: Faculty of Civil Engineering, CTU in Prague, Thákurova 7, 166 29, Prague; CZ, e-mail: jan.vorel@fsv.cvut.cz

assumption that a geometry of the composite with a ceramic matrix doesn't almost change in comparison to the composite with a polymer matrix from the perspective of porosity, which is the phase the most affecting the final effective properties, the polymer matrix composite is sufficient for mechanical modeling and geometric model creation. This fact comes from the earlier experimental temperature influence research, see (Šejnoha et al., 2012).

Effective elastic properties were experimentally determined by ultrasonic method in laboratory LCTS, Université de Bordeaux, 3 allée de la Boétie, 33600 Pessac, France.

Numerical evaluation of effective elastic properties was carried out employing the Mori-Tanaka scheme and the finite element method.

3. Results

Table 1 stores final effective elastic properties of analyzed materials acquired by the Mori-Tanaka method, finite elements method and experimental measurements.

Tab.1: Effective Young's and shear elasticity moduli

Method	*Effective Young's elasticity moduli* [GPa]				*Effective shear elasticity moduli* [GPa]			
	Basalt reinforcement		*Carbon reinforcement*		*Basalt reinforcement*		*Carbon reinforcement*	
	E_{11} , E_{22}	E_{33}	E_{11} , E_{22}	E_{33}	G_{12}	G_{23} , G_{13}	G_{12}	G_{23} , G_{13}
Mori-Tanaka	*12.7*	*3.2*	*40.5*	*3.3*	*1.2*	*1.2*	*1.2*	*1.3*
FEM	*12.8*	*0.3*	*39.3*	*1.5*	*1.7*	*0.2*	*1.6*	*0.7*
EXP - warp	*16.3*	*3.8*	*42.2, 41.6*	*3.5*	*11.5*	*1.7*	*35.9*	*0.7*
EXP - weft	*7.9, 6.9*	*3.2*	*41.6, 47.7*	*3.5*	*11.9*	*1.6, 1.8*	*32.5*	*1.2*

It is evident from Table 1 that results delivered by all methods are comparable. In the transverse direction the results experimentally obtained seem to be influenced by large error when compared with the moduli in the longitudinal direction. This is especially evident from the shear modulus (G_{12}) for the composite with a carbon reinforcement. The error is probably caused by a low quality of fabricated samples and by the problematic experimental setup for this direction, see (Vorel et al., 2013).

4. Conclusion

Taking account of all the introduced simplifications in determining the effective elastic properties of composites investigated by the Mori-Tanaka scheme and the finite element method, the agreement with the values obtained by experimental measurements is relatively good, and therefore computer modeling in this case seems to be a very effective tool for saving time and money resources.

Acknowledgement

The financial support provided by the GAČR grant no. P105/11/0224 and also the research project by the Grant Agency of the Czech Technical University in Prague grant no. SGS OHK1-042/13 are gratefully acknowledged.

References

Němeček, J. (2010): *Nanoindentation Heterogeneous Structural Materials.* Technical report, CTU in Prague

Šejnoha, M. (2007): *Micromechanical modeling of heterogeneous materials and structures*. PhD thesis, CTU in Prague

Šejnoha, M., Urbanová, S., Salačová, J., Maršálková, M. (2012): *Effective mechanical and transport properties of polysiloxane matrix based composites.* Published in: *High Performance Structures and Materials VI, 2012*

Vorel, J., Urbanová, S., Grippon, E., Jandejsek, J., Maršálková, M., Šejnoha, M. (2013): *Multi-Scale Modeling of Textile Reinforced Ceramic Composites.* In proceedings ICACC 2013

19th International Conference
ENGINEERING MECHANICS 2013
Svratka, Czech Republic, May 13 – 16, 2013

EFFECT OF THE SIZE OF PIRIFORM SINUSES ON THE VOICE QUALITY

T. Vampola[*], J. Horáček[**]

Abstract: *The influence of piriform sinuses (PS) on the resonance and antiresonance characteristics of the vocal tract is investigated. The change in sizes of PS cavities alters the resulting voice quality. Pilot studies reveal that additional formants caused by PS can occur in the frequency range of 3 – 5 kHz, i.e., in the range which is important for the production of the so called singer's or speaker's formant. This contribution therefore aims at investigating the influence of the side cavities of the vocal tract in more detail using two computational models of the vocal tract. First, is presented analysis of the influence of the acoustic spaces of PS on the existence of resonances and antiresonances in the spectra of the acoustic signal simulated using a reduced finite element (FE) model of the human vocal tract. Then the full FE model is used for the analysis by using direct numerical simulations of phonation.*

Keywords: ***Voice quality, singers's formant, biomechanics of voice, human vocal tract, numerical simulation of phonation***

1. Introduction

The influence of the vocal tract on vocal output has been presented in many articles. The influence of side cavities of human vocal tract, such as the piriform sinuses (PS) has received much less attention. Generally, these cavities have been reported to cause antiresonances in the resulting vocal spectrum, i.e., largely decreasing the radiation of some frequencies out of the mouth, particularly around 4-5 kHz. (Motoki, 2002; Mokhtari, *et al.*, 2008). As such, their role for the resulting vocal intensity may be considered undesirable, since it contrasts with the general goal of achieving maximum vocal output with the smallest vocal effort. However, a more detailed analysis reveals that besides the antiformants there are also new formants which occur due to these side cavities (Honda *et al.*, 2004).

Pilot studies reveal that additional formants caused by PS can occur in the frequency range of 3 – 5 kHz, i.e., in the range which is important for the production of the so called singer's formant (in operatic voices) or speaker's formant (observed in professional speakers) (Vampola *et al.*, 2013). It can thus be speculated that these cavities can help in establishing a "better" voice quality in speaking and singing. Considerable progress has been made lately in medical investigation methods like computer tomography which enables to create high quality three-dimensional (3D) models of the vocal tract taking into account details of the laryngeal cavity, valleculae and piriform sinuses. Use of these precise models for the evaluation of acoustic characteristics due to changed geometric configuration of the vocal tract is rather time consuming process.

2. Computational efficient model of the human vocal tract

For a quick evaluation of geometric configuration of PS on the generated acoustic characteristics the simplified one-dimensional (1D) reduced model was developed (Vampola & Horáček, 2012). This model was derived from the 3D FE model by the reduction process (Vampola *et al.*, 2008). Because the relatively dramatic reduction of the original 3D FE model was used, it was necessary to tune the basic acoustic resonance characteristics of the reduced model so that they correspond to the fundamental resonances and antiresonances of the full 3D FE model. The global multicriteria

[*] Doc. Dr. Ing. Tomáš Vampola: Department of Mechanics, Biomechanics and Mechatronics, Faculty of Mechanical Engineering, CTU, Technická 4; 166 07, Prague 6; CZ, e-mail: tomas.vampola@fs.cvut.cz

[**] Ing. Jaromír Horáček, DrSc.: Institute of Thermomechanics, Academy of Science of the Czech Republic; Dolejškova 5, 182 00 Praha 8; CZ, e-mail:jaromirh@it.cas.cz

optimization method was used for tuning of the stiffness parameters of the reduced model according to the chosen fundamental eigenfrequencies and anti-resonance frequencies of the 3D model (see Fig. 1).

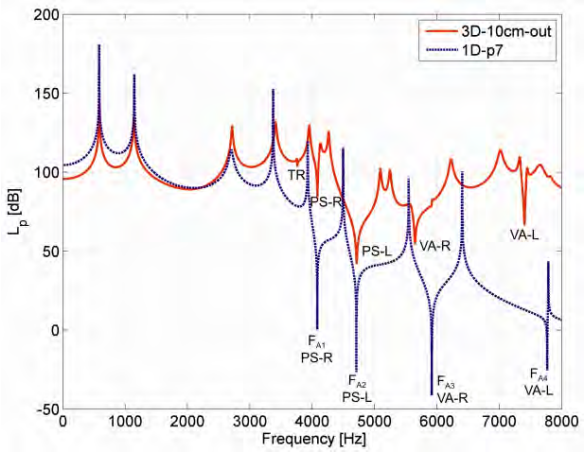

Fig. 1. Acoustic pressure response computed at the distance of 10 cm in front of the mouth using the full 3D FE model of the vocal tract (red full line) and at the output from the reduced (1D) model (blue dashed line).

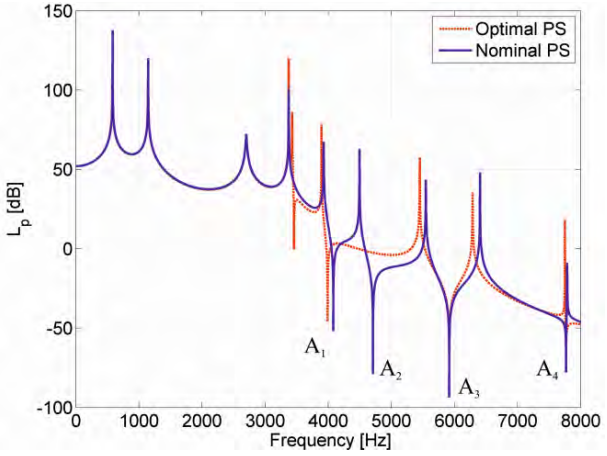

Fig. 2. Spectrum of the simulated acoustic pressure in front of the lips using the reduced model of the vocal tract harmonically excited at the vocal folds for increased PS volumes up to an optimum.

3. Conclusions

Figure 2 demonstrates that an optimum size of the PS can be found when the first antiresonance-resonance pair is approaching the 4th resonance frequency and consequently when the acoustic response in front of the lips results in the highest SPL in the frequency range 3-4 kHz, where a cluster of three resonances can be created in this way. It is apperent that the resonances caused by PS cavities can amplify the resulting voice signal. These phenomena may play an important role for producing a resonant voice, when adjusted properly. These extra resonances may join the other resonances of the vocal tract to form a complex speaker's / singer's formant cluster.

Acknowledgement

This work is supported by the Grant Agency of the Czech Republic by the project No P101/12/1306 "Biomechanical modeling of the human voice production – way to artificial vocal folds".

References

Honda, K., Takemoto, H., Kitamura, T., Fujita, S., & Takano, S. (2004). Exploring Human Speech Production Mechanisms by MRI. *IEICE Transactions on Information and Systems, E87-D,* 1050-1058.

Mokhtari, P., Takemoto, H., & Kitamura, T. (2008). Single-matrix formulation of a time domain acoustic model of the vocal tract with side branches. *Speech Communication, 50,* 179-190.

Motoki, K. (2002). Three-dimensional acoustic field in vocal-tract. *Acoustical Science and Technology, 23,* 207-212.

Vampola, T., Horáček, J. (2012). Influence of geometric configurations of the human vocal tract on the voice production. In Náprstek, J.; Fischer, C. (ed.). *Engineering Mechanics 2012*. Prague: ITAM AS CR, v.v.i., *2012*, pp. 1475-1483. ISBN 978-80-86246-40-6.

Vampola, T., Horáček, J., Laukkanen, A.-M., & Švec, J. G. (2013). Human vocal tract resonances and the corresponding mode shapes investigated by three-dimensional finite-element modelling based on CT measurement. *Logopedics Phoniatrics Vocology*, pp.1-10, DOI: 10.3109/14015439.2013.775333.

Vampola, T., Horáček, J., & Švec, J. G. (2008). FE modeling of human vocal tract acoustics. Part I: Production of Czech vowels. *Acta Acustica United with Acustica, 94,* 433-447.

19th International Conference
ENGINEERING MECHANICS 2013
Svratka, Czech Republic, May 13 – 16, 2013

UNSTEADY AERODYNAMIC FORCES MEASURED ON A FLUTTERING PROFILE

Václav Vlček, Igor Zolotarev, Jan Kozánek*

Summary: *The evaluations of optical measurements of the flow field near the fluttering profile NACA0015 with two-degrees of freedom are presented. Mach number of the airflow was M = 0.21 and M = 0.45, the boundaries of the flutter occurrence. Aerodynamic forces acting on the profile were evaluated in the drag and lift components which enabled to obtain independently the forces corresponding to the upper and lower surfaces of the profile. Using the mentioned decomposition, the new information about mechanism of flutter properties was obtained. The force effects on the upper and lower surfaces are in opposite phases and they are partially eliminated as a result of the circulation around the profile. The cycle changes of this forces cause the permanent energy contribution from the airflow to the vibrating system.*

1. Introduction

The schematic arrangement of the experiment is shown in Vlcek et al. (2013). The flow field near the vibrating NACA0015 profile was visualized by the interferometry in the flutter regime. Interferograms were recorded by the high-speed camera using 1000 frames/sec frequency. During the flutter, the profile, as two degrees of freedom dynamic system, oscillated by the coupled translational and rotational motion with large amplitudes. Two cases ($M = 0.21$, $Re = 0.25.10^6$ and $M = 0.45$, $Re = 0.54.10^6$) were evaluated. The eigenfrequencies of this system corresponding to zero flow velocity were 19.0 Hz (translation) and 21.5 Hz (rotation). In flutter regime, the flutter frequencies were 21.6 Hz (M = 0.21) and 32.3 Hz (M = 0.45).

2. Experimental results

The changes of the lifting forces acting on the upper and lower surfaces and the total lift as the function of the translation centre of the profile rotation during one oscillation period are shown in Fig. 1. The lifting force is depicted on the vertical axis, then the area of the loop represents the quantity which is proportional to the energy transferred from the fluid flow to the vibrating profile. Here, the positive direction of the closed loop corresponds to the clockwise motion.

* Ing. Václav Vlček, CSc., Ing. Igor Zolotarev, CSc., Ing Jan Kozánek, CSc., Institute of Thermomechanics, v.v.i., Academy of Sciences of the Czech Republic, Dolejškova 5, 182 00, Prague 8, Czech Republic, tel.: +420.266053402, fax: +420.286584695, e-mail: vlcek@it.cas.cz

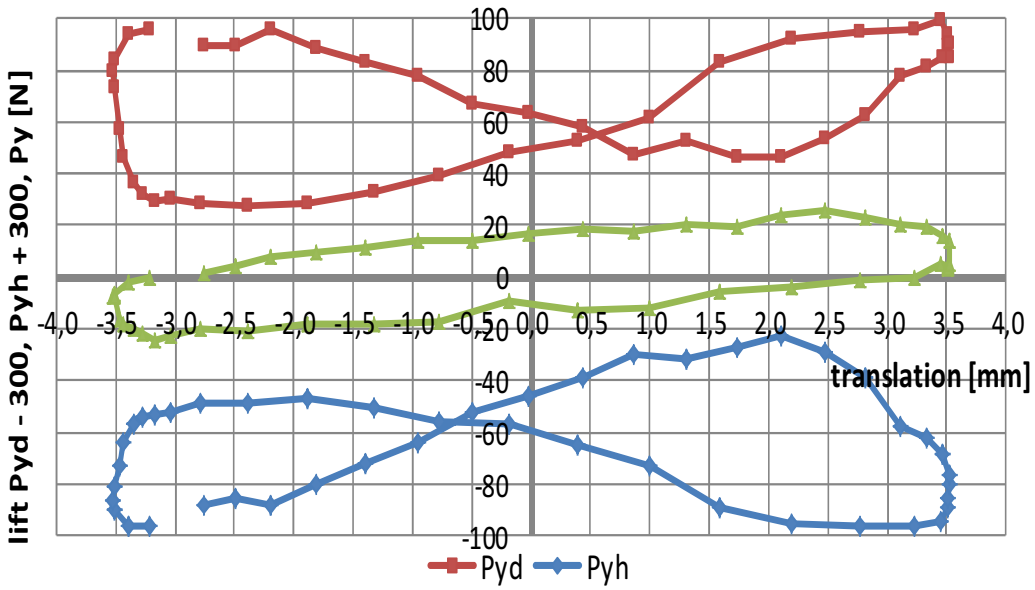

Fig. 1 The lift as the function of the translation (M = 0.21, Pyd – lower, Pyh – upper surface).

There are two types of cycles with starting points at translation value -3.2 mm, see the Fig. 1:

- The elliptical curve situated in the middle of the figure represents the cycle of the resulting lifting force with negative rotation (in this case the elevation in upper direction corresponds to the positive lifting force). Than the self-excited vibration exists and the energy flow from the fluid to the dynamic system take place.
- In the upper and lower part of the diagram there are trajectory loops – the additive components of the middle elliptical curve. These loops are going in opposite sense and represent variable forces existing separately on the upper and lower surfaces. The forces are interconnected by means of the circulation.

3. Conclusion

The interferometric measurements of forces acting on the profile NACA 0015 surface were evaluated during one period of vibration, the flow velocity was M = 0.21 and M = 0.45. The decomposition of the lifting forces into two parts (upper and lower surfaces) enables to obtain original results that describe the dynamical behaviour of the system after the loss of aeroelastic system stability in the flutter regime.

4. Acknowledgement

The authors gratefully acknowledge the Grant Agency of the Czech Republic for supporting this work under Grant No. 13-10527S „Subsonic flutter analysis of elastically supported airfoils using interferometry and CFD“.

5. References

Vlček, V., Kozánek, J., Zolotarev, I. (2013) Optical measurement of the flow field around the aerodynamic profile in flutter regime. Proc. Colloquium Dynamics of Machines 2013, Institute of Thermomechanics AS CR, v.v.i., Prague, 2013, pp. 131-138, (in Czech).

19th International Conference
ENGINEERING MECHANICS 2013
Svratka, Czech Republic, May 13 – 16, 2013

NUMERICAL MODEL FOR DUCTILE FIBER-REINFORCED CEMENT-BASED COMPOSITE

J. Vorel [1], **W.P. Boshoff** [2]

Summary: *Strain Hardening Cement-based Composite (SHCC) is a type of High Performance Concrete that was developed to overcome the brittleness of conventional concrete. The primary objective of this contribution is to verify a developed constitutive model (Vorel and Boshoff, 2012) intended to be utilized in simulations of structural components with SHCC under different types of loading conditions.*

Keywords: ***Strain Hardening Cement-based Composite (SHCC), rotating crack model, three-point bending test***

Introduction

At the beginning of the 21st century, civil engineers more than before face the often-contradictory demands for designing larger, safer, and more durable structures at lower cost and shorter time. Concrete has been used over many centuries as a reliant, fairly durable building material. Two of the main advantages of concrete are that it has a high compressive strength and can be cast on the construction site into almost any shape and size. The most prominent disadvantages of concrete are the brittleness during failure and the low tensile strength. The Strain Hardening Cement-based Composite (SHCC) is a type of High Performance Concrete (HPC) that was developed to overcome the brittleness of conventional concrete. Even though there is no significant compressive strength increase compared to conventional concrete, it exhibits superior behavior in tension. It has been shown to reach a tensile strain capacity of more than 4% during a pseudo strain hardening phase (Boshoff and van Zijl, 2007). The primary objective of the presented research is to verify a constitutive model presented in (Vorel and Boshoff, 2012) that is intended to be used in simulations of structural components with SHCC under different types of loading conditions. In particular, different flexural tests are examined to verify the constitutive model analyses and show advantages and disadvantages of the model. Therefore, the three-point bending test is introduced using parameters based on the tensile tests and data presented by Boshoff (2007). The obtained results are compared with experimental data.

Numerical simulations

The complete description and definition of the model used for simulation of SHCC can be found in (Vorel and Boshoff, 2012). To model the specific behavior of SHCC in tension,

[1] Ing. Jan Vorel, Ph.D., Department of Mechanics, Faculty of Civil Engineering, Czech Technical University in Prague, Thákurova 7, 166 29 Prague, CZ, tel. +420 224 354 375, e-mail jan.vorel@fsv.cvut.cz
[2] Dr William Peter Boshoff, Stellenbosch University, Department of Civil Engineering, Private Bag X1 Matieland 7602, South Africa, e-mail bboshoff@sun.ac.za

the application of classical constitutive material models used for quasi-brittle materials is not straightforward. The utilized numerical model is based on a rotating crack assumption to capture the strain hardening and softening, the multiple cracking, the crack localization, multiple orthogonal crack patterns (Suryanto et al., 2008) and nonlinear unloading.

This model is implemented in the open source finite element code OOFEM (Patzák and Bittnar, 2001). Isoparametric four-node quadrilateral plane-stress finite elements with four integration points (PlaneStress2d) are employed for the discretisation of the numerical models presented in this paper. The aforementioned numerical model is used to obtain the force-deflection diagrams of three-point bending tests. Two different numerical studies for two different sizes of beams are presented in this paper. First, the mesh-dependency of the model is investigated by varying the element size. Second, the edge-effect caused by the aligned fibers along the bottom surface of beams is studied.

Conclusions

In this paper a two-dimensional numerical model for Strain Hardening Cement-based Composites is studied. The accuracy of the introduced approach is investigated by means of a three-point flexural tests. The numerical simulations match reasonably the experimental data for both beam types. The mesh-dependency investigation revealed certain influence of the mesh size on the softening part of the force-displacement curve. On the other hand, the influence of the extra layer representing the aligned fibers along the surface of the beam is not strongly pronounced for any of the mesh sizes of the beam 100x100x300 mm. As expected, the influence of enhanced layer is more pronounced for the beam 16x70x400 mm where it represents significant portion of the beam height.

Acknowledgment

The financial support provided by the GAČR grant No. 105/12/P353 is gratefully acknowledged.

References

Boshoff, W. (2007). *Time-Dependant Behaviour of Engineered Cement-Based Composites*. PhD thesis, University of Stellenbosch. Ph.D. thesis.

Boshoff, W. and van Zijl, G. (2007). Time-dependant response of ECC: Characterisation of creep and rate dependence. *Cement and Concrete Research*, 37:725–734.

Patzák, B. and Bittnar, Z. (2001). Design of object oriented finite element code. *Advances in Engineering Software*, 32(10-11):759–767.

Suryanto, B., Nagai, K., and Maekawa, K. (2008). Influence of damage on cracking behavior of ductile fibre-reinforced cementitious composite. In *Proceedings of 8th International Conference on Creep, Shrinkage and Durability of Concrete and Concrete Structures*, pages 495–500.

Vorel, J. and Boshoff, W. (2012). Numerical modelling of engineered cement-based composites. In *Proceedings for Engineering Mechanics 2012*, pages 1555–1564.

19th International Conference
ENGINEERING MECHANICS 2013
Svratka, Czech Republic, May 13 – 16, 2013

THE STABILITY INVESTIGATION OF VIBRATIONS OF FLEXIBLY SUPPORTED RIGID ROTORS DAMPED BY HYBRID MAGNETORHEOLOGICAL DAMPING ELEMENTS

J. Zapoměl[*], J. Kozánek[**], P. Ferfecki[***]

Abstract: *A flexible suspension with added damping elements makes it possible to reduce the time varying forces transmitted between the rotor and its casing. For this purpose a concept of a hybrid damping device working on the principle of squeezing the layers of normal and magnetorheological oils have been developed. Its influence on stability of the rotor vibration caused by its unbalance is studied by two approaches: by utilization of the Floquet theorem and by the evolutive method. The former determines the stability by means of magnitude of the largest eigenvalue of the transition matrix set up over the span of time of one period, the later by evolution of eigenvalues of the system linearized in a small neighbourhood of the steady state phase trajectory of the rotor.*

Keywords: ***rotors, controllable dampers, vibration stability, Floquet theorem, evolution method.***

1. Introduction

Unbalance of rotating parts excites the time varying forces transmitted between the rotor and its casing. A usual technological solution how to reduce their magnitude consists in application of a flexible suspension and in adding the damping devices to the rotor supports. A simple analysis shows that to achieve their optimum performance their damping effect must be controllable to be possible to adapt it to the current operation conditions. This is enabled by magnetorheological damping devices.

2. Mathematical model of the constraint element and of the investigated rotor system

The principal parts of the studied damping element (Figure 1) are three rings mutually separated by lubricating films formed by normal (inner) and magnetorheological (outer) oils. The lateral vibration of the rotor squeezes the lubricating layers which produces the damping effect. The damper is equipped with an electric coil generating magnetic flux passing through the magnetorheological liquid. As its resistance against the flow depends on magnetic induction, the change of the applied current can be used to control the damping force.

In the mathematical model of the damping element the normal and magnetorheological oils are represented by Newtonian and Bingham materials. The pressure in the oil layers is governed by the Reynolds equations. Components of the damping forces are calculated by integration of the pressure distributions around the circumference and along the length of the damping element taking into account a cavitation in the lubricating films where the pressure remains constant.

The investigated rotor (Figure 2) consists of a shaft and of one disc and is coupled with the frame by the studied constraint elements at both its ends. The rotor turns at constant angular speed and is loaded by its weight and excited by the disc unbalance. The squirrel springs can be prestressed to be eliminated their deflection caused by the rotor weight. The whole system is symmetric relative to the disc middle plane. The task was to analyse stability of the rotor vibration.

[*] Prof. Ing. Jaroslav Zapoměl, DrSc.: Institute of Thermomechanics, Dolejškova 1402/5,182 00 Praha 8; 182 00, Prague, Czech Republic, e-mail: jaroslav.zapomel@vsb.cz

[**] Ing. Jan Kozánek, CSc.: Institute of Thermomechanics, Dolejškova 1402/5,182 00 Praha 8; 182 00, Prague, Czech Republic, e-mail: kozanek@it.cas.cz

[***] Ing. Petr Ferfecki, PhD.: Institute of Thermomechanics, Dolejškova 1402/5,182 00 Praha 8; 182 00, Prague, Czech Republic, e-mail: petr.ferfecki@vsb.cz

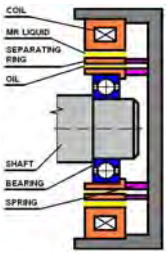

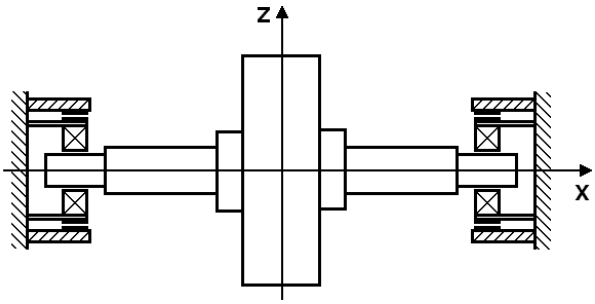

Fig. 1: Scheme of the studied damping device. *Fig. 2: Scheme of the investigated rotor system.*

3. The equations of motion and the vibrations stability evaluation

Lateral vibration of the rotor system is governed by a set of four nonlinear equations of motion. Their steady state solution was obtained by application of a trigonometric collocation method.

The first approach to assessment of the steady state vibration stability is based on a perturbation method and the Floquet theorem. This requires to set up the transition matrix over the span of time of one period and to calculate its eigenvalues. If moduli of all of them are less than 1, the vibration is stable. The second approach utilizes the evolutive method. The equation of motion is linearized in the neighbourhood of the steady state phase trajectory and the time histories of all eigenvalues of the linearized system are calculated. If the real parts of all of them are negative at any moment of time during one period, then the rotor vibration is stable.

4. Results of the computational simulations

Results of the carried out computational simulations are summarized in Figures 3 - 6. The analysis was performed for the conditions when the rotor journals in the constraint elements are not sufficiently centred by prestressing the squirrel springs. Therefore, the steady state orbits of the centres of the rotor journal and the separating ring shown in Figure 3 are slightly non-circular and shifted in the vertical direction. All eigenvalues of the transition matrix set up over the span of time of one period, as evident from Figures 4, are less than one and this implies the steady state vibrations of the rotor are stable. The undamped natural frequency of the system is 149 rad/s. In Figures 5 and 6 there are depicted the time histories of the damped natural frequencies and corresponding damping ratios during one period belonging to two partial motions of rotor that have the oscillatory character. The results show that presence of the damping devices increases the stiffness of the system as the natural frequencies are shifted to higher values. The damping ratios are positive which means the rotor oscillations are stable.

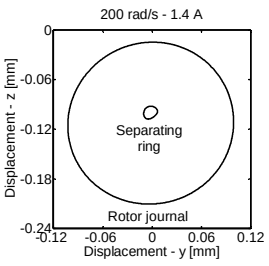

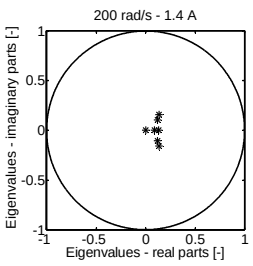

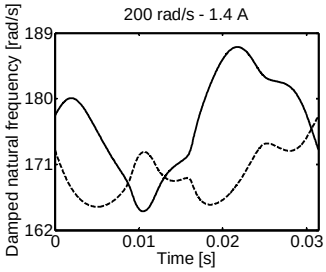

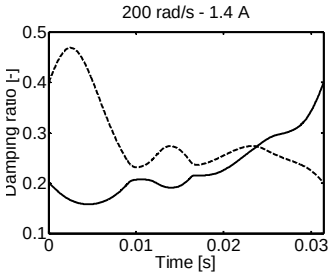

Fig. 3 *Fig. 4* *Fig. 5* *Fig. 6*

5. Conclusions

The performed computational simulations proved that the studied magnetorheological damping element enabled to reduce the force transmitted between the rotor and its casing, to supress the rotor oscillations and that for evaluation of stability of the system vibrations the approaches based on utilization of the Floquet theorem and the evolutive method could be applied.

Acknowledgement

The work reported in this article has been done with the institutional support RVO:61388998.

19th International Conference
ENGINEERING MECHANICS 2013
Svratka, Czech Republic, May 13 – 16, 2013

MODELLING OF THE TURBOCHARGER VIBRATIONS

V. Zeman, Z. Hlaváč *

Abstract: *The paper deals with derivation of the dynamical model of the turbochargers with rotor supported on the two floating ring bearings. The model respect the bearing forces acting upon the journals and floating bearing rings by means of inner and outer oil films. The gyroscopic effects, external and internal damping of the flexible rotor shaft and the rigid turbine and compressor wheels are respected. The modal analysis and the Campbell diagram is used in the turbocharger linearized model to find the critical speeds.*

Keywords: ***Turbocharger vibrations, eigenvalues, Campbell diagram, critical speeds.***

1. Introduction

The automotive turbochargers work at very high rotor speeds. Therefore the turbocharger vibrations caused by the rotor unbalance is fundamental phenomenon influencing a turbocharger operation. Consider the very high-speed automotive turbocharger (Shäfer (2012)) including the flexible rotor shaft (R), rigid turbine (T) and compressor (C) wheels and two cylindrical floating ring bearings ($\mathrm{B_a}$, $\mathrm{B_b}$) displayed in Fig.1. The aim of this article is to present a generally accepted methodology for modelling of the turbocharger vibration, calculation of complex modal values and critical speeds.

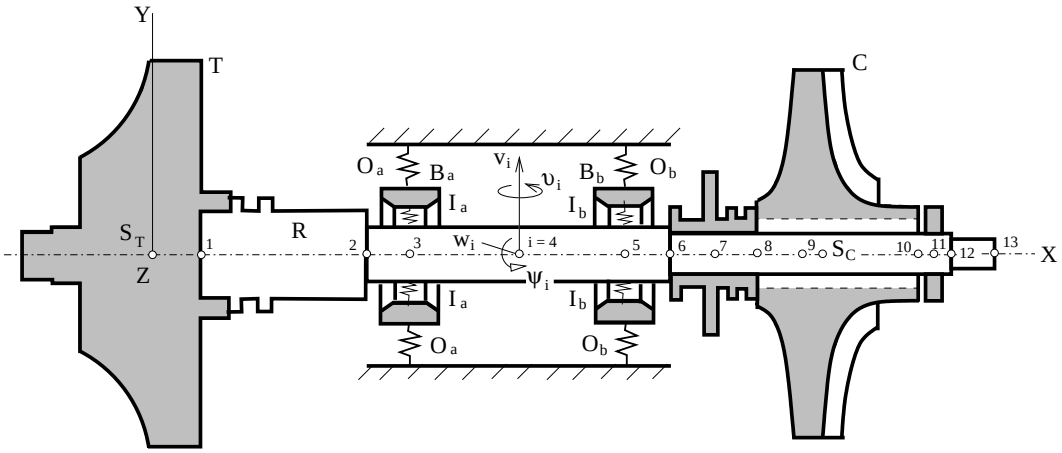

Fig. 1: Computational model of the turbocharger rotor

2. Equations of rotor motion

In the application of automotive turbochargers, the torsion and longitudinal vibrations amplitudes of the rotor are relatively small compared to the lateral-bending amplitudes caused by the rotor unbalance. Therefore, only four degrees of freedom (DOF) expressed by lateral and bending angular displacements of the rotor shaft nodal points i are taken into account in modelling. The mathematical model of the flexible rotor shaft with rigid turbine and compressor wheels rotating by constant angular speed ω, in the inertial coordinate system XYZ (see Fig.1)

$$\boldsymbol{q}_R = [\ldots, v_i, w_i, \vartheta_i, \psi_i, \ldots]^T \in R^{4N} \tag{1}$$

*Prof. Ing Vladimír Zeman, DrSc., Doc. RNDr. Zdeněk Hlaváč, CSc.: NTIS-New Technologies for Information Society, University of West Bohemia, Univerzitní 22, 306 14 Plzeň, tel. 420 377 63 23 32, e-mail zemanv@kme.zcu.cz

has the form (Byrtus et al. (2010))

$$\boldsymbol{M}_R\ddot{\boldsymbol{q}}_R + (\boldsymbol{B}_R^{(e)} + \boldsymbol{B}_R^{(i)} + \omega\boldsymbol{G}_R)\dot{\boldsymbol{q}}_R + (\boldsymbol{K}_R + \omega\boldsymbol{C}_R)\boldsymbol{q}_R = \boldsymbol{f}_R(t)\,. \tag{2}$$

The mass $\boldsymbol{M}_R$, external $\boldsymbol{B}_R^{(e)}$ and internal $\boldsymbol{B}_R^{(i)}$ damping and stiffness $\boldsymbol{K}_R$ matrices are symmetrical of order $4N$ (N is number of shaft nodal points i). The circulatory matrix $\omega\boldsymbol{C}_R$ generated by internal damping of the shaft and gyroscopic matrix $\omega\boldsymbol{G}_R$ are antisymmetrical. The vector $\boldsymbol{f}_R(t)$ expresses the turbine and compressor wheels unbalance.

On condition that floating ring bearings R_a (left) and R_b (right) vibrate only lateral in Y, Z directions, the vector of bearing ring displacements with respect to frame is

$$\boldsymbol{q}_B = [\boldsymbol{q}_{R_a}^T, \boldsymbol{q}_{R_b}^T]^T\,;\ \boldsymbol{q}_{R_x} = [v_x, w_x]^T,\ x = a, b \tag{3}$$

and the corresponding bearing mass matrix is diagonal

$$\boldsymbol{M}_B = \mathrm{diag}[m_a, m_a, m_b, m_b]\,, \tag{4}$$

where m_a, m_b are ring masses. In the first approximation the bearing forces $\boldsymbol{f}_x^{(I)} = [F_{Y,x}^{(I)}, F_{Z,x}^{(I)}]^T$ transmitted by inner oil film (superscript I) between journal and ring and bearing forces $\boldsymbol{f}_x^{(O)} = [F_{Y,x}^{(O)}, F_{Z,x}^{(O)}]^T$, $x = a, b$ transmitted by outer oil film (superscript O) for the well-balanced rotor can be linearized in the neighbourhood of the static equilibrium positions resulted from static load. The changes of bearing forces relating to small displacements and velocities of the journals and floating ring bearings at the static equilibrium position can be expressed as (Krämer (1993), Shäfer (2012))

$$\Delta\boldsymbol{f}_x^{(I)} = -\boldsymbol{K}_x^{(I)}(\omega)(\bar{\boldsymbol{q}}_{J_x} - \bar{\boldsymbol{q}}_{R_x}) - \boldsymbol{B}_x^{(I)}(\omega)(\dot{\boldsymbol{q}}_{J_x} - \dot{\boldsymbol{q}}_{R_x}),\ \Delta\boldsymbol{f}_x^{(O)} = -\boldsymbol{K}_x^{(O)}(\omega)\bar{\boldsymbol{q}}_{R_x} - \boldsymbol{B}_x^{(O)}(\omega)\dot{\boldsymbol{q}}_{R_x},\ x = a, b, \tag{5}$$

where stiffness $\boldsymbol{K}_x^{(I)}(\omega)$, $\boldsymbol{K}_x^{(O)}(\omega) \in R^{2,2}$ and damping $\boldsymbol{B}_x^{(I)}(\omega)$, $\boldsymbol{B}_x^{(O)}(\omega) \in R^{2,2}$ matrices of inner (I) and outer (O) film of both bearings ($x = a, b$) are nonsymmetrical. Vectors $\bar{\boldsymbol{q}}_{J_x}$ of journals and $\bar{\boldsymbol{q}}_{R_x}$ of bearing rings express lateral displacements of their centres from static equilibrium position. According to (2), (4), (5), the linearized turbocharger motion equations are

$$\begin{bmatrix} \boldsymbol{M}_R & \boldsymbol{0} \\ \boldsymbol{0} & \boldsymbol{M}_B \end{bmatrix}\begin{bmatrix} \ddot{\boldsymbol{q}}_R \\ \ddot{\boldsymbol{q}}_B \end{bmatrix} + \left(\begin{bmatrix} \boldsymbol{B}_R^{(e)} + \boldsymbol{B}_R^{(i)} + \omega\boldsymbol{G}_R & \boldsymbol{0} \\ \boldsymbol{0} & \boldsymbol{0} \end{bmatrix} + \boldsymbol{B}_B(\omega)\right)\begin{bmatrix} \dot{\boldsymbol{q}}_R \\ \dot{\boldsymbol{q}}_B \end{bmatrix} + \left(\begin{bmatrix} \boldsymbol{K}_R + \omega\boldsymbol{C}_R & \boldsymbol{0} \\ \boldsymbol{0} & \boldsymbol{0} \end{bmatrix} + \boldsymbol{K}_B(\omega)\right)\begin{bmatrix} \bar{\boldsymbol{q}}_R \\ \bar{\boldsymbol{q}}_B \end{bmatrix} = \begin{bmatrix} \boldsymbol{f}_R(t) \\ \boldsymbol{0} \end{bmatrix}, \tag{6}$$

where vectors marked with strip express rotor component displacements from equilibrium position. The stiffness and damping bearing matrices presented here in the reduced form (null blocks are not presented) are

$$\boldsymbol{K}_B(\omega) = \begin{bmatrix} \boldsymbol{K}_a^{(I)} & & -\boldsymbol{K}_a^{(I)} & \\ & \boldsymbol{K}_b^{(I)} & & -\boldsymbol{K}_b^{(I)} \\ -\boldsymbol{K}_a^{(I)} & & \boldsymbol{K}_a^{(I)} + \boldsymbol{K}_a^{(O)} & \\ & -\boldsymbol{K}_b^{(I)} & & \boldsymbol{K}_b^{(I)} + \boldsymbol{K}_b^{(O)} \end{bmatrix}\begin{matrix} \}\bar{\boldsymbol{q}}_{J_a} \\ \}\bar{\boldsymbol{q}}_{J_b} \\ \}\bar{\boldsymbol{q}}_{R_a} \\ \}\bar{\boldsymbol{q}}_{R_b} \end{matrix}\ ;\ \boldsymbol{B}_B(\omega) \sim \boldsymbol{K}_B(\omega)\,. \tag{7}$$

3. Conclusion

The described method was applied to investigate the complex eigenvalues, stability, unbalance response and critical speeds of the well-balanced concrete turbocharger rotor supported on two floating ring bearings. The adjusted nonlinear mathematical model including nonlinear characteristics of the bearing forces will be used for vibration analysis at the large journals and floating bearing rings deflections.

Acknowledgement

This work was supported by the European Regional Development Fund (ERDF), project "NTIS", European Centre of Excellence, CZ.1.05/1.1.00/02.0090.

References

Byrtus, M., Hajžman, M. & Zeman, V. (2010) *Dynamika rotujících soustav.* Monograph. UWB, Pilsen.

Krämer, E. (1993) *Dynamics of Rotors and Foundations.* Springer, Berlin.

Shäfer, H. N. (2012) *Rotordynamics of Automotive Turbochargers.* Springer, Heidelberg.

19th International Conference
ENGINEERING MECHANICS 2013
Svratka, Czech Republic, May 13 – 16, 2013

EXPERIMENTAL-AND-COMPUTATIONAL PREDICTION OF AEROELASTIC STABILITY IN BLADE ASSEMBLIES AGAINST SUBSONIC FLUTTER

A.P. Zinkovskii [*], V.A. Tsymbalyuk*

Abstract: *The basic principles of the experimental-and-computational complex for predicting the subsonic flutter stability of aircraft gas turbine compressor blading are stated. The methodology is described for the experimental determination of non-stationary aerodynamic forces and moments acting on blades during their in-flow vibrations; the calculation of the dynamic stability of a blade assembly against flutter; the aerodynamic rig design and peculiar features of its components to perform testing of airfoil cascades. The results of testing of the developed experimental-and-computational complex are presented.*

Keywords: ***blade assembly, modeling, airfoil cascade, subsonic flutter, aeroelastic stability prediction***

The most dangerous vibrations of axial compressor blades are those that occur most frequently during operation of the modern aircraft gas-turbine engines (AGTE) and can cause fatigue failures, namely: resonant vibrations, which are caused by circumferential nonuniformity of the flow due to gas dynamic wakes from the stator blades, struts and etc., nonresonant vibrations induced by rotating stall, nonresonant vibrations induced by turbulent flow fluctuations and flutter (self-excited vibrations in fluid flow).

Full-scale engine testing for blade stability against flutter is very expensive. Laboratory testing of aerodynamic loads and determination of dynamic stability of blade assemblies of rotor wheels make it possible to reduce their scope of testing. This exactly defines the purpose of the paper, which lies in scientific and technical justification and development of the experimental and computational complex for predicting the stability of AGTE blade assemblies against subsonic flutter, which involves the experimental determination of aerodynamic loads acting on blades during their vibration in a flow and computation determination of the flutter stability limit by calculating the natural frequencies of coupled vibrations of blades in a flow using the obtained experimental data.

Based on the approaches of physical modeling of phenomena observed under full-scale conditions, the similarity criteria are defined, which allow modeling the behavior of blade assemblies at their interaction with flow. It is shown, that unsteady aerodynamic loads Q_A acting on the blade assembly are the function of three similarity criteria, namely: reduced frequency, the Mach number M and the peripheral-to-axial velocity ratio, which for airfoil cascades is replaced with the angle of attack i.

The methodology is described for the experimental determination of non-stationary aerodynamic forces and moments acting on blades during their in-flow vibrations. The most susceptible to subsonic flutter are the first flexural and torsional modes of blade vibrations. As far as such modes of vibrations are concerned, virtually all exchange of energy with flow is implemented in the peripheral section of the blades where the vibration amplitudes are the largest. That is why during analyzing their dynamic stability against flutter it can be sufficient to determine loads for peripheral section, and these values can be regarded as constant along the blade length provided that the flow surfaces are close to cylindrical.

Considering the above-mentioned, the experimental investigations on determining aerodynamic loads have been performed using the straight cascade of airfoil models shown in Fig.1, *a*. These models are located parallel in a cascade and their cross sections are equal in height, which simulate the

[*] Prof. Ing. A.P. Zinkovskii, DSc., Ing. V.A. Tsymbalyuk, CSc.: G.S. Pisarenko Institute for Problems of Strength, Nat. Ac. Sci. of Ukraine, 01014, 2, Timiryazevskaya str., Kiev, Ukraine, tel.: +380442851687; fax: +380442861684; zinkovskii@ipp.kiev.ua, e-mail: zinkovskii@ipp.kiev.ua, tsymbalyukv@ipp.kiev.ua .

development of the chosen cylindrical section of the blade assembly. Then, the blade airfoil model is considered to be known as airfoil, whereas the straight cascade of airfoil models is referred to as airfoil cascade.

To various vibration modes of the blade assembly there correspond different combinations of translational (x, y) and angular (α) displacements of airfoils, while aerodynamic loads acting on them can be represented in terms of forces L_A, K_A and moment M_A, as is seen in Fig. 1, *b*, where β is the stagger angle; t_s is the cascade spacing.

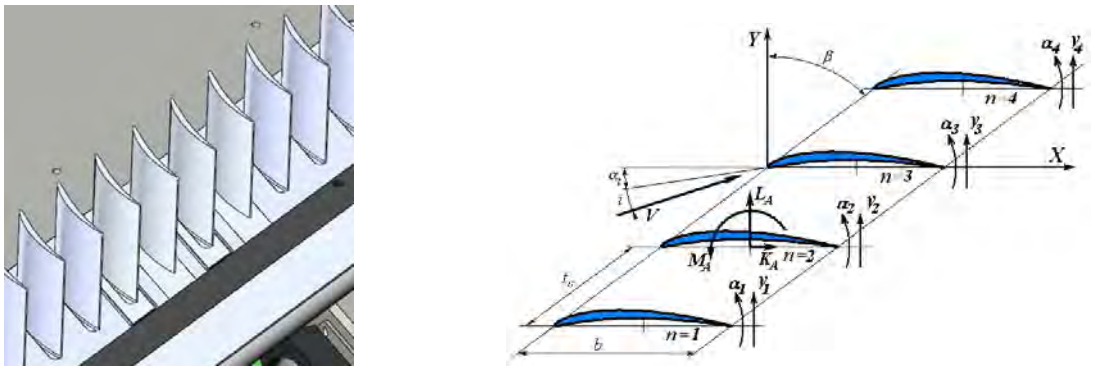

(а) (б)

Fig. 1 Straight cascade of airfoils (a) and scheme of acting loads (b)

Measurement of aerodynamic loads, which act on the airfoils vibrating in a flow, is performed using the developed automated test bench. The test bench is the open circuit subsonic wind tunnel with which the air is drawn from the atmosphere and rejected back into the surroundings. To ensure the preset rates and angles of attack of the flow around airfoils, the cascade of airfoils is put into the working section. The maximum four central airfoils can be active. Each of them is fixed on individual vibration unit, which structure and function will be provided in detail below. The other (background) airfoils are mounted rigidly to the rotating base plates. Setting of the airfoil cascade to the required angles of attack is performed by rotating the base plate and frame with vibration units.

A methodology has been developed for experimental determination of unsteady aerodynamic loads acting on GTE compressor blade assemblies under laboratory conditions, which ensures the enhancement of accuracy of test results and substantiated selection of the parameters for the model and test bench.

The computational model of the blade assembly with flexural-torsional vibrations of its blades and procedure for determination of the flutter stability limit based on it have been developed.

The results of approbation of the proposed methods using the analysis of dynamic stability of AGTE compressor blade assemblies as an example were provided.

The test bench, which has been developed at the G.S.Pisarenko Institute for Problems of Strength, makes it possible to determine aerodynamic loads (forces and moments) acting on blades in a flow by implementing unique experimental and computational complex and based on their use to predict stability of AGTE compressor blade assemblies against subsonic flutter over a wide range of variation of their mechanical parameters and flow characteristics. Moreover, it should be noted that the developed complex is a fully automated system with modern measurement and computer facilities.

The developed experimental and computational complex aimed at predicting the stability of blade assemblies against subsonic flutter can be deployed for the design and manufacture of gas turbine engines, which are used in aircraft manufacturing, ship building, steam turbines and other fields, also it can be adjusted to predicting the dynamic stability of tube bundles of steam condensers and heat exchangers of NPP.

This study was performed within the framework of the joint research project between the G.S.Pisarenko Institute for Problems of Strength of the NAS of Ukraine and Institute of Thermomechanics AS CR for conducting investigations on „Interaction of Elastic Bodies with Air Flow“.

19th International Conference
ENGINEERING MECHANICS 2013
Svratka, Czech Republic, May 13 – 16, 2013

MECHANICAL PROPERTIES OF CEMENT PASTE WITH 50% FLY ASH AT HIGH TEMPERATURES

O. Zobal[*], R. Lovichová[**], P. Padevět[***]

Abstract: *The current trend in society is the broader and appropriate use of waste materials. In the construction industry, for example, this effort is represented by using a larger quantity of power plant fly ash in cement and concrete mixtures. This article is dedicated to the comparison of the mechanical properties of a reference cement paste and binders where 50% of cement is replaced by power plant fly ash at high temperatures. Specifically, the experimentally obtained density values, compressive strength, tensile strength and static modulus of elasticity are presented here. The specimens for the experiment were 28 days old and the water-binder ratio was 0.4.*

Keywords: ***Cement, fly ash, high temperatures, compressive strength, tensile strength.***

1. Methodology of the experiment

The first mixture (referred to as CFA 1000 sat) was produced using the cement CEM I 42, 5R from Radotín and a given amount of water. The second mixture was made from the same cement and 50% of cement by weight was replaced by fly ash from Mělník referred to as EME et EN 450. This mixture is referred to as CFA 5050 sat and CFA 5050 dry, depending on whether the specimens were stored in a water bath or dried at 105 °C before testing. The water-binder ratio was always 0.4 and the age of the test samples was 28 days. Test samples had the shapes of small beams with sides of 20 x 20 mm and a length of 100 mm.

2. Evaluation of the experiment

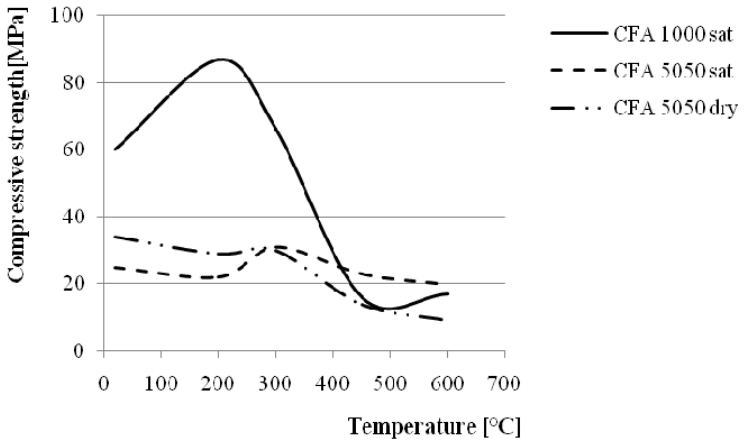

Fig. 1: Graphic representation of the development of compressive strength versus time and the type of mixture, the ratio of water and the binder has a value of 0.4, and aging specimens for 28 days.

[*] Ing. Ondřej Zobal: Faculty of Civil Ingineering, CTU in Prague, Thakurova 7, 166 29, Prague; CZ, e-mail: ondrej.zobal@fsv.cvut.cz

[**] Bc. Romana Lovichová: Faculty of Civil Ingineering, CTU in Prague, Thakurova 7, 166 29, Prague; CZ, e-mail: romana.lovichova@fsv.cvut.cz

[***] Ing. Pavel Padevět, Ph.D.: Faculty of Civil Ingineering, CTU in Prague, Thakurova 7, 166 29, Prague; CZ, e-mail: pavel.padevet@fsv.cvut.cz

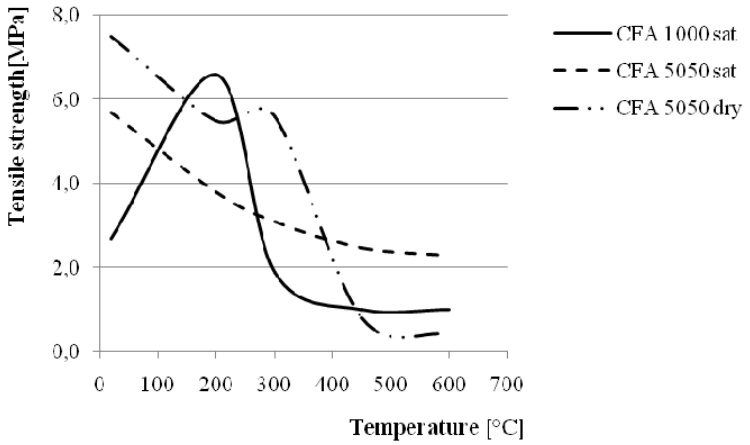

Fig. 2: Graphical representation of the evolution of tensile strength depending on the time and type of mixture; ratio of water and binder has a value of 0.4 and age of specimens is 28 days.

3. Conclusions

The subject of the experiment was the mechanical properties of cement paste and cement pastes with a 50% share of fly-ash in a mixture affected by high temperatures. The results of individual measurements and calculations were statistically processed and compared with each other. Test specimens in the form of beams were produced from the cement paste. Dimensions were always measured for all specimens and the weight was determined in order to obtain the necessary information about changes in the density of the tested material. Cement paste was prepared from CEM I 42.5 R , fly ash EME et EN 450 with the water-binder ratio value of 0.4. The testing of specimens was performed at five temperatures: 20°C, 200°C, 300°C, 450°C and 600°C. The assumption was that the mechanical properties would deteriorate with increasing temperature because the structure of specimens would be damaged. Surface damage of cement paste without fly ash at temperatures of 450°C and more was considerable, but the added fly ash significantly mitigated this damage.

Acknowledgement

The financial support of this experiment by the Faculty of Civil Engineering, Czech Technical University in Prague (SGS project No. 12/117/OHK1/2T/11) is gratefully acknowledged.

References

http://www.cez.cz/cs/vyroba-elektriny/uhelne-elektrarny/informace-o-uhelne-energetice.html

Soroka, I. (1993) *Concrete in Hot Environments*, Alden Press, Oxford, Great Britain

Neville, A., M. (2009) *Properties of concrete*

Zobal, O., Padevět, P., Šmilauer, V., Kopecký, L., Bittnar, Z. (2012) *Experimental analysis of material and mechanical properties of the concrete dam Orlik after 50 years*, In: Betonářské dny 2012. Praha: Česká betonářská společnost ČSSI

Zobal, O., Kopecký, L., Padevět, P. (2012) *Interaction of Cement with Fly Ash at the Micro Level*, In: 10th International Comferernce on New Trends in Statics and Dynamics of Buildings, Slovak University of Technology, Bratislava.

Lovichová, R. (2013) *Influence of high temperatures on the material properties of cement paste with fly ash*, Student text, CTU Press, Prague.

Zobal, O. (2009) *Influence of temperature on the material properties of cement paste*, Student text, CTU Press, Prague.

19th International Conference
ENGINEERING MECHANICS 2013
Svratka, Czech Republic, May 13 – 16, 2013

PARALLEL COMPUTATION OF MICROSTRUCTURAL FIELDS BASED ON EXTENDED WANG TILE SETS

L. Zrůbek [1], J. Kruis[1], J. Novák [2] and A. Kučerová[1]

Summary: *This contribution addresses the method of Wang tilings used to reproduce fluctuating stresses, strains and displacements in materials with random microstructure subject to uniform strain excitation. Using small sets of Wang tiles allows to avoid an abrupt evaluation of fluctuating fields in a large macro-scopic domain, carrying a complete number of non-local solutions to desired mechanical quantities and synthesized by means of stochastic tiling algorithm. Assuming each tile discretized by the same regular finite element mesh, all admissible micro-scale problems can be obtained effectively by the Schur complement method.*

Keywords: ***microstructure, Wang tilings, stress field synthesis, Schur complement method***

1. Extended abstract

In this contribution, we draw our attention in high performance analysis of micro-scale quantities as stresses, strains and displacements at strongly heterogeneous materials. We first recall a recently reported technique based on Wang tilings (Wang (1961)) that instead of an abrupt evaluation of micro-scopic fields in entire macro-scopic domains uses a small set of statistical volume elements - tiles, from which the fields are synthesized via stochastic tiling algorithms (Cohen, Shade, Hiller, Deussen (2003)).

Wang tilings are rendered by square tiles, quatrominoes, gathered in sets. Tiles of a single set involve complete morphological information of synthesized quantity. The assembly of adjacent tiles in a regular lattice is called valid tiling, provided the macro-scopic domain is completely covered. This is allowed through congruent interfaces of different codes representing equilibrated tractions and compatible displacements.

As the sought fields are nonlocal, at least the nearest neighbours of each tile in the tiling must be taken into account. Therefore, thousands of micro-scale problems, square tilings of nine tiles in the simplest setting, have to be solved. At this time, structured discretizations arising from a raster image representation of microstructures are used and solved efficiently by Moulinec-Suquet Fast Fourier Transform algorithm (FFT) (Moulinec & Suquet (1994)). Nevertheless,

[1] Ing. Lukáš Zrůbek; Doc. Ing. Jaroslav Kruis, Ph.D.; Ing. Anna Kučerová, Ph.D.; Department of Mechanics, Faculty of Civil Engineering, Czech Technical University in Prague, Thákurova 7, 166 09, Prague 6
[2] Ing. Jan Novák, Ph.D.; Department of Mechanics, Faculty of Civil Engineering, Czech Technical University in Prague, Thákurova 7, 166 09 Prague 6 and Institute of Structural Mechanics, Faculty of Civil Engineering, Brno University of Technology, Antonínská 548/1, 601 90, Brno

strongly heterogeneous materials as metallic foams, for example, cause serious difficulty and the micro-scale problem suits better to conventional Finite Element Methods.

Keeping up with the fact that there are only eight different tiles, each may be discretized by a finite element mesh with a regular distribution of nodes on edges. It means, if any of two tiles are placed side by side in either of a spatial direction, their finite element meshes are conforming. Hence, the solution to all admissible micro-scale problems can be obtained effectively by the Schur complement method (Kruis (2004); Medek, Kruis, Tvrdík, Bittnar (2007)), which is the domain decomposition method of a non-overlapping type. The parallelization process is as follows. First, small number of processors eliminate internal unknowns in the reference tiles in order to obtain the Schur complements. This brings us at the position where each micro-scale problem can be defined only by means of the tile interfaces and the appropriate system of equations is reduced by assembling only the Schur complements. The interior field values are simply obtained by the backward substitution, if required.

Regarding the independent solution of all admissible tilings, the problem is ideal for processor farming, since the number of processors is usually significantly smaller. All available processors will share the computational effort when tackling the basic Schur complements with very fine meshes.

2. Acknowledgment

This work was supported by the Czech Science Foundation, through projects No. 13–24027S (L. Zrůbek, A. Kučerová), P105/12/0331 (J. Novák) and GACR 13–18652S (J. Kruis) and by the Czech Technical University in Prague through project No. OHK1–042/13 (L. Zrůbek, J. Kruis, J. Novák, A. Kučerová). In addition, we would like to thank the European Social Fund endowment under Grant No. CZ.1.07/2.3.00/30.0005 (J. Novák) of Brno University of Technology (Support for the creation of excellent interdisciplinary research teams at Brno University of Technology).

3. Reference

M.F. Cohen, J. Shade, S. Hiller, O. Deussen, “Wang tiles for image and texture generation”, ACM Transactions on Graphics, Citeseer, 287–294, ISSN 0730–0301, 2003.

J. Kruis, “Domain Decomposition Methods on Parallel Computers”, Progress in Engineering Computational Technology, 299–322, ISBN 1–874672–22–9 hardback, 2004.

O. Medek, J. Kruis, P. Tvrdík, Z. Bittnar, “Static Load Balancing Applied to Schur Complement Method”, 489–498, ISSN 0045–7949, 2007.

H. Moulinec, P. Suquet, “A fast numerical method for computing the linear and nonlinear mechanical properties of composites”, Comptes rendus de l’Académie des sciences. Série II, Mécanique, physique, chimie, astronomie, 1417–1423, 1994.

H. Wang, “Proving theorems by pattern recognition–II”, Bell Systems Technical Journal, 1–41, ISSN 0005–8580, 1961.

19th International Conference
ENGINEERING MECHANICS 2013
Svratka, Czech Republic, May 13 – 16, 2013

COARSE-GRAINED PARTICLES CONVEYING ALONG A PIPE BED

Pavel Vlasák [*], Zdeněk Chára [**], Jiří Konfršt[***], Bohuš Kysela[****]

Abstract: *The paper describes the results of a flow visualisation of model coarse-grained fully stratified particle-water mixtures. Investigation was focussed on study of the particle behaviour and carrier liquid and conveyed particles local velocities. Glass balls and washed graded pebble gravel of mean diameter of 6 mm were conveyed by water in a horizontal smooth pipe loop with a transparent pipe viewing section of inner diameter 40 mm. Particle movement along the pipe invert and particulate stationary bed, created by two layers of spherical particles of the same size as the conveyed particles, was studied. The effect of stationary bed on local velocity values of the carrier liquid and conveyed particles were determined. It was conducted that the maximum liquid velocity is significantly shifted from pipe centre to a higher position in the flow pattern with stationary bed.*

Keywords: ***Coarse-grained slurry, flow structure, visualisation, liquid local velocity, particle velocity.***

1. Results and Discussion

Pipeline transport of coarse-grained material is not very frequently used due to the problems of severe wear, material degradation, high operational velocities and energy requirement. However, it is of potential importance in mining industry. Slurry transport and handling in pipes require advance knowledge of their flow behaviour, which is important for the safe and economical design of the transport technology. For that reason, great attention was paid to the understanding of slurry flow behaviour and pressure drop mechanism. The understanding of the slurry flow behaviour makes it possible to optimize transport parameters and energy requirements, to improve quality, safety, economy and reliability of transport.

Heterogeneous slurries may be defined as the flow with asymmetrical concentration and velocity distribution, where a Coulomb friction contributes significantly to the friction losses. A flow pattern with a bed layer and a skew concentration distribution generally exist for these slurries. Wilson (1976) proposed a two-layer model for settling slurries with fully stratified flow pattern, where all particles are supposed to be concentrated in the lower portion of the pipe, in the upper layer only carrier liquid is presented. The Coulombic contribution to particle-wall friction is dominant. Based on experimental data of the Saskatchewan Research Council (Shook & Roco, 1991) the two-layer model was extended even for finer particles, it may be used for the description of the fully or partially stratified flow patterns and also in the case of the non-Newtonian carrier.

The mixture flow behaviour and velocity, particle velocity, motion and distribution in the pipe were recorded using the digital camera, NanoSenze MKIII+ (Vlasak et al., 2012) on an experimental pipe loop with a glass pipe viewing section of inner diameter 40 mm. The measured mixtures consisted of the glass balls of uniform size distribution (particle diameter d = 6 mm, density ρ_p = 2 540 kg/m^3), and the washed graded pebble gravel of uniform size distribution (particle diameter d ranged from 4 to 8 mm, ρ_p = 2 650 kg/m^3). Water was used as the carrier liquid.

[*] Prof. Ing. Pavel Vlasák, DrSc.: Institute of Hydrodynamics AS CR, v. v. i., Podbabská 30/5; 166 12, Prague 6; CZ, e-mail: vlasak@ih.cas.cz

[**] Doc. Ing. Zdeněk Chára, CSc.: Institute of Hydrodynamics AS CR, v. v. i., Podbabská 30/5; 166 12, Prague 6; CZ, e-mail: chara@ih.cas.cz

[***] Ing. Jiří Konfršt, Ph.D.: Institute of Hydrodynamics AS CR, v. v. i., Podbabská 30/5; 166 12, Prague 6; CZ, e-mail: konfrst@ih.cas.cz

[****] Ing. Bohuš Kysela, Ph.D.: Institute of Hydrodynamics AS CR, v. v. i., Podbabská 30/5; 166 12, Prague 6; CZ, e-mail: kysela@ih.cas.cz

When fully stratified mixture flows in horizontal pipes, the bed load layer originates and the pipe cross-section changes from circular to segment of a circle, and the velocity field becomes asymmetrical. The local velocities of carrier liquid and conveyed particles in case of the fully stratified flow pattern, including the flow pattern with stationary bed were studied.

The effect of stationary bed on local carrier liquid velocity u, the relative local particle velocity u_p/u_{max}, and carrier liquid u/u_{max} velocity profiles is illustrated in Fig. 1. The local velocity values were evaluated by PIV (Particle Image Velocity) method. The measured water velocity profiles were asymmetrical, maximum velocity values were at distance h about 23 mm above the pipe invert. The velocity gradient is steeper in the lower part of the profile, independently on the flow rate Q. Experimental local velocities near the stationary bed (from h = 9 to 12 mm) were practically equal zero due to the high value of the bed roughness. The velocities of particles rolling along stationary bed ($0.3 < h/D < 0.45$) is significantly lower than velocities of saltating particles, especially of the particles moving in area of the maximum water velocity.

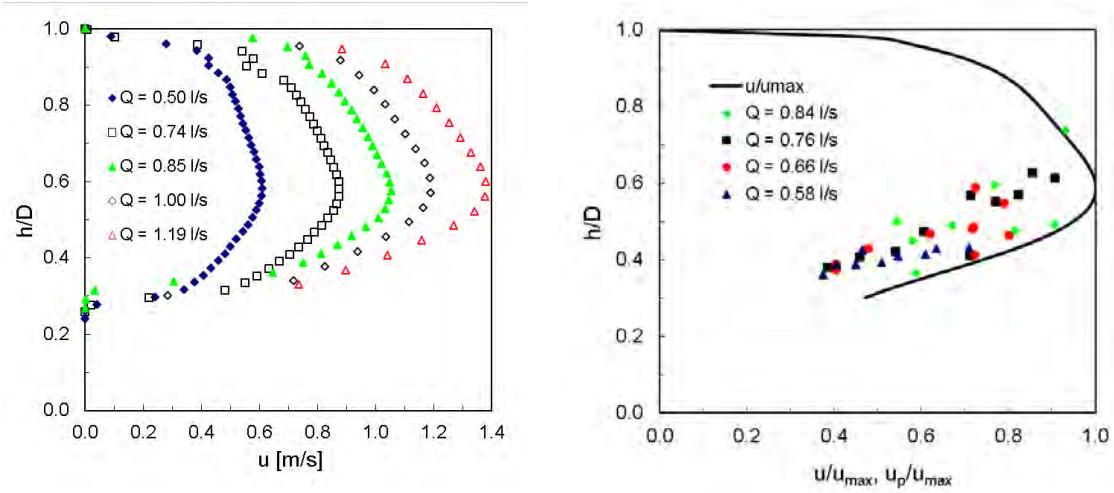

Fig. 1: Carrier-liquid and particles velocity profiles in pipe with stationary bed layer (S.B.).

2. Conclusions

The coarse-grained particle-water mixtures studied in the smooth pipe were significantly stratified. It was conducted asymmetrical carrier liquid velocity distribution in the pipe with stationary bed, the local velocity values increased in comparison with the flow without bed formation.

The coarse-grained particles conveyed by liquid in pipe moved principally in a layer close to the pipe invert, however for moderate and high flow velocities particle saltation becomes dominant mode of transport and particles were also observed in the central and upper part of the pipe cross-section.

The particle velocities increased with increasing distance from pipe invert, velocities of the saltating particles were significantly higher than that of the sliding or rolling particles.

Acknowledgement

Supports under the project P105/10/1574 of the Grant Agency of the Czech Republic and RVO: 67985874 of the Academy of Sciences of the Czech Republic are gratefully acknowledged.

References

Shook C.A. & Roco M.C. (1991) *Slurry Flow: Principles and Practice*, Butterworth/Heinemann, 1991.

Vlasak P., Kysela B. & Chara Z. (2012) Flow Structure of Coarse-Grained Slurry in Horizontal Pipe. *J Hydrol Hydromech*, 60, 2, pp. 115-124

Wilson K.C. (1976) A unified physically based analysis of solid-liquid pipeline flow. *Proc. of Hydrotransport 4*, Banff, Alberta (Canada), BHRA (U.K.), Paper A1, 1–16.